Dedicated to:

My Parents

Department of Chemical Engineering

Indian Institute of Technology Guwahati

Gwahati-781039, Assam, India

.....CERTIFICATE.....

This is to certify that the thesis entitled "*Preparation, Characterization and Applications of clay supported composite membranes*" being submitted by **Somen Jana** for the award of PhD degree has been carried out under our guidance and supervision. The work documented in this thesis has not been submitted to any other University or Institute for the award of any degree or diploma.

Dr. Kaustubha Mohanty

Associate Professor
Department of Chemical Engineering
Indian Institute of Technology Guwahati
Gwahati-781039, Assam, India

Dr. Mihir K. Purkait

Associate Professor
Department of Chemical Engineering
Indian Institute of Technology Guwahati
Gwahati-781039, Assam, India

Acknowledgement

First and foremost I want to thank both of my supervisors **Dr. Kaustubha Mohanty**, Assosiate Professor, Department of Chemical Engineering and **Dr. Mihir K. Purkait**, Assosiate Professor, Department of Chemical Engineering. It has been an honor to be the first Ph.D. student of Dr. Mohanty. I appreciate all their contributions of time and ideas. Above all and the most needed, they provided me unflinching encouragement, help and support in various ways. This thesis would not have been possible unless their guidance and enormous assistance.

Further I owe my deepest gratitude to the doctoral committee members viz. **Dr. G. Pugazhenthi** (Chairman), Department of Chemical Engineering, **Dr. P. Ghosh** (Member) and **Dr. V. Venkata Dasu** (External Member), Department of Biotechnology for their kind technical help and friendly support whenever I needed. I want to extend my appreciation towards the previous and current HOD, **Dr. Aloke K. Ghoshal** and **Dr. Prabirkumar Saha** respectively. I'll never forget their important advices during my thorny days of PhD. Further I'm also thankful to other faculty members of our department who taught me many things knowingly or unknowingly.

I am grateful to all of the **departmental technical and non-technical staffs** for their kind cooperation during my staying in the department. I would also like to show my gratitude to **Mr. K. K. Senapati** and **Mr. C. Borogohain**, SO, CIF for their genuine help during the using of the scanning electron microscope and differential scanning calorimeter. I would like to broaden my thanks to the **Central Workshop, IIT Guwahati** for making a part of my experimental set up and to **Mr. A. Gogoi,** Junior technical superintendent, Department of Chemistry for doing my FTIR analysis.

I feel myself lucky enough to get very good batchmates like **Biraj**, **Ashoke** and **Kabita Mam**. I am indebted to many of my senior research scholars like **Bisuda, Debada, Shiva-bhaiya, Subham, Barun, Pradip, Mehabub, Bandana Mam, Monash** and **P. Aadaleesan** for helping me many times in different ways. I can remember some of my juniors like **Avijit Ghosh, S. Murugavelh, Soumya Sasmal, Kartick Mondal, Santhi Raju Pilli, Hemant Kumar, R. Anantharaj, D. Vasanth, Vijay**

Singh and last but not the least **Sabuj Das.** All of them also helped technically and personally during the period. Especially **Pradip, Mehabub, Biraj, Murugavelh, Medhi, Sabuj** and **Avijit** were some excellent persons who lend there hand without any hesitation whenever I needed. Special thank to **Srinivas** for helping me during the placements.

Most of all, I would like to express my deepest gratitude to all of my family members. **My Father** is the person who put the fundamental of my learning character, showing me the joy of intellectual pursuit ever since I was a child. **My Mother** is the one who sincerely raised me with her caring and gently love. Words fail me to express my appreciation to my wife **Rani** and to my dearest friend **Manindra** whose dedication, love and persistent confidence in me, has taken the load off my shoulder. Thanks to **Tuli** for being caring sister.

Finally, I would like to thank everybody who was important to the successful realization of thesis, as well as expressing my apology that I could not mention personally one by one.

Somen Jana

Abstract

Low cost ceramic membranes were prepared by paste casting followed by sintering at various temperatures using natural clay (– 150 mesh) of IIT Guwahati as the main raw material. The mechanical strength of the membrane was successfully increased by addition of small amount of sodium carbonate, sodium metasilicate and boric acid. The pore size of the prepared membrane was found to be 4.58 µm (for the membrane sintered at 1000 ºC). For decreasing the pore size of the membrane, kaolin was mixed with the natural clay in different proportions which resulted in various microfiltration (MF) membranes with a wide range of pore size (4.58 µm to 0.31 µm). The membrane pore size and pore density were predicted directly from the particle size distribution of the clay and kaolin and were suitably represented by second-order polynomials. These microfiltration membranes were successfully applied in hybrid processes such as Micellar Enhanced Microfiltration (MEMF) for removal of chromate ions and Advanced Oxidation Process (AOP) followed by MF for the removal of crystal violet dye. With an aim to reduce the pore size of these membranes to Ultrafiltration (UF) range, polymers such as chitosan and polyvinyl acetate were used to coat a thin layer over it using dip-coating method. The glutaraldehyde cross-linked chitosan membrane resulted in a pore size of 14 nm and was successfully applied for the removal of heavy metals (As and Hg) from synthetic groundwater using polymer enhanced UF. Almost 100 % removals were observed for both 500 µg L^{-1} mercury and 1000 µg L^{-1} arsenic. A modified dip coating method was used for preparing the polyvinyl acetate coated membrane whose pore size was found to be 9 nm. This membrane was successfully applied to fractionate lysozyme and ovalbumin from chicken egg white. An overall rejection of 94 % ovalbumin and transmission of 95% lysozyme was achieved. Another mixed matrix membrane was prepared using one polymer (cellulose acetate) and one inorganic precursor (LTA zeolite) with a pore size of 10 nm and the membrane efficiency was tested by rejection of bovine serum albumin (BSA). An overall BSA rejection of more than 95% was obtained.

Index

List of Tables

List of Figures

Nomenclatures

ABBREVIATIONS

AAS	Atomic absorption spectroscopy
AOP	Advanced oxidation process
BSA	Bovine serum albumin
CA	Cellulose acetate
CEW	Chicken egg white
CI	Confidence interval
CPC	Cetylpyridinium chloride
CV	Crystal violet
DD	Diffusion dialysis
DMAc	Dimethylacetamide
DSC	Differential scanning calorimetry
ED	Electrodialysis
EDX	Energy-dispersive X-ray spectroscopy
FESEM	Field emission scanning electron microscopy
FS	Ferrous sulfate heptahydrate
FTIR	Fourier transform infrared spectroscopy
HPLC	High-performance liquid chromatography
LS	Lysozyme
LPSA	Laser particle size analyzer
MEMF	Micellar enhanced microfiltration
MD	Membrane distillation
ME	Membrane extraction
MF	Microfiltration
MEUF	Micellar enhanced ultrafiltration
NF	Nanofiltration
OV	Ovalbumin

PAA	poly (acrylic) acid
PAUF	Polymer assisted ultrafiltration
PEI	Polyethyleneimine
PEUF	Polymer enhanced ultrafiltration
PSD	Particle size distribution
PV	Pervaporation
PVA	Polyvinyl alcohol
PVAc	Polyvinyl acetate
PVP	Polyvinylpyrrolidone
RO	Reverse osmosis
SDS	Sodium dodecile sulfate
SEM	Scanning electron microscopy
TDS	Total dissolved solid
TGA	Thermogravimetric analysis
TSS	Total suspended solids
UF	Ultrafiltration
UV	Ultraviolet
XRD	X-Ray diffraction analysis
XRF	X-Ray fluorescence

NOTATIONS

A, B	Intercept and slope of Equation 4.1 respectively
A_{sp}	Specific Area of membrane precursor
ΔC	Concentration differential
$D_{1,0}$	Average particle diameter surface
$D_{3,2}$	Weighted mean diameter
$D_{4,3}$	Volume weighted mean diameter
D_{avg}	Average pore diameter
ΔE	Electrical potential differential
J	Liquid flux ($m^3m^{-2}sec^{-1}$)

K	Effective permeability factor (m/s)
L	Pore length (m)
L_h	Hydraulic permeability ($m^3m^{-2}sec^{-1}$ Pa^{-1})
l	Pore length (m)
N_p	Pore density
n	Number of pores per unit area
n_i, d_i	n_i is the (number-based) frequency of occurrence of particles in size class i, having a mean diameter d_i
ΔP	Pressure differential
P_2	Membrane pressure at permeate side (Pa)
p	Average pressure on the membrane
Q	Volumetric flow rate (m^3/s)
R	Rejection (%)
r_g	Average pore radius found from gas permeability
r_l	Average pore diameter (µm)
S	Permeable area of the membrane (m^2)
ΔT	Temperature differential
${}_{25}X_{75}$	Quartile ratio
ε	Porosity of membrane (unit less)
η	Viscosity of gas (Pa s)
μ	Viscosity (Pa.s)
v	Molecular mean velocity of the gas (m/s)

Summary

Separation is an indispensible part of downstream operation in chemical, petrochemical, biochemical, food and several other allied process industries. Almost all kinds of separation can be accomplished by exploiting the differences between the matters to be separated: size, shape, vapor pressure, solubility and so on. Membrane based separation process is an emerging technology and is being used in a large number of process and allied industries. Membrane processes have several advantages such as, low energy consumption, easy up-scaling, non requirement of any additives. Moreover they can be applied for continuous separation and easily coupled with other separation processes (hybrid processes). Nevertheless, this process has some drawbacks such as concentration polarization/membrane fouling, low life time and low selectivity or flux.

Now-a-days, membrane processes are used in a wide range of applications and the numbers of applications are still growing. From an economic point of view, the present time is intermediate between the development of first generation of membrane processes like microfiltration (MF), ultrafiltration (UF), nanofiltration (NF), reverse osmosis (RO), electro-dialysis (ED), membrane electrolysis (ME), diffusion dialysis (DD) and dialysis and second generation membrane processes like gas separation (GS), vapor permeation (VP), membrane distillation (MD) and carrier mediated processes.

There are more than 100 different materials in the patent and scientific literature from which membranes have been made and many more such will be added in near future. In the following section a brief discussion of the salient chemistry and characteristics of the few widely used materials for preparing membranes were given. All the materials have some advantages and disadvantages. Materials are chosen depending on their characteristics and applicability.

Ceramic membrane: α-alumina, γ-alumina, zirconia, silica, titania and kaolin are the most common inorganic materials used for preparation of ceramic membranes. Some common advantages of ceramic membranes are: high resistivity to corrosive feed, high temperature applicability, long life, low fouling tendency and higher mechanical strength. However, there exist a few drawbacks like: mostly applicable to MF and UF range and comparatively high cost. Thus, there is always a challenging research area for preparing ceramic membrane with low cost which can be competitive with the polymeric membrane.

Polymeric membrane: Polysulfone, cellulose acetate, styrene acrylonitrile, polyethersulfone, polyvinylidene fluoride, polyvinyl acetate, polytetrafluroethylene, polyetherimeide and polyvinyl pyrrolidone are most widely used polymeric materials for the polymeric membrane. The advantages are: wide range of application from MF to RO, availability of both hydraulic and hydrophobic materials, low cost and easy to fabricate while the disadvantages are: low solvent and temperature resistance, lower applicable range of pH and lower life span.

Zeolite membrane: LTA, FAU, MOR, FER, CHA, SAPO-34, DDR, and mixed tetrahedral–octahedral oxides are the most common types of zeolites used as membrane material. The advantages of zeolite membranes over polymeric membranes are that these membranes have high selectivity; they have long term stability in high temperature and pressure, easy for cleaning and catalytic activation. The disadvantages are: high capital cost, brittleness, low membrane surface per module volume and difficulty in achieving high selectivity in large scale microporous membranes.

Mixed matrix membrane: Zeolite/polymer mixed matrix membranes are excellent candidate to address the issue of both polymer membrane and zeolite membranes. Zeolite/polymer mixed-matrix membranes combine the superior selectivity and permeability of inorganic zeolite with the low cost and ease of processability of polymer membranes. Kulprathipanja and coworkers at UOP first introduced the term "mixed matrix membrane" and performed the pioneering study on zeolite/polymer mixed-matrix membrane in the mid-1980s. Later on, both rubbery polymer and glassy polymers were combined with a variety of zeolite and aluminosilicates. Still there is enough scope of research for preparing mixed matrix membranes with different combination of polymers and zeolites and studying the effect of zeolite and polymer percentage on the morphology and pore size.

The development of asymmetric membranes made a breakthrough in industrial applications. This consists of a very dense top layer or skin with a thickness of 0.1 to 0.5 μm supported by a porous sub-layer. These membranes combine the high selectivity of a dense membrane with the high permeation rate of a very thin membrane. Another advantage of these membranes is that, each layer can be optimized independently to obtain optimal membrane performance with respect to selectivity, permeation rate, thermal and chemical stability. Different methods such as dip-coating, spray coating, spin coating, interfacial polymerization, in-situ polymerization, grafting and plasma polymerization can be used for preparing composite membranes.

Dip coating method is very easy and non expensive, thus suitable for industrial applications. But, there is no work reported using polyvinyl acetate (PVAc) or polyvinylpyrrolidone (PVP) as the polymer

layer over ceramic support using dip coating method. Thus, a detail investigation about the problem/process can be a challenging research area.

The composite membranes are very successful towards industrial application. Thin film composite membranes were used for aromatic recovery. Carbon fiber/carbon/alumina tubular composite membranes were used for the treatment of wastewater. Except these, composite membranes were used for separation of organic liquid, used in membrane reactor and for separation of vapor gas mixture.

Thus, based on the above brief discussion, it seems that there is enough scope to carry out further work on preparation and characterization of composite membranes using low cost locally available raw materials and use the prepared membranes for various applications such as water/wastewater treatment, bioseparation etc. To achieve this overall aim, present research work has been undertaken with the following objectives:

- Preparation of low cost ceramic membrane using locally available raw material (clay of IIT Guwahati).
- Application of the prepared membrane for the removal of chromate ions by micellar enhanced separation using a suitable surfactant.
- Decreasing the pore size of the membrane by using a suitable material (whose particle size is smaller than clay) with clay as the main raw material.
- Development of relationships to predict the membrane pore size and density from the particle size of membrane precursors.
- Application of the prepared membrane for the removal of crystal violet dye by advanced oxidation process (AOP) followed by membrane filtration.
- Preparation of the composite membrane by using the ceramic membrane as the support and impregnating this support by crosslinked chitosan to decrease the pore size further.
- Removal of arsenic and mercury from synthetic groundwater using this composite membrane by polymer enhanced filtration using a suitable polymer.
- Development of a novel dip-coating method for applying a thin layer of polyvinyl acetate (PVAc) over the ceramic support and studying the effect of dip coating parameters like solution concentration and dipping time.
- Fractionation of lysozyme and ovalbumin from chicken egg white (CEW) using the PVAc-ceramic composite membrane.

- ❖ Preparation and characterization of a mixed matrix membrane using cellulose acetate (CA) and LTA zeolite and testing the suitability of the prepared membrane by the rejection of bovine serum albumin (BSA).

Thesis Outline

As described before, the work was started with the preparation of low cost ceramic membrane from local clay of IIT Guwahati campus. Further to reduce the pore size, kaolin was used with clay as the raw material. Over again, to prepare the membranes in the ultrafiltration range, different types of coating viz. crosslinked chitosan, polyvinyl acetate and a combination of LTA zeolite and cellulose acetate were used. With this, the prepared membranes were applied for the removal of chromate ions, crystal violet dye, heavy metals (As, Hg), for the separation of lysozyme from chicken egg white and for bovine serum albumin. The thesis is organized in the following seven chapters:

Chapter I: Introduction and literature review.

Chapter II: Preparation of low cost macroporous support from local clay and application for the removal of CrO_4^{2-} by micellar enhanced microfiltration (MEMF).

Chapter III: Preparation of submicron range membrane from kaolin and local clay: Effect of precursor particle size on membrane morphology and application for the removal of crystal violet dye by advanced oxidation process (AOP) followed by microfiltration.

Chapter IV: Preparation of chitosan impregnated ultrafiltration membrane and application for the removal of arsenic and mercury by polymer enhanced ultrafiltration (PEUF).

Chapter V: Preparation and characterization of polyvinyl acetate-ceramic composite membrane by modified dip coating method and application for the fractionation of lysozyme and ovalbumin from chicken egg white.

Chapter VI: Preparation of LTA zeolite – cellulose acetate mixed matrix membrane and studies on the rejection of bovine serum albumin (BSA).

Chapter VI: Conclusion.

A brief description of the content of each of the chapters is furnished below:

Chapter I: Introduction and literature review

In the starting of this chapter a concise basic discussion of the membrane technology viz. definition, classification, advantages/disadvantages and industrial applications are discussed. Further discussion on different membrane materials like ceramic, polymeric, zeolite and mixed-matrix are followed by the discussion on different membrane preparation methods. And finally major research areas are compared with the current trend and work plan was organized from the literature review.

Chapter II: Preparation of low cost macroporous support from local clay and application for the removal of CrO_4^{2-} by micellar enhanced microfiltration (MEMF)

This chapter presents the preparation and characterization of low cost ceramic microfiltration membranes from natural clay of IIT Guwahati and its application to remove chromate ions from wastewater. Two membranes were prepared by paste casting method followed by sintering at different temperatures, first one from only clay (Membrane A) and the second one from clay with small amount sodium carbonate, sodium metasilicate and boric acid (Membrane B). Both the membranes have been characterized by TGA, SEM, XRD, water permeability test and acid-base treatment. It was observed that with the increase of sintering temperature, pore size as well as permeability and flexural strength increased while porosity and pore density decreased. The overall performance of Membrane B was found to be better than Membrane A. The average pore size for membrane B was increased from 3.74 μm to 4.58 μm when sintering temperature increases from 800 °C to 1000 °C.

Membrane B sintered at 1000 °C was successfully used for the removal of chromate from aqueous solution by micellar enhanced microfiltration (MEMF) using cetyl pyridinium chloride (CPC) as the surfactant. 100% rejection of chromate ions were reported at a very high feed ratio (CPC/chromate) of 10.

Based on raw material prices the membrane cost was estimated to be $\$19/m^2$. The prepared low-cost membrane shows good promise for the treatment of wastewater containing such heavy metals.

Chapter III: Preparation of submicron range membrane from kaolin and local clay: Effect of precursor particle size on membrane morphology and application for the removal of crystal violet dye by advanced oxidation process (AOP) followed by microfiltration.

In the first part of this chapter, ceramic disc type microfiltration membranes (50 mm diameter and 5 mm thickness) were prepared by the paste casting method from different compositions of clay,

kaolin, and binding agents like sodium carbonate, sodium metasilicate, boric acid, and sintered at different temperatures. All the membranes were characterized by TGA, SEM, XRD, water permeability test, and acid–base treatment. With the increase of sintering temperature, the pore size as well as the permeability and flexural strength increased while porosity and pore density decreased. It was found that with increasing the amount of kaolin and decreasing the amount of clay the pore diameter decreased. A membrane prepared from 18% clay, 62% kaolin, and 20% binding material and sintered at 1000 °C has shown the lowest average pore size of 0.31 µm with porosity, pore density, and flexural strength of 0.22, 4.80×10^{12} m^{-2} and 12.81 MPa respectively. The membrane pore size and pore density were predicted directly from the particle size distribution of the clay and kaolin and were suitably represented by second-order polynomials.

In the second part[3], a hybrid process of advanced oxidation (AOP) followed by microfiltration (MF) was proposed for the removal of crystal violet dye from aqueous solution in order to save energy, time and cost. Fenton's reagent was used to degrade the dye by varying the concentrations of $FeSO_4{\cdot}7H_2O$ and H_2O_2. The optimal composition of Fenton's reagent for an initial dye concentration of 100 mg L^{-1} was found to be 1000 mg L^{-1} of H_2O_2 and 100 mg L^{-1} of $FeSO_4{\cdot}7H_2O$.

EDX and FTIR spectra of crystal violet and AOP post-product were compared to understand the molecular changes during AOP. The aromatic and chlorine groups were found to be degraded during the process. The lowest pore size microfiltration membrane prepared from clay and kaolin (disused in the first part) was used to remove the AOP post-products at three different transmembrane pressures of 138, 207 and 276 kPa. Small change in pH (6.41 to 6.18), total dissolved solid (360 mg L^{-1} to 350 mg L^{-1}) and density (999.7 kg m^{-3} to 997.1 kg m^{-3}) were observed during microfiltration. Subsequently, no dye and suspended solids were found in the permeate. Thus, 100 % dye removal was achieved with this scheme of AOP followed by MF.

Chapter IV: Preparation of chitosan impregnated ultrafiltration membrane and application for the removal of arsenic and mercury by polymer enhanced ultrafiltration (PEUF).

This chapter presents the fabrication of chitosan based ceramic composite membranes using dip coating technique. Low-cost ceramic supports were prepared from local clay of IIT Guwahati and kaolin with an average pore size of 1093 nm and porosity of 0.37. Different composite membranes were prepared by varying chitosan concentration and dipping time and were characterized using scanning electron microscope (SEM), air and hydraulic permeability tests.

The average pore sizes were in the range of 760 nm to 13 nm which confirmed that the prepared composite membranes were applicable for both microfiltration (MF) and ultrafiltration (UF) applications. An increase in both chitosan concentration and dipping time was found to reduce the pore size. The composite membrane (pore size: 13 nm) was used for the removal of mercury and arsenic from synthetic groundwater by polymer enhanced ultrafiltration (PEUF) technique using polyvinyl alcohol (PVA) as the chelating agent. The effects of initial concentrations of mercury, arsenic and PVA on the extent of removal of both the heavy metals were investigated in detail. The efficiency of PEUF was explored in terms of rejection of metals and permeates flux. Almost 100% removals were observed for both 500 μg L^{-1} mercury and 1000 μg L^{-1} arsenic.

Chapter V: Preparation and characterization of polyvinyl acetate-ceramic composite membrane by modified dip coating method and application for the fractionation of lysozyme and ovalbumin from chicken egg white.

Composite ultrafiltration membrane was prepared by applying thin coating of polyvinyl acetate (PVAc) over a ceramic support by using a novel dip-coating method. Traditional dip coating method was found to be unsuitable for the coating of PVAc. Due to the low viscosity of the polymer solution (N,N-di-methyl acetamide solvent), the polymer doesn't form layer rather penetrate into the macropores of the support during drying. In the proposed modified technique, a secondary solvent (water) was used for the removal of DMAc rather than drying it from the solution. For studying the effect of polymer concentration and dipping time over membrane parameters, twelve different membranes were prepared using four different concentrations (10%, 20%, 30% and 40%) and three dipping time (30s, 60s and 120s). Membranes were characterized with TGA, SEM, air and hydraulic permeability, acid/base treatment. PVAc was found to be thermally stable up to 275 °C and no crack/uneven coating was found from the surface morphology study. The pore size was observed to decrease with increase in both the polymer concentration and dipping time and was found to be between 150 to 9 nm.

The lowest pore size membrane was applied for the separation of lysozyme (LS) and ovalbumin (OV) from chicken egg white (CEW). Studies were done with three different concentration of CEW in water with a fixed concentration of NaCl (200 mM) and at a fixed transmembrane pressure (206.8 kPa). Feed and permeate concentrations of LS and OV were analyzed in HPLC.

Effect of pH was studied and pH 11.0 was found as optimum for the transmission of LS to permeate side. Rejections of both the LS and OV were found to increase with time and over 94% rejection of OV and 95% transmission of LS was found.

Chapter VI: Preparation of LTA zeolite – cellulose acetate mixed matrix membrane and studies on the rejection of bovine serum albumin (BSA).

This chapter presents the preparation and characterization of a mixed matrix membrane which is an organic-inorganic hybrid composite membrane containing dispersed zeolite particles in a continuous organic polymer matrix. These types of membranes provide the advantages of both polymer membranes such as low cost and ease of processing and the zeolite membranes like high selectivity and permeability. In this work, cellulose acetate (CA) and LTA zeolite were used as the membrane forming materials. Zeolite was prepared and characterized with XRD and LPSA. Coating of mixed matrix material was applied over a low cost ceramic support. The effect of CA %, LTA % and dipping time on membrane pore size and morphology was studied. The prepared membranes were characterized with TGA, SEM, air and hydraulic permeabilities. CA was found to be thermally stable up to 300 °C and the zeolite has not shown any changes during thermal application. Morphologically zeolite and CA construct good matrix and no non-uniform layer/uncoated sections were found. The pore sizes varied between 80 to 10 nm depending upon the LTA, CA composition and dipping time. The effectiveness of the prepared membrane was tested by the rejection of bovine serum albumin (BSA).

The rejection of 1000 mgL^{-1} BSA with every membrane was compared and the rejection of three different concentrations (500, 1000 and 2000 mgL^{-1}) of BSA solution was tested with lowest pore size membrane (M-5.0-4-90). Rejection and flux were found to be increased and decreased with time respectively. Finally at 120 min of operation, over 96% rejection was observed for 2000 mg L^{-1} BSA.

Chapter VII: Conclusion

This chapter summarizes the inferences drawn from the present work and recommendations for future work. The overall aim of the thesis is to prepare low cost ceramic and composite membrane for different microfiltration and ultrafiltration applications. Low cost ceramic membranes were prepared using natural clay as the main raw material along with some other binding agents. The pore sizes of these ceramic membranes were found to be in the microfiltration range and the lowest pore size membrane was successfully applied for the removal of chromate ions by micellar enhanced microfiltration method. Kaolin was mixed with clay in different proportions with an aim to reduce the pore size of the ceramic membrane further and the lowest pore size (0.31 μm) membrane was applied

successfully for the removal of carcinogenic crystal violet dye using the hybrid process of advanced oxidation followed by microfiltration. Different composite membranes were prepared and characterized using these ceramic membranes as the support. Polymers such chitosan, polyvinyl acetate were used to coat a thin layer over the ceramic support which resulted in membranes with pore sizes suitable for both microfiltration and ultrafiltration applications. The lowest pore size chitosan crosslinked membrane was successfully applied for the removal of mercury and arsenic by polymer enhanced ultrafiltration (PEUF) using polyvinyl alcohol as the chelating agent. Similarly the lowest pore size polyvinyl acetate coated membrane was used for the fractionation of lysozyme and ovalbumin from chicken egg white. Finally a mixed matrix membrane was prepared by dip coating method using cellulose acetate as the polymer and LTA zeolite as the inorganic material. The pore size was found to be 10 nm and the suitability of the membrane was tested by the rejection of bovine serum albumin (BSA). The overall results from this work are encouraging and conclude that the prepared composite membranes can be utilized for various applications.

Chapter I

Introduction

In this chapter, an outline of membrane separation processes, membrane materials, preparation methods, advantages, disadvantages and major research areas of membrane technology is discussed. From the discussion, state of art for the current work is derived and finally the organization of the total thesis has been presented.

1.1 Background

Membrane technology has drawn a lot of attention as a dignified separation technology in past few decades. Membrane technology is a term that refers to a number of different filtration processes that are used to separate substances. With this technology, membranes are used as filters in separation processes, with a wide variety of applications, both industrial and scientific. The membranes used in membrane technology may be regarded as barriers separating two fluids and allowing certain substances to be either transported or retained across the membrane.

Membrane technology has been found to be advantageous and promising when compared to other separation processes such as adsorption, distillation, extraction and crystallization. The primary advantages of this process are, lower capital cost, lower energy requirement, higher separation factors, compact design and elimination of secondary separation units. Moreover this process can be combined with other separation processes (hybrid process) to achieve a higher separation factor. The success of this technology depends on various factors such as porosity, pore diameter, pore size distribution, particle size distribution of the solutes in addition to the solubility/diffusivity of the permeating molecules and the membrane material. Various methods have been used to prepare different types of membranes using a wide range of membrane materials. Still there is enough scope to study this process in detail while ensuring its versatility for a wide range of applications.

1.2 Overview of Membrane Separation Process

1.2.1 What is a Membrane?

The word membrane originates from the Latin word *membrana* which means a skin. Membrane keeps things separated in the living world and passes materials selectively [1]. Although it's difficult to give an exact definition of a membrane, a general definition could be: **a membrane is a thin barrier, placed between two phases, or mediums, which allow one or more constituents to selectively pass from one medium to the other in the presence of an appropriate driving force while retaining the rest [2].** The term 'selective' being inherent to a membrane or a membrane process. It should be noted that this is a macroscopic definition while separation should be considered at the microscopic level. The definition says nothing about membrane neither structure nor membrane function [3]. Contrary with the conventional mass transfer operation, the two phases between which transfer of one or more species occurs are not in direct contact in membrane separation [2]. Further, the transports of molecules through the pores of membrane belongs to fluid dynamics. Thus, membrane processes are the combination of two unit operations *i.e.*, mass transfer and momentum transfer.

1.2.2 Basic Principle of Membrane Separation

Some mechanism must exist in the membrane which facilitate the transport of one component and impedes the transport of the other. In a first approximation, membranes can be classified according to the means of such impediment. Porous membranes discriminate according to the size of particles of molecules. Non-porous membranes discriminate according to the chemical affinities between components and membrane materials. Membranes can sharply alter the rates of mass transfer. These altered rates occur because of physical and chemical interactions between the membranes and separating components. The physical interaction includes those encountered in filtration, where different components pass through the membrane at different rates determined by the size of the component.

The flux through the membrane can be generally expressed as:

$$Flux = \frac{Membrane\ \ permeability}{Membrane\ thickness} \times Driving\ \ force \qquad (1.1)$$

This means that the flux depends linearly on both the permeability (a membrane parameter) and the driving force. The driving force may be difference in pressure, concentration, temperature, chemical potential and so on. The flux also depends inversely upon the thickness of the membrane. The thinner the membrane; the higher the flux.

From thermodynamic point of view, there may be three types of transport through membrane. These are active transport, passive transport and facilitated and carried mediated transport. In a system characterized by a single force and a single flow, the flow must be directed from a region of higher electrochemical potential to one of lower electrochemical potential. In other words, the flow and the force must be of same sign. However, if there are two or more flows and force, negative coupling between flows can drive a substance in a direction opposite to its conjugate force. The term 'active transport' should be applied to flows that are directed against their conjugate driving forces and conversely the 'passive transport' are those where flows are directed in the direction of conjugate driving force. In facilitated or carrier mediated transport, the carrier molecules which reside in the membrane, can interact with a given permeant. Hence the transport of a permeant through the membrane is accomplished by means of three steps: association with a carried molecule at the interior surface of the membrane, transport of permeant-carrier complex across the surface, the dissociation of the permeant molecule across the surface [1].

A schematic representation of membrane separation is shown in Figure 1.1

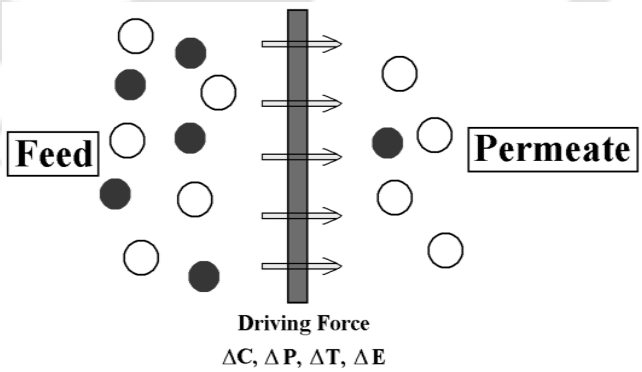

Figure 1.1. Schematic representation of a two-phase system separated by a membrane.

1.3 Classification of Membranes

A membrane can be natural or synthetic, thick or thin, its structure can be homogeneous or heterogeneous, neutral or charged. Transport across membrane can be active or passive, passive transport can be driven by various means (e.g. pressure, concentration, electrical difference). As such, membranes can be classified according to different viewpoints. The first classification is by nature, i.e. biological or synthetic membranes. This is the clearest distinction possible. Synthetic membranes can be subdivided into organic (polymeric or liquid) and inorganic (e.g. ceramic, metal) membranes.

Another means of classifying membranes is by morphology or structure - for the case of solid synthetic membranes, the two types of membrane structures are: symmetric and asymmetric (anisotropic) membranes [3]. The principal types of synthetic membranes are classified as shown in the Figure 1.2.

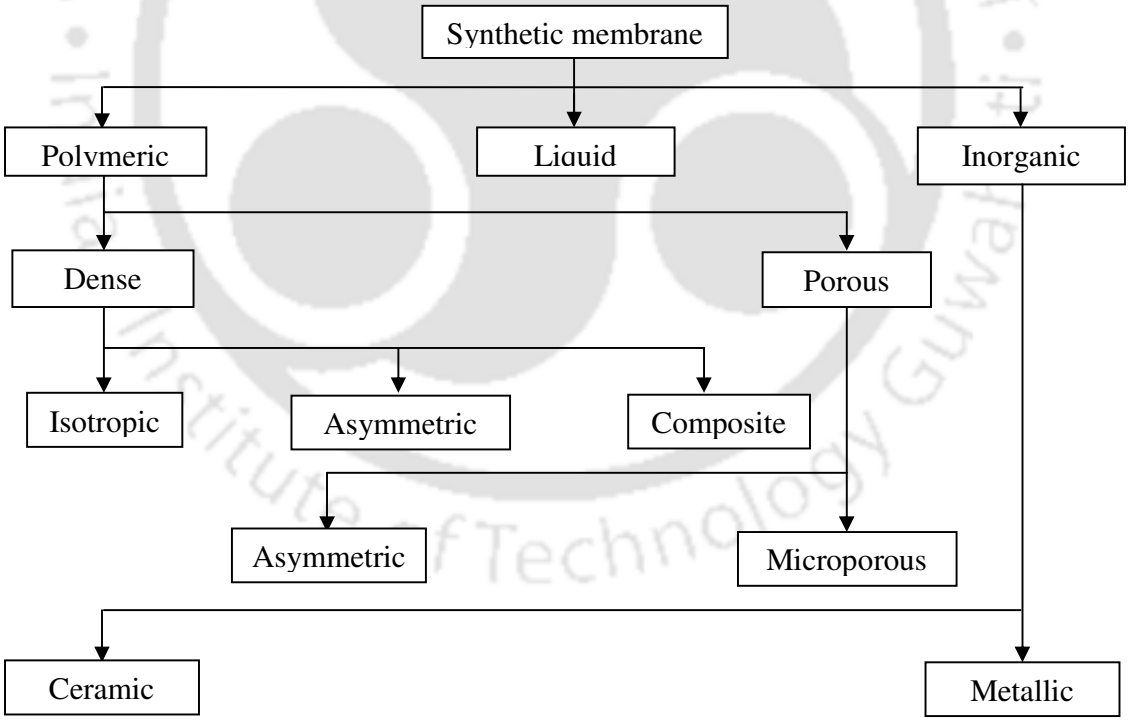

Figure 1.2. Types of membranes [2]

1.4 Classification of Membrane Separation Processes

The membrane processes can be classified according to the driving force used in the process. Technically and commercially most relevant processes are pressure driven processes. Apart from this, concentration gradient and electrical potential also act as driving force for some of the membrane processes. Table 1.1 summarizes the classifications and general characteristics of various membrane processes.

Table 1.1. Classifications and characteristics of membrane processes [1, 2].

Driving force	Membrane process	Permeate	Retentate	Type of membrane
Pressure difference	Microfiltration (MF) (0.5-2 bar)	Dissolved solutes, water	Suspended solids	Symmetric microporous
	Ultrafiltration (UF)	Small molecules, water	Polymers, proteins, micelles, colloid particles	Asymmetric microporous
	Nanofiltration (NF)	Monovalent ions, water	Small molecules, divalent salts	Thin-film membrane
	Reverse osmosis (RO)	Small polar solvents, salts, water	All solutes	Asymmetric skin type
	Pervaporation (PV)	Volatile small molecules, water	Low volatility species; species less soluble in the membrane	Asymmetric homogenous polymer
Concentration difference	Diffusion dialysis (DD)	Small molecules, water	Large molecules	Nonporous or microporous
	Membrane extraction (ME)	Gases, solutes, vapors soluble in the extractant	Components of feed insoluble in extractant	-----
Electrical potential difference	Electrodialysis (ED)	Ionized solutes, water	Non-ionic solutes	Ion-exchange membrane
Temperature difference	Membrane distillation (MD)		Molecules < 1 nm	Microporous

The difference between the pressure driven processes (microfiltration, ultrafiltration, nanofiltration, reverse osmosis and pervaporation) are the transmembrane pressure difference and pore sizes. The pore size is the most important parameter for size based membrane separation processes. The pore sizes of different types of membranes are compared in Figure 1.3.

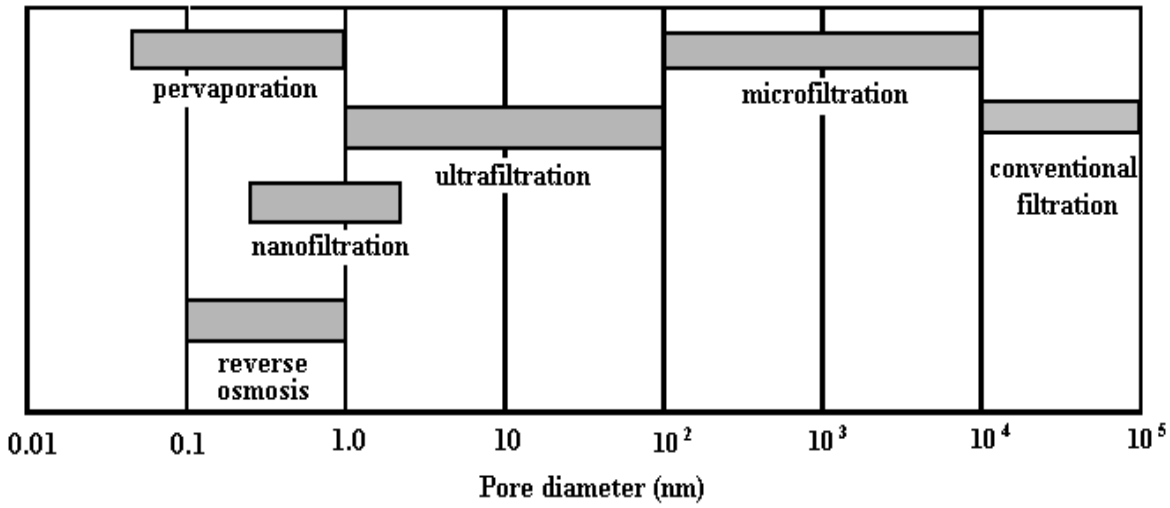

Figure 1.3. Pore size range in pressure driven membrane processes

Except the pressure driven processes, there are a number of membrane separation process based on selective transport of a target species under concentration difference, electrical potential difference and temperature difference. Dialysis and membrane extraction functions on concentration difference. In dialysis, diffusion of solutes occurs across a semi-permeable membrane whereas in membrane extraction, gas and solute vapors pass through the membrane. In electrodialysis, electrical potential difference is used to transport some selective ions from one solution to another through an ion-exchange membrane. Membrane distillation method uses a non-wetting, microporous membrane, with a liquid feed phase on one side and a condensing permeate phase on the other. The vapor molecules transmit through the membrane due to temperature difference.

In membrane technology, pressure driven processes have taken the lead over all the processes. There is an explosive growth observed recently in the usage of membranes and development of newer and cost effective membrane materials.

1.5 Advantages and Disadvantages of Membrane Separation Processes

Like other processes, membrane process also has some advantages and disadvantages.

Comparing to the other conventional processes membrane technology permits concentration/separation, without the use of heat. Evaporation and freeze concentration are common dewatering techniques used for liquid products. Evaporation requires the input of about 2.33 MJ/kg of water evaporated while freezing requires about 335 KJ/kg water frozen. On the other hand, membrane separation doesn't need any change in the state of the solvent to effect a dewatering, thus results in considerable saving in energy.

No complicated design of heat transfer or evaporator unit is required. Membrane processes can be operated even in ambient atmosphere. These make the process more efficient and convenient.

As technology develops, more and more situations arise where substance of high unit value are formed in very low concentration. In conventional separation processes, the separation efficiency drops rapidly as the concentration of the desired component fails. Membrane separation techniques, on the contrary, can give better answer to these problems.

With the development of new membranes along with improved transport properties and better chemical and thermal stability in recent years, a large number of new potential applications are identified. The membrane industries are responding to the market needs by rapidly exploiting these applications on an industrial scale.

Membrane units can be easily combined with other processes. These hybrid processes can successfully increase capacity of existing plants and improve product quality. Hybrid processes are also successful in terms of overall improvement in performance and cost.

Membrane fouling is a pertinent problem in membrane separation process. Deposited solid particles over membrane surface increases the rate of membrane fouling and decreases the flow rate gradually. This problem is especially observed in hollow fiber membrane/dead-end filtration module.

Sometimes, membrane processes show limitation to higher solid content feed. In RO, it is frequently the osmotic pressure of the concentrated solutes that limits the process. In the UF or MF, the problem doesn't arise much but high viscosity of the solutions sometimes lead to lower flow rate.

In general, membrane processes are expensive comparing to the other process due to the fabrication method, occasional replacement, fouling and poor cleanability of the membrane.

1.6 Membrane Materials

Polymeric and ceramic materials are most common membrane materials used for the preparation of symmetric membrane. Asymmetric membranes are generally prepared with the following combination of materials such as, ceramic-polymeric [4], ceramic-zeolite [5] or ceramic mixed matrix [6]. Usually, in asymmetric membranes, ceramic layer provides desired mechanical strength and the skin layer (polymeric, zeolite or mixed matrix) gives the required pore size. The resistance of the asymmetric membrane was mainly due to the skin layer.

1.6.1 Ceramic Membrane

α-alumina [7], γ-alumina, zirconia, silica, titania [8] and kaolin [9] are the most common inorganic materials used for preparation of ceramic membranes. Some common advantages of ceramic membranes are: high resistivity to corrosive feed, high temperature applicability, long life, low fouling tendency and higher mechanical strength [3]. However, there exist a few drawbacks such as: mostly applicable to MF-UF–range and comparatively high cost. Thus, there is always a challenge to prepare ceramic membrane from low cost material so as to make it competitive with the commercial polymeric membrane.

1.6.2 Polymeric Membrane

Polysulfone [10], cellulose acetate [4], styrene acrylonitrile [11], polyethersulfone, polyvinylidene fluoride, polyvinyl acetate, polytetrafluroethylene, polyetherimeide and polyvinyl pyrrolidone [12] are most widely used polymeric materials for the polymeric membrane. The advantages are: wide range of application from MF to RO, availability of both hydraulic and hydrophobic materials, low cost and easy to fabricate while the disadvantages are: low solvent and temperature resistance, lower applicable range of pH and lower life span [3].

From the previous studies, it was found that ceramic membranes are better than the polymeric membranes in many aspects. But, generally ceramic membranes are 10 times costlier than polymeric membranes. Thus, there exists an evergreen area of research to make a low cost ceramic membrane which can be commercially competitive to the polymeric membrane.

1.6.3 Zeolite Membrane

LTA [13], FAU [14], MOR [15], FER [16], CHA [17], SAPO-34 [18], DDR [19], and mixed tetrahedral–octahedral oxides [20] are the most common types of zeolites used as membrane material. The advantages of zeolite membranes over polymeric membranes are that these membranes have high selectivity; long term stability in high temperature and pressure, easy for cleaning and catalytic activation. The disadvantages are: high capital cost, brittleness, low membrane surface per module volume and difficulty in achieving high selectivity in large scale microporous membranes [21].

1.6.4 Mixed matrix Membrane

Zeolite/polymer mixed matrix membranes are excellent candidate to address the issue of both polymeric and zeolite membranes. Zeolite/polymer mixed matrix membranes combine the superior selectivity and permeability of inorganic zeolite with the low cost and ease of processability of polymeric membranes. Kulprathipanja and coworkers at UOP first introduced the term “mixed matrix membrane” and performed the pioneering study on zeolite/polymer mixed matrix membrane in the mid-1980s [22]. Later on, both rubbery polymer and glassy polymers [23] were combined with a variety of

zeolite and aluminosilicates [24]. Still there is enough scope of research for preparing mixed matrix membranes with different combination of polymers and zeolites and studying the effect of zeolite and polymer percentage on the morphology as well as pore size.

1.7 General Methods for Membrane Preparation

There are different methods for preparing membranes. The underlying basic principles of the preparation process are to control the pore size and the pore size distribution at the surface layer and to decrease the thickness of the surface layer. Some of the commonly practiced methods of membrane preparation are discussed below.

1.7.1 Symmetric Ceramic Membrane

Synthetic Symmetric ceramic membranes are fabricated using uniaxial and paste methods. Both these methods involve the preparation of an inorganic mixture using suitable pore forming organic and inorganic mixtures along with binding materials. The uniaxial method involves casting an inorganic mixture in a suitable disk or tubular shape and kept under very high pressure (30 – 50 MPa). Subsequently, the disk or tubular type mould is sintered to prepare the membrane. The paste method involves the preparation of a paste using the inorganic mixture using suitable solvent which is eventually casted into suitable shape and sintered at high temperatures. The properties of the ceramic membrane are highly influenced by the composition of the raw materials, sintering temperatures as well as the process including the schedule of heating, sintering and cooling [25, 26].

1.7.2 Asymmetric Ceramic Membrane

Asymmetric ceramic membranes are prepared by the deposition of thin film of inorganic materials over the porous symmetric ceramic membrane (or support). Slip coating followed with casting, sol-gel and dip coating methods are usually deployed for the fabrication of asymmetric membranes whose properties are dependent upon both the support as well as the thin skin layer morphology. The slip coating sintering process involves coating the support surface with a suspension of finer particles in

a solution of a cellulosic polymer or polyvinyl alcohol that acts as a binder and viscosity enhancer to hold the particles in the suspension. Subsequently the membrane is dried and sintered at high temperature to obtain a fine microporous surface layer. Usually, several slip coated layers are applied in series with each layer formed from a suspension of progressively finer particles to yield an isotropic structure. Many commercial ceramic UF membranes are made using slip casting technique to achieve skin layer pore diameters within 100 – 200 Å. Membranes with even finer pore sizes are fabricated using sol gel technique. This method involves the transition of the slip casting technique to the colloidal level. The colloidal or polymeric gel solutions of an inorganic hydroxide are initially prepared using controlled hydrolysis of metal salts or metal alkoxides. The particulate sol method involves the dissolution of alkoxide dissolved in alcohol followed by the hydrolysis using excess water or acid. The precipitate thus obtained is maintained as a hot solution for extended time periods to yield a stable colloidal solution. The colloidal solution is then cooled and coated onto the microporous membrane support. Later the membrane is carefully dried to avoid surface defects such as cracks and sintered at usually 500 – 800 °C. During the dip coating process, the support is dipped in an inorganic suspension and the inorganic materials passed through the pores of the support and as well as deposit over the support surface. Subsequently the membrane is dried and sintered at high temperatures [25, 26].

1.7.3 Polymeric-Ceramic Composite Membrane

Polymer-ceramic composite membranes are prepared by deposition of polymeric film over a porous ceramic support. These membranes are characterized with superior combinations of structural integrity, fouling resistance, flux and selectivity and have been applied for UF [27] and pervaporation applications [12]. These membranes have a top skin layer consisting of polymers such as polysulfone [10], styrene acrylonitrile [11], polyvinyl acetate, polyvinyl pyrrolidone [12], cellulose acetate [4], polydimethylsiloxane [28] over a ceramic support having nominal pore sizes of 0.2 – 2 μm made from materials such as kaolin, alumina and zirconia. There are several methods available for the preparation of polymer ceramic composite membrane such as spray coating [11], spin coating [29], grafting [12], self assembly [30], dip coating [4] and vapor deposition [31]. The dip coating technique involves dipping the ceramic support in the polymeric sol for a specific amount of time to yield the polymeric-ceramic membrane. Spray coating, spin coating and self assembly are modified versions of dip coating technique and are applied depending upon various issue such as the physio-chemical properties of the

polymeric sol as well as the ceramic support. While spray coating involves spraying the polymeric sol onto the support, spin coating involves rotation of the support in a polymeric sol. Grafting polymerization method involves three steps namely, pretreatment, surface activation and grafting the polymer over the support. Therefore, though the method is efficient, it is marginally complicated when compared to other processes. The vapor deposition method involves deposition of the polymeric film by condensation of vapor on the membrane support.

The advantages of composite membranes can be represented as:

- High selectivity of a dense membrane.
- High permeation rate of a very thin membrane.
- Each layer can be optimized independently to obtain optimal membrane performance with respect to selectivity, permeation rate, thermal and chemical stability.

1.7.4 Phase Inversion Method

Phase inversion is a very flexible technique to obtain membrane with a large sort of morphologies. Membrane properties can vary greatly depending on the kind of polymers used. The classical phase inversion method follows a ternary phase diagram. When the homogeneous solution of a polymer is quenched in the precipitant, the material moves towards a two phase region and the membrane (a solid porous phase) forms with a liquid phase filling the pores.

For commercial membrane preparation, the film is cast on a non woven fabric moving in a rotating drum. Doctor's blade is used to control the thickness. Phase inversion takes place in a in gelation tank containing a non-solvent. The fabric with the film on top moves through the non-solvent. An ultrathin top layer is formed and finally the membrane is passed through a drying chamber to evaporate the solvent.

1.7.5 Track Itch Method

This method is used to prepare membranes where the pores are not tortuous but straight like cylindrical pores. In the first step of track etch process, polycarbonate or polyester films are bombarded

with massive energetic nuclei in a combined beam of U235 fission fragment in a nuclear reactor. In the second step, the track left by the particles are preferentially etched into uniform, cylindrical pores in etch bath, generally warm caustic soda solution. Pore size is controlled by residence time in etch bath.

1.7.6 Surface Impregnation Method

The micropores of the ceramic support were used to impregnate by insoluble polymer to make it an UF membrane. Chitosan can be a good option for this purpose. Chitosan is soluble in pH < 5.0. In that pH, chitosan is crosslinked with glutaraldehyde and just after the reaction, reactant suspension was spread over ceramic support by dip coating or spin coating. The crosslinked reaction turns the chitosan insoluble even in lower pH. The crosslinked molecules are penetrated into the pores and finally the support was dried to make the pores in UF range.

1.7.7 Interfacial Polymerization

Interfacial polymerization is one more method of depositing thin layer upon a porous support. In this case, a polymerization reaction occurs between two very reactive monomers. The support layer, which is generally an ultrafiltration or microfiltration membrane, is immersed in an aqueous solution containing a reactive monomer or a pre-polymer, frequently of the amine type. Then the membrane is immersed into the second bath containing a water immiscible solvent in which another reactive monomer, often an acid chloride has been dissolved. These two reactive monomers (i.e. acid chloride and amine) react with each other to form a dense polymeric top layer. Sometimes, heat treatment is applied to complete the interfacial reaction. The advantage of this process is that the reaction is self inhibiting through passage of a limited supply of reactants through the already formed layer, resulting in an extremely thin film of thickness within 50 nm range [2].

1.7.8 Preparation of Zeolite Membrane

Zeolite membranes have gained much interest recently. Zeolites are crystalline microporous aluminosilicates and is build up by a three dimensional network of SiO_4 and AlO_4 tetrahedra. Zeolites have a much defined pore structure. LTA [13], FAU [14], MOR [15], FER [16], CHA [17], SAPO-34

[18], DDR [19], and mixed tetrahedral–octahedral oxides [20] are the most common types of zeolites used as membrane material. Due to the high amount of aluminum, zeolite LTA is ~~a~~ very hydrophilic in nature. The pore size depend on the type of cation and Ca^{2+}, Na^{+} and K^{+} gives 5Å, 4Å and 3Å respectively. On the other hand, silicalite-1 is very hydrophobic zeolite since it does not contain any aluminum and has no charge which must be compensated by a counter-ion.

Most of the synthetic zeolite membranes are prepared on a microporous support that provides good mechanical strength to thin zeolite film. Several strategies have been developed for preparing such layers and among them the following three are very popular [32]:

1. In-situ Crystallization
2. Vapor-Phase Transport
3. Secondary Growth Synthesis/Seeding Technique

In-situ crystallization: For preparing synthetic zeolite membrane, first the zeolite sol is prepared. The sol is obtained by mixing two solutions, one of which is alumina source while the other is the silica source. The alumina source is obtained by addition of requisite amount of sodium aluminates in sodium hydroxide solution, while the silica source is obtained by the addition of sodium silicate to sodium hydroxide solution. By mixing these two solutions in different ratios, the Si/Al ratio of the particular zeolite is maintained [33].

In in-situ crystallization method, the nucleation and growth occurs in a single step. The support is made to contact with the prepared sol and placed in an autoclave for hydrothermal treatment.

Vapor phase transport: A second method aims to favor nucleation processes by using a dry-gel conversion in the so-called “vapor phase transport” method. It is a two-step method. An amorphous gel containing silica, aluminum is first coated on the support. The crystallization occurs in the second step, the water for the hydrothermal synthesis coming as saturated vapor from the bottom of the autoclave. The template may be present either in the water or in the gel. This approach allows a strict control of the zeolite amount deposited. Also, the location and concentration of seeds is favored. A drawback is the possibility of cracks formation in the amorphous gel layer [34].

Secondary growth synthesis/seeding technique: The third method, known as "secondary growth synthesis" includes an initial seeding step, during which small zeolite seed crystals are deposited on top of the support (sometimes by rubbing the crystal of the zeolite). These seeds are then grown under hydrothermal zeolite synthesis conditions in order to form a continuous zeolite layer on the substrate surface. This two-step method favors the density of initial nuclei and has been widely used. The choice of the seed allows determining the nature of the membrane zeolite. Seed characteristics (size, shape, concentration) can also affect the zeolite crystal orientation in the layer which may influence the overall transport properties [34].

Mixed matrix Membrane Preparation: Similar to commercial composite membranes, mixed matrix membranes should have asymmetric membrane geometry with a thin selective layer on a porous support to be commercially viable. The skin layer should be made from a zeolite/polymer mixed matrix material to provide the membrane high selectivity, but the non selective porous support can be made from the ceramic or polymer. Zeolite/polymer mixed matrix membranes can be fabricated into dense film, asymmetric flat sheet or asymmetric hollow fiber.

Mixed matrix dense film: The process for preparing dense film mixed matrix membrane is described below:-

i) Dispersing the zeolite particles in an organic solvent or a mixture of two or more organic solvents by ultrasonic mixing and high speed stirring to form a zeolite slurry.

ii) Dissolving a polymer that serves as a continuous polymer matrix in the zeolite slurry to form a stable zeolite/polymer casting dope.

iii) Fabricating the mixed matrix dense film by a solution casting method, by pouring the stable zeolite/polymer casting dope into a glass ring on top of a clean glass plate or using a doctor knife to spread the stable zeolite /polymer casting solution on a flat and clean support.

Flat sheet asymmetric mixed matrix membrane: The process for preparing flat sheet asymmetric mixed matrix membrane is described below:-

i) Setting the solution layer by doctor's blade over a support fabric.

ii) Letting a controlled amount of evaporation occurs.

iii) Immersing the partially dried nascent mixed matrix membrane in to a gelation medium with controlled temperature.

iv) Waiting until all solvents are replaced by the gelation fluid.

v) Putting the membrane in to a drying chamber at controlled temperature.

Asymmetric hollow fiber mixed matrix membrane: The method for preparation of hollow fiber mixed matrix geometry is same as the method of flat sheet, but there is no requirement of fabric. In addition, the dope was forming an integrally skinned asymmetric hollow fiber mixed matrix membrane has a relatively higher viscosity than that for forming an integral sinned asymmetric flat sheet mixed matrix membrane. An extrusion spinneret instead of a doctor's blade is needed for spinning hollow fibers.

1.8 Industrial Application of Membranes

Membrane processes are no longer bound in the domain of laboratory but have found their way into industries as viable separation technique. These processes have achieved impressive industrial importance for the resolution of aqueous liquid mixtures, purification of chemical and biological products, wastewater reclamation, hydrometallurgical processing and many more. The principle characteristics of various commercialized membrane process separation processes can be specified based on several aspects [35]:

- Size of the species to be retained.
- Nature of the species to be transmitted through the membrane (i.e. volatile, electrolyte etc.).
- Mechanism of transport.
- Selectivity between the components.

The application of different membrane processes are summarized in Table 1.2.

Table 1.2. Selected industrial applications of membrane processes.

Membrane process	Industrial application
Microfiltration	Wastewater treatment, membrane bioreactor, sugar, fruit, wine tea industry, fermentation broth concentration.
Ultrafiltration	Drinking water, membrane bioreactor, diary, meat, fruit and brewery industry, protein/enzyme purification, heavy metal removal by micellar enhanced ultrafiltration
Nanofiltration	Drinking water, wastewater treatment, sugar and tea industry, dye removal
Reverse osmosis	Deionized/drinking water preparation, wastewater treatment, diary, fruit/vegetable, wine and sugar industry, heavy metal removal
Gas separation	H_2 recovery, CO_2 separation
Pervaporation	Ethanol dehydration, organic material recovery
Electrodialysis	Demineralized water, wastewater treatment, diary and Sugar industry

Over the years, the focus of the chemical and process industry has shifted towards the development and application of integrated processes combining the mechanism of reaction and separation in one single unit. This trend is motivated by benefits such as reduction in equipment and plant size and improvement of process efficiency and hence, a better process economy. Some of the major examples are the ones dealing with equilibrium reactions such as: esterification, ester hydrolysis and etherification and breaking of the azeotropes [36]. Combination of membrane processes with other methods were reviewed by Lipnitzki et al. [37].

Thus, from the discussions, it can be concluded that for removal of organic and inorganic components such as heavy metals or dye molecules by membrane processes, nanofiltration or reverse osmosis is required. But, these processes require high pressure and suffer from the problems of lower flow rate and high fouling. For overcoming these problems, different unit processes can be combined with membrane filtration. Surfactant enhanced methods followed by microfiltration can be used for removal of metal ions, toxic dye molecules can be destroyed and removed from wastewater by advanced

oxidation and microfiltration. Apart from these, ultrafiltration can be used for the removal of heavy metals by polymer enhanced methods, and for the fractionation of a binary proteins.

1.9 Aim of the Current Study

Thus, based on the above brief discussion, it seems that there is enough scope to carry out further work on preparation and characterization of composite membranes using low cost raw materials and use the prepared membranes for various applications such as water/wastewater treatment, bioseparation etc. To achieve the goal, present research work has been undertaken with the following objectives:

- Preparation of low cost ceramic microfiltration membrane using locally available raw material (e.g., clay of IIT Guwahati) and application for the removal of chromate ions by micellar enhanced separation using a suitable surfactant.
- Decreasing the pore size of the membrane by using a suitable material (whose particle size is smaller than clay) mixed with clay as the main raw material and application for the removal of crystal violet dye by advanced oxidation process (AOP) followed by membrane filtration.
- Development of relationships to predict the membrane pore size and density from the particle size of membrane precursors.
- Preparation of the composite membrane by using the ceramic membrane as the support and impregnating this support by crosslinked chitosan to decrease the pore size further and application for the removal of arsenic and mercury from synthetic groundwater using this composite membrane by polymer enhanced filtration using a suitable polymer.
- Development of a novel dip-coating method for applying a thin layer of polyvinyl acetate (or other low viscous polymer) over the ceramic support and studying the effect of dip coating parameters like solution concentration and dipping time.
- Fractionation of lysozyme and ovalbumin from chicken egg white (CEW) using the prepared ceramic composite ultrafiltration membrane.
- Preparation and characterization of a mixed matrix membrane using cellulose acetate (CA) and LTA zeolite and testing the suitability of the prepared membrane by the rejection of bovine serum albumin (BSA).

1.10 Thesis Outline

1.10.1 Chapter I: Introduction.

1.10.2 Chapter II: Preparation of low cost macroporous support from local clay and application for the removal of CrO_4^{2-} by micellar enhanced microfiltration (MEMF).

1.10.3 Chapter III: Preparation of submicron range membrane from kaolin and local clay: Effect of precursor particle size on membrane morphology and application for the removal of crystal violet dye by advanced oxidation process (AOP) followed by microfiltration.

1.10.4 Chapter IV: Preparation of chitosan impregnated ultrafiltration membrane and application for the removal of arsenic and mercury by polymer enhanced ultrafiltration (PEUF).

1.10.5 Chapter V: Preparation and characterization of polyvinyl acetate-ceramic composite membrane by modified dip coating method and application for the fractionation of lysozyme and ovalbumin from chicken egg white.

1.10.6 Chapter VI: Preparation of LTA zeolite – cellulose acetate mixed matrix membrane and studies on the rejection of bovine serum albumin (BSA).

1.10.7 Chapter VI: Conclusion.

References

1. K. Nath, Membrane Separation Processes. Prentice Hall of India, (2008)

2. B.K. Dutta, Principles of Mass Transfer and Separation Processes. Prentice Hall of India, (2007)

3. M. Mulder, Basic Principles of Membrane Technology. Springer, (2007)

4. B.K. Nandi, R. Uppaluri, M.K. Purkait, Effects of dip coating parameters on the morphology and transport properties of cellulose acetate–ceramic composite membranes. J. Membr. Sci. (2009) 330, 246–258.

5. J. Dong, K. Wegner, Y.S. Lin, Synthesis of submicron polycrystalline MFI zeolite films on porous ceramic supports. J. Membr. Sci. (1998) 148, 233-241

6. S. Hussain, W.J. Koros, Mixed matrix hollow fiber membranes made with modified HSSZ-13 zeolite in polyetherimide polymer matrix for gas separation. J. Membr. Sc. (2007) 288, 195-207.

7. K.A. DeFriend, M.R. Wiesner, A.R. Barron, Alumina and aluminate ultra-filtration membranes derived from alumina nanoparticles. J. Membr. Sci. (2003) 224, 11–28.

8. Y. Yoshino, T. Suzuki, B.N. Nair, H. Taguchi, N. Itoh, Development of tubular substrates, silica based membranes and membrane modules for hydrogen separation at high temperature. J. Membr. Sci. (2005) 267, 8–17.

9. B.K. Nandi, R. Uppaluri, M.K. Purkait, Preparation and characterization of low cost ceramic membranes for micro-filtration applications. Appl. Clay Sci. (2008) 42, 102–110.

10. Y. Matsumoto, M. Sudoh, Y. Suzuki, Preparation of composite UF membranes of sulfonated polysulfone coated on ceramics. J. Membr. Sci. (1999) 158, 55–62.

11. S. Sachdeva, A. Kumar, Synthesis and modeling of composite poly(styrene-coacrylonitrile) membrane for the separation of chromic acid. J. Membr. Sci. (2008) 307, 37–52.

12. W. Yoshida, Y. Cohen, Ceramic-supported polymer membranes for pervaporation of binary organic/organic mixtures, J. Membr. Sci. (2003) 213, 145–157.

13. D. Shah, K. Kissick, A. Ghorpade, R. Hannah, D. Bhattacharyya, Pervaporation of alcohol–water and dimethylformamide–water mixtures using hydrophilic zeolite NaA membranes: mechanisms and experimental results. J. Membr. Sci. (2000) 179, 185–205.

14. V. Nikolakis, G. Xomeritakis, A. Abibi, M. Dickson, M. Tsapatsis, D. G. Vlachos, Growth of a faujasite-type zeolite membrane and its application in the separation of saturated/unsaturated hydrocarbon mixtures. J. Membr. Sci. (2001) 184, 209–219.

15. A. Tavolaro, A. Julbe, C. Guizard, A. Basile, L. Cot, E. Drioli, Synthesis and characterization of a mordenite membrane on Al_2O_3 tubular support. J. Mater. Chem. (2000) 10, 1131–1137.

16. T. Matsufuji, S. Nakagawa, N. Nishiyama, M. Matsukata, K. Ueyama, Synthesis and permeation studies of ferrierite/alumina composite membranes, Micropor. Mesopor. Mater. (2000) 38, 43–50.

17. H. Lee, P.K. Dutta, Synthesis of free-standing chabazite-type films, Micropor. Mesopor. Mater. (2000) 38, 151–159.

18. S.G. Li, J.L. Falconer, R.D. Noble, SAPO-34 membrane for CO_2/CH_4 separation. J. Membr Sci. (2004) 241, 121–135.

19. T. Tomita, K. Nakayama, H. Sakai, Gas separation characteristics of DDR type zeolite membrane, Micropor. Mesopor. Mater. (2004) 68, 71–75.

20. K.G. Shattuck, B. Yilmaz, J. Warzywoda, A. Sacco, Hydrothermal synthesis of oriented ETS-4 films on porous α-alumina substrates, Micropor. Mesopor. Mater. (2006) 88, 56–62.

21. J. Caro, M. Noack, P. Kölsch, R. Schäfe , Zeolite membranes – state of their development and perspective, Micropor. Mesopor. Mater. (2000) 38, 3–24

22. S. Kulprathipanja, E.W. Funk, S.S. Kulkarni, Y.A. Chang, Separation of a monosaccharide with mixed matrix membrane US patent 4735193. (1988).

23. R. Mahajan, W.J. Koros, Mixed matrix membrane material with glassy polymers Part 2. Polymer engg sci. (2002) 42, 1432-1441.

24. R. Mahajan, W.J. Koros, Mixed matrix membrane material with glassy polymers Part 1. Polymer engg sci. (2002) 42, 1420-1431.

25. R.W. Baker, Membrane Technology and Applications, John Willey & Sons Ltd, West Sussex, England (2004)

26. S. Judd, B. Jefferson, Membranes for Industrial Wastewater Recovery and Re use, Elsevier, Oxford, UK (2003).

27. R.S. Faibish, Y. Cohen, Fouling resistance ceramic supported polymeric membranes for ultrafiltration of oil-in-water microimulsion. J. Membr. Sci., (1999) 158 55-62.

28. Y. Ki. Hong, W.H. Hong, Influence of ceramic support on pervaporation characteristics of IPA/water mixtures using PDMS/ceramic composite pervaporation membranes using response surface methodology. J. Membr. Sci., (2008) 311 23-33.

29. K.M. Song, W.H. Hong, Dehydration of ethanol and isopropanol using tubular type cellulose acetate membrane with ceramic support in pervaporation process. J. Membr. Sci., (1997) 123 27-33.

30. Y. Chen, F. Xiangli, W. Jin, N. Xu, Organic inorganic composite pervaporation membranes prepared by self-assembly of polyelectrolyte multilayers on macroporous ceramic supports. J. Membr,. Sci., (1999) 159 29-39.

31. H. Yanagishita, D. Kitamoto, K. Haraya, T. Nakane, T. Tsuchiya, N. Kaura, Preparation and pervaporation performance of polyimide composite membrane by vapor deposition and polymerization (VDP). J. Membr. Sci., (1997) 136 121-136.

32. S. Miachon, E. Landrivon, M. Aouine, Y. Sun, I. Kumakiri, Y. Li, P. Prokopová, N. Guilhaume, A. Giroir-Fendler, H. Mozzanega, J. Dalmon, Nanocomposite MFI-alumina membranes via pore-plugging synthesis: Preparation and morphological characterization. J. Membr. Sci., (2006) 281 228-238.

33. S. Workneh, A. Shukla, Synthesis of sodalite octahydrate zeolite-clay membrane and its use in separation of SDS. J. Membr. Sci., (2008) 309 189-195.

34. N. Saffaj, M. Persin, S. A. Younsi, A. Albizane, M. Cretin, A. Larbot Elaboration and characterization of microfiltration and ultrafiltration membranes deposited on raw support prepared from natural Moroccan clay: Application to filtration of solution containing dyes and salts. App. Clay Sci. (2006) 31, 110–119.

35. R.E. Kesting, Synthetic Polymeric Membrane: A Structural Perspective. 2nd Edition, John Wiley and Sons, Inc, New York, (1985).

36. G. Kaibel, T. Holtmann, C. Miller, H. Schoenmakers, Reaktivdestillation. Chem. Ing.Tech. (2005) 77, 1749–1758.

37. F. Lipnizki, R.W. Field, P.K. Ten, Pervaporation-based hybrid process: a review of process design, applications and economics. J. Membr. Sci., (1999) 153, 183–210.

Chapter II

Preparation of low cost macroporous support from local clay and application for the removal of CrO_4^{2-} by micellar enhanced microfiltration

2.1. Introduction and Literature Survey

Ceramic membranes are a type of artificial membranes made from inorganic metarials (such as alumina, titania, zirconia oxides or some glassy materials). By contrast with polymeric membranes they can used in separations where aggressive media (acids, strong solvents) are present. They also have excellent thermal stability which make them usable in high temperature membrane operations [1]. Although it is well known that ceramic membranes are costlier than polymeric membranes, however they are superior with respect to long life, their uses in harsh chemical environment, and fouling characteristics [2].

Early research on the preparation of ceramic membranes have utilized expensive α- Al_2O_3 as precursor [3]. Later on γ- Al_2O_3, zirconia, titania, silica etc. were used for membrane synthesis [4, 1]. Recently some researchers have started to work with cheaper raw materials like apatite powder [5], fly ash [6], kaolin [7, 8] etc. to reduce the cost of the membrane.

Due to the well-known structural adsorption, rheological and thermal properties of clay minerals, membranes from clay are gaining a lot of attention these days. Initial days of research on ceramic membrane preparation were concentrated on pillared clays [9, 10]. Preparation of ceramic membranes using pure clay has started very recently. Moroccan clay was used to prepare different kinds of porous ceramic membranes deposited on tubular support and a pore size of 9.25 to 10.5 micron was reported [11]. The mechanical strength of the support was 10 MPa at 1250 °C sintering temperature. In a very recent work, ceramic microfiltration membrane was prepared from Tunisian natural material with a pore size of around 10 micron [12]. The prepared membrane was successfully applied for the treatment of cuttlefish effluent.

The potential use of ceramic microfiltration membranes in various fields like chemistry, food, biotechnology and wastewater treatments are increasing day by day [13]. Wastewater from different industries like metal plating, metal mines or coal refining contains many heavy metal ions which are potential environmental pollution source. Previously different processes like precipitation [14], flocculation [15], adsorption [16], and ion-exchange [17] were used for removal of these ions. With the progress of technology, membrane processes like reverse osmosis has been applied for removal of metal ions. However, main drawback of the process is that it requires high operating pressure (sometimes more than 25 atm) leading to high capital and operating cost.

Micellar enhanced ultrafiltration (MEUF) is one of the promising technology in which surfactant molecules absorbs inorganic and organic molecules from water solution [18]. A more recent approach is micellar flocculation followed by microfiltration. By this technology membrane process can run at much lower pressure (6-8 atm), thus reducing the operating cost [19].

During micellar flocculation, high charge ions binds to the surface of the micelle and those surface charges leads to the flocculation of the micelle. Micellar flocculation with sodium dodecile sulfate (SDS) has been studied by many researchers [20-22]. Mixture of different surfactants like cetylpyridinium chloride (CPC) and SDS were used for the simultaneous removal of cation and anion [19]. Purkait et. al. have studied the precipitation of CPC with potassium dichromate and potassium permanganate up to feed CPC to $K_2Cr_2O_7$ and $KMnO_4$ concentration ratio of 10 [23]. In these experiments 85% dichromate and 100% permanganate has been removed. However, at higher ratio of CPC to dichromate, removal of $K_2Cr_2O_7$ has not been reported yet.

The present work reports the preparation of low cost ceramic membrane from natural clay collected from IIT Guwahati campus. Two different membranes are prepared with two different compositions, one with pure clay and another with clay mixed with other chemicals. Comparison of these two membranes has been done in all aspects. TGA of both the compositions are done and all the membranes are characterized by XRD and SEM. Average pore size have been found and compared from SEM images and as well as from water permeability test. Other characteristics like porosity, flexural strength, and chemical stability have also been determined. The prepared membrane has been applied for removal of chromate ions from aqueous solutions. Flux decline and rejection of potassium dichromate has been observed with respect to time and different ratios (0.25 to 100) of CPC to dichromate. Finally

the cost analysis of the prepared membrane has been done to compare the membrane with the similar membranes and polymeric membranes available in the market.

2.2. Materials and Methods

2.2.1 Raw Material

Clay: The raw muddy clay was collected from IIT Guwahati campus and dried in hot air oven at 120 °C. The dried clay was ground in a ball mill and passed through 150 mesh screen. The preparation method of the dry powdered clay from muddy clay is presented in Figure 2.1.

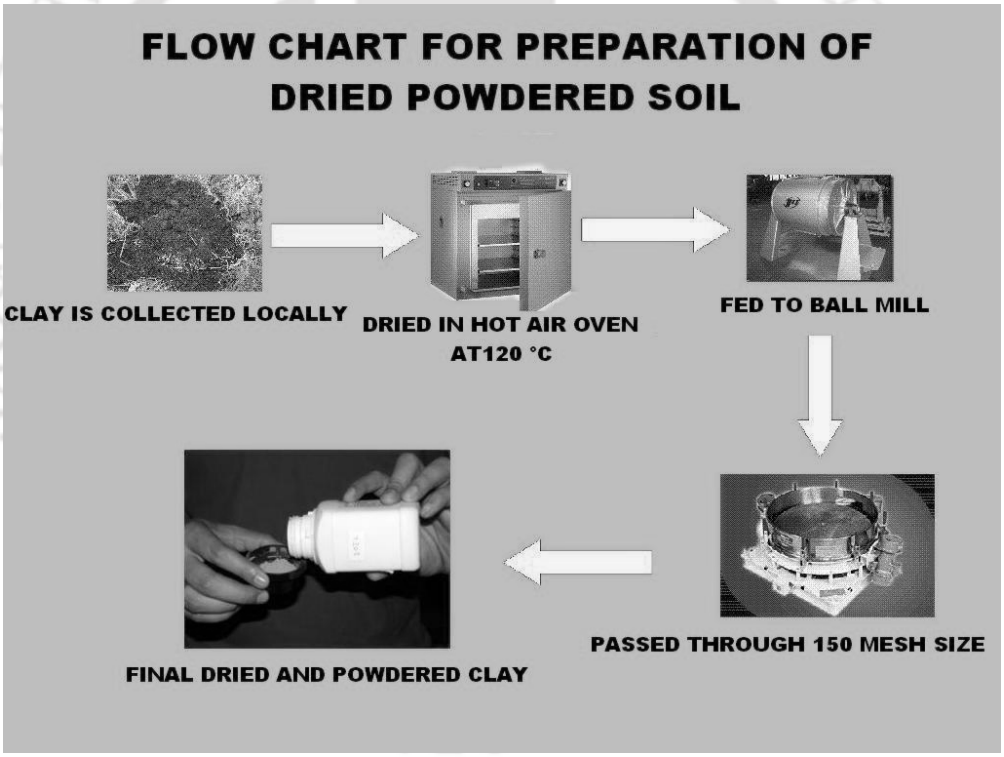

Figure 2.1. Preparation of dried, powdered clay

All the membranes were prepared with –150 mesh clay powder. The total component analysis of the clay sample was done by X-ray fluorescence (Philips, PW 2440 MagiXPRO). The analysis report is shown in Table 2.1. Further, the X-Ray Diffraction (Bruke D8, advanced X-ray diffraction measurement system) analysis of clay powder was done to determine the compounds present. The graph is shown in Figure 2.2 and the reflections of illite, quartz and kaolinite were found. Basic properties of clay like

pH, bulk density, organic matter content and soluble matter content were determined. The bulk density was found to be 30 kg m^{-3} and the value of soluble matter content was 3.03%.

Table 2.1. XRF report of clay

Main components									
Analyte	Na	Mg	Al	Si	K	Ca	Fe		
Compound formulas	Na_2O	MgO	Al_2O_3	SiO_2	K_2O	CaO	FeO		
Concentration, %	2.065	1.518	17.097	71.595	1.901	1.465	3.236		
Trace components									
Analyte	P	S	Ti	Cr	Mn	Co	Ni	Cu	Cl
Compound formulas	P_2O_5	SO_3	TiO_2	Cr_2O_3	MnO_2	Co_3O_4	NiO	CuO	Cl
Concentration, %	0.263	0.217	0.541	0.012	0.059	0.003	0.001	0.002	0.026

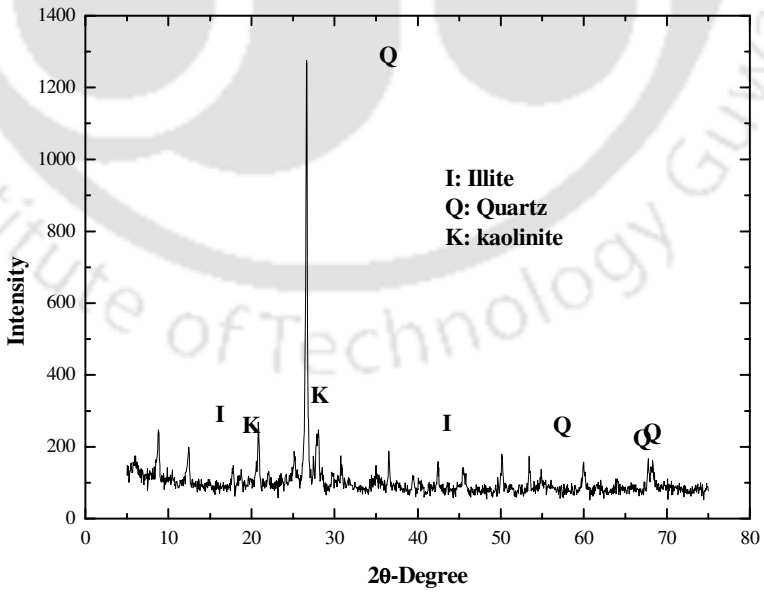

Figure 2.2. XRD report of the powdered clay.

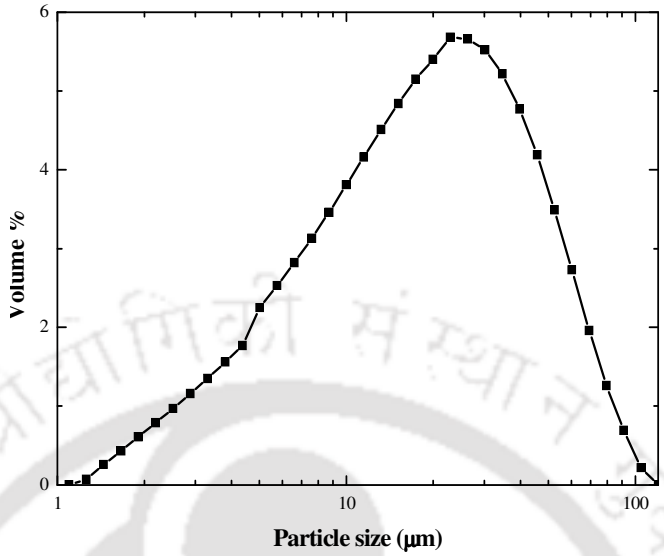

Figure 2.3. Particle size distribution of powdered clay.

Clay pH was measured by the standard method [24] and it was found that the used clay was slightly acidic (pH = 6.62). Clay organic matter was calculated by the method of Loss On Ignition (LOI) [25]. The % organic matter content was calculated to be 0.96%. Particle size distribution of the clay material was measured in laser particle size analyzer (Malvern, Masterizer-2000. Model: APA-5005) and is shown in Figure 2.3.

Chemicals: Different raw materials were used in this study for synthesis of membrane and for the chromate ion removal studies. Sodium metasilicate, sodium carbonate and boric acid have been used as the components for membrane preparation. Sodium metasilicate increases mechanical strength by creating silicate bonds within the elements. Sodium carbonate acts as a colloidal agent and improves dispersion properties thereby creates homogeneity. Boric acid also increases mechanical strength by creating metallic metaborate during sintering [26]. Potassium dichromate was used as the source of chromate ions and cetyl pyridinium chloride as cationic surfactant. Sodium metasilicate, boric acid and CPC were purchased from Loba Chemie Pvt. Ltd. Sodium carbonate and potassium dichromates were purchased from Rankem, India and SD Fine Chemicals respectively. All the chemicals used in these studies are of analytical grade.

2.2.2 Membrane Preparation

Membranes were prepared by paste casting method [7, 8]. First the raw materials were mixed according to the compositions given in Table 2.2. Membrane A was prepared from the clay only without adding any other chemicals. For the preparation of Membrane B, small amount of sodium metasilicate, sodium carbonate and boric acid were used. The amount of the materials play vital role during the preparation of membranes. Different membranes were prepared at various proportion of membrane precursor. In some composition membranes are not formed at all or brittle or melt during sintering. By trial and error methods the composition of membrane precursor were optimized. Final composition of 'Membrane B' was arrived after several trial and errors. The materials were mixed with distilled water and a paste was prepared. The paste was then casted over gypsum surface in the shape of a circular disc of 52 mm diameter and 5 mm thickness by a dice made from perspex sheet. The paste with the dice was placed in room temperature for 24 h for drying partially. Afterwards the paste was removed from the dice carefully and placed in room temperature for another 36 h. Thereafter was placed in hot air oven at 100 °C for 12 h. Eventually the caste disc was heated step by step (50 °C in every 15 min) in programmable muffle furnace (Naskar & Co.; 140QT) to the desired sintering temperature and kept in that temperature for 6 h. Then the temperature of muffle furnace was cooled gradually to room temperature and the prepared membrane was removed. The membrane thus obtained was polished with silicon carbide abrasive paper (C-180) to give a final shape of around 50 mm diameter and 5 mm thickness. Finally, the membrane was washed in distilled water and dried at 100 °C. Membrane A was prepared at three different sintering temperatures viz. 900 °C, 950 °C and 1000 °C. On the other hand Membrane B was prepared at 800 °C, 900 °C and 1000 °C. Membrane A sintered at 800 °C was not further considered for experiments due to its very lower flexural strength.

Table 2.2. Compositions of two different membranes

Materials	Membrane A (Wet basis)	Membrane B (Wet basis)
Clay (%)	70	70
Sodium carbonate (%)	Nil	3
Sodium metasilicate (%)	Nil	1.5
Boric acid (%)	Nil	1.5
Water (%)	30	24

2.2.3 Characterization Techniques

For the analysis of thermal transformations during the whole sintering process, thermogravimetric analysis (TGA) (Mettler-851e) of membrane A and membrane B were conducted from 30 °C to 950 °C at the heating rate of 10 °C/minute under air. XRD (Bruke D8, advanced X-ray diffraction measurement system) of prepared membranes at different sintering temperatures was done to study the phase changes. Before putting in to the XRD instrument, the sample is powdered and dried. After that, the dried sample is placed in between two glass slides in the form a thin film and inserted in to the specific cavity for analysis. Other parameters like porosity, flexural strength (Universal tensile testing machine, Dutt-101) were also determined for all the membranes prepared. SEM pictures (Leo 1430 vp) of all membranes were taken for judgment of the morphology and to estimate the pore size distribution and average pore size. During the sample preparation of the SEM, some steps are used to follow. A small portion of the sample with tiny thickness is first dried and then placed over the mount by means of carbon conducting tape. Then the mount is placed into gold coater. The gold coating was conducted for 60 s at 4 mA volt under 1×10^{-3} Pa pressure. Finally the sample with the mount is fixed on the sample holder. Water permeation experiments were carried out to evaluate the average pore size and permeability. Chemical stability of the membranes was checked by comparing the porosity, pore size, permeability and mechanical strength before and after acid and base treatment.

2.2.4 Water Permeability Experiment

All the prepared membranes were subjected to water permeation experiment. The dimensions of used membranes are 5 mm thick and 50 mm diameter. From this experiment, hydraulic permeability (L_h), average pore diameter (r_l) were determined. All of these experiments were carried out using the experimental set-up shown in Figure 2.4. The schematic of the set up was shown in Figure 2.5. All the permeation experiments were done in deionized water taken from Millipore water synthesis system (Elix-3).

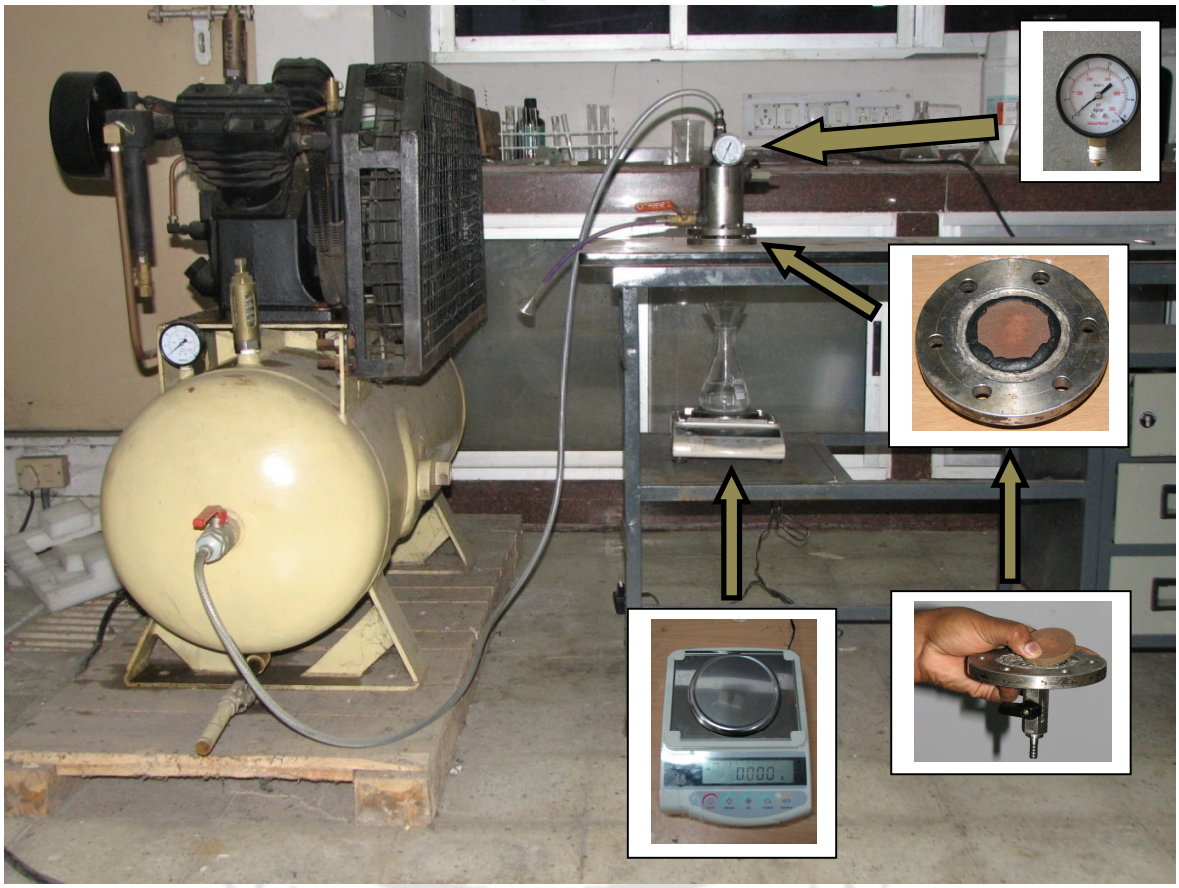

Figure 2.4. Photograph of the experimental set up used for water permeability test and microfiltration experiment

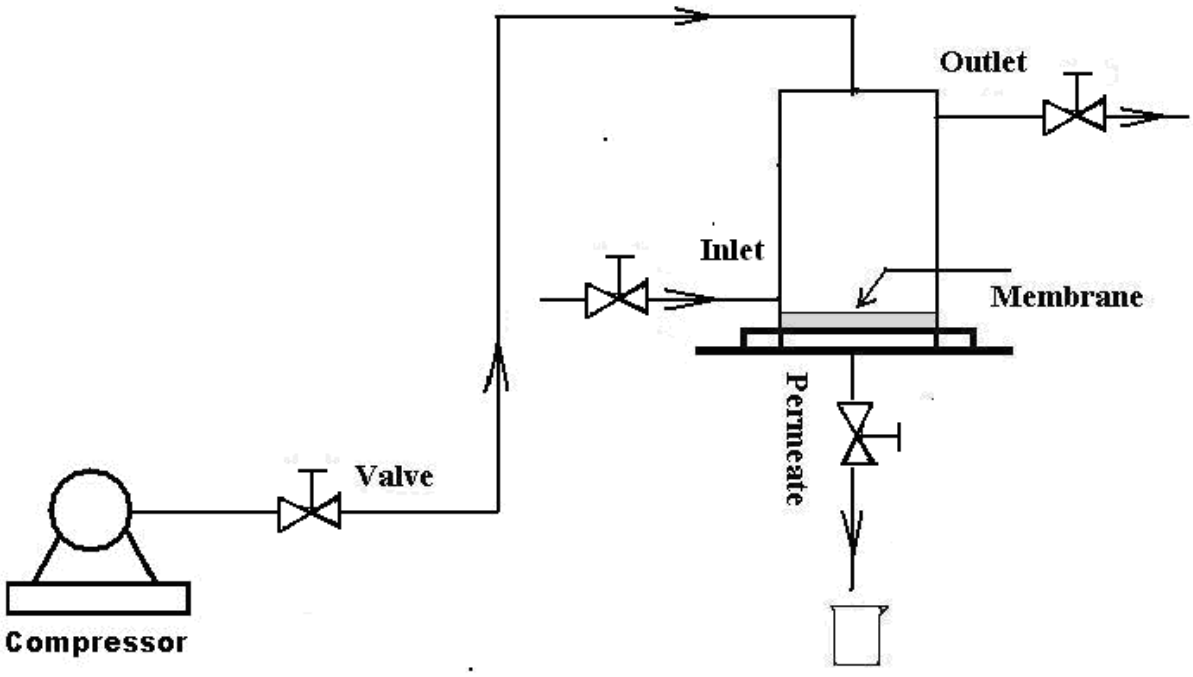

Figure 2.5. Schematic of experimental set up used for water permeability test and microfiltration experiment

The hydraulic permeability and average pore radius can be calculated from the following equations [7, 8].

$$J = \frac{n\pi r^4 \Delta P}{8\mu l} = L_h \Delta P \qquad (2.1)$$

where, J is liquid flux ($m^3m^{-2}sec^{-1}$), ΔP is transmembrane pressure (kPa), μ is viscosity of water, l is pore length (i.e. thickness of membrane, assuming the pores are cylindrical). Taking porosity, $\varepsilon = n\pi r^2$ (n = number of pores per unit area and r = radius of pore), equation (1) can be changed to [7, 8] equation (2)

$$r = \left[\frac{8\mu l L_h}{\varepsilon}\right]^{0.5} \tag{2.2}$$

The porosity was figured out by pycnometric method using water as the wetting liquid [7]. The transmembrane pressure drop for these experiments was in the range of 10 – 325 kPa. Before the experiment, all the membranes' standard compaction test was conducted at a pressure of 380 kPa which was well above the operating pressure. This test involves the measurement of permeate liquid volume as a function of time. The flux was observed to be high initially and reduced to a steady value afterwards. For membrane A sintered at 900 °C, the flux decreased from 5.03×10^{-3} $m^3\,m^{-2}\,s^{-1}$ to 3.6×10^{-3} $m^3\,m^{-2}\,s^{-1}$ in 3 h. Similarly for membrane B (1000 °C), the flux in the beginning was 2.2×10^{-2} $m^3\,m^{-2}\,s^{-1}$ and reached to a steady value of 1.9×10^{-2} $m^3\,m^{-2}\,s^{-1}$ in 2.5 h. These data has been taken by collecting permeate in every 10 sec interval of time. In the next stage of the experiment, the flux through the membrane was observed with respect to different pressures. From the slope of ΔP vs. J (r^2 values are in between 0.98 to 0.99), values of hydraulic permeability (L_h) were obtained by Eq. (1) and reported in Table 3. With this value and respective porosity value of the same membrane, average pore radius was calculated from Eq. (2).

2.2.5 Chromate Removal Using MEMF

To test the suitability of prepared membrane, studies on the removal of chromate ions using micellar flocculation was carried out. Potassium dichromate was chosen as sources of chromate ions. Cetyl pyridinium chloride was used as the surfactant. During the mixing of the surfactant with dichromate, two cetyl pyridinium (CP) ions bind with one chromate oxyanion. Monomer CP ions form $(CP)_x$-oxyanions and flocculation starts. Studies were done up to the surfactant to dichromate feed ratio of 10, and it was seen that over 80% potassium dichromate creates flocculation [23]. So, in this work higher feed ratios were used and the flocks were tried to remove by microfiltration. Flocculations of micelles depend on different ratios of surfactant to dichromate. Different feed ratios starting from 0.1 to 160 were prepared. Experiments were conducted on a fixed concentration of CPC (1000 mg L^{-1}) and varying the potassium dichromate concentration to maintain CPC/$K_2Cr_2O_7$ ratios as 0.25, 0.5, 1.0, 1.5, 2.0, 2.5, 5, 10, 20, 50, 100 and 160. The total observations are reported in Table 4. It can be seen that in the lower ratio (up to 2.0), flocculation occurred. In a slight higher ratio (2.0 to 5), the solution was appearing hazy. Eventually, the micelles started to settle down (ratios from 6 to 50) and thereupon

(ratios from 75 to 160) there were no settling even after 12 h. This may be due to the fact that with the increase of the feed ratios, micelle formation increased and after a particular ratio decreased. Similar results were reported by Purkait et al., 2008. All these experiments are carried out in a constant room temperature (~25 °C) using deionized water of Millipore water purification system (Elix-3) as it is known that these phenomena are temperature sensitive.

During microfiltration experiments, 200 mL of all the mentioned solutions were prepared and passed through the fabricated membrane B (sintered at 1000 °C). Membrane A was not used due to its lower flexural strength. The permeate from the bottom of the cell was collected in a small beaker (10 mL capacity), with this, its cumulative weight was continuously measured by an electronic balance. Then the cumulative weights were converted to cumulative volumes and from the slope of the cumulative volume versus time curve, the permeate flux was obtained as a function of operating time [18]. The flux decline with respect to time was observed for a particular ratio (1.0) at three different pressure viz. 69, 104 and 134 kPa. Another flux change profile was determined for different ratios used at a particular pressure (104 kPa) and particular time (300 sec.). The final concentrations (C_f) of CPC and potassium dichromate after the membrane operation were measured and compared with the initial concentration (C_i). The rejection % (R) is calculated based on the formula,

$$R = (1 - \frac{C_f}{C_i}) \times 100 \tag{2.3}$$

Rejection was calculated with respect to time for a particular ratio at three different pressures (same as maintained above) and with respect to different ratios tested. Standard technique [27] was applied to determine the concentration of CPC and potassium dichromate using UV-vis spectrophotometer (Varian-Cary 50 Bio).

The images of the freshly prepared micelle, micelle kept overnight and the filtrate are presented in Figure 2.6

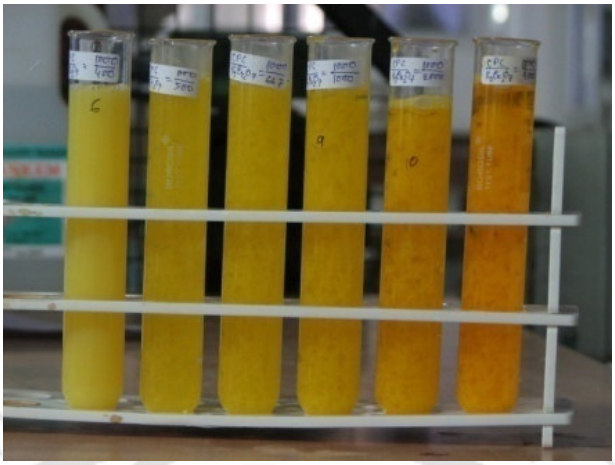

Figure 2.6 (a) Freshly prepared micelle.

Figure 2.6 (b) Micelle kept overnight.

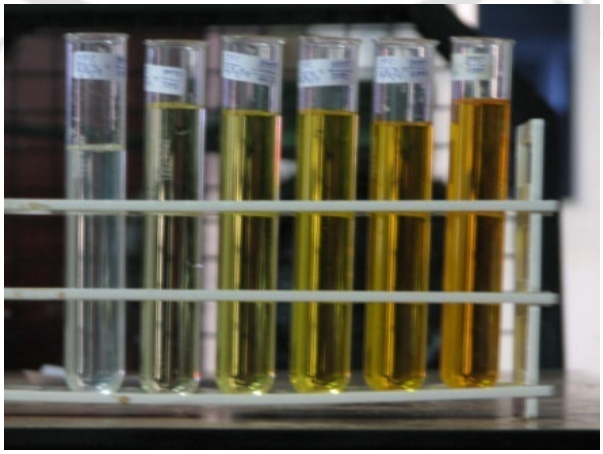

Figure 2.6 (c) After filtration.

2.3. Results and Discussion

The images of prepared membranes are shown in Figure 2.7.

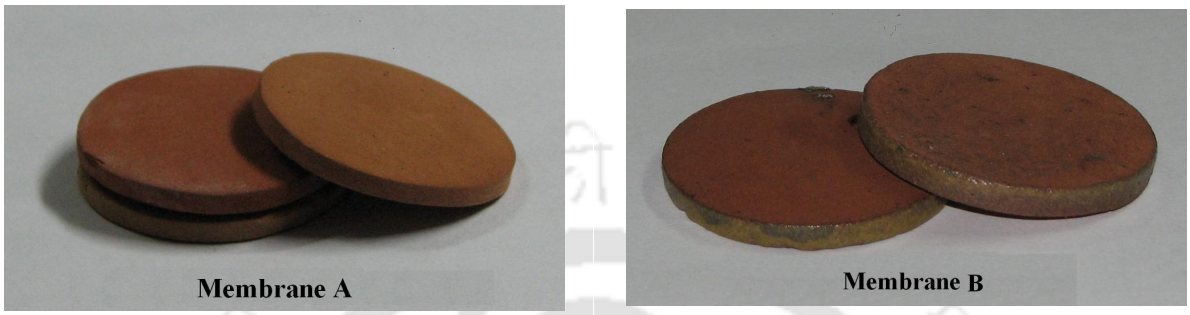

Figure 2.7. Images of Membrane A and Membrane B

2.3.1 Structural Characterization of Membrane

Thermogravimetric analysis: The objective of TGA experiment is to determine the various temperature zones where prominent weight loss occurred. The experiment was carried out in alpha-alumina crucible from 30 °C to 950 °C. Figure 2.8 represents the TGA results obtained from the instrument for Membrane A and Membrane B.

From Figure 2.8, it was observed that during the first phase of heating the weight loss of membrane B was more than the membrane A. Up to 90 °C weight loss of membrane A was 0.23% and membrane B was 3.07% and up to 150 °C the membrane A weight loss was 0.38% where as membrane B has shown a weight loss of 4.2%. These weight losses can be attributed to the loss of loosely bound water molecule [7]. More weight loss of membrane B during this phase was due to the presence of some hygroscopic materials (like sodium metasilicate, boric acid). At higher temperature up to 950 °C membrane A and membrane B has shown overall 4.07% and 9.68% weight loss, respectively. From the comparison of the two TGA graphs, it was observed that higher weight loss of membrane B has occurred between 300 °C to 500 °C. This phenomenon may be attributed to the fact that the boiling point of boric acid was 300 °C which was a component of membrane B. After 675 °C, for both the compositions, weight change was marginal. This result concluded that the minimum sintering temperature for both the membrane should be above 675 °C.

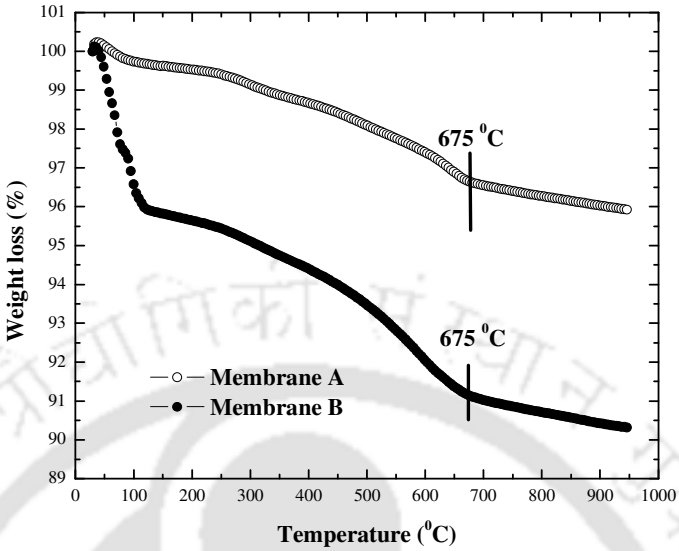

Figure 2.8. Thermogravimetric analysis of Membrane A and Membrane B.

X-ray diffraction analysis: Figure 2.9 represents the X-ray diffraction analysis of compositions before sintering and after sintering at different temperatures. From XRD analysis of both compositions before sintering reflections of illite, kaolinite and quartz were observed. In the sintered samples, no reflection of kaolinite was found. This can be explained by the fact that over 513 °C, kaolinite changes to metakaolinite. For the sample of membrane A (sintered at 900 °C) and membrane B (sintered at 800 °C), still reflections of illite was found where at higher temperatures, these reflections were not seen. Another observation was that, in the higher temperature, mullite reflections were appearing. For both the membranes, higher temperature sintered samples were characterized by more number of mullite reflections. This proves the formation of mullite with the increasing sintering temperatures. In membrane B another characteristic reflection of nephiline (Na_2O, Al_2O_3, $2SiO_2$) was detected. On the other hand, quartz reflections were not changed distinguishably. With these, it can be concluded that the skeletal structure of membrane A consists of mullite and quartz where as membrane B composed of mullite, quartz and nephiline.

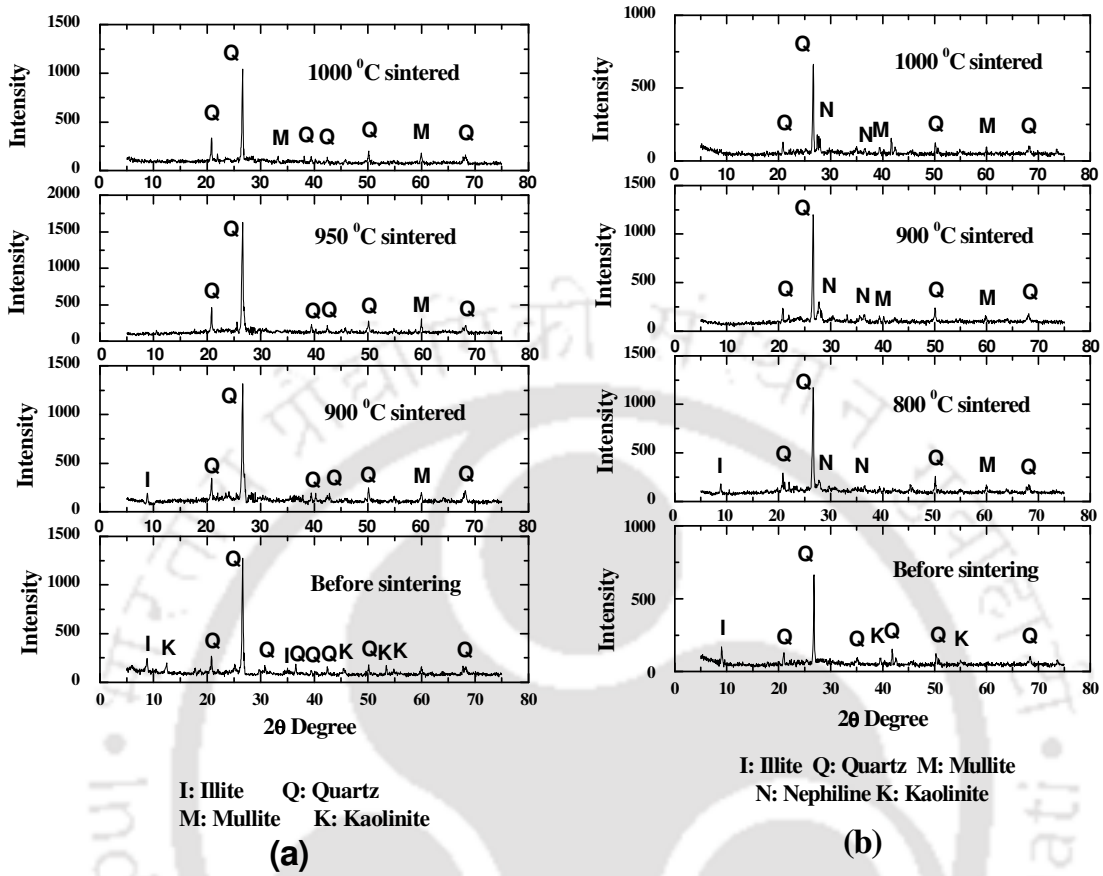

Figure 2.9. XRD analysis of prepared membrane at different temperature. (a) Membrane A; (b) Membrane B.

Surface morphology from SEM: In Figure 2.10, SEM images of different membrane prepared at different sintering temperatures are shown. These pictures gave elaborated information about the texture of the membrane surfaces. As a general observation, with the increasing temperature, the structure of the membrane becomes dense. This result can be due to the fact that the porosity was decreasing with sintering temperature, which is discussed in subsequent section. Another objective of SEM was to detect the small cracks on the membrane surface (if any). No such cracks were observed.

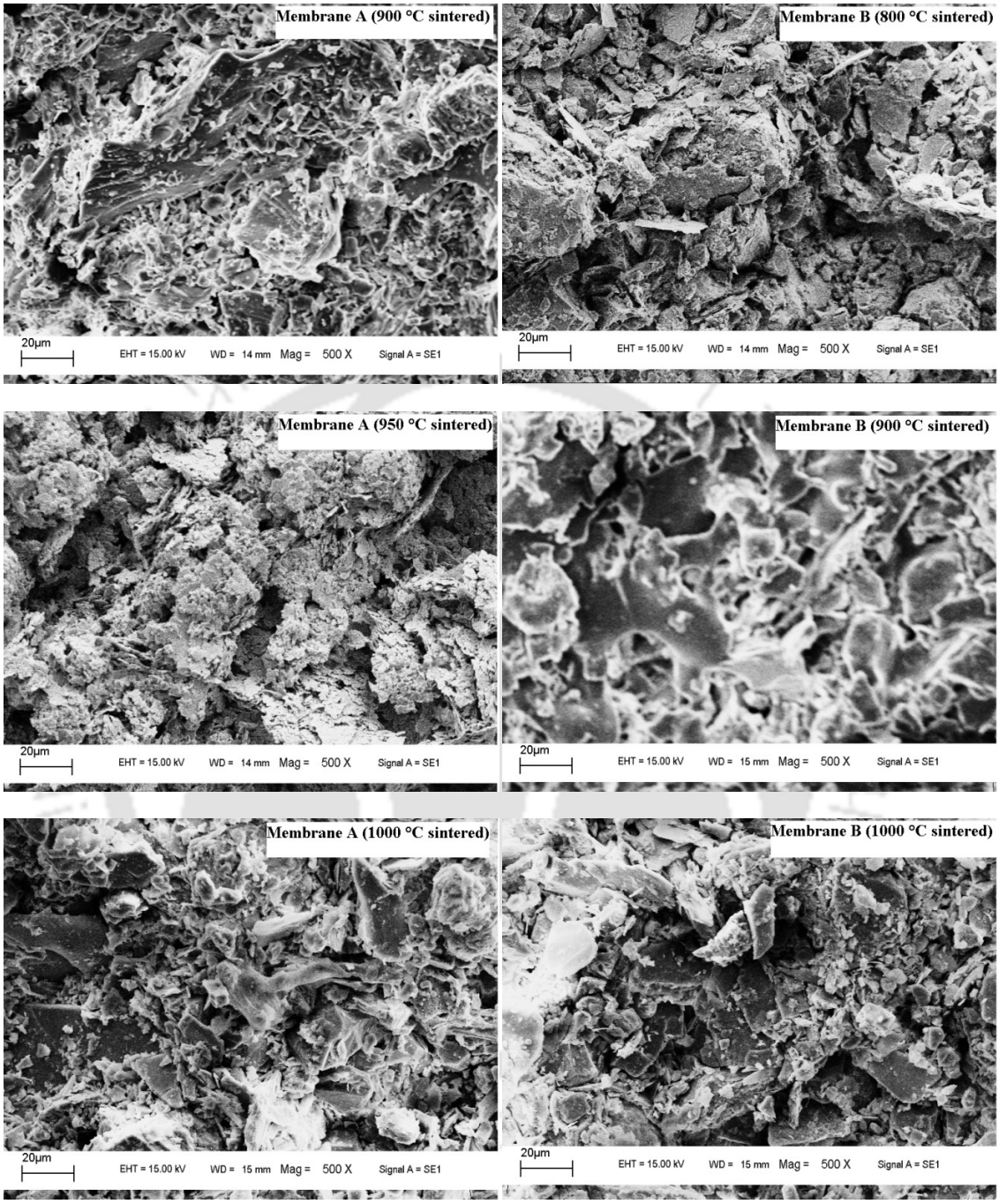

Figure 2.10. SEM pictures of membrane A and membrane B, prepared at different sintering temperatures.

Pore size distribution and area average pore diameter from SEM: Pore diameters have been measured from different SEM images by ImageJ software. These images were taken from different positions of surfaces of the membrane at different magnifications. For every membrane, around 600 pores were considered. After opening the specific image in the software (File--> Open), first the scale of the original SEM image is related with the distance in pixel (Analyze--> Set scale). Afterwards, the pore diameters were measured by the tool ''Straight line selection''. The distances in pixels were converted to the known distance (micron) by the software itself. And finally, the measured data were transferred to MS-excel for further calculations. Average pore diameters (d_s) were calculated by the following Eq. (4)

$$d_s = \left[\frac{\sum_{i=1}^{n} n_i d_i^{\,2}}{\sum_{i=1}^{n} n_i} \right]^{0.5} \qquad (2.4)$$

where, n is the number of pores, d_i is pore diameter (μm) of i-th pore. The pore size distributions are shown in Figure 2.11 and the area average pore diameters are reported in Table 2.3. It was found that the average pore size of membrane A was lower than the average pore size of membrane B. At 900 °C sintering temperature, average pore diameter of membrane A and membrane B were found to be 2.16 and 4.73 μm respectively. It can be seen that the average pore size was increasing with the increasing sintering temperatures for both the compositions. For membrane A, average pore diameter was changed from 2.16 to 3.91 μm with increasing of sintering temperature from 900 °C to 1000 °C. Similarly, for membrane B, the pore diameter was increased from 4.08 μm to 4.92 μm during sintering from 800 °C to 1000 °C. The reason behind the increase of pore diameter was the overlapping of small pores during creation of large pores at the time of higher sintering temperature. Similar results has been reported by other researchers for microfiltration membrane prepared from kaolin and clay [7, 11].

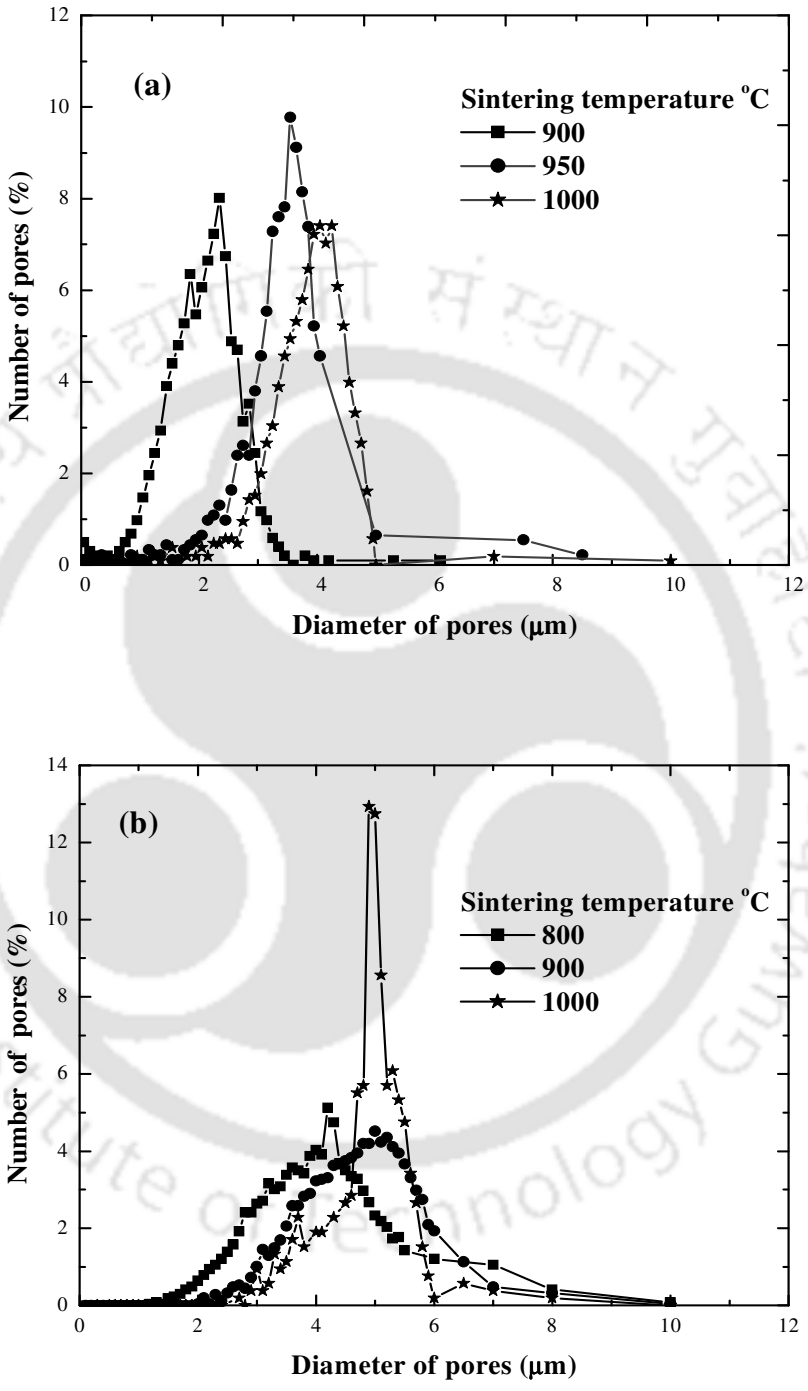

Figure 2.11. Pore size distribution of prepared membrane at different sintering temperature. (a) Membrane A and (b) Membrane B.

Table 2.3. Various parameters for membrane A and membrane B prepared at different sintering temperatures

Membrane	Sintering temperature	Average pore diameter		Porosity	Pore density (m^{-2})	Water permeability ($m^3m^{-2}kPa^{-1}s^{-1}$)	Flexural strength (MPa)
		From SEM images (μm)	From water permeability (μm)				
Membrane A	900 °C	2.16	1.84	0.45	1.33×10^{11}	9.522×10^{-6}	2.54
	950 °C	3.42	2.93	0.43	5.00×10^{10}	2.307×10^{-5}	3.35
	1000 °C	3.91	3.48	0.42	3.50×10^{10}	3.179×10^{-5}	3.79
Membrane B	800 °C	4.08	3.74	0.50	3.60×10^{10}	4.371×10^{-5}	1.54
	900 ° C	4.73	4.41	0.40	3.50×10^{10}	4.862×10^{-5}	9.1
	1000 °C	4.92	4.58	0.38	2.06×10^{10}	4.982×10^{-5}	11.55

Surface pore density: Surface pore density represents the average number of pores present per unit area of the membrane surface. It was calculated from the SEM images. The results are shown in Table 2.3. It was observed that the surface pore density was decreasing with the increase in sintering temperature. For membrane A, pore density was decreased from $13.3\times10^{10}m^{-2}$ to $3.50\times10^{10}m^{-2}$ during changing of the sintering temperature from 900 °C to 1000 °C. And for membrane B, the values have been decreased from 4.28×10^{10} to 2.09×10^{10} during sintering from 800 °C to 1000 °C. This change was due to the overlapping of small pores during creation of large pores at the time of higher temperature sintering.

2.3.2 Water Permeation Experiment

Porosity: Porosity was calculated by pcynometric method using water as the wetting liquid. All the values of porosity of membrane A and membrane B sintered at different temperatures are reported in Table 2.3. It was observed that porosity decreased with the increasing of the sintering temperature. This was mainly due to squeezing of the membrane body at the time of sintering and overlapping of small pores during creation of large pores. For membrane A, porosity decreased from 0.45 to 0.42 for

increasing of sintering temperature from 900 °C to 1000 °C. Similarly for membrane B, porosity changed from 0.50 to 0.38 with increase sintering temperatures from 800 °C and 1000 °C.

Average pore diameter: All the values of porosity and pore diameter are reported in Table 2.3. It can be concluded that porosity increased and pore size decreased with the increase in sintering temperature. This was due to the shrinkage of small pores during the creation of large pores during high temperature sintering. Other researchers also reported the similar findings for microfiltration membrane prepared from kaolin and clay [7, 11]. Another observation was that the pore sizes obtained from SEM images were larger than the same obtained from water permeability experiments. This was due to the presence of dead-end-pores which were incorporated in SEM image analysis but not integrated at the time of water permeability experiments.

2.3.3 Mechanical Strength

The flexural strength was calculated by three point bending strength method. The standard ASTM method is followed i.e., the sample is prepared in the size of 250 mm × 20 mm × 4 mm and the measurement was done. The results are reported in Table 2.3. It was observed that the flexural strength increased with increasing sintering temperature. The densification of the ceramic material during sintering was the reason behind it [7]. In addition to this, the strength of membrane B was far better than the membrane A. For membrane A, flexural strength increased from 2.54 MPa (900 °C sintered) to 3.79 MPa (1000 °C sintered) and for membrane B, the values were 1.54 MPa (800 °C sintered) and 11.55 MPa (1000 °C sintered) respectively. This was due to the formation of nephiline during sintering of membrane B, which was supported by the XRD analysis. Literature also revealed that nephiline gave higher mechanical strength to ceramic structures [28].

2.3.4 Chemical Stability

The chemical stability of all the membranes prepared was found by subjecting them to acid and base treatment. The membranes were immersed in the solution of NaOH (pH = 13.5) and HCl (pH = 1.0) separately for 72 h. Then the membranes were cleaned with distilled water and dried. The porosity, average pore size (by water permeability test), water permeability and flexural strength were measured for all the acid and base treated membranes separately. The results are shown in detail in Table 2.4. The

initial values of porosity, average pore diameter and water permeability of membrane A sintered at 1000 °C were 0.42, 3.48 μm and 3.179×10^{-5} $m^3m^{-2}kPa^{-1}sec^{-1}$ and after base and acid treatment those became 0.44, 3.56 μm and 3.485×10^{-5} $m^3m^{-2}kPa^{-1}sec^{-1}$ and 0.46, 3.60 μm and 3.730×10^{-5} $m^3/m^2/bar/h$. respectively. Similarly for membrane B sintered at 1000 °C the values were 0.38, 4.58 μm and 4.982×10^{-5} $m^3m^{-2}kPa^{-1}sec^{-1}$ and after base and acid treatment those became 0.43, 4.71 μm and 5.962×10^{-5} $m^3m^{-2}kPa^{-1}sec^{-1}$ and 0.42, 4.68 μm and 5.749×10^{-5} $m^3m^{-2}kPa^{-1}sec^{-1}$ respectively. It was observed that, membranes were chemically resistant as the changes of parameters were nominal. Further it was observed that membrane B was more chemically stable than membrane A and chemical stability increased with increase in sintering temperature. This could be due to the formation of mullite at higher sintering temperature and nephiline during the sintering of membrane B. The reason for increasing the porosity was due to the fact that, during the chemical treatment, some materials of membrane were corroded and void space was being generating. Similarly average pore size and permeability are also increased. Some simple mathematical correlation can be given such as; percentage change of water permeability and porosity is directly proportional to the square of percentage changes of pore size. Because, both increased due to the increase in the pore area, assuming the pores are cylindrical and the thickness of the membrane is not changing during chemical treatment.

Table 2.4. Variation of different membrane parameters after chemical treatment

Membrane	Sintering temperature	Porosity	Average pore size (μm)	Water permeability ($m^3m^{-2}kPa^{-1}s^{-1}$)	Flexural strength (MPa)
Membrane A (after base treatment)	900 °C	0.57	1.91	1.300×10^{-5}	1.08
	950 °C	0.51	3.03	2.926×10^{-5}	1.68
	1000 °C	0.44	3.56	3.485×10^{-5}	2.04
Membrane A (after acid treatment)	900 °C	0.60	1.92	1.382×10^{-5}	0.44
	950 °C	0.53	3.05	3.081×10^{-5}	0.92
	1000 °C	0.44	3.56	3.485×10^{-5}	1.64
Membrane B (after base treatment)	800 °C	0.55	3.86	5.122×10^{-5}	1.21
	900 °C	0.45	4.57	5.874×10^{-5}	7.17
	1000 °C	0.43	4.71	5.962×10^{-5}	8.22
Membrane B (after acid treatment)	800 °C	0.53	3.84	4.884×10^{-5}	1.05
	900 °C	0.43	4.54	5.539×10^{-5}	6.20
	1000 °C	0.42	4.68	5.749×10^{-5}	6.55

2.3.5. Chromate Ions Removal Studies

The flux through the membrane was noted throughout the process. The experiment was done in two ways. Initially, experiments were performed at a particular ratio (1.0) at three different pressures viz. 69, 104 and 138 kPa. and the flux decline profile throughout the process is represented in Figure 2.12 (a).

It was seen that the flux decreased with time. In the first stage of the experiment the decline was very fast and then (after 300 sec) a steady decline of flux was observed. The first phase flux declining was due to the concentration polarization and the second stage steady state decrease was due to fouling. Another general and obvious ascertainment was that the flux was higher for the higher pressure.

Later on, the changes of flux with the change of ratios, after achieving the steady state profile are compared in Figure 2.12 (b). Flux decreased with the increase in ratio of surfactant to dichromate up to 10 and thereafter with increase in the ratios, the flux increased. The reason can be explained from the visual observations reported in Table 2.5. Up to the feed ratio of CPC and $K_2Cr_2O_7$ of 10, the micelle formation increases. The flux is reduced due to the deposition of the micelle over the membrane surface. Even, with the increase of the ratios, the micelle formation decrease which causes the increase of the flux.

For both CPC and dichromate the % rejection was almost constant (with ±10% variation) with respect to time and also independent with respect to pressure. The chromate ions are not directly rejected by the membrane. The ions react with CPC and forms micelle, which was rejected by the membrane. This is the reason for not variation in the rejection with respect to time and pressure. Chromate ion rejection results are reported in Figure 2.13 (a).

The results of chromate ion rejection with respect to different ratios are shown in Figure 2.13 (b). It was observed that rejection increased massively with the increase in the feed ratios. For CPC it decreased with respect to the ratios (up to the feed ratio of 1.0, the rejection 100%, at ratio = 5 it is 65% and at the ratio of 20, it decreased to almost 15.5%). This may be due to the fact that only the micelles were removed by the membrane. In the lower ratio, all CPC molecules were forming micelles whereas many excess dichromate molecules were not removed. On the other hand at the higher feed ratios, all dichromate molecules were forming micelles and removed but excess CPC molecules were not removed. So at higher ratios (10 onwards), complete removal of chromate ions can be achieved by MEMF.

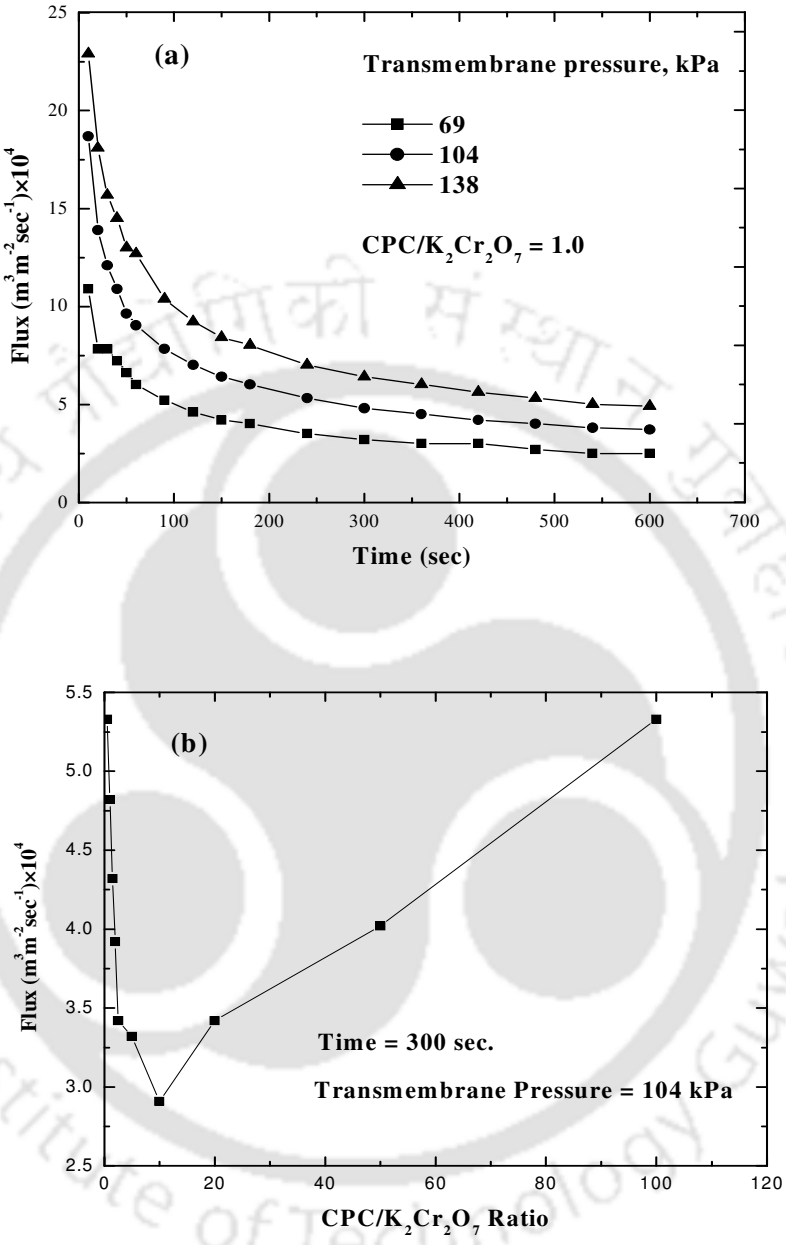

Figure 2.12. Variation of permeate flux during microfiltration of $K_2Cr_2O_7$ and CPC mixture.

(a) At constant CPC/ $K_2Cr_2O_7$ ratio of 1.0 and transmembrane pressure of 69, 104 and 138 kPa during the whole experiment

(b) For all CPC/ $K_2Cr_2O_7$ ratios at time = 300 sec and pressure 104 kPa

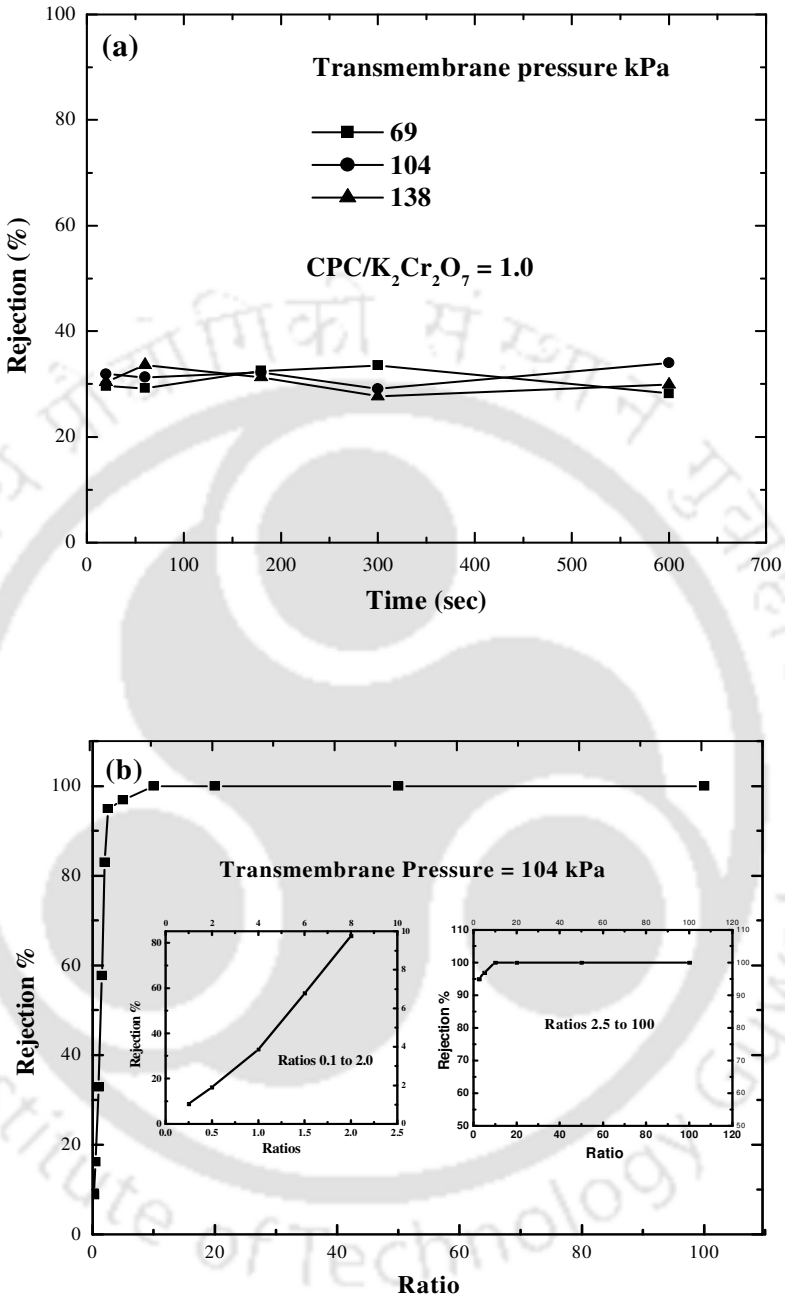

Figure 2.13. Variation percentage of Cr (VI) rejection with respect to the (a) different transmembrane pressure of 69, 104 and 138 kPa at the fixed ratio of 1.0. (b) different ratios at a fixed transmembrane pressure of 104 kPa.

Table 2.5. Visual observation of the mixture of cetylpyridinium chloride (CPC) and potassium dichromate at different CPC/$K_2Cr_2O_7$ ratios

Sl. no.	CPC concentration (mg L^{-1})	$K_2Cr_2O_7$ concentration (mg L^{-1})	Ratio: CPC/ $K_2Cr_2O_7$	Precipitation
01	500	5000	0.1	Floatation of micelle after 12 hr.
02	500	2000	0.25	Floatation of micelle after 12 hr.
03	500	1000	0.5	Floatation of micelle after 12 hr.
04	500	500	1	Floatation of micelle after 12 hr.
05	500	250	2	Flotation within 5 min (floating micelle)
06	500	175	2.85	Hazy
07	1000	200	5	Hazy
08	1000	165	6.06	Sedimentation of some portion after 12 hr still hazy
09	1500	150	10	Sedimentation after 12 hr
10	2000	100	20	Sedimentation after 12 hr
11	3000	100	30	Sedimentation after 12 hr
12	4000	100	40	Sedimentation after 12 hr
13	5000	100	50	Sedimentation after 12 hr
14	6000	80	75	No sedimentation appeared
15	7000	70	100	No sedimentation appeared
16	8000	50	160	No sedimentation appeared

2.4. Membrane Cost

Industrially competitiveness depends on the manufacturing cost of the membrane. In general costs of ceramic membranes are ten times greater than the cost of polymeric membrane. Conventional industrial scale polymeric membranes are available at the cost of \$50-200/m^2 [29] and ceramic membranes are at \$500-2000/m^2 [30]. Assuming the thickness of the prepared membrane (5 mm), the cost of the membrane per square meter was calculated on the basis of prices of the chemicals from corresponding company listed in the section 2.1.2. Details of the cost analysis are shown in Table 6. As per this analysis, the material cost was around \$ 19/m^2. Taking the cost of manufacturing and shipment the cost may reach up to \$ 100/m^2, which is competitive to the cost of the polymeric membranes. Additionally, depending on the fouling characteristics and long term stability, ceramic membranes produced from clay can be taken as cheaper than polymeric membranes. Depending on the fouling characteristics, on time performance and long term stability of the ceramic membrane in process applications, the reported value of the membrane cost may vary significantly. However, corrosion resistance and mechanical strength data presented in this work instill confidence in the long term performance and hence the projected membrane cost is anticipated to be close to the reported value.

Table 2.6. Cost analysis of prepared membrane from the unit cost of raw materials

	%	Unit price(\$/kg)	*Material required/m^2 (g)	Cost/m^2 (\$)
clay	92	0	37.48	0
Sodium carbonate	4	4.6	1.63	7.50
Sodium metasilicate	2	5.6	0.81	4.56
Boric acid	2	8.4	0.81	6.84
Total	100	-	40.74	18.91

* 5 cm diameter and 5 mm thick membrane has been prepared from total 80 gm materials.

2.5. Conclusion

Microfiltration membranes were prepared from locally available clay collected from IIT Guwahati campus. Membrane A was prepared from clay only and Membrane B was prepared from clay with small amount of sodium carbonate, sodium metasilicate and boric acid. The prepared membranes have average pore sizes of around 3.75 μm to 4.5 μm. After using a minute amount of other chemicals, membranes have shown much higher mechanical strength (11.55 MPa) at lower sintering temperature (1000 °C). The XRD results proved that nephiline formed during sintering of Membrane B which was mainly responsible for the higher mechanical strength. All the membranes are characterized by SEM, XRD, water permeability and chemical stability test. Due to the overall best performance of Membrane B sintered at 1000 °C, it was tested for removal of chromate ions by micellar flocculation using cetyl pyridinium chloride as the surfactant. It was also contemplated that at higher ratio (10 onwards) of CPC to potassium dichromate, 100% dichromate was removed. It was also seen that there was not much fluctuation in the permeate concentrations during the whole experiment. This study indicated that with addition of small amount of chemicals with local clay, a high flux microfiltration membrane was prepared and successfully applied for the removal of chromate ions from aqueous solution by micellar flocculation. The approximate cost of the prepared membrane was less than the module cost of polymeric membranes. The results so obtained in this study are encouraging and can be used to develop low cost ceramic microfiltration membrane from clay for industrial applications.

References

1. Y.H. Wang, T.F. Tian, X.Q. Liu, G.Y. Meng, Titania membrane preparation with chemical stability for very harsh environments applications. J. Membr. Sci. (2006.) 280, 261–269.

2. S. Lee, J. Cho, Comparison of ceramic and polymeric membranes for natural organic matter (NOM) removal, Desalination (2004) 160, 223-232.

3. K.A. DeFriend, M.R. Wiesner, A.R. Barron, Alumina and aluminate ultra-filtration membranes derived from alumina nanoparticles. J. Membr. Sci. (2003) 224, 11–28.

4. Y. Yoshino, T. Suzuki, B.N. Nair, H. Taguchi, N. Itoh, Development of tubular substrates, silica based membranes and membrane modules for hydrogen separation at high temperature. J. Membr. Sci. (2005) 267, 8–17.

5. S. Masmoudi, A. Larbot, H.E. Feki, R.B. Amara, Elaboration and characterisation of apatite based mineral supports for microfiltration and ultrafiltration membranes. Ceram. Int. (2007) 33, 337–344.

6. Y. Dong, X. Liu, Q. Ma, G. Meng, Preparation of cordierite-based porous ceramic microfiltration membranes using waste fly ash as the main raw materials. J. Membr. Sci. (2006) 285 173-181.

7. B.K. Nandi, R. Uppaluri, M.K. Purkait, Preparation and characterization of low cost ceramic membranes for micro-filtration applications, Applied Clay Sci. (2008) 42, 102-110.

8. M.C. Almandoz, J. Marchese, P. Prádanos, L. Palacio, A. Hernández, Preparation and characterization of non-supported micro-filtration membranes from aluminosilicates. J. Membr. Sci. (2004) 241, 95–103.

9. T. Mishra, K. Parida, Transition-metal oxide pillared clays. Part 2. A comparative study of textural and acidic properties of manganese(III) pillared montmorillonite and pillared acid-activited montmorillonite, J. Mater. Chem, (1997) 7, 147–152.

10. R. Cool, A. Clearfiled, V. Mariagnanam, L.J.M. Ellistrem, R.M. Crooks, E.F. Vansant, Self-assembly of aluminium-pillared clay on a gold support, J. Mater. Chem, (1997) 7, 443–448.

11. N. Saffaj, M. Persin, S.A. Younsi, A. Albizane, M. Cretin, A. Larbot Elaboration and characterization of microfiltration and ultrafiltration membranes deposited on raw support prepared from natural Moroccan clay: Application to filtration of solution containing dyes and salts App. Clay Sci. (2006) 31, 110– 119.

12. S. Khemakhem, A. Larbot, R.B. Amar, New ceramic microfiltration membranes from Tunisian natural materials: Application for the cuttlefish effluents treatment. Ceramics Intern. (2009) 35, 55-61.

13. K.K. Cham, A.M. Brownstein, Ceramic membranes growth prospects and opportunities, Am. Ceram. Soc. Bull, (1991) 70, 703–707.

14. J.G. Dean, F.L. Bosqui, K.H. Lanouette, Removing heavy metals from waste water. Environ. Sci. Technol. (1972) 6, 518-522.

15. T.K. Rout, D.K. Sengupta, G. Kaur, S. Kumar, Enhanced removal of dissolved metal ions in radioactive effluents by flocculation. Int. J. Miner. Process. (2006) 80, 215-222.

16. K. Mohanty, M. Jha, B.C. Meikap, M.N. Biswas, Removal of chromium (VI) from dilute aqueous solutions by activated carbon developed from Terminalia arjuna nuts activated with zinc chloride. Chem. Eng. Sci. (2005) 60, 3049–3059.

17. J.A.S. Ten´orio, D.C.R. Espinosa, Treatment of chromium plating process effluents with ion exchange resins. Waste Manage. (2001) 21, 637-642.

18. M.K. Purkait, S. Dasgupta, S. De, Resistance in series model for micellar enhanced ultrafiltration of eosin dye. J. Colloid Interface Sci. (2004) 270, 496–506.

19. C. Das, P. Maity, S. Dasgupta, S. De, Separation of cation–anion mixture using micellar-enhanced ultrafiltration in a mixed micellar system. Chem. Engg. J. (2008) 144, 35–41.

20. F.I. Talens-Alesson, A. Anthony, M. Bryce. Removal of phenol by adsorptive micellar flocculation: Multi-stage separation and integration of wastes for pollution minimization. Colloids and Surfaces. A: Physicochem. Eng. Aspects, (2006) 276, 8–14.

21. P. Paton-Morales, F.I. Talens-Alesson, Effect of Competitive Adsorption of Zn^{2+} on the Flocculation of Lauryl Sulfate Micelles by Al^{3+}. Langmuir, (2002) 18, 8295–8301.

22. F.I. Talens-Alesson, Behavior of anionic surfactant micelles in the presence of Al^{3+} and Ca^{2+}. J. Disp. Sci. Technol. (1999) 20, 1861–1872.

23. M.K. Purkait, S. Dasgupta, S. De, Precipitation of cetyl (hexadecyl) pyridineum chloride using mono and divalent oxyanions. J. of Hazardous Mat. (2008) 160, 502- 507.

24. W. Chesworth, Enclycopedia of soil science, 2008 Springer, 103-104.

25. Soil and Plant Analysis Council Inc, 1999, Soil analysis: handbook of reference methods., 178-179.

26. J.S. Reed, Principles of Ceramics Processing. John Wiley & Sons,NewYork (1995)

27. A.I. Vogel, Textbook of Practical Organic Chemistry, The English Language Book Society and Longmans, London (1970) 385, 818.

28. V.M. Sglavo, S. Maurina, A. Conci, A. Salviati G. Carturan, G. Cocco, Bauxite `red mud' in the ceramic industry. Part 2: production of clay-based ceramics. J. of the Europ. Ceram. Soc. (2000) 20, 245-252.

29. B.D. Bhide, S.A. Stern, A new evaluation of membrane processes enrichment of air. II. Effects of economic membrane properties. J. Membr. Sci. (1991) 62, 37–58.

30. W.J. Koros, R. Mahajan, Pushing the limits on possibilities for large scale gas separation: which strategies? J. Membr. Sci. (2000) 175, 181–196.

Chapter III

Preparation of submicron range membrane from kaolin and local clay: Effect of precursor particle size on membrane morphology and application for the removal of crystal violet dye by advanced oxidation process (AOP) followed by microfiltration

3.1 Introduction and Literature Survey

In the past two decades membrane technology has significantly progressed. Many applications were proposed where microfiltration and ultrafiltration were applied like, biotechnology [1], wastewater treatment [2], fruit juice clarification [3], wine filtration [4], fermentation broth clarification [5]. These technologies are regarded as economically competitive due to the availability of membranes with higher flux and lower process cost. Recently ceramic membranes are drawing a lot of attraction due to its advantages like resistant to corrosive feed, high temperature and high pressure applications and long life. On the other hand ceramic membranes are at least ten times costlier than polymeric membranes. Different types of morphology, stability and porous texture of inorganic membranes were created with different combination of precursors with a final aim of good separation characteristics. Precursors were aggregated by paste method or uniaxial pressing to the desired shape of the membrane followed by sintering [6, 7]. Different raw materials as precursors have different functional attributes for the membrane structure. Kaolin provides low plasticity and high refractory properties to the membrane. Quartz provides thermal and mechanical stability. Calcium carbonate during sintering evolves CO_2 thus creating porous texture in the ceramics. Sodium metasilicate increases mechanical strength by creating silicate bonds. Sodium carbonate improves dispersion properties, thereby creating homogeneity. Boric acid also increases mechanical strength by creating metaborates during sintering [8].

During the early research on ceramic membrane preparation, expensive alumina powder was used as the main precursor. DeFriend et. al. [9] reported pore size of 15-25 nm from the α-alumina powder with average particle size of 15-40 nm. Afterwards Felamaki et. al. [10] obtained pore size of

around 0.5 μm from 160 μm average particle sized γ-alumina powder. However, cost of such precursors, remains a cause of concern. Search for cheaper raw materials ended with the use of titania powder (pore size 0.1-0.2 μm; precursor size: 0.37 μm), apatite powder (pore size 5-7 μm; grain size: 50-350 μm), natural clay (pore size 9-10 μm; grain size : 9 μm) etc for the preparation of ceramic membrane [11-13]. Nandi et. al. [14] prepared ceramic membrane using kaolin as the main raw material. The pore sizes reported were 0.75 – 1.5 μm for the average particle size of 5 μm. Das et. al. [15] had shown that the particle size and its distribution of membrane preparing materials have important effect on the pore size, pore size distribution and porosity of the membrane. Apart from these, the effect of sintering temperature on the pore diameter was also studied [16]. In general the pore size increases with the increase of the sintering temperature. This happens partially due to the overlapping of the small sized pores by large sized pores during sintering. Saffaj et. al. [16] reported the increase of the pore size from 9.4 μm to 10.8 μm during the increase of the sintering temperature from 1100 °C to 1250 °C for membranes prepared from natural clay. According to Masmoudi et. al. [17] pore size were increased from 5 μm to 7 μm during the increase of the temperature from 1150 °C to 1200 °C for the membranes prepared from apatite powder.

Critical review of the above works reveals that the most important controlling parameter for pore size variation is the particle size of the membrane precursor, though sintering temperature also plays an important role. Most of the literatures focused on the variation of pore diameter with sintering temperatures. Very few literatures discussed the role of membrane precursor diameter on the membrane pore size [15]. Moreover the relationship of the surface weighted mean diameter [$D_{3,2}$], volume weighted mean diameter [$D_{4,3}$] of the particle size distribution (PSD) with pore size and the variation of the pore density with PSD were not studied yet.

The wastewater from textile, dyeing, printing and other related industries has long been a major environmental problem for all over the world. It is estimated that over 100,000 kind of synthetic dyes are available in the world and almost 7×10^5 tons of dye stuff are produced annually [18]. Such colored wastewater streams could pose serious detrimental effects to the environment and thus to human health also. Hence, these effluents must be treated or decolorized prior to discharge. Among various dyes, crystal violet is a well-known dye being used for various purposes such as, biological stain, dermatological agent, veterinary medicine, an additive in poultry feed to inhibit propagation of mold, intestinal parasites and fungus etc. Apart from these, this dye is also extensively used in textile dying

and paper printing. The most serious factor is that the dye is a mitotic poison and it can induce a genetic mutation [19].

There are several methods available for dye removal such as coagulation/flocculation [20], adsorption [21], chemical oxidation and photo catalytic processes [22, 23], ozone treatment [24], biological treatment [25], and membrane processes [26, 27]. Ionic dye like crystal violet was removed using commercially available cation exchange membrane [28]. Another potential process for the treatment of wastewater containing dye is advanced oxidation process (AOP) with Fenton's reagent [29, 30]. Arslan-Alaton et. al. [30] removed Acid Red 183, Acid Orange 51 and Reactive Blue 4 by aerobic, anoxic and anaerobic processes with the help of Fenton's reagent. Fenton's reagent is a homogeneous catalytic oxidation solution. The solution is prepared by mixing hydrogen peroxide and ferrous ions, in an acidic environment resulting in a complex redox reaction. During the reaction, a highly reactive non-specific oxidant called hydroxyl radicals [$HO^{\bullet}$] is produced which is capable of destroying a wide range of organic pollutants in water and wastewater [31]. The catalysis is initiated by ferrous ions whereas decomposition of H_2O_2 generates $HO^{\bullet}$ [32] (equation. 3.1).

$$H_2O_2 + Fe^{++} \rightarrow Fe^{+++} + HO^- + HO^{\bullet} \qquad (3.1)$$

In physical methods like, coagulation, flocculation or adsorption, pollutants do not degrade rather transferred from liquid phase to solid phase, thus causing secondary pollution. Regeneration of the adsorbents in adsorption is a costly and time consuming process. Chemical methods like photo catalytic processes, ozone or hydrogen peroxide treatment requires high dosage of expensive chemicals and produces large quantity of sludge. Moreover, the resulting by-products by chemical degradation may be themselves colored and/or even toxic. On the other hand, biological degradation of dyes is cost effective, environment friendly and not produce huge amount of sludge, but is very selective, time consuming and thus not suitable for most of the dyes [33].

Besides those processes, membrane technology was also used for removing dye from wastewater. Generally, due to the smaller particle diameter, the required pore size of the membrane should be in the ultrafiltration/nanofiltration range which requires high pressure. In an earlier work, Nowak et. al. has reported 90-100% removal of organic dye with the help of polysulfone ultrafiltration membrane [34]. Literature survey also reveals that over 99% removal of reactive dye from dye/salt mixture was achieved by asymmetric cellulose acetate and composite polyamide

nanofiltration membranes [35]. However, the major problem in membrane-based separation process is the decline in the flux and subsequent fouling of the membrane [36].

To overcome these problems, a combination of various separation methods has been adopted in recent years to achieve a high quality of separation. Hybrid or integrated membrane processes compared with traditional wastewater treatment processes provide some advantages such as high quantity of treated wastewater, high removal efficiency, fouling control, low energy consumption and lower back-washing time [37]. Dye removal from textile effluent was tried by other researcher with the combination of coagulation-flocculation and nanofiltration [18]. Another application of the hybrid processes was photocatalysis–ultrafiltration and photocatalysis–membrane distillation for degradation of azo-dye in an aqueous solution reported by Mozia et al. (2006) [38]. Banerjee et al. (2007) [39] proposed an energy and cost effective separation of dyes by a combination of advanced oxidation process (AOP) using Fenton's reagent and nanofiltration (NF) [39]. After the AOP with Fenton's reagent, some precipitate (by product of ferric hydroxo complexes) used to form and generally removed by decanting [40]. However, it takes long time for settlement of the entire molecules, sometimes days together thereby making the decantation process for treatment of large amount of industrial wastewater too unrealistic. There is a need for the faster removal of the AOP-post products to make the process more practical. Low-cost MF membranes may provide an alternative to the faster removal of these products.

The objective of the present chapter is to prepare membranes with wide ranges of pore size using different PSD of membrane precursor and to find suitable relation of pore size with PSD of membrane precursor. The precursors with different average particle size were prepared by mixing kaolin and clay powder in different ratios. Characterization of the prepared membranes by TGA, SEM, XRD, water permeability test and acid–base treatment for analyzation of different membrane morphological parameters were also studied. A relationship was developed to predict the membrane pore size from the PSD of the membrane precursor. Further, the prepared membrane was tried to apply for the removal of crystal violet with the combination of AOP and MF. In AOP, the degradation of dye is faster if dye concentration is high and MF membrane with an appropriate pore size can successfully remove the post-AOP products. Thus, in this work AOP followed by MF is used to remove crystal violet. The optimal composition of the Fenton's reagent is determined by varying different concentrations of H_2O_2 and ferrous sulfate. The pH, total suspended solid (TSS), total dissolved solid (TDS), conductivity and density of the feed and permeate are measured for checking the suitability of the MF process. Further,

EDX and FTIR of the crystal violet and the membrane retentate are obtained for analyzing the compositional and structural changes in the dye molecule.

3.2 Materials and Methods

3.2.1 Raw Materials

– 150 mesh natural clay (collected from IIT Guwahati campus) was used as clay powder. The preparation method, chemical analysis and properties of the clay powder were presented in Chapter II in detail. Clay powder and kaolin (CDH (P.) Ltd.) were used for the preparation of the membranes where as sodium metasilicate (Loba Chemie Pvt. Ltd.), sodium carbonate (Rankem, India), boric acid (Loba Chemie Pvt. Ltd.) were used as binding materials. Crystal violet (Qualigens Fine Chemicals) was used as the source of dye whereas hydrogen peroxide 30% solution (Merck) and ferrous sulfate heptahydrate (Rankem, India) were used for preparing Fenton's reagent.

3.2.2 Membrane Preparation and Characterizations

Membranes were prepared by paste casting as per the compositions given in Table 3.1. The compositions were not chosen randomly; rather those were determined by trial-and-error method. Several membranes having different composition were prepared and characterized. In some cases membranes were not formed at all, sometimes membranes formed are of distorted shaped. After many trials the composition reported here was found to be the best. During selection of various compositions, we have considered the role of different membrane forming precursors. For example, the binding materials (sodium carbonate, sodium metasilicate and boric acid) provide mechanical strength to the membranes; use of less amount of binding material makes the membrane brittle. On the other hand, excess use of binding material may lead to many problems like, the binding materials may come out from the membrane during sintering or it can stick to the furnace floor.

The 'Membrane A' is the same membrane 'Membrane B' of Chapter II. Here it is used to compare the properties and pore sizes with the other membranes.

Table 3.1. Different compositions (dry basis) of raw materials used for preparing membranes.

Compositions	Membrane material		Binding material			% of binding material used
	Clay (%)	Kaolin (%)	Sodium carbonate (%)	Sodium metasislicate (%)	Boric acid (%)	
Membrane A	92	0	4	2	2	8
Membrane B	70	18	6	3	3	12
Membrane C	50	34	8	4	4	16
Membrane D	32	50	9	4.5	4.5	18
Membrane E	18	62	10	5	5	20

The membranes were prepared by paste casting followed by sintering at various temperatures (Membrane A, B, C and D were prepared at 1000 °C. Membrane E was sintered at different temperature (850 °C, 900 °C, 950 °C and 1000 °C) for observing the effect of temperature on the pore size of the membrane). The preparation method was discussed in detail in Chapter II.

Prepared membranes were characterized by TGA, SEM, XRD, water permeability. Porosity and flexural strength were determined and the chemical stability was determined by acid-base treatment. The detail procedures of the experiments were given in Chapter II.

3.2.3 Relationship between PSD of Membrane Precursor with Membrane Pore Size and Pore Density

Mixtures of kaolin and clay powder in different compositions were used for obtaining different particle size distribution (PSD) and average particle size of the membrane precursor. PSD of all the mixture of clay and kaolin were determined by Laser Particle Size Analyzer (Malvern, Masterizer-2000). The values of average particle diameter [$D_{1,0}$], surface weighted mean diameter [$D_{3,2}$], volume weighted mean diameter [$D_{4,3}$] and specific area for all the mixtures were directly obtained from the PSD report. Whereas, the mean diameter quantities were calculated by the following formulae:

$$D_{1,0} = \frac{\sum n_i d_i}{\sum n_i} \qquad (3.2)$$

$$D_{3,2} = \frac{\sum n_i d_i^{\,3}}{\sum n_i d_i^{\,2}} \qquad (3.3)$$

$$D_{4,3} = \frac{\sum n_i d_i^{\,4}}{\sum n_i d_i^{\,3}} \qquad (3.4)$$

Here n_i means the (number-based) frequency of occurrence of particles in size class i, having a mean diameter d_i [41] The spread of the particle size distribution of the powders was expressed by "quartile ratio" which represents the size ratio corresponding to the cumulative finer percentage of 75 and 25 in the particle size distribution curve [15]. The relationship of the average pore size with $D_{1,0}$, $D_{3,2}$, $D_{4,3}$ and specific area and the relationship of pore density with respect to average particle diameter and quartile ratio were determined. For this, first the values were plotted in MS Excel 2003. Afterwards different correlations were checked by comparing the R^2 values for finding the best correlation**.**

3.2.4 Confidence interval

In statistics, a confidence interval (CI) estimate and represent uncertainty or imprecision associated with estimates of population parameters from sample data. Instead of estimating the parameter by a single value, an interval likely to include the parameter is given. In that way, confidence intervals indicate the reliability of an estimate.

A confidence interval is always qualified by a particular confidence level, usually expressed as a percentage; thus one speaks of a "95% confidence interval". The end points of the confidence interval are referred to as confidence limits.

How likely the interval is to contain the parameter is determined by the confidence level or confidence coefficient. Increasing the desired confidence level will widen the confidence interval.

3.2.5 Advanced Oxidation Process on Crystal Violet

During AOP, dye molecules are degraded by the hydroxyl radicals [OH^*]. As the radicals are unstable in nature, those are required to generate continuously during the process. This is done by the reaction of H_2O_2 and ferrous ions. After the degradation of dye highly reactive organic radicals (R^*) are generated and further oxidized by Fe^{3+}, reduced by Fe^{2+} or dimerised. On the other hand, ferrous and ferric ions react with hydroxyl ions to from ferric hydroxo complexes and create suspended solids [40].

To find the most efficient composition of Fenton's reagent, different ferrous sulfate heptahydrate (FS) and hydrogen peroxide concentrations were considered for decoloration of 100 mg L^{-1} crystal violet (CV) solution. The prepared dye solution was mixed with Fenton's reagent (different compositions) and kept in test tube for visual observation of the decolorations. With an aim to obtain the most favorable composition, experiments were conducted for very high concentration of H_2O_2 (3600 mg L^{-1}) and ferrous sulfate (750 mg L^{-1}) with gradually decreased concentrations. The starting values of H_2O_2 and ferrous sulfate were taken from the available literature [39]. To determine the optimum dosage of H_2O_2 and $FeSO_4$, for a particular crystal violet concentration, $[H_2O_2]$/[FeSO4] and $[H_2O_2]$/[Dye] ratios were calculated for every run.

The images of the visual observation experiment were shown in Figure 3.1.

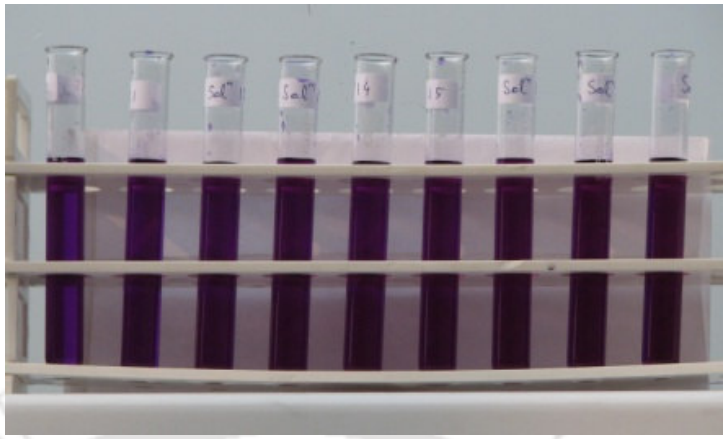

(a)

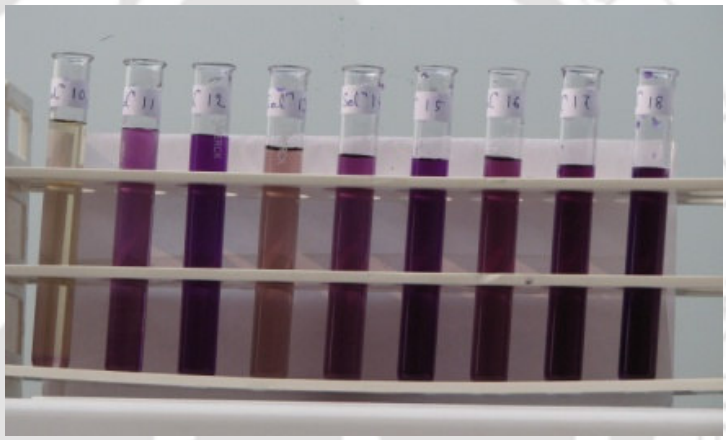

(b)

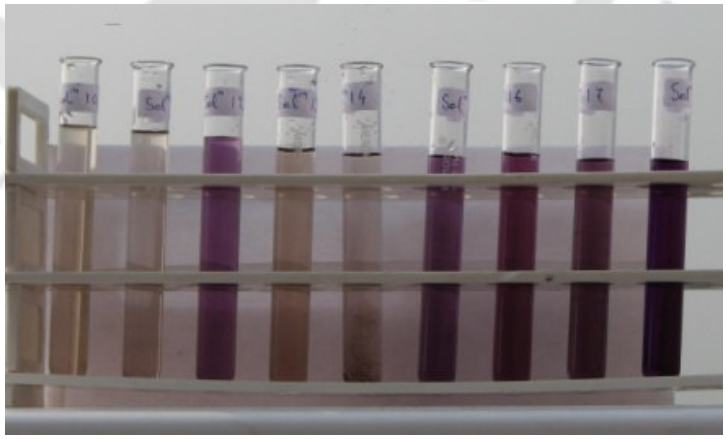

(c)

Figure 3.1. Visual observation experiment **(a)** Initial; **(b)** After 10 min and **(c)** After 2 h.

The dye degradation profiles were observed with respect to time while varying the concentrations of all the reactants (crystal violet, H_2O_2 and ferrous sulfate). For every experiment, one reactant concentration is changed while keeping the two other reactant concentrations unchanged. This was done for understanding the effect of the reactants separately, over the degradation. The experimental conditions are shown in Table 3.2. All the experiments were carried out in the absence of direct sunlight at room temperature (~ 25 °C) using 500 mL glass beaker as the reaction vessel. UV-vis spectrophotometer (Varian-Cary 50 Bio) was used to measure the absorbance of the dye (λ_{max} = 583 nm) [42]. The absorbance values were calibrated with previously known concentration of the dye. During the study, 10 mL of the reaction mixture were taken out from the beaker every 3-5 min interval and absorbance values were measured.

Table 3.2. Experimental conditions for AOP study with Fenton's reagent on crystal violet dye.

	Crystal violet concentration (mg L^{-1})	H_2O_2 Concentration (mg L^{-1})	Ferrous sulfate concentration (mg L^{-1})
Variation of crystal violet	200	1000 (unchanged)	150 (unchanged)
	150		
	100		
Variation of ferrous sulfate	100 (unchanged)	1000 (unchanged)	200
			100
			75
Variation of H_2O_2	200 (unchanged)	2000	150 (unchanged)
		1500	
		500	

3.2.6 Microfiltration Experiments

Before microfiltration experiments, progression of settlement of the suspended solids were estimated. For this, 1000 mL solution with concentrations of 200 mg L^{-1} crystal violet, 2000 mg L^{-1} hydrogen peroxide and 150 mg L^{-1} ferrous sulfate was prepared. The mixture was kept 1 h for the completion of the reaction and then mixed well. The mixed AOP post product was kept in a vessel. Then

some samples were collected from the 30 mm below the top surface of the solution (total depth of the suspension was 60 mm) after 15 min, 1 h, 3 h and 24 h. The particle size distribution (PSD) and total suspended solid (TSS) of the collected samples at different time were determined. Microfiltration experiments were done with post AOP solution of the composition mentioned above. The experiments were conducted in a dead end membrane cell at 138, 207 and 276 kPa pressure. The membrane was thoroughly cleaned after each experiment. The schematic diagram of the experimental set-up was shown in chapter II. The permeable area of the membrane was 0.00126 m^2. The permeate flux during the microfiltration was observed up to 30 min for all the three pressures to determine the flux decline profile. Physical and chemical properties like pH, total suspended solid, total dissolved solid (TDS), conductivity and density of the inlet and permeate solution were determined to check the feasibility of using microfiltration after AOP. pH, TDS and conductivity were measured in Digital Portable Water/Soil Analysis Kit (VSI Electronics Pvt. Ltd.; VSI-06D1). TSS were measured by drying 10 mL of the respective solutions (at 120 °C for 3 h) and by taking the dry weight of the residue. Densities were measured from the weight of the 10 mL respective solutions. Finally, the dye concentration in the permeate (if any) was measured by UV-Vis spectrophotometer.

3.2.7 Chemical Change Analysis

For analyzing the structural changes in the molecules of dye during AOP, spectras of the crystal violet dye and AOP post-product were obtained by using FTIR (Perkin Elmer, Model Spectrum one FTIR) and EDX (LEO, Model 1430VP).

3.3 Results and Discussion

3.3.1 Particle Size Distribution of Membrane Precursor

Kaolin was mixed with clay in different ratios for making membranes of different pore size. The PSD of different membrane precursors and kaolin are shown in Figure 3.2. It can be seen that kaolin has much finer particles than clay. The average particle size was decreasing as compositions were varied from A to E. For membrane A, B, C, D and E, the average particle size was 34.66 μm, 30.37 μm, 26.07 μm, 21.79 μm and 17.51 μm respectively.

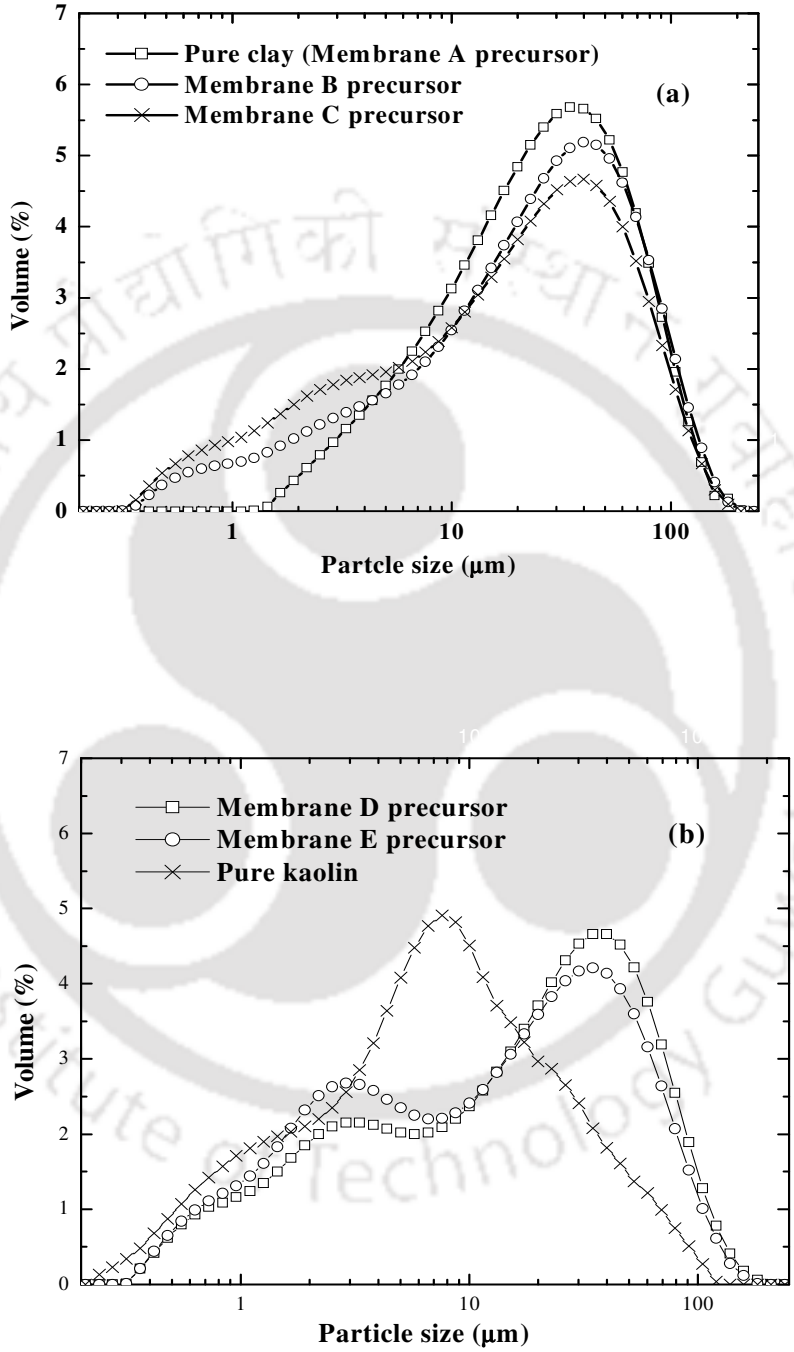

Figure 3.2. Particle size distributions of different membrane precursors.

3.3.2 Characterization of the Prepared Membranes

Thermogravimetric Analysis: As a general observation, mass loss was increased with the successive compositions (Figure 3.3). During the first phase of heating (up to 100 °C) the mass loss for membrane A, and membrane E was 1.5% and 4.2% respectively. These mass losses can be attributed to the loss of loosely bound water molecules [14]. The sequential increase of mass losses in this phase can be explained by the enhanced amount of hygroscopic materials (like sodium metasilicate, boric acid) in the compositions. Afterwards up to 300 °C the mass losses for all the membranes were very less. During the second phase drastic falling in weight loss was observed after 300 °C. As a consequence, membrane A and membrane E has shown 1.35 % and 6.05 % mass losses in between 300 °C and 500 °C. This phenomenon may be attributed to the fact that the boiling point of boric acid, whose composition was increased subsequently, is around 300 °C. Afterwards, another strong fall in weight loss was observed after 500 °C. In comparing with membrane B and membrane E, the mass loss in the range of 500 °C to 700 °C, was 2.83 % and 7.28 % consecutively. This was corresponding to the loss of structural hydroxyl groups at 513 °C due to the transformation of kaolinite to metakaolinite according to the following reaction [43]:

$$Al_2O_3 \cdot 2SiO_2 \cdot 2H_2O \rightarrow Al_2O_3 \cdot 2SiO_2 + 2H_2O \qquad (3.5)$$

(Kaolinite) (metakaolinite)

This phase change was not detected in membrane A since kaolin was not present in that composition. And finally, after 700 °C, for all the compositions, mass changes were marginal. Thus, it can be concluded that the minimum sintering temperature for all the membranes should be above 700 °C.

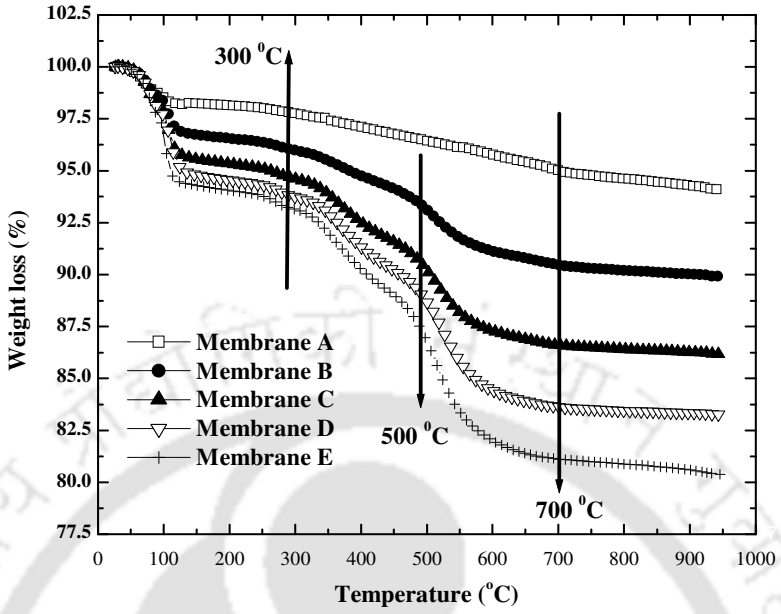

Figure 3.3. Thermogravimetric analysis of the prepared membranes.

X-ray Diffraction Analysis: For the 1000 °C sintered membranes, reflections of quartz (Q), mullite (M) and nephiline (Na_2O, Al_2O_3, $2SiO_2$) (N) were detected (Figure 3.4 a). In case of membrane B, another characteristic reflection of corundum (C) was observed. Same types of peaks were observed by Löffler et. al. during dehydration of natural and synthetic goethite [44]. Corundum is a crystalline form of aluminum oxide (Al_2O_3) with traces of iron, titanium and chromium. In 1837, Gaudin made the first synthetic rubies (structure is very closer to corundum) by fusing alumina at a high temperature with a small amount of chromium as a pigment. As, kaolin contains large amount of aluminum oxide and the clay contains very small amount of chromium (0.012%), titanium (0.541%) and iron (3.326%), so, generation of corundum at high temperature sintering is possible for membrane B, C, D and E. But for membrane C, D and E, due to lower clay percentage in the composition, may be the available chromium; titanium and iron are not enough for generation of corundum. Temperature effects for phase changes were observed for membrane E (Figure 3.4 b). At 600 °C sintered membrane, reflection of illite (I), nephiline (N) and quartz (Q) were observed. No reflection of kaolinite was found due to transformation to metakaolinite which was confirmed by TGA experiment also. At the higher temperature sintered membranes (1000 °C), no reflection of illite was observed. Comparable result was reported in the literature for Moroccan clay membranes [16]. At higher temperature (800 °C and 1000 °C), mullite reflections were appearing, quartz reflections did not change significantly. Thus, membrane A, C, D, and

E contains mullite, quartz and nephiline where as membrane B contains mullite, quartz, nephiline and corundum.

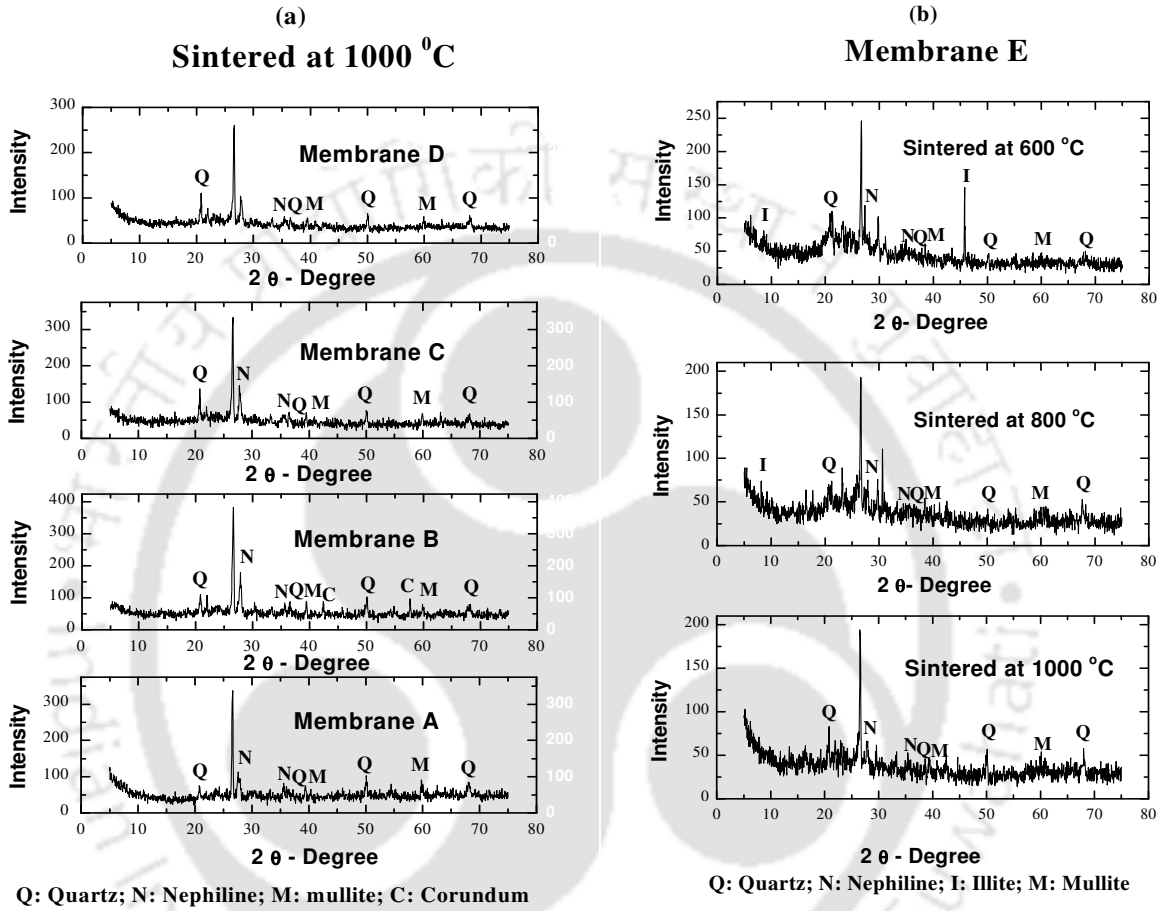

Figure 3.4. XRD of prepared membranes **(a)** 1000 °C sintered Membrane A, Membrane B, Membrane C and Membrane D. **(b)** Membrane E sintered at 600 °C, 800 °C and 1000 °C.

Surface Morphology and Pore Size Distribution from SEM Images: To determine the area average pore size and the pore size distribution of the prepared membranes, morphological studies were conducted using SEM (Figure 3.5). SEM also detects the small cracks on the membrane surface (if any). No such cracks were observed in any of the membranes. It was seen that with increasing the amount of kaolin in the membrane precursors, the structure was becoming denser. This was due to the fact finer particles of kaolin were blocking the inter-particle space of clay, thus making the structure more condensed. Additionally, with the increase of the sintering temperature, the membrane became dense.

SEM images from different sections of the membrane (and in different magnification) were considered and around 600 pore diameters from every membrane were measured using the ImageJ software [14]. After opening the specific image in the software (File → Open), first of all the scale of the original SEM image is related with the distance in pixel (Analyze → Set scale). Afterwards, the pore diameters were measured by the tool "Straight line selection". The distance in pixels, were converted to the known distance (micron) by the software itself. And finally, the measured data were transferred to MS-excel for further calculations. Average pore diameters (d_s) were calculated by the following equation (3.6)

$$d_s = \left[\frac{\sum_{i=1}^{n} n_i d_i^{\,2}}{\sum_{i=1}^{n} n_i} \right]^{0.5} \qquad (3.6)$$

where n is the number of pores, and d_i is the pore diameter (μm) of the i-th pore. With the decrease of the average particle size of the membrane preparing materials, the pore size was decreasing (Membrane A to Membrane E) (Fig. 3.6). The average pore size of membrane A and membrane D, sintered at 1000 °C was 4.91 and 0.78 μm respectively (Table 3.3). This was due to the densification of the material. Similar results was reported by Das et. al. [15] for membranes prepared from alumina. It was found that for a particular composition (membrane E), pore size was increasing with the sintering temperatures. The reason was the overlapping of small pores creating large pores at higher sintering temperature. For membrane E, average pore size was increased from 0.46 μm to 0.51 μm for corresponding sintering temperature of 850 °C and 1000 °C. Similar trend was reported by Saffaj et. al. [16] for membranes prepared from Moroccan clay.

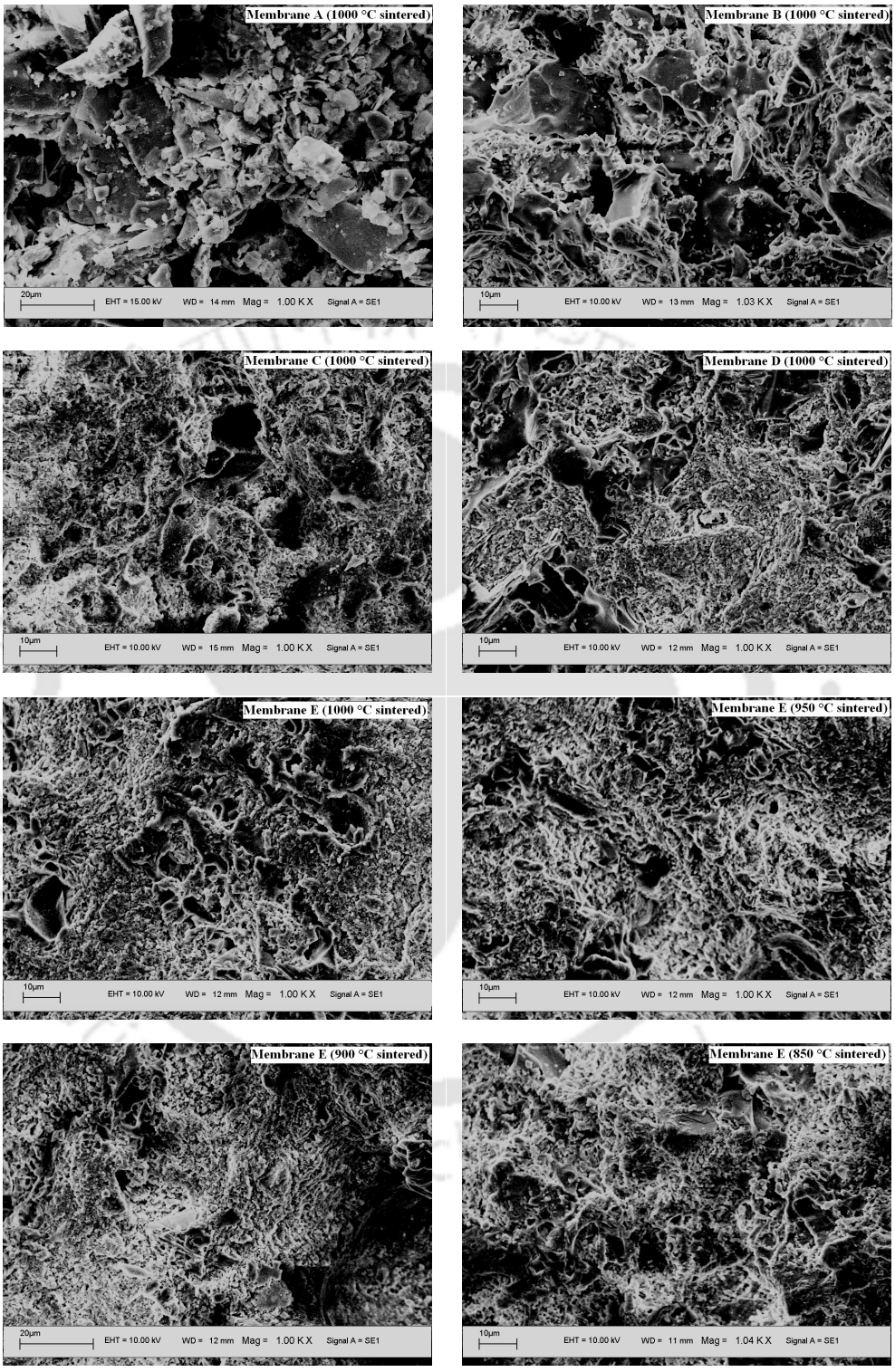

Figure 3.5. SEM micrographs of prepared membranes for different compositions and different sintering temperatures.

Table 3.3. Different parameters of the prepared membranes

Membrane	Sintering temperature (°C)	Average pore diameter		Porosity	Pore Density (m^{-2})	Water permeability ($mPa^{-1}s^{-1}$)	Flexural strength (MPa)
		From SEM images (μm)	From water permeability (μm)				
Membrane A	1000	4.91	4.58	0.38	2.47×10^{10}	4.98×10^{-08}	11.55
Membrane B	1000	3.11	2.28	0.37	1.24×10^{11}	1.20×10^{-08}	17.25
Membrane C	1000	1.10	0.71	0.35	1.37×10^{12}	1.10×10^{-09}	15.45
Membrane D	1000	0.78	0.49	0.29	2.45×10^{12}	4.35×10^{-10}	12.80
Membrane E	1000	0.51	0.31	0.22	4.80×10^{12}	1.32×10^{-10}	12.81
	950	0.48	0.29	0.24	6.01×10^{12}	1.26×10^{-10}	11.50
	900	0.48	0.27	0.25	7.76×10^{12}	1.14×10^{-10}	10.11
	850	0.46	0.24	0.26	1.10×10^{13}	9.36×10^{-11}	7.01

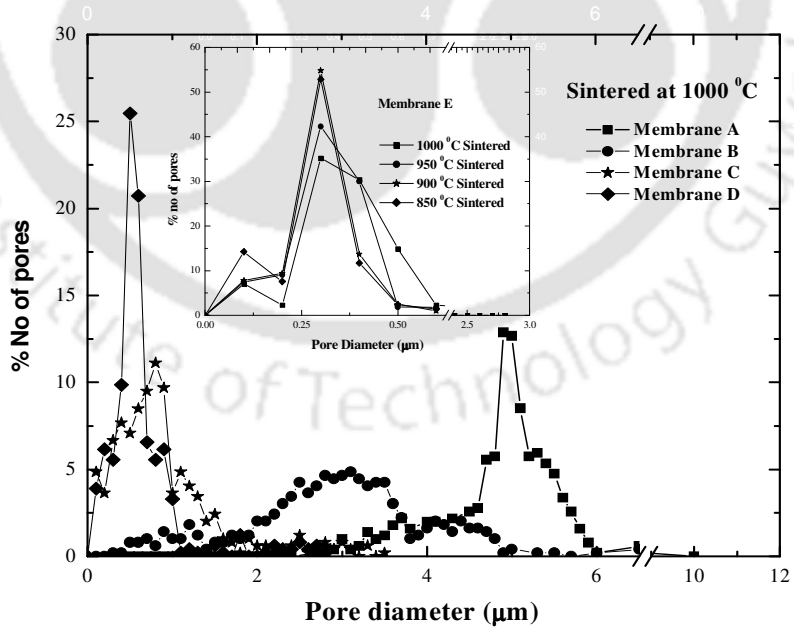

Figure 3.6. Pore size distribution of prepared membranes

Surface Pore Density: Surface pore density corresponds to the average number of pores counted per unit area of the membrane surface. It was calculated from the SEM images and reported in Table 3.3. Pore density was increasing with the decrease of the particle size of membrane preparing materials. The pore density of membrane A and membrane D (sintered at 1000 °C) were 2.47×10^{10} and 1.24×10^{11} m^{-2} respectively. As the size of the average particle sizes were decreasing, more number of particles were appearing within the same volume, hence number of pores were increasing. Furthermore, for a particular composition, pore density was decreased with increasing of the sintering temperatures. For membrane E, pore density was decreased from 1.10×10^{13} m^{-2} to 6.01×10^{12} m^{-2} during the increasing of the sintering temperature from 850 °C to 1000 °C successively. This change was also representative of the overlapping of many small pores to a smaller number of large pores at higher sintering temperature.

Water Permeability Experiment: From the porosity values obtained by pycnometric method, it was observed that porosity decreased with the decreasing of the average particle size of the membrane preparing materials. Membrane A and membrane D have shown porosity of 0.38 and 0.29, respectively. This is due to the densification of the membrane structure. In the same way, it was increasing with the sintering temperature (Table 3.3). This was mainly due to squeezing of the membrane body during sintering and overlapping of small pores during creation of large pores. Membrane E has shown porosity of 0.22 and 0.26 for 850 °C and 1000 °C sintered samples successively.

The average pore diameter decreased with the smaller particle size (i.e with the increase of the kaolin percentage and decrease of the clay percentage) of membrane preparing materials and on the contrary, increased with the increase of the sintering temperature (Table 3.3). The average pore diameter obtained from membrane A and membrane D were 4.58 and 0.49 µm correspondingly. For membrane E, the values were 0.24 and 0.31 for 850 °C and 1000 °C sintered temperatures respectively. The pore size obtained from SEM images was larger than from water permeability experiments. This was due to the presence of dead-end-pores which were incorporated in SEM image analysis but not integrated in the water permeability experiments. Details of the water permeability experiments are explained in Chapter II.

From the determined pore sizes, it can be forecasted, that the prepared comparatively higher pore size membranes (membrane A and B) can be applicable for surfactant based separation like micellar enhanced microfiltration (MEMF) whereas comparatively lower pore size membranes (membrane C, D and E) can be applicable for oily-wastewater separation or fruit juice clarification. Though the micelles

having larger particle sizes can be removed by filter paper, however, for large-scale separation, filter paper option is unrealistic. The alternative ways for separation of oil-water are: coagulation followed by flock forming, freeze-thaw and electrochemical method, whereas fruit juice can be clarified by electro-flotation and enzyme based methodology. However the advantages of using these prepared membranes over all those conventional processes are that these are low cost as well as less time consuming.

Mechanical Strength: The flexural strength was calculated by a three point bending strength method and reported in Table 3.3. The flexural strength was increased with increasing sintering temperature. For membrane E, flexural strength increased from 7.01 MPa (850 °C sintered) to 12.81 MPa (1000 °C sintered). This is due to the formation of mullite and nephiline in the higher sintering temperatures. Similar results were reported by other researchers also [14] Comparing with other compositions, membrane B has shown maximum mechanical strength (17.25 MPa). The reason behind this was the presence of corundum in the framework. As XRD analysis of membrane A, C and D were not shown much difference, it can be concluded that the higher strength of membrane C (15.45 MPa) and D (12.80 MPa), with respect to membrane A (11.55 MPa) were due to its more dense structure.

***Chemical Stability against Acid and Bases*:** As an overall analysis, membranes have shown 2-10% weight loss during the treatments. The change in porosity, pore size, water permeability and flexural strength were found to be marginal (Table 3.4). Thus all the membranes can be considered as chemically resistant. Membrane B has shown maximum chemical stability. Presence of corundum in the structure could be the reason for this. Chemical stability was increased with the higher sintering temperatures (Membrane E). This may be due to the formation of mullite and nephiline at the higher temperature sintered samples. The reason for the increasing porosity was due to the fact that, during the chemical treatment, some materials of the membrane were corroded thereby generating voids. Average pore size and permeability also increased. For membrane E (sintered at 1000 ºC), the pore diameter, porosity, permeability and flexural strength were changed from 0.31 µm, 0.22, 1.32×10^{-7} m^3m^{-2} kPa^{-1} sec^{-1} and 12.81 Mpa to 0.32 µm, 0.26, 1.66×10^{-7} m^3m^{-2} kPa^{-1} sec^{-1} and 9.32 Mpa after acid treatment. The membrane has shown 6.05% weight loss.

Table 3.4. Variation of different membrane parameters after chemical treatment

After acid treatment					
Composition (Sintering temperatures, °C)	Weight loss (%)	Porosity	Pore Size (µm)	Permeability ($mPa^{-1}sec^{-1}$)	Flexural Strength (MPa)
A (1000)	5.37	0.42	4.68	5.63×10^{-08}	9.37
B (1000)	2.15	0.38	2.31	1.27×10^{-08}	14.44
C (1000)	4.38	0.37	0.73	1.23×10^{-09}	12.13
D (1000)	5.22	0.32	0.51	5.20×10^{-10}	12.86
E (1000)	6.05	0.26	0.32	1.66×10^{-10}	9.32
E (950)	6.63	0.29	0.29	1.52×10^{-10}	8.25
E (900)	8.23	0.32	0.28	1.57×10^{-10}	7.15
E (850)	9.38	0.34	0.25	1.33×10^{-10}	4.91
After base treatment					
Composition (Sintering temperatures, °C)	Weight loss (%)	Porosity	Pore Size (µm)	Permeability ($mPa^{-1}Sec^{-1}$)	Flexural Strength (MPa)
A (1000)	6.89	0.43	4.71	5.72×10^{-08}	9.94
B (1000)	1.72	0.38	2.30	1.26×10^{-08}	14.32
C (1000)	2.83	0.37	0.72	1.23×10^{-09}	13.58
D (1000)	4.37	0.32	0.50	4.84×10^{-10}	13.15
E (1000)	5.65	0.26	0.31	1.56×10^{-10}	10.95
E (950)	7.13	0.30	0.30	1.69×10^{-10}	10.25
E (900)	8.41	0.32	0.28	1.57×10^{-10}	9.23
E (850)	10.02	0.35	0.25	1.37×10^{-10}	5.86

3.3.3 Variation of Average Pore Size and Pore Density

Pore Size: All the membranes were prepared from clay, kaoline and binding materials without using any pore forming material like calcium carbonate. It was assumed that pores were created only by intra-particle spaces of the framework. Boric acid, sodium metasilicate and sodium carbonate were used to generate hardness in the ceramic structure [8]. Variation of the average pore diameter [D_{avg}] of the prepared membranes were compared with average particle diameter [$D_{1,0}$], surface weighted mean [$D_{3,2}$], volume weighted mean [$D_{4,3}$] and specific area [A_{sp}] (Figure 3.7). It is known that only the average mean particle diameter doesn't give a complete view of the statistical variation of the PSD. So, in general, it is advised to use some form of weighted mean diameter, where both particle quality (e.g. size, volume) and weighing (e.g. by number, area) relate the parameters of interest [45]. Relationship of average pore size with specific area was also considered due to the fact that overall area of the particles was not represented by any of the above parameters.

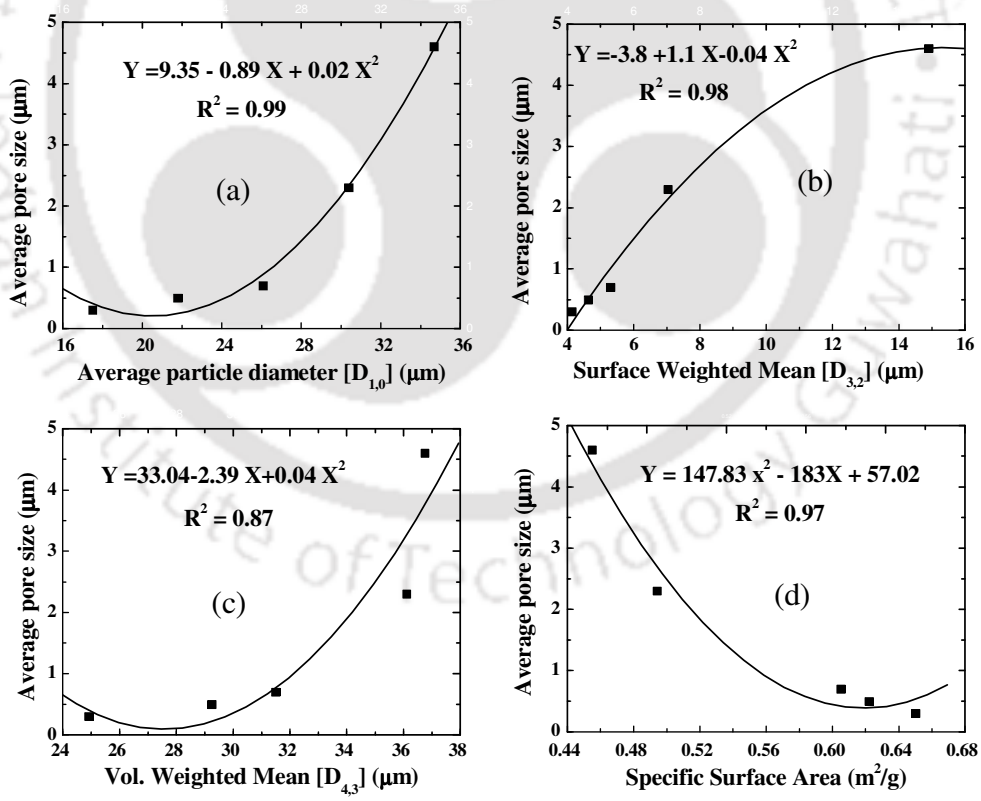

Figure 3.7. Variation of average pore size with respect to (a) Average particle size, (b) Surface weighted mean, (c) Volume weighted mean and (d) Specific area

It was observed that pore diameter was decreasing with the decrease of the $D_{1,0}$, $D_{3,2}$, $D_{4,3}$ (Figure 3.7). On the contrary, it was decreasing with the increase of the specific area. The average pore size was decreased from 4.6 µm to 0.3 µm for the value of average particle diameter 34.66 µm to 17.51 µm. It was due to the fact that, with the decrease of the particle size, more materials were aggregating within the volume, hence making the structure denser. Besides, specific area increases when the particle diameter decreases, as a result pore size also decreases. It was also seen that all the relationship can be represented by second order polynomials (equation (3.7), (3.8), (3.9) and (3.10)) for which the R^2 values were found to be between 0.99 to 0.87.

$$D_{avg} = 9.35 - 0.89 \times D_{1,0} + 0.02 \times D_{1,0}^{\ 2} \qquad (3.7)$$

$$D_{avg} = -3.8 + 1.1 \times D_{3,2} - 0.04 \times D_{3,2}^{\ 2} \qquad (3.8)$$

$$D_{avg} = 33.04 - 2.39 \times D_{4,3} + 0.04 \times D_{4,3}^{\ 2} \qquad (3.9)$$

$$D_{avg} = 147.83 \times A_{sp}^{\ 2} - 183 \times A_{sp} + 57.02 \qquad (3.10)$$

The 95% confidence intervals for the developed relationships were shown in Table 3.5. As, the less difference between the upper and lower limit represent a better estimation, the coefficients of equation (3.8) have shown best among all the relationships. Depending on the confidence interval and R^2 values, the relationship with $D_{3,2}$ was found to be the best. These equations gave clear evidence that membrane pore sizes can be predicted from the membrane precursor PSD even before preparing the membrane.

Table 3.5. Confidence interval of the fitted second order polynomials.

	$D_{1,0}$ vs. D_{avg}		$D_{3,2}$ vs. D_{avg}		$D_{4,3}$ vs. D_{avg}		A_{sp} vs. D_{avg}	
	Lower 95%	Upper 95%	Lower 95%	Upper 95%	Lower 95%	Upper 95%	Lower 95%	Upper 95%
Variable x	1.667	0.117	0.152	2.345	9.683	4.903	490.3	124.3
Variable x^2	0.007	0.037	0.099	0.028	0.074	0.160	131.0	426.7

Pore Density: For pore density [N_p], not only the average particle diameter, but the spread of the PSD also have strong influence over the pore diameter. To get an idea about this spread of PSD, a simple way is to measure the difference between the particle sizes corresponding to the cumulative finer percentage of 75% and 25% in the PSD curve. Such a quantity is normally referred to as the quartile range and designated as "$_{25}X_{75}$" [46]. The pore density was compared with average particle diameter and quartile ratio (Figure 3.8).

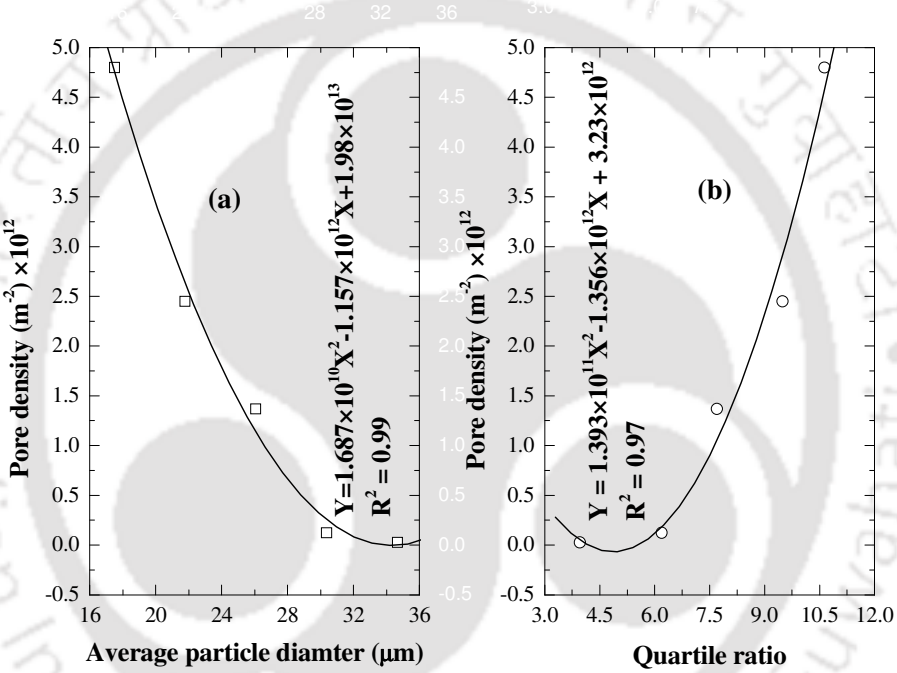

Figure 3.8. Variation of pore density with respect to, (a) Average particle size and (b) Quartile ratio.

It was observed that the pore density was decreasing with the increase of the particle diameter. Pore density was decreased from 4.8×10^{12} to 0.0247×10^{12} for increase of the particle size from 17.51 μm to 34.66 μm. This aspect can be explained by the fact that during the agglomeration of the particles, more pores were forming. On the other hand, pore density was decreasing with the decrease of the quartile ratio. For the decrease of quartile ratio from 10.64 to 3.96, the pore density was decreased as mentioned above. Increase in the quartile ratio means, a wider PSD, more uneven distribution, hence increase in the pore density. These relationships were also represented by second order polynomials (equation (3.11) and (3.12)) with R^2 values of 0.99 to 0.97

$$N_p = 1.69\times10^{10}\times D_{1,0}{}^2 - 1.16\times10^{12}\times D_{1,0} + 1.98\times10^{13} \qquad (3.11)$$

$$N_p = 1.393\times10^{11}\times({}_{25}X_{75})^2 - 1.36\times10^{12}\times({}_{25}X_{75}) + 3.23\times10^{12} \qquad (3.12)$$

From these equations, pore density can also be predicted from the PSD of the membrane preparing material.

The calculated 95% confidence intervals for all the developed second-order polynomials were shown in Table 3.6. Depending upon the R^2 values and confidence interval, the relationship of N_p with $D_{1,0}$ was found better than the relationship with ${}_{25}X_{75}$. From these equations, it is clear that pore density can also be predicted from the PSD of the membrane preparing material.

Table 3.6. 95% confidence intervals for the second order polynomials of pore density with $D_{1,0}$, and ${}_{25}X_{75}$

	$D_{1,0}$ vs. N_p		${}_{25}X_{75}$ vs. N_p	
	Lower 95%	Upper 95%	Lower 95%	Upper 95%
Variable x	1.9×10^{12}	3.9×10^{11}	-4×10^{12}	1.2×10^{12}
Variable x^2	2.2×10^{9}	3.2×10^{10}	3.7×10^{10}	3.2×10^{11}

3.3.4 AOP Study

Finding the Optimal Ratio of the Reactants: All the experimental conditions and visual observations are shown in Table 3.7. It was observed that higher concentrations of H_2O_2 (3600 mg L^{-1}) and ferrous sulfate (750 and 500 mg L^{-1}), has made the 100 mg L^{-1} dye solution colorless instantaneously. The time of decoloration increased with lowering the concentrations of the reactants. Another observation was that, the solution was not totally clear below a critical concentration of 1000 mg L^{-1} of H_2O_2 and 100 mg L^{-1} of ferrous sulfate. Thus, for 100 mg L^{-1} dye solution, the optimal concentration of H_2O_2 and ferrous sulfate was found to be 1000 mg L^{-1} and 100 mg L^{-1} respectively. It was observed that total degradation of the dye was achieved at a ratio of $[H_2O_2]$/[Dye] above 10 and at a ratio of

$[H_2O_2]/[FeSO_4]$ below 10. This was due to the decrease of the $[Fe^{2+}]$ and $[OH^*]$ in the solution at these particular reactant concentrations. Below these concentrations, some of the dye molecules were degraded and some of those remain within the solution.

Table 3.7. AOP study on crystal violet dye (100 mg L^{-1} concentration) for finding the optimal ratios of the reactants.

Run no	H_2O_2 concentration (mg L^{-1})	Ferrous sulfate heptahydrate concentration (mg L^{-1})	Ratios		Observations
			$[H_2O_2]/[FeSO_4]$	$[H_2O_2]$/[Dye]	
1	3600	750	4.8	360	Instantly colorless
2	3600	500	7.2	360	Instantly colorless
3	3600	250	14.4	360	Colorless after 3 min
4	2500	200	12.5	250	Colorless after 10 min
5	2500	100	25	250	Colorless after 2 h
6	2500	50	50	250	Almost clear
7	1000	200	5	10	Colorless after 10 min
8	1000	100	10	10	Colorless after 2 h
9	1000	50	20	10	Not clear even after 4 h
10	500	200	2.5	5	Not clear even after 4 h
11	500	100	5	5	Not clear even after 4 h
12	500	50	10	5	Not clear even after 4 h

These determined optimized ratios of $[H_2O_2]$/[Dye] and $[H_2O_2]/[FeSO_4]$ can be useful for on-line monitoring of real-time industrial processes. By detecting the concentration of the dye, relative amount of $FeSO_4$ and H_2O_2 can be added and consequently a continuous process can be controlled.

Effect of the Variation of the Reactants: During the AOP experiments, it was observed that for the initial 5 min, the reaction rates were very fast and then gradually decreased. After 60 min, degradation of dye was marginal. This was due to the presence of the large number of Fe^{2+} ions in the initial stage. However, during the process Fe^{2+} was converted to Fe^{3+}. The regeneration of Fe^{2+} was a slow process and hence rate determining step after the first phase. Similar type of findings was reported earlier [39].

Figure 3.9 shows the concentration profile of the dye with time for various initial crystal violet concentrations. It can be seen from the figure that with decreasing the concentration of crystal violet, the rate of degradation of dye decreased. 200, 150 and 100 mg L^{-1} initial dye solution were reacted with 1000 mg L^{-1} H_2O_2 and 150 mg L^{-1} ferrous sulfate. Subsequently, these solutions have shown 14.87, 9.16 and 4.73 mg L^{-1} dye concentration after 21, 26 and 22 min, respectively. The initial dye concentrations also affected the amount of dye degradation. Dye degradation increased with the increase of the initial dye concentration. The increase in the dye concentration leads to increase in the reaction rate. Thus, initial dye concentration of 200 mg L^{-1} dropped down to about 13.79 mg L^{-1} in 30 min and 100 mg L^{-1} decreased to about 3.72 mg L^{-1} in 28 min.

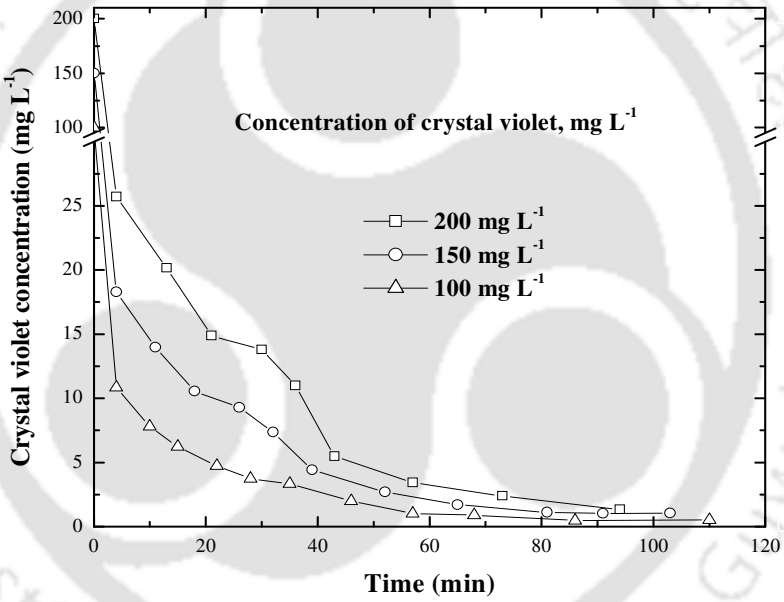

Figure 3.9. Dye degradation profile with Fenton's reagent varying the concentration of crystal violet with fixed concentration of H_2O_2 (1000 mg L^{-1}) and ferrous sulfate heptahydrate (150 mg L^{-1}).

Variation of dye concentration with time for different ferrous sulfate heptahydrate dosage is presented in Fig. 3.10. With the increase of the $FeSO_4 \cdot 7H_2O$, the rate of the degradation of dye increased. This was due to the addition of more number of the Fe^{2+} ions with the increase of the $FeSO_4 \cdot 7H_2O$ concentrations. With the increase of the ferrous ions, concentration of [OH^*] radicals were also increased, thus rate of dye degradation increased. With the $FeSO_4 \cdot 7H_2O$ concentration of 75 and 200 mg L^{-1} in a solution containing initial concentration of 100 mg L^{-1} dye and 1000 mg L^{-1} H_2O_2, the dye concentration decreased to 16.27 and 1.58 mg L^{-1} in 29 and 28 min respectively.

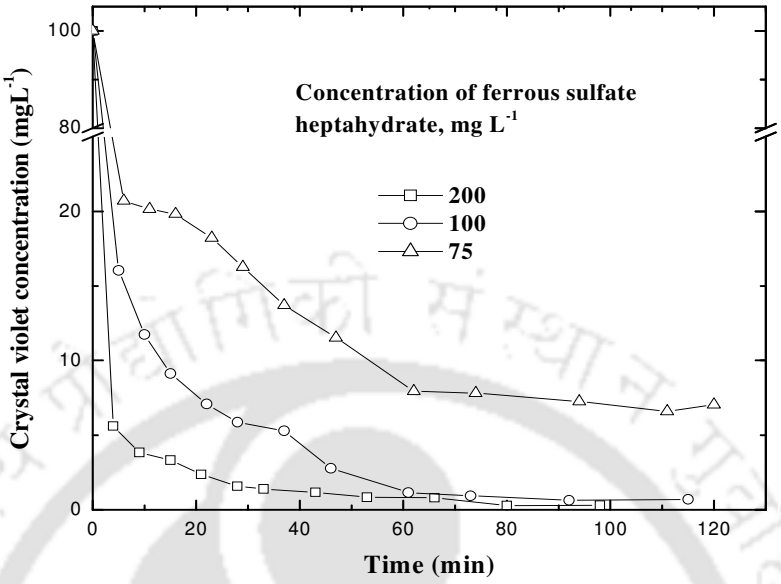

Figure 3.10. Dye degradation profile with Fenton's reagent varying the concentration of ferrous sulfate with fixed concentration of H_2O_2 (1000 mg L^{-1}) and crystal violet (100 mg L^{-1}).

Effect of H_2O_2 concentration on dye degradation is shown in Figure 3.11. By increasing the H_2O_2 concentration, increase in the rate of dye degradation was observed. The reason behind this is the increase of the hydroxyl radicals with the increase of the H_2O_2 concentration. The [OH*] radicals further reacted with the dye molecules and degrade those. For the H_2O_2 concentration of 500 and 2000 mg L^{-1}, 200 mg L^{-1} crystal violet (with fixed 150 mg L^{-1} ferrous sulfate) reaches to 31.07 and 11.49 mg L^{-1} after 23 and 22 min respectively.

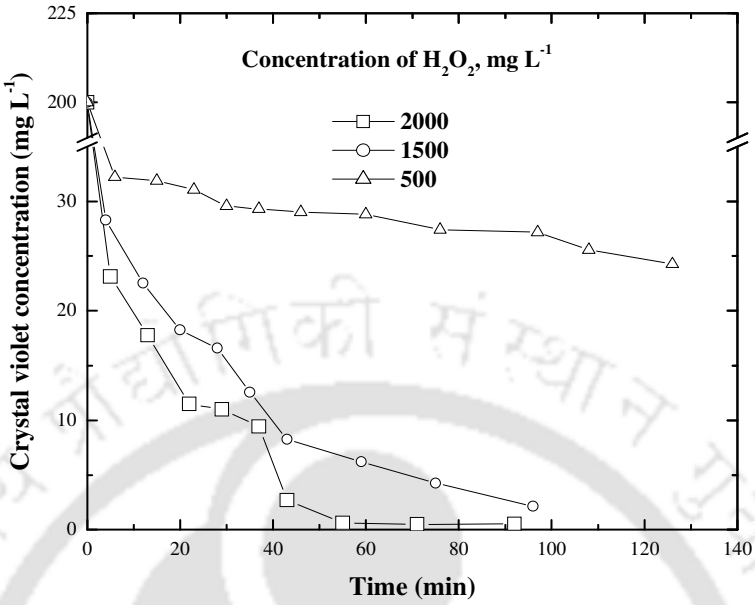

Figure 3.11. Dye degradation profile with Fenton's reagent varying the concentration of hydrogen peroxide with fixed concentration of crystal violet (200 mg L^{-1}) and ferrous sulfate heptahydrate (150 mg L^{-1}).

3.3.5 Microfiltration Experiments

As described in the experimental section, the total suspended solid (TSS) was measured at different time, while keeping the solution at rest. The value was initially 6.2×10^{-4} mg L^{-1} and gradually decreased to 5.5×10^{-4} mg L^{-1} (after 5 min), 4.9×10^{-4} mg L^{-1} (after 1 h), 3.0×10^{-4} mg L^{-1} (after 3 h) and 1.6×10^{-4} mg L^{-1} (after 24 h). It was observed that all the particles were not settled down with time. Particle size distribution results also revealed the same (Figure 3.12). With progress in time, the larger particles were settled down but particles below 5 μm were not settled even after 24 h. Thus, for quick and complete removal of suspended solids, microfiltration is necessary. From the PSD of suspended solids, the smallest particle size was in the range of 0.6 μm. Hence, the used membrane (average pore size = 0.31 μm) was considered suitable for removal of the suspended solids.

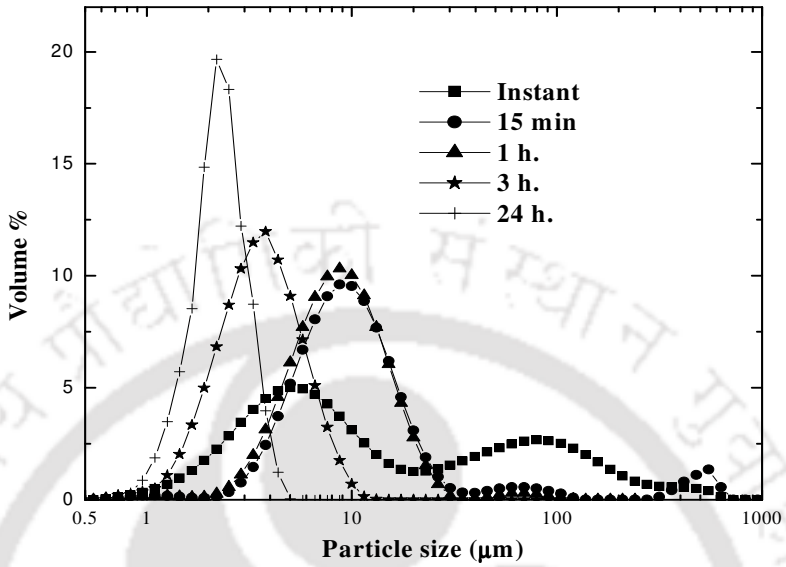

Figure 3.12. PSD of suspended solids of the AOP post product kept in rest for different time.

Variation of Flux throughout the Experiment: Before microfiltration, the water permeability of the membrane was measured as 1.32×10^{-7} $m^3m^{-2}kPa^{-1}s^{-1}$. During microfiltration experiments, flux was observed to decrease slowly. The flux decline profiles for three different transmembrane pressures are shown in Figure 3.13. Two trends can be observed from this figure. Initially, the flux was decreased very sharply (up to 10 min) and then the declination was steady. The first phase flux declination may be due to the concentration polarization and the second stage steady state decrease was due to cake formation over the membrane surface [47].

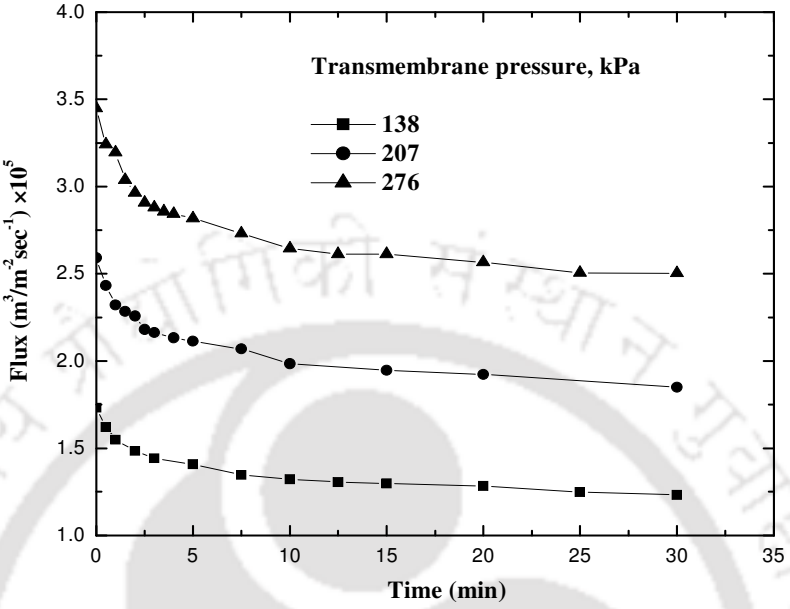

Figure 3.13. Flux decline profile during microfiltration experiment.

Physical and Chemical Properties of Feed and Permeate: The physical properties of the feed and permeate for microfiltration experiment were shown in Table 3.8. It was found that the pH was decreased slightly (from 6.41 to 6.18) after microfiltration. This may be due to the separation of slight basic $Fe(OH)_3$ during microfiltration. TSS were completely removed which was confirmed by laser particle size analyzer (LPSA) also. The LPSA has not detected any particle in permeate. The conductivity (0.5 mmoh) values were same for before and after microfiltration. TDS was changed marginally (from 360 mg L^{-1} to 350 mg L^{-1}) which could be due to the instrumental error (the instrument error is specified as ± 10%). Density value was decreased slightly (from 999.7 kg m^{-3} to 997.1 kg m^{-3}). No dye molecules were detected in the permeate, thereby achieving a 100% rejection of suspended solids as well as dye.

Table 3.8. Physical and chemical properties of the feed and permeate

Property	Feed	Permeate
pH	6.41	6.18
TSS (mg L^{-1})	620	0
TDS (mg L^{-1})	360	350
Conductivity (mmoh)	0.5	0.5
Density (kg m^{-3})	999.7	997.1

3.3.6 Analyzation of the AOP-post-product

EDX Results: From the EDX spectra of the crystal violet dye and the membrane retentate (Table 3.9), it was found that the original dye consists of carbon, nitrogen, oxygen and chlorine whereas, AOP post-product, consists of carbon, nitrogen, oxygen, and iron. Presence of carbon and nitrogen proves the precipitation of the dye. Other researchers also reported the presence of carbon in AOP post-product during treatment of wastewater [48]. Iron in the membrane retentate has come from the precipitate of ferric hydroxo complexes generated from ferrous sulfate. Besides, chlorine, which was present in the crystal violet molecules, was not found in the membrane retentate. This may be due to the oxidization of the chloride group during AOP. Thus, AOP followed by microfiltration efficiently removed crystal violet dye from aqueous solution.

Table 3.9. EDX of the dye and AOP post product (membrane retentate).

Element	Atomic %	
	Dye	Membrane retentate
C	75.24	69.61
N	17.40	9.17
O	3.05	16.92
Cl	4.32	—
Fe	—	4.29

FTIR Analyzation: The FTIR spectra of the crystal violet and the membrane retentate are shown in Figure 3.14. The changes in the band peaks during the process are analyzed in Table 3.10. It was observed that the bands around 1474, 1295, 940, 911 and 723 cm^{-1} present in the crystal violet are absent in the post AOP product. The bands of 1474 and 1295 cm^{-1} represent typical ν(C=O) of cyclic group. Bands from 940 and 911 cm^{-1} also represent loss of aromaticity during the process. Apart from this, the band around 723 cm^{-1} represents chlorine. In the EDX spectra also, chlorine was not found in the AOP post-product. FTIR result also confirmed the same. On the other hand, bands of – CH_3 (bend) (1363 cm^{-1}) and – CH_3 (stretch) (2924 cm^{-1}) are present in both crystal violet and AOP post product. From this, it was concluded that, during the advanced oxidation process, the aromatic group and chlorine of the dye molecules are oxidized. Similar results were reported in literature [40].

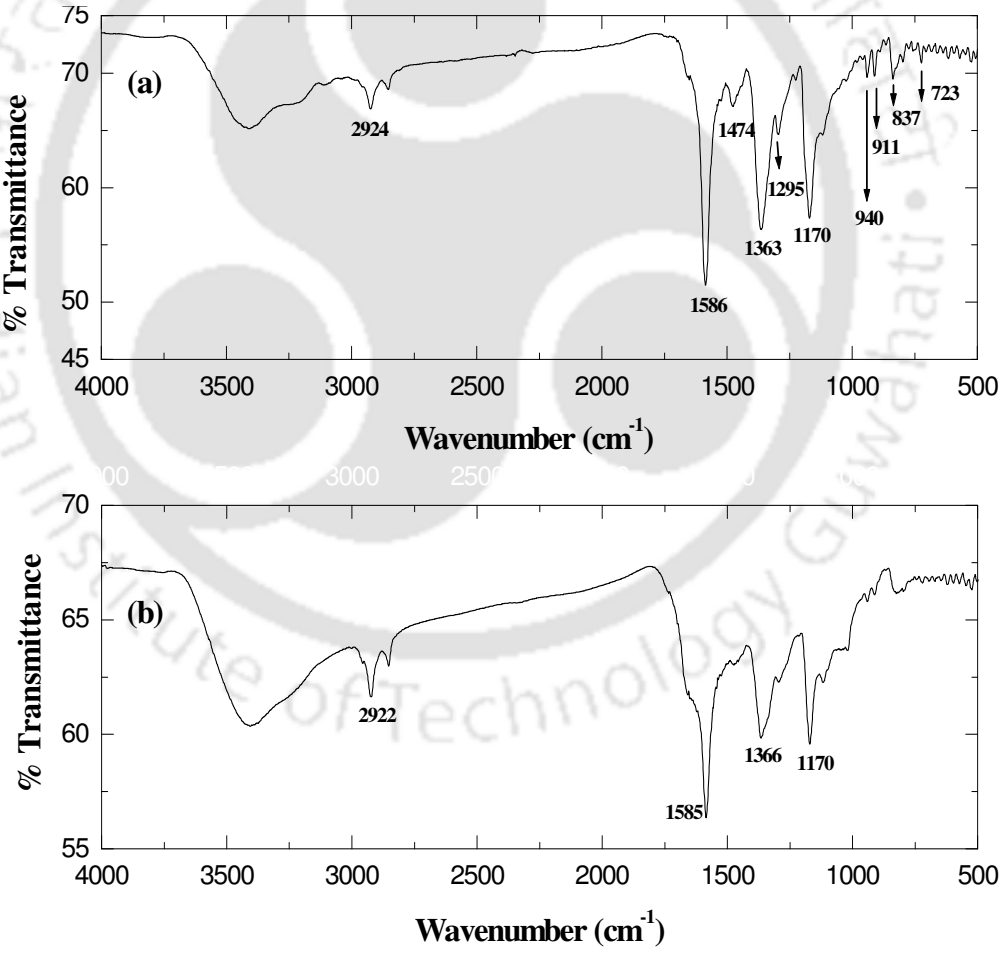

Figure 3.14. FTIR analysis of the a) Crystal violet and b) AOP post product.

Table 3.10. FTIR band analyzation of crystal violet and AOP post product.

Band Peak (cm^{-1})	Crystal violet	AOP post product	Representing group/bond
3400	Present	Present	Alkyle C=C
1586	Present	Present	Aromatic C=C
1474	Present	Not present	ν(C=O) of cyclic group
1363	Present	Present	$-CH_3$ (bend)
1295	Present	Not present	ν(C=O) of cyclic group
2924	Present	Present	$-CH_3$ (stretch)
1170	Present	Present	$-CH_3$
940	Present	Not present	Aromaticity
911	Present	Not present	Aromaticity
723	Present	Not present	Chlorine

3.4 Cost Estimation of Prepared Membranes

In general, ceramic membranes are ten times costlier than polymer membranes. Conventional industrial scale polymeric membranes are available for \$50–200/m^2 [49] and ceramic membranes for \$500–2000/m^2 [50]. The thickness of the prepared membrane was 5 mm. The cost of the membrane per square meter is calculated on the basis of prices of the chemicals from corresponding companies (Table 3.11). The total material cost is varying from \$7.65/m^2 to \$65.61/m^2. Taking the cost of manufacturing and shipment, the cost may reach up to \$100 - 150/m^2, which is competitive to the cost of the polymer membranes.

Table 3.11. Cost analysis of the prepared membranes from the unit cost of raw materials.

Raw materials		Clay	Kaolin	Sodium carbonate	Sodium metasilicate	Boric acid	Total cost ($/m^2)
	Unit price ($/kg)	--	7.36	7.36	14.23	8.59	
Membrane A	Material required* (m^2/kg)	9.37	0.00	0.41	0.20	0.20	--
	Cost/m^2 ($)	--	0.00	3.00	2.90	1.75	7.65
Membrane B	Material required* (m^2/kg)	7.13	1.83	0.61	0.31	0.31	--
	Cost/m^2 ($)	--	13.50	4.50	4.35	2.62	24.97
Membrane C	Material required* (m^2/kg)	5.09	3.46	0.81	0.41	0.41	--
	Cost/m^2 ($)	--	25.50	6.00	5.80	3.50	40.79
Membrane D	Material required* (m^2/kg)	3.26	5.09	0.92	0.46	0.46	--
	Cost/m^2 ($)	--	37.49	6.75	6.52	3.94	54.70
Membrane E	Material required* (m^2/kg)	1.83	6.32	1.02	0.51	0.51	--
	Cost/m2 ($)	--	46.49	7.50	7.25	4.37	65.61

* 5 cm diameter and 5 mm thick membrane were prepared from 20 g material.

3.5 Conclusion

The aim of this work was to prepare microfiltration membranes from locally available clay and study the effect of inorganic precursors on the membrane morphology. Further the prepared membrane was applied for the removal of crystal violet dye by the hybrid process of advanced oxidation process followed by microfiltration. Five number of microfiltration membranes were prepared with different compositions of clay, kaolin and other binding materials. It was found that, with the increase of sintering temperature, pore size as well as permeability and flexural strength were increasing while porosity and pore density were decreasing. It was observed that initial average particle size of the membrane precursor is the key factor for controlling the pore size and pore density of the membrane. Pore size of membrane was related with average particle diameter [$D_{1,0}$], surface weighted mean diameter [$D_{3,2}$], volume weighted mean diameter [$D_{4,3}$] and specific area where as pore density was related with average particle diameter [$D_{1,0}$] and quartile ratio [$_{25}X_{75}$]. It can be concluded that pore diameter and density can be predicted directly from the particle size distribution of membrane precursors.

In the second stage of the work, carcinogenic crystal violet dye was removed successfully by a sequential combination of advanced oxidation process and microfiltration. Different ratios of the reactants (H_2O_2, $FeSO_4 \cdot 7H_2O$) were tried with 100 mg L^{-1} dye solution for finding the best combination. For total degradation of dye, ratios of the reactants were found as: $[H_2O_2]/[\text{Dye}] \geq 10$ and $[H_2O_2]/[FeSO_4] \leq 10$. The effects of the dye, ferrous sulfate heptahydrate and hydrogen peroxide concentration on the degradation of dye were studied. It was observed that the rate of degradation of the dye decreased with the increase of the dye concentration and increased with the increase in the concentration of $FeSO_4 \cdot 7H_2O$ and H_2O_2. It was observed that the AOP post-products were not settled down totally even after 24 h. Thus, microfiltration was applied for removal of the suspended solids. A membrane, prepared from clay and kaolin with average pore size of 0.31 µm was used for this work. The conductivity value were not changed (0.5 mmoh) whereas minute changes were observed for pH (6.41 to 6.18), TDS (360 mg L^{-1} to 350 mg L^{-1}) and density (999.7 kg m^{-3} to 997.1 kg m^{-3}) during microfiltration. The EDX and FTIR analyzation of the crystal violet and the membrane retentate clearly showed the oxidization of the aromatic group and chlorine from the dye molecular structure. After microfiltration, no suspended solid and dye was found in the permeate. Thus, the process flourished good promise for the treatment of wastewater containing dyes.

References:

1. C.S. Parnham; R.H. Davis, Protein recovery from bacterial cell debris using crossflow microfiltration with backpulsing. J. Membr. Sci. (1996) 118, 259-268.

2. 2. C. Song, T. Wang, Y. Pan, J. Qiu, Preparation of coal-based microfiltration carbon membrane and application in oily wastewater treatment. Sep. Purif. Technol. (2006) 51, 80-84.

3. B. K. Nandi, B. Das, R. Uppaluri, M. K. Purkait, Microfiltration of mosambi juice using low cost ceramic membrane. J. of Food Engg. (2009) 95, 597-605.

4. A. Urkiaga A.L. De L. Fuentes, M. Acilu, J. Uriarte Membrane comparison for wine clarification by microfiltration. Desalination. (2002) 148, 115-120.

5. J. Sikder, C. Pereira, S. Palchoudhury, K. Vohra, D. Basumatary, P. Pal, Synthesis and characterization of cellulose acetate-polysulfone blend microfiltration membrane for separation of microbial cells from lactic acid fermentation broth. Desalination. (2009) 249, 802-808.

6. M.C. Almandoz, J. Marchese, P. Prádanos, L. Palacio, A. Hernández, Preparation and characterization of non-supported micro-filtration membranes from aluminosilicates. J. Membr. Sci. (2004) 241, 95–103.

7. Y.H. Wang, X.Q. Liu, G.Y. Meng, Preparation of asymmetric pure titania ceramic membranes with dual functions. Matl Sci. Engg. (2007) 445-446, 611-619.

8. J.S. Reed, Principles of Ceramics Processing, 2nd Ed. John Wiley & Sons, (1995). NewYork.

9. K.A. DeFriend, M.R. Wiesner, A.R. Barron, Alumina and aluminate ultra-filtration membranes derived from alumina nanoparticles. J. Membr. Sci. (2003) 224, 11–28.

10. C. Falamaki, A.M. Shafiee, A. Aghaie, Initial sintering stage pore growth mechanism applied to the manufacture of ceramic membrane supports. J. Eur. Ceram. Soc. (2004) 24, 2285–2292.

11. Y.H. Wang, T.F. Tian, X.Q. Liu, G.Y. Meng, Titania membrane preparation with chemical stability for very hash environments applications. J. Membr. Sci. (2006) 280, 261–269.

12. S. Masmoudi, A. Larbot, H.E. Feki, R.B. Amara, Elaboration and characterisation of apatite based mineral supports for microfiltration and ultrafiltration membranes. Ceram. Int. (2007) 33, 337–344.

13. S. Khemakhem, A. Larbot, R. Ben Amar, New ceramic microfiltration membranes from Tunisian natural materials: Application for the cuttlefish effluents treatment. Ceram. Int. (2009) 35, 55-61.

14.B.K. Nandi, R. Uppaluri, M.K. Purkait, Preparation and characterization of low cost ceramic membranes for micro-filtration applications. Appl. Clay Sci. (2008) 42, 102–110.

15. N. Das, H.S. Maiti, Effect of size distribution of the starting powder on the pore size and its distribution of tape cast alumina microporous membranes. J. of Europ. Cer. Soc. (1999) 19, 341-345.

16. N. Saffaj, M. Persin, S.A. Younsi, A. Albizane, M. Cretin, A. Larbot, Elaboration and characterization of microfiltration and ultrafiltration membranes deposited on raw support prepared from natural Moroccan clay: application to filtration of solution containing dyes and salts, Appl. Clay Sci. (2006) 31 110–119.

17. S. Masmoudi, A. Larbot, H.E. Feki, R.B. Amara, Elaboration and characterisation of apatite based mineral supports for microfiltration and ultrafiltration membranes. Ceram. Int. (2007) 33 337–344.

18. M. Riera-Torres, C. Gutiérrez-Bouzán, M. Crespi., Combination of coagulation–flocculation and nanofiltration techniques for dye removal and water reuse in textile effluents. Desalination. (2010) 252, 53–59.

19. A. Adak, M. Bandyopadhyay, A. Pal, Removal of crystal violet dye from wastewater by surfactant-modified alumina. Sep. Purif. Technol. (2006) 44, 139-144.

20.P. Cooper, Removing colour from dye house wastewaters—a critical review of technology available. J. Soc. Dyers Colourists. (1993) 109, 97-100.

21. S. Netpradit, P. Thiravetyan, S. Towprayoon, Application of 'waste' metal hydroxide sludge for adsorption of azo reactive dyes. Water Res. (2003) 37, 763-772.

22. H.L. Liu, Y.R. Chiou, Optimal decolorization efficiency of reactive red 239 by UV/ZnO photocatalytic process. J. Chin. Inst. Chem. Eng. (2006) 37, 289.

23. E.G. Solozhenko, N.M. Soboleva, V.V. Goncharuk, Decolourization of azo dye solutions by Fenton's oxidation. Water Res. (1995) 29, 2206-2210.

24. C. Allegre, P. Moulin, M. Maisseu, F. Charbit, Treatment and reuse of reactive dyeing effluents. J. Membr. Sci. (2006) 269, 15-34.

25. I.K. Kapdan, F. Kargi, Simultaneous biodegradation and adsorption of textile dyestuff in an activated sludge unit. Process Biochem. (2002) 37, 973-981.

26. C.A. Buckley, Membrane technology for the treatment of dyehouse effluents. Water Sci. Technol. (1992) 25, 203-209.

27. I. Koyuncu, Reactive dye removal in dye/salt mixtures by nanofiltration membranes containing vinylsulphone dyes: effects of feed concentration and cross flow velocity. Desalination. (2002) 143, 243-253.

28. J.S. Wu, C.H. Liu, K.H. Chu, Removal of cationic dye methyl violet 2B from water by cation exchange membranes. J. Membr. Sci. (2008) 309, 239-2445.

29. M.S. Lucas, A.A. Dias, A. Sampaio, A. Amaral, Degradation of a textile Azo dye by a combined chemical-biological process: Fenton's reagent-yeast. Water research. (2007) 41, 1103-1109.

30. I. Arslan-Alaton, B.H. Gursoy, J. Schmidt, Advanced oxidation of acid and reactive dyes: Effect of Fenton treatment on aerobic, anoxic and anaerobic processes. Dyes and Pigments. (2008) 78, 117-130.

31. O. Legrini, E. Oliveros, A.M. Braun, Photochemical processes for water treatment. Chem. Rev. (1993) 93, 671–698.

32. C. Walling, Intermediates in the reactions of Fenton type reagents. Acc. Chem. Res. (1998) 31, 155–157.

33. X. Tan, N.N. Kyaw, W.K. Teob, K. Li., Decolorization of dye-containing aqueous solutions by the polyelectrolyte-enhanced ultrafiltration (PEUF) process using a hollow fiber membrane module, Sep. Purif. Technol. (2006) 52, 110–116.

34. K.M. Nowak, T. Winnicki, Decolorization of dye solutions by continuous ultrafiltration. Desalination. (1986) 60, 59-66.

35. S. Yu, M. Liu, M. Ma, M. Qi, Z. Lü, C. Gao, Impacts of membrane properties on reactive dye removal from dye/salt mixtures by asymmetric cellulose acetate and composite polyamide nanofiltration membranes. J. Membr. Sci. (2010) 350, 83-91.

36. S. Chakraborty, S. De, J.K. Basu, S. DasGupta, Treatment of a textile effluent: Application of a combination method involving adsorption and nanofiltration. Desalination. (2005) 174, 73–85.

37. C.A. Basar, C. Aydiner, S. Kara, B. Keskinler, Removal of CrO_4 anions from waters using surfactant enhanced hybrid PAC/MF process. Sep. Purif. Technol. (2006) 48, 270-180.

38. S. Mozia, M. Tomaszewska, A.W. Morawski, Removal of azo-dye Acid Red 18 in two hybrid membrane systems employing a photodegradation process. Desalination. (2006) 198, 183–190.

39. P. Banerjee, S. DasGupta, S. De, Removal of dye from aqueous solution using a combination of advanced oxidation process and nanofiltration. J. Hazar. Mat. (2007) 140, 95-103.

40. E. Neyens, J. Baeyens, A review of classic Fenton's peroxydation as an advanced oxidation technique. J. Hazardous Mat. (2003) 98, 33-50.

41. G.M. Merkus, Particle Size Measurements: Fundamentals, Practice, Quality, Springer., 2009.

42. Y. Liu, B.H. Han, Y.T. Chen, Molecular Recognition and Complexation Thermodynamics of Dye Guest Molecules by Mdified Cyclodextrins and Calixarenesulfonates. J. Phys. Chem. B. (2002) 106, 4678-4687.

43. Y.F. Chena, M.C. Wang, M.H. Hon, Phase transformation and growth of mullite in kaolin ceramics. J. Afr. Earth Sci. (2006) 46, 245–252.

44. L. Löffler, W. Mader, Anisotropic X-ray diffraction peak broadening and twinning in diaspore-derived corundum. J. Europ. Ceram. Soc. (2005) 25, 639-648.

45. W. Chesworth, Encyclopedia of Soil Science. Springer, 2008.

46. T. Allen, Particle size measurement, Chapman & Hall, London, New York, 1981.

47. A.S. Jönsson, G. Trägårdh, Ultrafiltration applications. Desalination. (1990) 77, 135-179.

48. P. Westerhoff, H. Moon, D. Minakata, J. Crittenden, Oxidation of organics in retentates from reverse osmosis wastewater reuse facilities. Water research. (2009) 43, 3992–3998.

49. B.D. Bhide, S.A. Stern, A new evaluation of membrane processes enrichment of air. II. Effects of economic membrane properties. J. Membr. Sci. (1991) 62, 37–58.

50. W.J. Koros, R. Mahajan, Pushing the limits on possibilities for large scale gas separation: which strategies? J. Membr. Sci. (2000) 175, 181–196.

Chapter IV

Preparation of chitosan impregnated ultrafiltration membrane and application for the removal of arsenic and mercury by polymer enhanced ultrafiltration

4.1 Introduction and Literature Survey

The uses of ultrafiltration membranes are gaining a lot of interest now-a-days due to their higher selectivity, permeation rate, and chemical and thermal stability. In recent years, various UF membranes were synthesized with very good structural integrity, fouling resistance and high selectivity. These membranes were not tried industrially due to the high cost of the support (1600 $/m^2 to 20,000 $/m^2) [1]. Generally, the ceramic supports were prepared from alumina, kaolin, ball clay and quartz [2]. So there is a need to look for alternative low-cost materials for preparing the ceramic support so as to make the prepared membrane commercially competitive.

The composite UF membranes constitute of different types of thin polymeric layers such as; polysulfone [3], styrene acrylonitrile [2], cellulose acetate [4], polyvinyl acetate, polyvinyl pyrrolidone [5], polydimethylsiloxane [6]. Chitosan, which is an amino polysaccharide with many reactive amino and hydroxyl group, is a promising precursor for UF membrane preparation. During crosslinking with glutaraldehyde, solubility of chitosan is decreased sharply and hydrophilicity increased which are very important factors for a membrane precursor [7]. This chapter focused on the preparation of chitosan based ultrafiltration membrane using low cost ceramic support.

To prepare the UF top layer over the ceramic support, many techniques were reported such as spray coating [4], grafting [5], spin coating [8], self assembly [9], dip coating [4] and vapor deposition [10]. Among these methods, dip coating is simple, inexpensive and thus most desirable choice for industrial purpose. UF membranes were used for the removal of high molecular weight substrate, oil from water, colloidal material, polymer molecules and organic-inorganic pollutants.

Pollution due to the discharge of heavy metals to water bodies is one of the serious environmental problems worldwide. Metals like mercury and arsenic are found in industrial effluents and in groundwater and pose serious threats to the environment. These pollutants are not only non-biodegradable but are toxic even at low concentration. The general methodologies for removal of mercury ions (safe limit 2 ppb) from aqueous solution are absorption [11], chelation-enhanced method [12] and electrocoagulation [13]. Arsenic (safe limit 10 ppb) was separated by inorganic and organic adsorbents [14] including bioadsorbents [15]. However, these methods have several disadvantages like incomplete metal removal, generation of toxic sludge or other waste materials which require disposal and further treatment or consume huge reagent and energy [16]. Reverse osmosis (RO) provides an excellent substitute method for removal of these metals from aqueous solutions [17], but the process suffers due to its lower flux and requirement of higher pressure. A combined method that comprises chelation followed by ultrafiltration may be used to overcome these problems. This hybrid process was widely used from late 1960s [18]. Many researchers studied this process for the purification of metal ions by suitable water-soluble macromolecular substrates [19, 20]. Canizares et al. have studied the recovery of heavy metals like Cu (II), Ni (II), Pb (II) and Cd (II) from industrial wastewaters by polyethyleneimine (PEI) and poly (acrylic) acid (PAA). They have used an UF ceramic membrane and obtained an almost metal free permeate [12]. Another report described the removal of Ni and Co up to 95.0 % and 99.9 % respectively by UPM-20 membrane using PEI as the chelating agent [20].

The crux of the method follows the addition of a higher molecular weight polymer (a chelating agent) into the solution of the ions of metal to be separated. Size of the chelating complexes is much greater than that of the unbounded ions and sufficient to be retained by an UF membrane. The solution is then ultrafiltered through an appropriate membrane selected to ensure good rejection of the chelating complexes so that a metal ion–free permeate is obtained. This method may be termed as polymer assisted ultrafiltration (PAUF) or polymer enhanced ultrafiltration (PEUF). The key advantage of this method is high selectivity by virtue of the use of selective polymer and high productivity at insignificant power consumption.

In this work, ‘Membrane B’ of Chapter III was used as the support for the preparation of chitosan based ultrafiltration ceramic membrane. Glutaraldehyde was used as the crosslinking agent and the crosslinked chitosan was deposited on the top surface of the ceramic support by dip coating method. The chitosan concentration (1.0 %, 1.5 % and 2.0 %) and dipping time (240 s, 480 s and 720 s) were

varied during the dip coating process. Characterizations of the support and the membranes were done using thermogravimetric analysis (TGA), scanning electron microscopy (SEM) and hydraulic permeability (both air and water) measurement. The crosslinking of chitosan with glutaraldehyde was investigated by Fourier transform infrared spectroscopy (FTIR) and differential scanning calorimetry (DSC) analysis. The membrane with 2.0 % chitosan concentration and 720 s dipping time (pore size 13 nm) was used for the removal of low concentration (up to 1000 μg L^{-1}) mercury and arsenic from wastewater by PEUF using polyvinyl alcohol (PVA) as the chelating agent. The performance of PEUF was observed in terms of permeate flux and rejection of both metal and PVA. SEM and EDX of the membrane surface before and after UF experiment were also carried out to ensure the deposition of heavy metal and PVA over membrane surface. Another study was done on the removal of higher concentration of mercury (up to 60 mg L^{-1}) with another membrane prepared by 2.0 % chitosan concentration and 800 s dipping time (pore size 12 nm). The effect of pH on the rejection efficiency was also studied. Finally, a comparative study of the removal of heavy metals using reverse osmosis (RO), nanofiltration (NF) and PEUF was reported.

4.2 Materials and Methods

4.2.1 Raw Materials

–150 mesh (sieve size 104 μm) clay powder (collected from IIT Guwahati campus), sodium metasilicate (Loba Chemie Pvt. Ltd.), sodium carbonate (Rankem, India), boric acid (Loba Chemie Pvt. Ltd.) and kaolin (CDH Pvt. Ltd.) were used for the preparation of membrane support. Total component analysis and preparation method of the clay powder were given in Chapter II. Each component has its individual role during membrane preparation. Kaolin provides low plasticity and high refractory properties to the membrane. Sodium metasilicate increases mechanical strength by creating silicate bonds. Sodium carbonate improves dispersion properties, thereby creating homogeneity. Boric acid also increases mechanical strength by creating metaborates during sintering. Chitosan (Hi Media Laboratories Pvt. Ltd., India) was used to produce the ultrafiltration top layer over the ceramic support by using acetic acid (Merck, India) and glutaraldehyde (Merck, India). Arsenic trioxide (Loba Chemie, India) and mercuric chloride (Merck, India) were used as the source of arsenic and mercury respectively. Polyvinyl alcohol (Loba Chemie Pvt. Ltd) with a molecular weight of 115 kDa was used as the chelating agent whereas, elemental iodine (Merck, India) and boric acid (Loba Chemie Pvt. Ltd.) were utilized

during the spectrometric determination of PVA. Potassium iodide (Merck, India), sodium borohydrate (Sisco Research Lab. Pvt. Ltd.) and stannous chloride (Merck, India) were used during the analysis of arsenic and mercury respectively using atomic absorption spectroscopy (AAS).

4.2.2 Preparation of the Ceramic Support and the Membranes

Disc shaped ceramic support (50 mm diameter and 5 mm thickness) was prepared from the composition given in Table 3.1 (Membrane B), by paste casting followed by sintering at 1000 ℃. The details of the preparation method were described in Chapter III. The membranes were prepared by impregnation of the crosslinked chitosan over the top layer of ceramic support using dip-coating technique. The chitosan solution (1–2 wt %) was prepared by dissolving chitosan flakes in a 2 wt% aqueous acetic acid solution. The solution was then mixed with 0.12 % (v/v) glutaraldehyde solution in 1:1 ratio and stirred for 1 min. During this step the crosslink reaction took place [21].

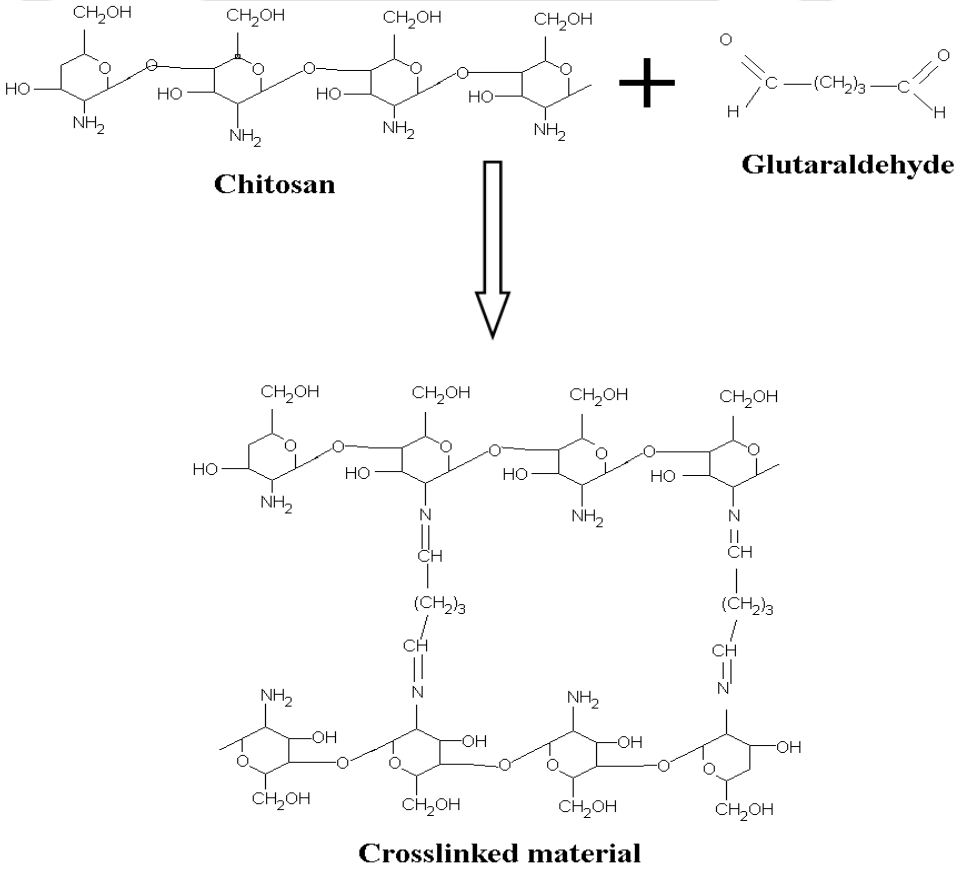

Figure 4.1. Mechanism for crosslinking of chitosan with glutaraldehyde.

The aldehyde groups of the glutaraldehyde form covalent imine bonds with the amino groups of chitosan, due to the resonance established with adjacent double ethylenic bonds via a Schiff reaction. The mechanism is described in Figure 4.1 [22].

To restrict the pore penetration of chitosan during the coating process, the ceramic support was dipped in water for 3-4 h before dip-coating. During this, all the air present in the porous structure inside the support was displaced by water. After taking out from water the support (except the top surface) was covered by aluminum foil for preventing chitosan deposition. Then, the support was placed in a 250 mL beaker and chitosan/glutaraldehyde solution was poured over it in such a way that the top surface was completely covered by the solution. The dipping time was varied from 240 s to 720 s. After the coating process, the membrane was taken out from the solution and dried at 100 ºC for 6 h in hot air oven for complete removal of water from the membrane. The nomenclature of various membranes fabricated with varying chitosan concentrations (1.0 %, 1.5 % and 2.0 %) and dipping time (240 s, 480 s and 720 s) are given in Table 4.1. Another membrane was prepared with 2.0 % chitosan concentration and 800 s dipping time for the removal of high concentration mercury.

Table 4.1. Nomenclature of the prepared composite membranes.

Time (s)	Chitosan concentration (weight %)		
	1%	1.5%	2%
240 s	M-1-240	M-1.5-240	M-2-240
480 s	M-1-480	M-1.5-480	M-2-480
720 s	M-1-720	M-1.5-720	M-2-720

4.2.3. Characterization of Glutaraldehyde Crosslinked Chitosan

Thermogravimetric analysis (TGA) and differential scanning calorimetry (DSC) studies of the crosslinked chitosan were performed to know its behavior under thermal application. TGA (Mettler-851e) experiments were done under inert atmosphere (nitrogen) and under air from 25 °C to 250 °C at the heating rate of 5 °C/min. Thermograms of chitosan and crosslinked chitosan were obtained using indium standards to calibrate the DSC (Mettler, Toledo – STAR^e System DSC 1/400) temperature and enthalpy scale. The samples were kept and sealed in aluminum pans and heated at a constant rate of 5 °C min^{-1}, over a temperature range of 25 to 450 °C. Inert atmosphere was maintained by purging nitrogen

at the flow rate of 100 mL min^{-1}. Fourier-transform infrared (Perkin Elmer, Model Spectrum one FTIR) spectra of the chitosan and crosslinked chitosan were obtained to assimilate the change in bonds during the crosslink reaction. The pellets were prepared on a KBr press and the spectra were scanned over the wave number range of 4000 to 400 cm^{-1}.

2.4. Characterizations of the Support and the Membrane

The characterization of both support and chitosan impregnated membranes were performed by scanning electron microscopic analysis and permeation experiments (air and water). The broad intension of the SEM (Make: Oxford; Model: LEO 1430VP) experiment was the morphological study aimed to evaluate the effect of dip coating parameters (solution concentration and dipping time) on ceramic matrix blocking and top layer growth as well as checking the sequential change of membrane morphology during dip coating process with respect to the coating parameters. SEM also detects the presence of surface/cross sectional defects such as pinholes and cracks (if any). Air flux characterization aims to quantify membrane morphological parameters such as average pore size and Viscous/Knudsen flux that contribute to transport. All the chitosan impregnated membranes were subjected to gas permeation test. The photograph of the gas permeation test experiment is shown in Figure 4.2.

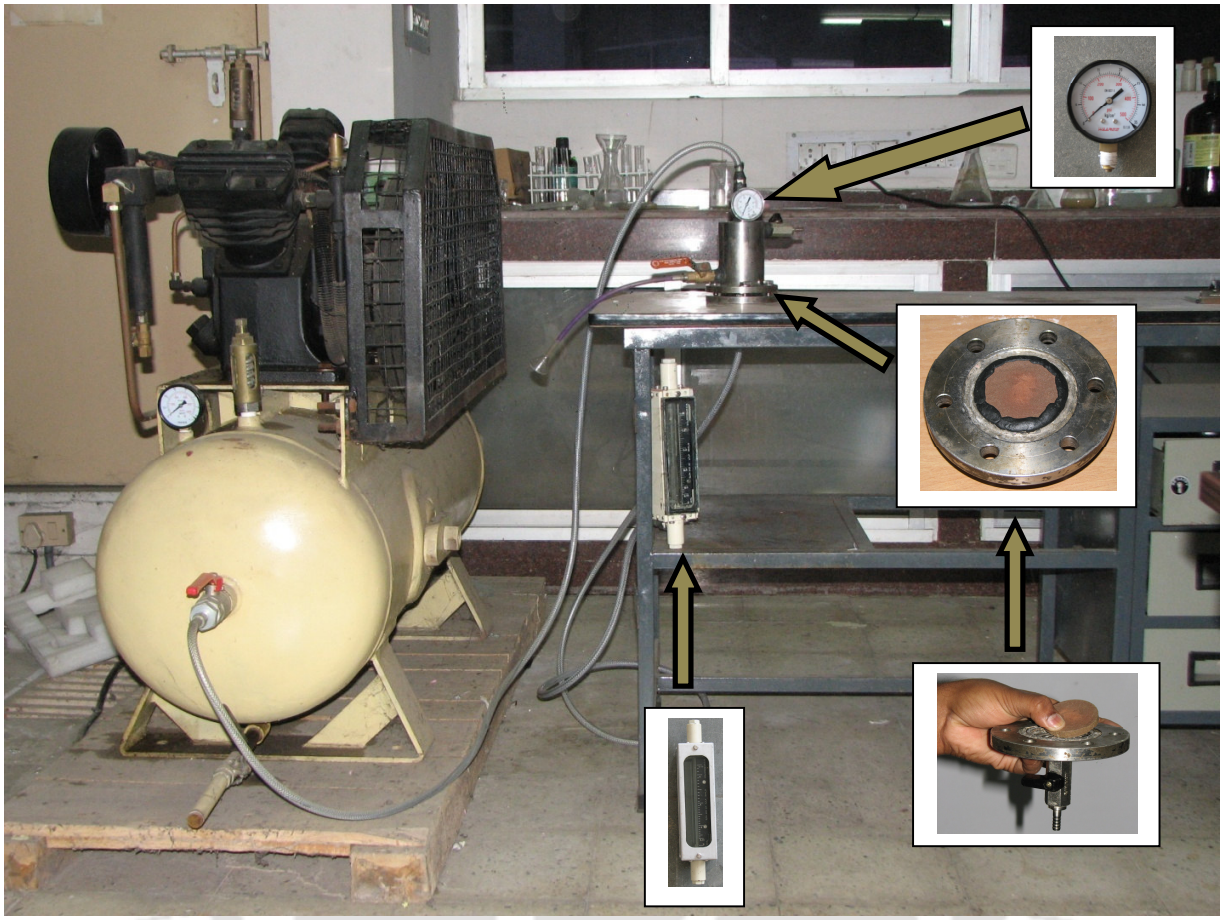

Figure 4.2. Photograph of the gas permeation experimental setup.

Based on the gas permeation data, average pore radius (r_g) can be estimated according to the following expression [4]:

$$K = 2.133\frac{r_g \cdot \nu \cdot \varepsilon}{l \cdot q^2} + 1.6\frac{r_g^{\,2} \cdot \varepsilon}{l \cdot \eta \cdot q^2} p \qquad (4.1)$$

where p is the average pressure on the membrane, ν (m/s) is the molecular mean velocity of the gas, l (m) is the pore length, q is the tortuosity, η (Pa s) is the viscosity of gas, K (m/s) is the effective permeability factor evaluated as:

$$K = \frac{Q \cdot P_2}{S \cdot \Delta P} \qquad (4.2)$$

where, S (m^2) is the permeable area of the membrane, Q (m^3/s) is the volumetric flow rate, P_2 is the membrane pressure at permeate side (Pa) and ΔP is the trans-membrane pressure drop (Pa). In Eq. (1), the first term corresponds to Knudsen permeance and the second term corresponds to the viscous permeance. Therefore, Eq. (1) can be represented as a straight line in a graph drawn between *K* and *p* where the slope and intercept represents the viscous and Knudsen permeability of the membrane respectively. Henceforth the values of the slope and intercept obtained from the graph can be used to evaluate the percentage contribution of pores (and pore sizes) that contribute towards viscous and Knudsen flow transport mechanisms. In other words, gaseous flux characterization of the ceramic support can yield qualitative information with respect to the pore size distribution applicable for the contribution of Knudsen or viscous flow regimes towards the overall ultrafiltration membrane flux. The average pore radius (r_g) of the membrane can be evaluated using the intercept (A) and slope (B) of the straight line expressed as:

$$r_g = 1.333\frac{B}{A}v\eta \qquad (4.3)$$

The hydraulic permeability experiments were conducted using deionized water and were determined by the following equation:

$$J = L_h \cdot \Delta P \qquad (4.4)$$

where, J is the liquid flux ($m^3m^{-2}s^{-1}$), L_h is the hydraulic permeability ($m^3m^{-2}s^{-1}kPa^{-1}$) and ΔP is the transmembrane pressure (kPa). The air and hydraulic permeability experiments were conducted in a dead end permeation cell. Details of the experimental set up were given in Chapter II. Chemical stability of the support and the chitosan impregnated membranes were investigated by measuring the weight loss, pore size, air and hydraulic permeability before and after acid and base treatment. The membranes were subjected to a solution of NaOH (0.075 M; pH~13.5) and HCl (0.075 M; pH~1.0) separately for 1 week under atmospheric condition. All the membranes were dried thereafter and the weight loss was measured. The characterization of all the membranes were performed as discussed in the preceding section.

2.5 Polymer Enhanced Ultrafiltration (PEUF)

The feed solutions were prepared by mixing required amount of PVA (chelating agent) and heavy metal (Arsenic trioxide/Mercuric chloride) in aqueous medium. The metal ion concentrations were taken as 1000 μg L^{-1}, 500 μg L^{-1} and 250 μg L^{-1} separately for arsenic and mercury. The concentrations were chosen in the orders which are generally found in groundwater. PVA was taken as 1.0 %, 0.5 % and 0.25 % (w/v). After mixing the required amount of PVA and heavy metal in aqueous solution, the mixture was kept in shaker for overnight to ensure the maximum diffusion of the metal ions towards the chelate compound. After that the solution was transferred to the ultrafiltration cell. The lowest pore size UF membrane (M-2-720) with pore size around 13 nm was used for all PEUF experiments. The experimental set up was a dead end permeation cell with 250 mL capacity with a membrane area around 12.56×10^{-4} m^2. The detailed description of the cell was shown in Chapter II. The experiments were conducted to observe the performance of the ultrafiltration membrane in terms of flux and rejection of metal ions. The effects of concentrations of PVA and metal ions on permeate flux and rejections were also investigated.

During the study for removal of high concentration of mercury also, the experiments were performed to observe the effect of the concentrations of both PVA and mercury and transmembrane pressure on the mercury removal efficiency. Thus, the first set of solutions were prepared with a fixed concentration of metal ion (30 mg/L) and varying PVA concentrations (1.0 %, 0.5 % and 0.25 %). Again, another set of solutions were prepared with a fixed PVA concentration (0.50 %) and varying metal ion concentrations (10 mg/L, 25 mg/L and 50 mg/L). After mixing the required amount of PVA and heavy metal in aqueous solution, the mixture was kept in a shaker for overnight to ensure the maximum transformation of the metal ions towards the chelate compound. All the above experiments were conducted at a fixed pH of 7.0. Further the Effect of pH on mercury rejection was studied by varying the pH and initial mercury concentration (30 mg L^{-1}), PVA concentration (0.50 %), transmembrane pressure (172.4 kPa) and time of operation (15 min) keeping constant.

During the experiment, permeate was collected from the bottom of the cell in different time intervals. For a particular time span, the collection time was taken as the midpoint of the particular time span. The collected sample was continuously measured by a digital weight balance to avoid the weight loss by evaporation and subsequently diluted before the analysis (the upper detection limit of the instrument is 20 μgL^{-1} for As and 40 μgL^{-1} for Hg). Atomic Absorption Spectra (Varian; AA240FS)

was used to determine the Hg and As concentrations. The concentration of PVA in the permeate was determined by spectrometric method using boric acid as complex formation agent and elemental iodine as the coloring agent [23]. The flux decline profiles and % rejections were determined at a constant pressure of 103.4 kPa. This was done by collecting permeate from the bottom and continuously measuring the cumulative mass. The cumulative masses were converted to cumulative volumes and from the slope of the cumulative volume versus time curve, the permeate flux was obtained as a function of operating time. The percent rejection (R) of heavy metals and PVA were calculated with respect to time for all the experiments using following formula:

$$R = \left(1 - \frac{C_f}{C_i}\right) \times 100 \qquad (4.5)$$

where, C_i is the initial concentration (µg/L) and C_f is the final concentration (µg/L). The SEM and EDX analysis of the membrane surface before and after PEUF were also obtained to verify the deposition of heavy metals and PVA over the surface of the membrane. Finally, the membranes were washed in hot water to remove the deposited PVA from the surface and dried. Then, the pure water fluxes of these membranes were compared with that of the unused membranes.

4.3 Results and Discussions

4.3.1. Analysis of the Coating Material

Thermal stability: The TGA analysis of coating material under air and inert atmosphere was presented in Figure 4.3. It was evident from the figure that there was no difference in weight loss pattern of the crosslinked material under both the conditions which proves the non-reactivity of the material with air even at higher temperature. Up to 100 °C, a sharp weight loss was observed (16.4 % and 14.9 % for air and inert atmosphere, respectively) which can be attributed to the loss of free water and afterwards between 100 °C to 200 °C, the mass loss was marginal (3.79 % and 4.46 % for air and inert atmosphere respectively). This mass loss was due to the loss of bonded water. And finally, after 200 °C, huge fall in the graph was observed. Thus the acceptable limit for the prepared membrane can be taken as 200 °C.

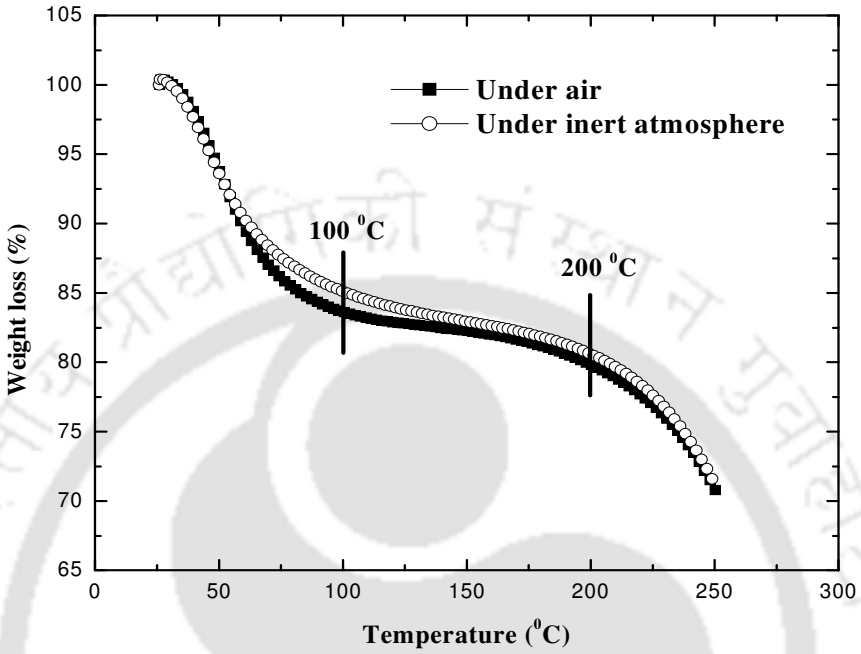

Figure 4.3. Thermogravimetric analysis of the coating material (chitosan crosslinked with glutaraldehyde) under inert atmosphere (Ar) and air.

DSC studies were performed to compare the hydrophilicity and the thermal stability of the crosslinked chitosan with raw chitosan. Generally, primary and supra molecular structures make the polysaccharide molecules hydrophilic. In the DSC graph (Figure 4.4), the endotherm of chitosan was seen at the 103.7 °C with the enthalpy of fusion (ΔH) 453.4 Jg^{-1}. On the contrary, for crosslinked chitosan, the endotherm was observed at 86.2 °C with the enthalpy of fusion 623.6 Jg^{-1}. Thus, the hydrophilicity of chitosan increased during the crosslinking reaction. Another observation was that, the temperature for occurrence of endotherm is decreased which can be due to the release of the absorbed moisture at lower temperature for the crosslinked chitosan. On the basis of these results it can be stated that polar groups increased and crystalline domains reduced during crosslinking. The second thermal event observed for chitosan at 303.0 °C as an exotherm due to the decomposition of the polymer with a ΔH value of 11.3 Jg^{-1}. No such peak was found for the crosslinked chitosan. So, it can be concluded that the crosslinked chitosan was more thermally stable than raw chitosan.

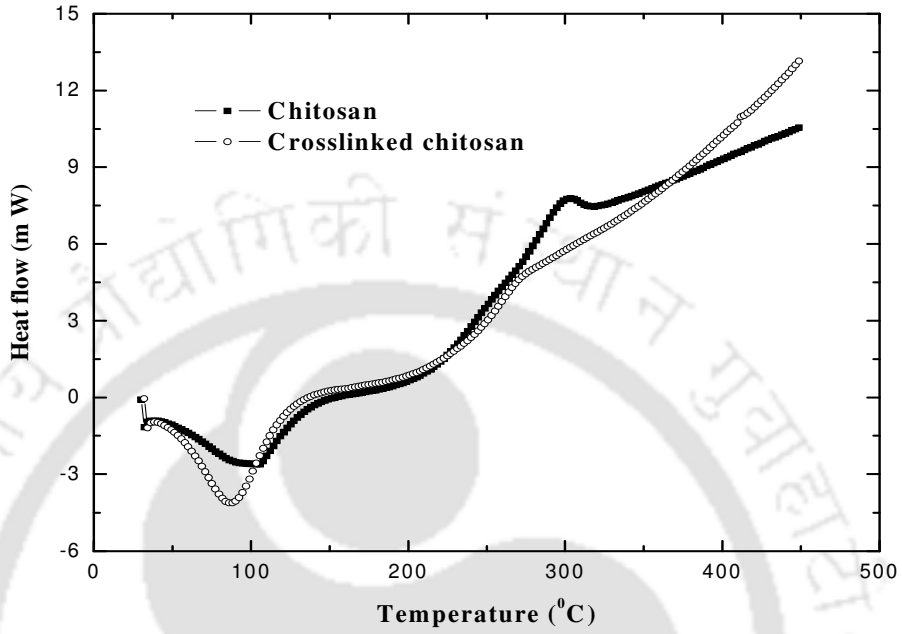

Figure 4.4. Differential scanning calorimetry of chitosan and the coating material (chitosan crosslinked with glutaraldehyde).

***FTIR Analysis*:** The FTIR spectra of chitosan and glutaraldehyde crosslinked chitosan were shown in Figure 4.5 and the bands analysis was given in Table 4.2. A characteristic band around 3429 cm^{-1} representing $–NH_2$ and –OH stretching were seen for both the chitosan and glutaraldehyde crosslinked chitosan. Another band around 1641 cm^{-1} which was present in raw chitosan was missing in the crosslinked chitosan that was attributed to the bending vibration of 1° amine. Furthermore, the crosslinked chitosan displayed two bands around 2923 cm^{-1} and 1637 cm^{-1} which can be ascribed to the C–H stretching of the secondary alcoholic groups and NH_2 bend respectively. This confirmed the occurrence of crosslinking reaction of glutaraldehyde with NH_2 groups present in chitosan. Other researcher also reported similar FTIR trend for the crosslinked reaction of chitosan with tannic acid [24].

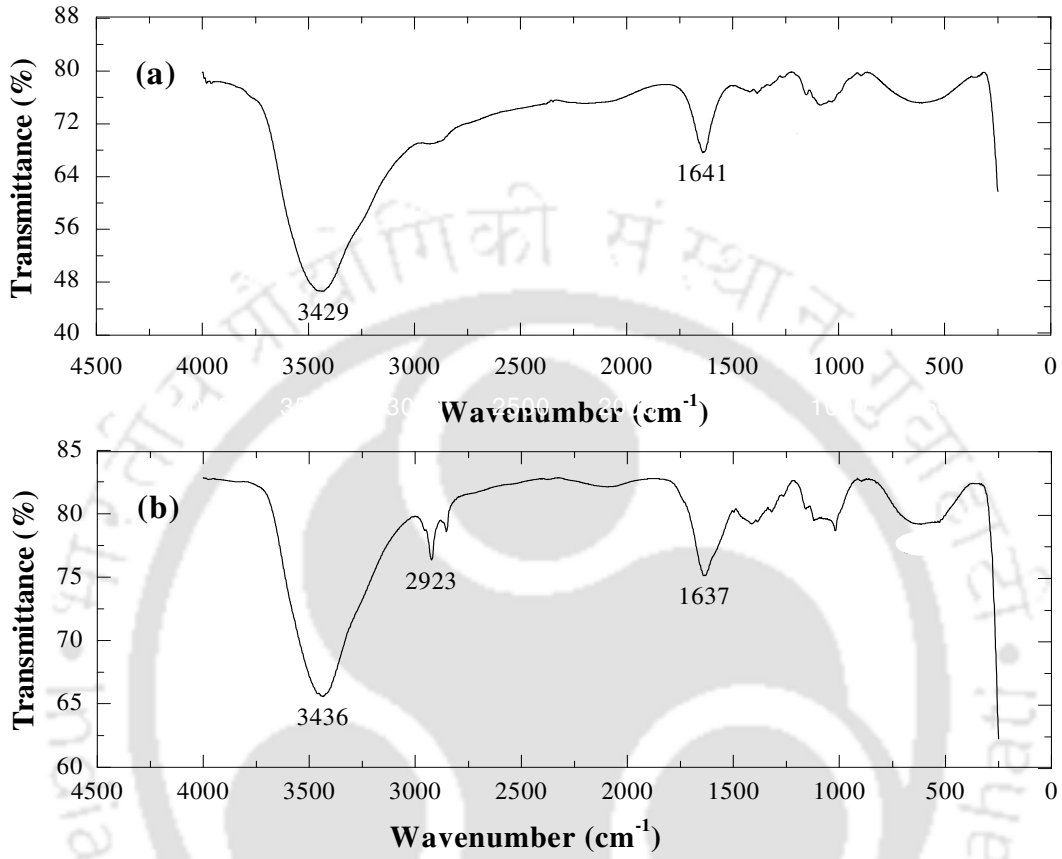

Figure 4.5. FTIR analysis of the (a) Chitosan and (b) Chitosan crosslinked with glutaraldehyde.

Table 4.2. FTIR band analysis of chitosan and glutaraldehyde crosslinked chitosan.

Band Frequency (cm^{-1})	Chitosan	Crosslinked Chitosan	Band assessments
3429	Present	Present	– NH_2
2923	Not present	Present	C – H stress
1641	Present	Not present	bending vibration of 1° amine
1637	Not present	Present	NH_2 bend

4.3.2 Characterizations of the Chitosan Impregnated Membranes

Morphological assessment: The SEM micrographs of the ceramic support and chitosan impregnated membranes are presented in Figure 4.6. From the figure it was clear that the surface of the support was covered with the coating material during the process. The extent of coating increased with the concentration of chitosan and duration of coating. From the images of 1.0 % chitosan coated membranes, it was seen that the large pores of the ceramic support was partially covered by the coating material, whereas the extent of coating was increased with time. For 1.5 % chitosan coating, a thin layer appeared over the top surface. Again, for 2.0 % chitosan coating, not only the total surface was covered by the coating material but also additional cluster of coating materials were noticed in some locations. It was thus concluded that the effective pore size of the chitosan impregnated membranes were reduced with increase in chitosan concentration as well as dipping time. It was also clear from the SEM images that there were no cracks or discontinuous coating over the membrane surfaces.

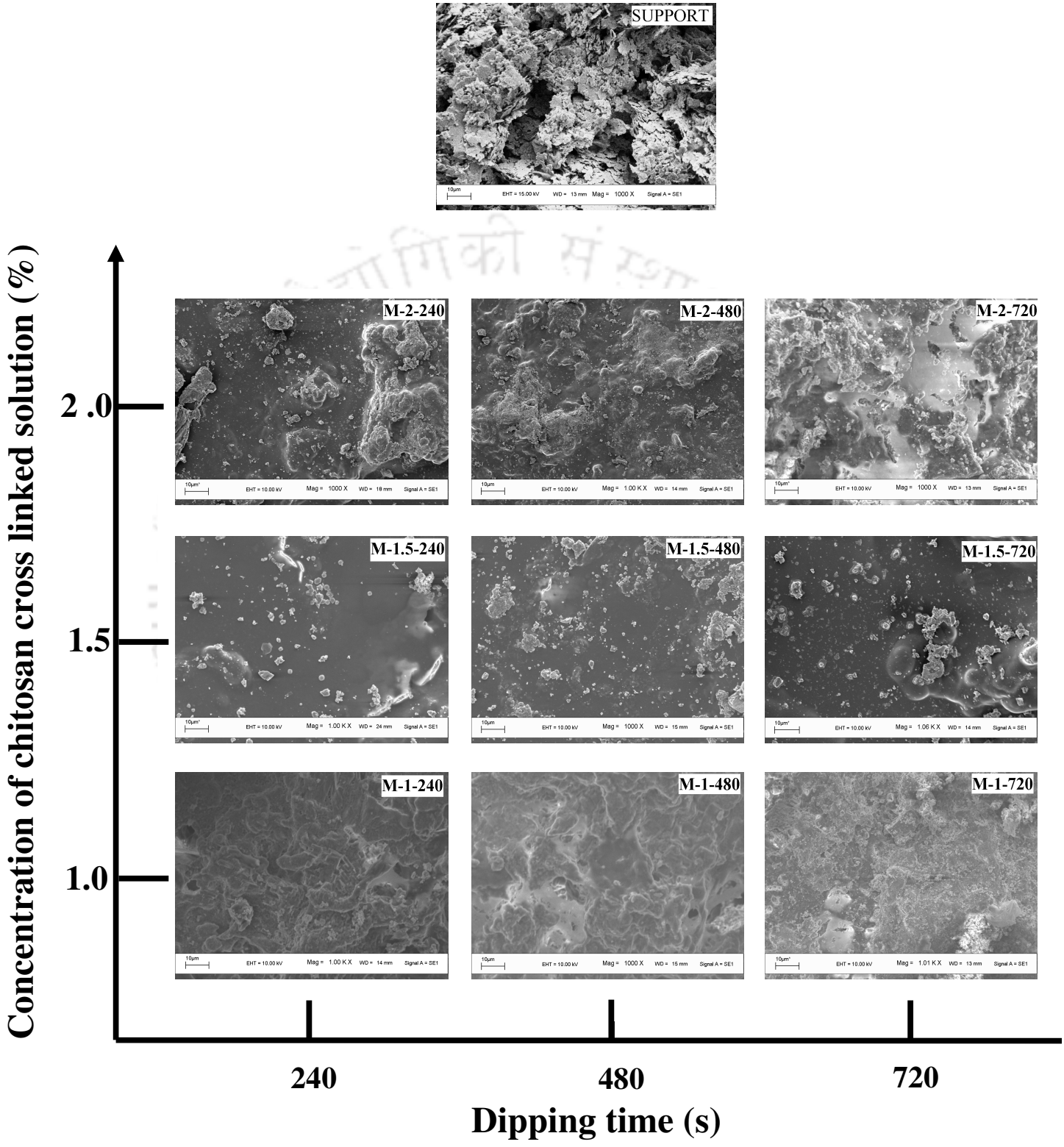

Figure 4.6. SEM micrographs of the top surface of ceramic support and different composite membranes.

Gas permeation:

Figure 4.7 shows the variation of effective permeability factor (K) with average pressure (*p*) for the support and all coated membranes. Table 4.3 summarizes parameters evaluated from the graphical analysis of transmembrane flux data. As shown in the table, the permeability of the support was found to be 6.90×10^{-1} $m^3m^{-2}kPa^{-1}s^{-1}$ and that of for different chitosan impregnated membranes were varied from 3.19×10^{-1} $m^3m^{-2}kPa^{-1}s^{-1}$ to 3.38×10^{-3} $m^3m^{-2}kPa^{-1}s^{-1}$. The average pore size of the support was found to be 1093 nm and that of for chitosan impregnated membranes were varied from 760 to 13 nm. Another observation was that with the increase in the chitosan concentration and dipping time, the contribution of viscous flux decreased and Knudsen flux increased. Viscous flux decreased from 75 % (M-1-240) to 6 % (M-2-720) and Knudsen flux increased from 25 % (M-1-240) to 94 % (M-2-720). This was due to the decrease in the pore sizes with the increase in the chitosan concentration and dipping time, which was confirmed from SEM images also. Nandi et al. also reported similar trend for the membranes prepared by dip coating of cellulose acetate over ceramic support [4].

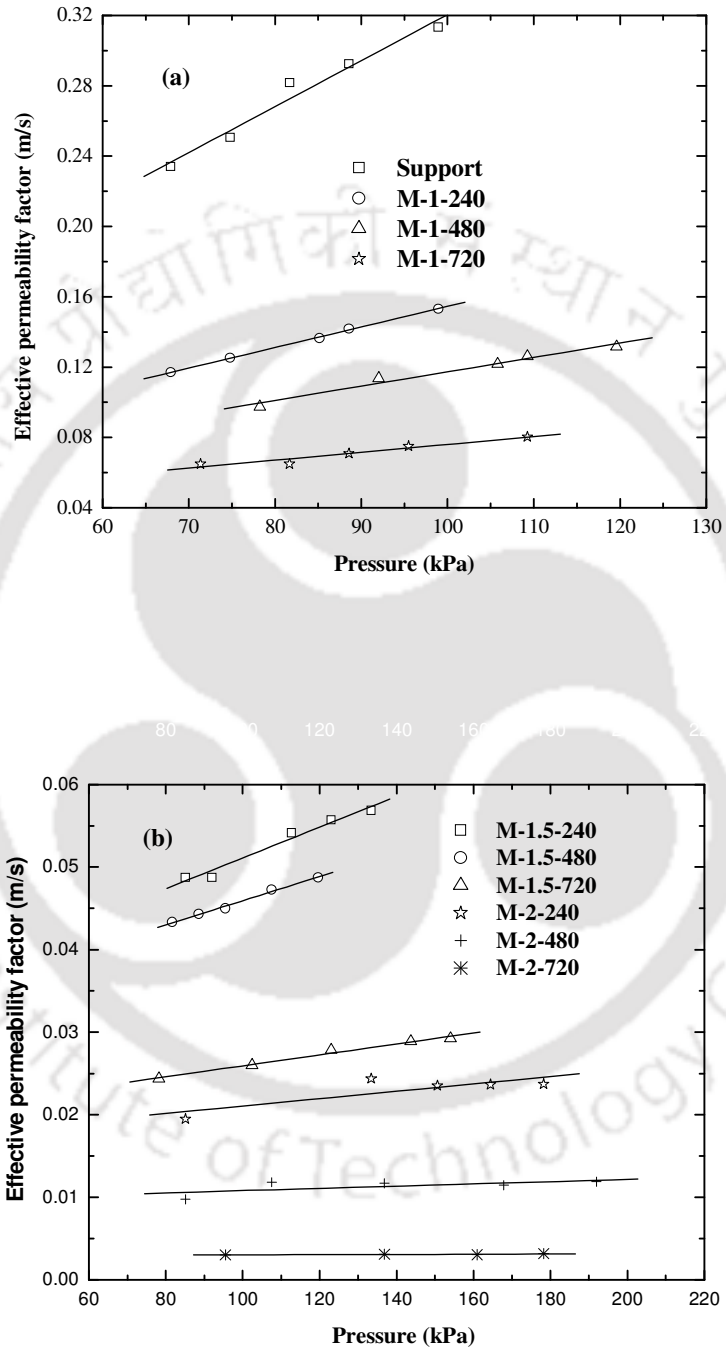

Figure 4.7. Variation of effective permeability factor (K) with average pressure (p) for (a) Support, M-1-240, M-1-480 and M-1-720 and (b) M-1.5-240, M-1.5-480, M-1.5-720, M-2-240, M-2-480, M-2-720.

Table 4.3. Various parameters evaluated from graphical analysis of gas permeation result.

Membrane type	Slope ($\times10^7$) ($m.s^{-1}Pa^{-1}$)	Intercept ($\times10^2$) ($m.s^{-1}$)	Air permeability* ($m^3m^{-2}kPa^{-1}s^{-1}$)	Pore size (nm)	Viscous flux (%)	Knudsen flux (%)
Support	26.15	5.89	6.90×10^{-01}	1093	60 – 81	19 – 40
M-1-240	11.67	3.78	3.19×10^{-01}	760	52 – 75	25 – 48
M-1-480	8.15	3.59	2.33×10^{-01}	560	56 – 76	24 – 44
M-1-720	4.45	3.15	1.39×10^{-01}	348	37 – 62	38 – 63
M-1.5-240	1.87	3.24	7.75×10^{-02}	142	28 – 49	51 – 72
M-1.5-480	1.46	3.13	6.65×10^{-02}	115	22 – 39	61 – 78
M-1.5-720	0.66	1.93	3.52×10^{-02}	85	16 – 41	59 – 84
M-2-240	0.45	1.66	2.75×10^{-02}	66	12 – 35	65 – 88
M-2-480	0.14	0.94	1.28×10^{-02}	36	09 – 30	70 – 91
M-2-720	0.02	0.29	3.38×10^{-03}	13	06 – 15	85 – 94

*At 241.3 kPa transmembrane pressure.

Hydraulic permeability: From the hydraulic permeabilities (Figure 4.8) it was observed that the permeability decreased with the chitosan concentration and dipping time. For 1.0 % chitosan concentration, the permeability was decreased from 1.01×10^{-8} $m^3m^{-2}Pa^{-1}s^{-1}$ to 5.83×10^{-9} $m^3m^{-2}Pa^{-1}s^{-1}$ with an increase in the dipping time of 240 s to 720 s. On the other hand, for 480 s dipping time, the permeability decreased from 8.37×10^{-9} $m^3m^{-2}Pa^{-1}s^{-1}$ to 1.23×10^{-10} $m^3m^{-2}Pa^{-1}s^{-1}$ with the increase in the chitosan concentration of 1.0 % to 2.0 %. This was due to the fact that, with increase in both dipping time and chitosan concentration, the average pore size of the membrane decreased and top layer thickness increased. The hydraulic permeability was observed to be lesser than the air permeability for the same membrane. This was due to the higher density and viscosity of water with respect to air.

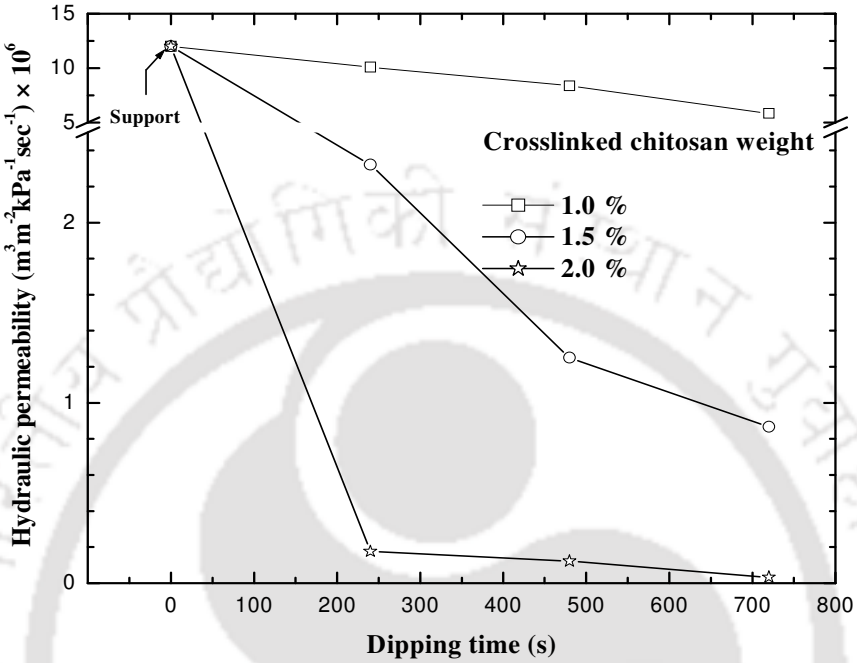

Figure 4.8. Hydraulic permeabilities of the prepared composite membranes.

Chemical resistivity: Table 4.4 summarizes the variations in different membrane parameters for the ceramic support and the chitosan impregnated membranes after acid and base treatments. It was found that the pore size, air and hydraulic permeabilities were slightly increased after both acid and base treatment. The mass loss of the support was found to be 5.37 % in acid solution and 6.89% in basic solution. For chitosan impregnated membranes, the mass loss was varied from 5.39 % (M-1-240) to 5.72 % (M-2-720) in acid solution and 6.89 % (M-1-240) to 7.44 % (M-2-720) in basic solution. Theoretically, the change of water permeabilities (in %) were proportional to the square of changes of pore size, because, both values increased with pore area, assuming the pores are cylindrical and the thickness of the membrane did not change during chemical treatment. Comparing the air permeability of the membranes before treatment (from Table 4.3), it was found that the air permeabilities of M-1-240 and M-2-720 were changed from 3.19×10^{-1} $m^3m^{-2}kPa^{-1}s^{-1}$ and 3.38×10^{-3} $m^3m^{-2}kPa^{-1}s^{-1}$ to 4.10×10^{-01} $m^3m^{-2}kPa^{-1}sec^{-1}$ and 4.38×10^{-02} $m^3m^{-2}kPa^{-1}sec^{-1}$ for acid treatment and 4.30×10^{-01} $m^3m^{-2}kPa^{-1}sec^{-1}$ and

6.77×10^{-02} $m^3m^{-2}kPa^{-1}sec^{-1}$ for base treatment, respectively. The water permeability of M-1.5-480 was changed from 1.25×10–6 $m^3m^{-2}kPa^{-1}sec^{-1}$ to 3.38×10^{-06} $m^3m^{-2}kPa^{-1}sec^{-1}$ and 4.14×10^{-06} $m^3m^{-2}kPa^{-1}sec^{-1}$ for acid and base treatment respectively. Although the lower pore size membranes showed some changes in terms of pore size and permeabilities during acid and base treatment, however they were very marginal. Moreover, in real life practice, PEUF usually never carried out in such harsh conditions.

Table 4.4. Variation of different membrane parameters after chemical treatment.

After acid treatment				
Membrane	Weight loss (%)	Pore size (nm)	Air permeability* ($m^3m^{-2}kPa^{-1}sec^{-1}$)×$10^2$	Water permeability ($m^3m^{-2}kPa^{-1}sec^{-1}$) ×$10^6$
Support	5.37	1211	73.0	12.7
M-1-240	5.39	888	41.0	11.5
M-1-480	5.40	682	32.0	10.3
M-1-720	5.41	465	22.6	7.08
M-1.5-240	5.43	252	13.3	3.90
M-1.5-480	5.45	222	11.6	3.38
M-1.5-720	5.49	184	9.51	2.74
M-2-240	5.55	158	7.94	2.27
M-2-480	5.62	126	6.12	1.72
M-2-720	5.72	96	4.38	1.19
After base treatment				
Membrane	Weight loss (%)	Pore size (nm)	Air permeability* ($m^3m^{-2}kPa^{-1}sec^{-1}$) ×$10^2$	Water permeability ($m^3m^{-2}kPa^{-1}sec^{-1}$) ×$10^6$
Support	6.89	1104	72.5	12.6
M-1-240	6.92	949	43.0	11.8
M-1-480	6.93	744	34.1	11.1
M-1-720	6.95	524	24.6	7.86
M-1.5-240	6.98	315	15.6	4.75
M-1.5-480	7.02	278	13.6	4.14
M-1.5-720	7.08	245	11.8	3.58
M-2-240	7.17	220	10.4	3.15
M-2-480	7.28	181	8.32	2.50
M-2-720	7.44	154	6.77	2.04

* At 241.3 kPa transmembrane pressure.

4.3.3. Removal of Low Concentration Mercury and Arsenic

***Permeate concentration of heavy metals*:** The effect of initial concentrations of PVA and metals on their removal efficiency were investigated separately and shown in Figures 4.9 and 4.10, respectively. Figure 4.9 (a) represents the permeate mercury concentration with respect to time (up to 2 h) at different PVA concentration. It was observed that, higher concentration of PVA lead to better removal. Complete removal was achieved for 1.0 % and 0.5 % PVA up to 2 h and 1 h of operation, respectively. On the other hand, mercury concentration of the permeate with 0.25 % PVA was found to be over safe limit of 2 μg L^{-1} even from the beginning of operation. This was due to the reason that the heavy metals were not directly rejected by UF membranes. The metal ions react with the PVA molecule to form chelate compound which were then separated by the UF membrane. Higher concentration of PVA lead to react with more number of mercury ions and further lowered mercury concentration in the permeate. The permeate concentration of mercury with respect to time (up to 2 h) for a fixed concentration of PVA (0.75 %) at different mercury concentration was shown in Figure 4.9 (b). It was found that the mercury concentration in permeate increased with higher feed concentration of mercury. This was due to the reaction of mercury ions with fixed concentration of PVA. For higher concentrations of mercury, all the ions did not react with the chelating agent thus not separated by UF membrane. For 250 μg L^{-1} and 500 μg L^{-1} feed concentrations, complete removal of mercury was observed up to 50 minutes of operation. Again, for 1000 μg L^{-1} feed concentration, the mercury concentration of permeate was found to be higher than the safe limit. It was evident from both the figures that the permeate mercury concentration increased with the progress of the experiment. This was due to the deposition of more chelate molecules over the membrane surface, leading to an increase in the membrane surface concentration (concentration polarization). This resulted in an increase in the convective transport of the mercury to the permeate side thereby increasing the permeate side concentration. Purkait et al. also reported similar trends for the removal of eosin dye by micellar enhanced ultrafiltration with cetylpyridinium chloride with a polyamide membrane of 1000 Da cutoff [25].

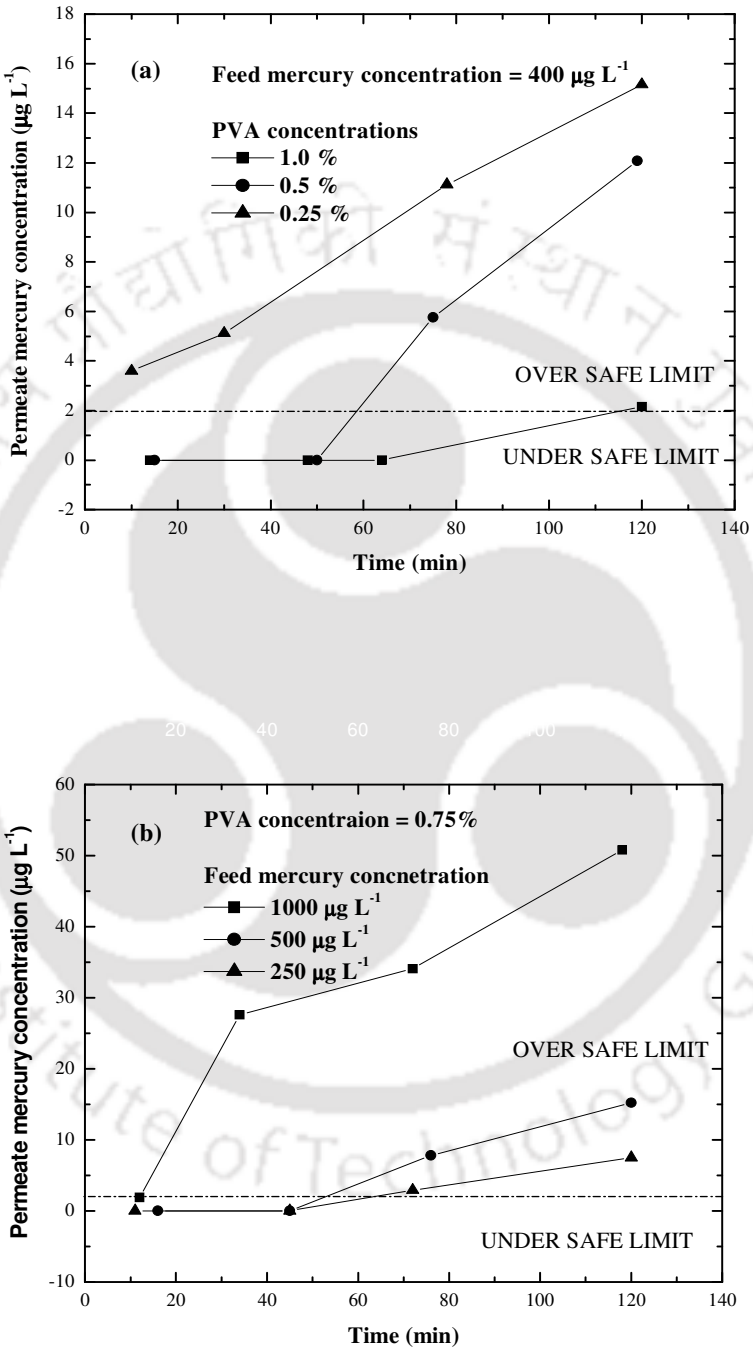

Figure 4.9. Concentration of mercury in permeate with respect to time. (a) Variation with PVA concentration, mercury: 400 µg L^{-1}, and (b) Variation with mercury concentration, PVA: 0.75 %.

Arsenic removal experiments also convey similar trends. Figure 4.10 (a) and 4.10 (b) represents permeate arsenic concentration with respect to time for a fixed concentration (400 µg/L) of arsenic by varying the concentrations of PVA and for a fixed concentration of PVA (0.75 %) by varying the concentration of feed arsenic concentration, respectively. For the first set of experiments, all the permeate solutions were found to be under safe limit. Among the second set of experiments, the permeate from 1000 µg L^{-1} feed concentration solution shown higher arsenic concentration than the safe limit of 10 µg L^{-1} after 46 min of the experiment. It can be concluded that 0.75% of PVA was optimum for the treatment of up to 500 µg L^{-1} of initial arsenic concentration. The reason behind the increase in permeate concentration with time was due to the increase in convective transport as discussed in case of mercury.

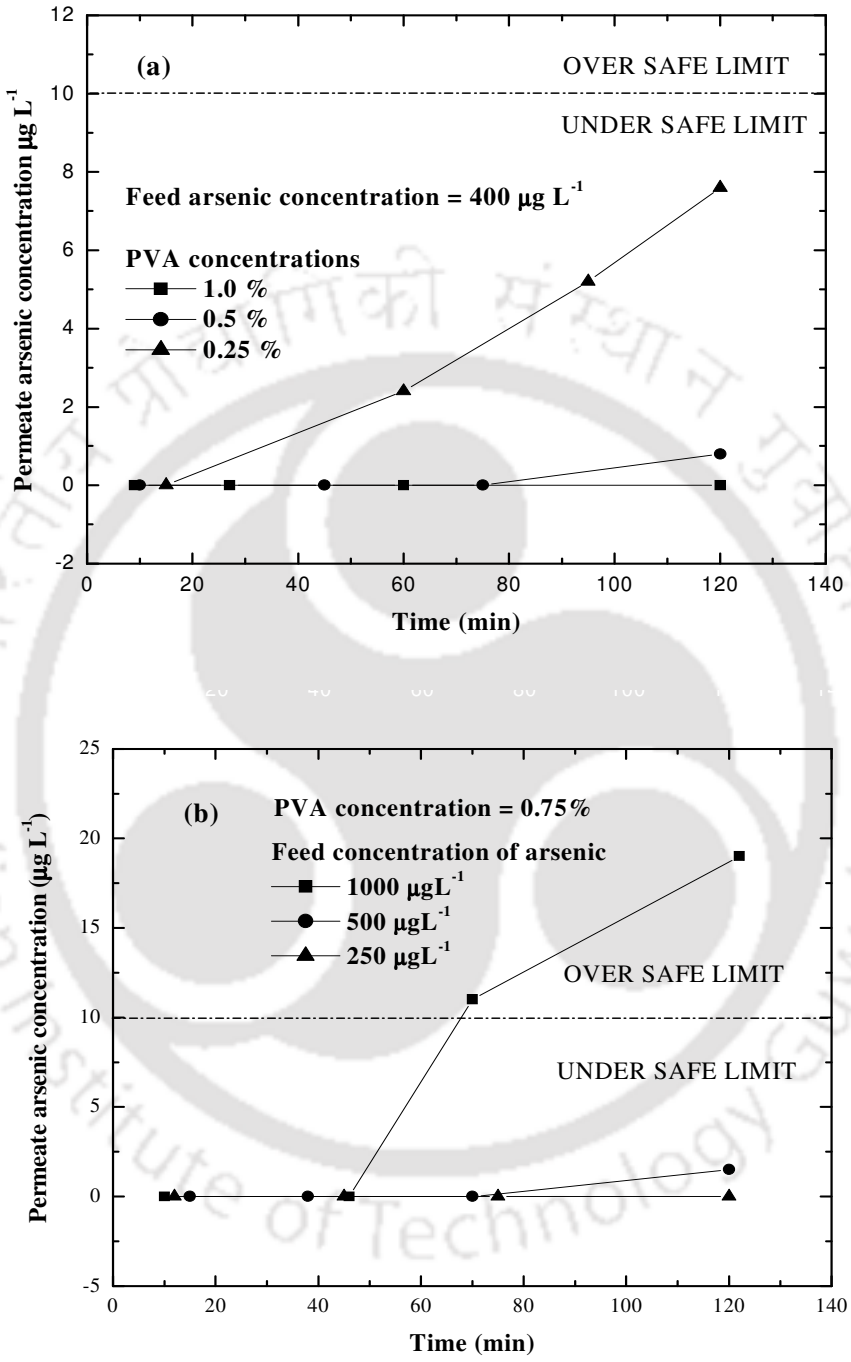

Figure 4.10. Concentrations of arsenic in permeate with respect to time. (a) Variation with PVA concentration, arsenic: 400 µg L^{-1}, and (b) Variation with arsenic concentration, PVA: 0.75 %.

Flux decline during the experiment: Before the experiment, the stable flux of the membrane (M-2-720) was observed as 3.44×10^{-06} $m^3m^{-2}s^{-1}$ for 103.4 kPa transmembrane pressure. During the experiment, the flux was observed to decrease slowly. From the flux decline profiles, two trends were observed. In Figure 4.11 flux decline profiles of 1.0 %, 0.5 % and 0.25% PVA with 1000 µg L^{-1} arsenic was reported whereas the flux decline trends were found to be independent of metal ion type and concentrations. This could be due to the very low concentration of metal ion with respect to that of PVA. Initially, the flux decreased very sharply and then the declination was gradual. The first phase flux declination was due to the concentration polarization and the second stage gradual decrease was due to gel formation over the membrane surface [26]. Another observation was that, the flux decline was more for higher concentration of PVA. The flux decreased to 2.19×10^{-8} $m^3m^{-2}s^{-1}$, 10.1×10^{-8} $m^3m^{-2}s^{-1}$, and 23.4×10^{-8} $m^3m^{-2}s^{-1}$ in 4823 s, 4287 s and 4401 s for 1.0 %, 0.5 % and 0.25 % PVA solutions, respectively. This was due to the increase in PVA concentration. At higher PVA concentration, more PVA molecules were deposited over the membrane surface resulting higher flux declination.

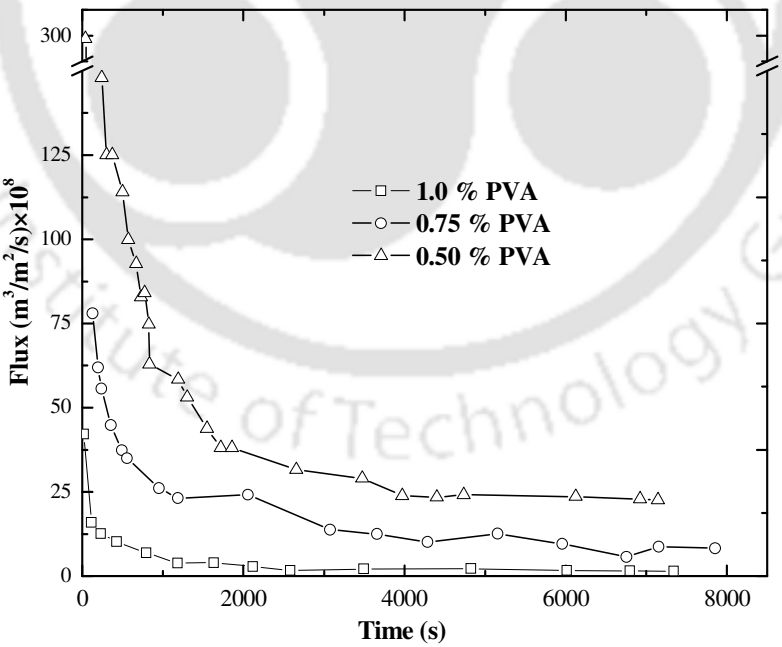

Figure 4.11. Flux decline profiles for 1000 µg L^{-1} arsenic concentration with different PVA concentrations at 103.4 kPa.

4.3.4 Studies on High Concentration Mercury Removal

Mercury Rejection Efficiencies: Figure 4.12 presents the mercury removal efficiency with time at different PVA concentrations. It was observed that, higher concentration of PVA lead to better removal of mercury. From the figure it was clear that 24.3 % and 85.1 % rejection was observed using 0.25 % and 1.0 % PVA at the end of 12 min for 30 mg L^{-1} mercury, respectively. Up to 1% rejection was observed without using PVA. The metal ions react with the PVA molecule to form chelate compound which were then rejected by the UF membrane. The increase in rejection efficiency with PVA concentration was due to the formation of more numbers of chelate compound which subsequently rejected by the UF membrane. It was also clear from the figure that mercury rejection decreased marginally with time. This was due to the deposition of more chelate molecules over the membrane surface, leading to an increase in the membrane surface concentration (concentration polarization). This resulted in an increase in the convective transport of the mercury to the permeate side thereby increasing the permeate side mercury concentration. Thus, the permeate mercury concentration increased and rejection decreased. Similar observations were reported during micellar enhanced ultrafiltration (MEUF) of eosin dye using polyamide membrane of 1000 Da cutoff [25].

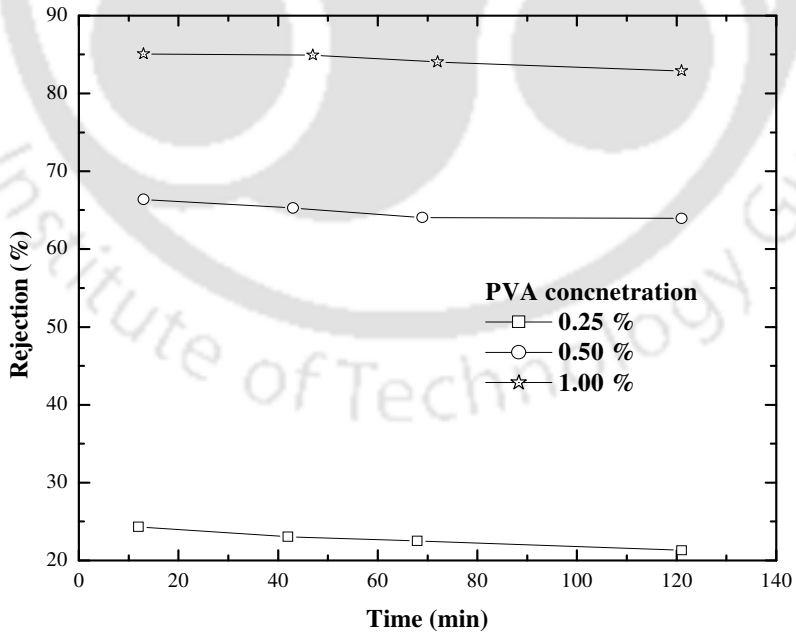

Figure 4.12. The effect of PVA concentration on mercury rejection (initial mercury concentration: 30 mg L^{-1}, transmembrane pressure: 172.4 kPa, pH: 7.0).

The variation in mercury removal efficiency with time at constant pressure and PVA concentration is shown in Figure 4.13 for three different initial mercury concentrations. It was observed that the mercury concentration in permeate increased with initial mercury concentration. The rejection increased from 63.7 % to 72.3 % when initial mercury concentration decreased from 50 mg L^{-1} 10 mg L^{-1} at the end of 12 min of the PEUF experiment. This was due to the extent of chelating reaction between mercury ions with fixed concentration of PVA. As the mercury concentration increased, all the mercury ions could not bind to the chelating agent and remains as free ions in the solution. This unreacted mercury passed through the UF membrane resulting in lower mercury rejection. From Figure 4.13 it was also clear that the rejection decreased with the progress of the experiment marginally. For example, rejection decreased from 72.4% to 69.3% when operating time increased from 12 min to 120 min for the initial mercury concentration of 10 mg L^{-1}. The decrease in mercury rejection was due to increase in convective transport as discussed in the preceding section.

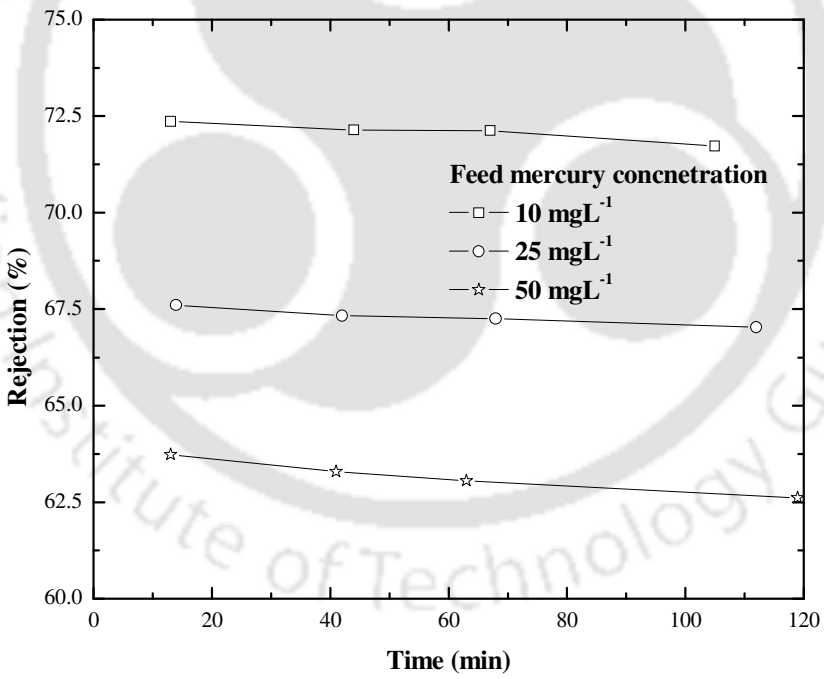

Figure 4.13. Effects of feed mercury concentration on mercury rejection (PVA concentration: 0.50 %, transmembrane pressure: 172.4 kPa, pH: 7.0).

Figure 4.14 shows the variation of mercury rejection with solution pH at a fixed transmembrane pressure of 172.4 kPa and constant concentrations of mercury (30 mg/L) and PVA (0.50 %). It was observed that rejection increased with pH of up to 7.0 and decreased thereafter. Maximum rejection was observed at pH of 7.0. The mercury removal was found to be 38.9 %, 65.9 % and 54.3 % at pH 3, 7 and 12, respectively. The maximum rejection was due the formation of more stable mercury - PVA chelate at pH 7 that reduced the free mercury in solution and hence lowered the permeate mercury concentration. Other researchers also reported similar trends for the removal of cupper with PVA as the chelating agent [27].

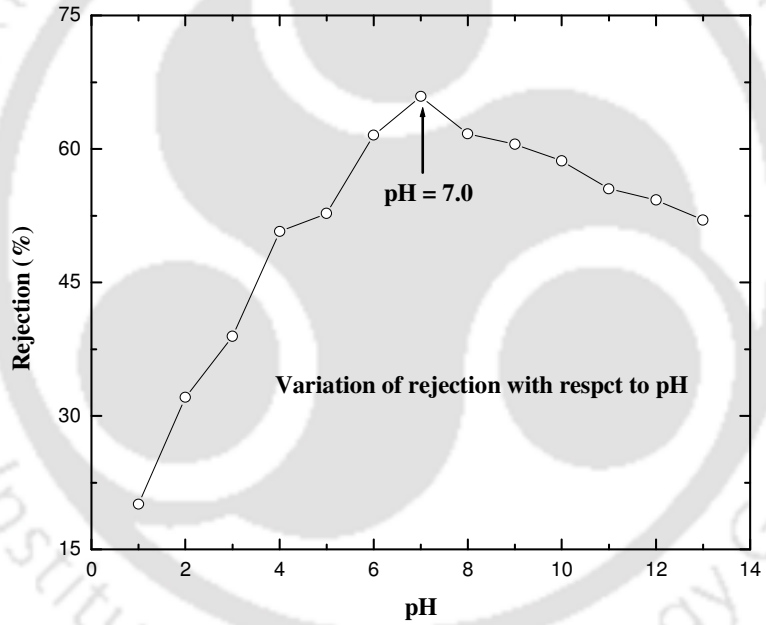

Figure 4.14. Variation of mercury rejection with solution pH (initial mercury concentration: 30 mg L^{-1}, PVA concentration: 0.50 %, transmembrane pressure: 172.4 kPa, time of operation: 15 min).

4.3.5 Rejection of PVA

The final concentrations of PVA were measured by spectrophotometric method and the rejections were determined using Equation (4.5). It was observed from the rejection vs time plot (Figure

4.15) that the rejection was higher for higher concentration of PVA. Rejection of 1000 µg L^{-1} arsenic and different PVA concentrations were reported in Figure 4.15. It was observed that the rejection of PVA was independent of the metal ion concentration and type. This could be due to the use of very low concentration of metal ions. For example, 98.88 % rejection was observed after 120 min for 1.0 % PVA while 0.5 % PVA solution shows 98.82 % rejection in 119 min. This was due to the appearance of more PVA molecules in the solution which lead to higher rate of gel layer formation and thus reduction in the permeate PVA concentration. Another observation was that the rejection was decreasing with time. The rejection decreased from 99.87 % to 98.74 % in 7 to 106 min for 0.25 % feed PVA concentration. This was also due to the higher PVA concentration over membrane surface with time. The selection of higher molecular weight and higher concentration of PVA may increase the % rejection of PVA.

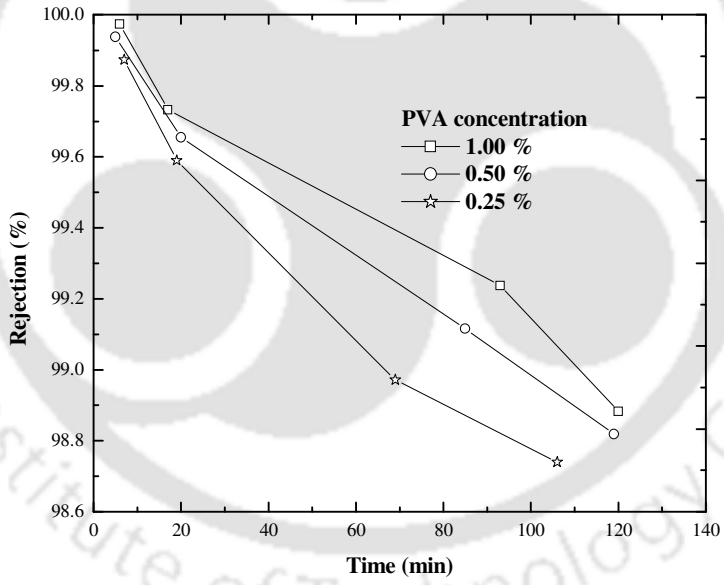

Figure 4.15. Rejection of polyvinyl alcohol (PVA) with respect to time for 1000 µg L^{-1} As and different PVA concentration.

4.3.6 Deposition of PVA and Heavy Metals over the Membrane Top Surface

Figures 4.16 (a) – 4.16 (c) represent the SEM micrographs of top surfaces of the membranes used before PEUF, after mercury removal and after arsenic removal, respectively. It was seen that the

rough membrane surface (before application) became very smooth after the removal experiments. This was due to the deposition of gel layer of chelate compound over the membrane surface. The EDX of the above three membranes were also shown in the inset of respective figures. It was seen from the inset of Figure 4.16 (a) that the peaks of the components of the support (Na, Mg, Al, Si, Ca and Fe) and chitosan (C, O and N) were prominent, whereas, after application, only C, O and the specific heavy metals were detected. C and O appeared as the components of PVA. Besides, presence of mercury and arsenic over the membrane top surface proved the deposition of chelate compounds. After every PEUF experiment, the membranes were thoroughly washed in tap water followed by distilled water for about 10 min. Distilled water was passed through the membrane for about 30 min and membrane compaction was done at 300 kPa for about another 30 min. The permeability of membrane was determined further and it was found that only 0.8-1.0 % reduction from its original one.

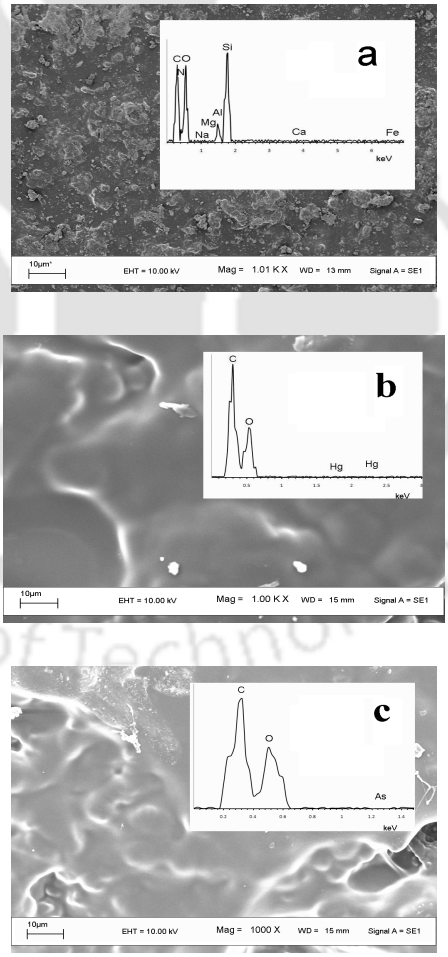

Figure 4.16. SEM and EDX of (a) Membrane top surface before application, (b) after mercury removal and c) after arsenic removal.

Finally, a comparative analysis of the removal efficiency of heavy metal by different membrane processes (reverse osmosis and nanofiltration) and PEUF was reported in Table 4.5. It was observed from the table that although the flux was in the same order but in the present PEUF process, 100 % removal was possible at very low pressure. Therefore, the use of PEUF using chitosan based ultrafiltration membrane may play a superior role over reverse osmosis and nanofiltration process.

Table 4.5. Comparative analysis for the removal of heavy metals using different membrane processes.

Metal removed	Membrane process	% removal	Flux $(m^3/m^2/s)\times10^6$	Pressure (kPa)	References
Co, Ni, Cr	RO	99.4 (Co), 99.5 (Ni), 99.9 (Cr)	4.16	300	[20]
Cd, Ni	NF	up to 99	13	820	[28]
Zn	NF	up to 90	4.0	950	[29]
Cu, Zn	NF, Chelation agent	53 (Cu), 40 (Zn)	13.8	1000	[30]
Cu	NF, Chelation agent	96-97	3.0-4.6	900, 1400	[31]
As, Hg	PEUF	up to 100	3.0	103.4	Present work

4.4. Membrane Cost

Conventional industrial scale ceramic membranes are available for \$500–2000/m^2 [32]. The thickness of the support was 5 mm and total 17.5 L/m^2 solution is required for the successful dip coating. The cost of the membrane per square meter was calculated on the basis of prices of the chemicals from corresponding companies (Table 4.6) and found as 523.68 \$/m^2. Taking the cost of manufacturing and shipment, the cost may reach up to \$600/m^2, which is competitive with the cost of the commercial ceramic membranes.

Table 4.6 Cost analysis of the prepared membranes from the unit cost of raw materials

	Raw materials	Material required (m^2/kg)	Unit price ($/kg or $/L)	Total cost ($/$m^2$)
Support	Clay*	7.13	--	--
	Kaolin*	1.83	7.93	14.50
	Sodium carbonate*	0.61	7.71	4.70
	Sodium metasilicate*	0.31	15.41	4.78
	Boric acid*	0.31	9.25	2.87
Coating material (17.5L)	Water#	8.75	--	--
	Acetic acid#	0.18	7.71	1.35
	Glutaraldehyde solution (25 %)#	4.20	90.75	381.17
	Chitosan#	0.18	653.24	114.32
	Total			523.68

* 5 cm diameter and 5mm thick membrane were prepared from 20 g material.
# Total 17.5 L/m^2 solution is required to conduct the dip coating process successfully. The acetic acid, glutaraldehyde and chitosan was used as discussed in the section 2.2.

4.5 Conclusion

Chitosan based ceramic ultrafiltration membranes were fabricated using low cost ceramic support using dip coating method and characterized. Nine membranes were prepared by varying three different concentrations of chitosan (1.0 %, 1.5 % and 2.0 %) at different dipping times (240 s, 480 s and 720 s). Chitosan was crosslinked with glutaraldehyde to increase the hydrophilicity and decrease the solubility in water. TGA and DSC analysis confirmed that the crosslinked material was thermally stable. The FTIR analysis of the chitosan and crosslinked chitosan inferred that the crosslinked reaction occurred in $-NH_2$ group of chitosan. The average pore sizes of the chitosan impregnated membranes were calculated using gas permeability data and found to be within 760 nm to 13 nm. The average pore size was observed to decrease with increase in both the chitosan concentration and dipping time. Acid and base treatments of the chitosan impregnated membranes confirmed that they were chemically stable and less prone to corrosion. From the average pore size, it was found that the fabricated chitosan impregnated membranes were applicable for both MF and UF range. The UF range membrane having the pore size of 13 nm was successfully used for the removal of mercury and arsenic from aqueous medium by polymer

enhanced ultrafiltration (PEUF) using polyvinyl alcohol as the chelating agent. It was found that the heavy metal concentration in permeate increased with the increase in its initial concentration and decreased with the increase in initial PVA concentration. Though the metal concentration in the permeate increased with time, initially 100% removal was observed for the 500 µg L^{-1} of both the metals. pH 7.0 was found as the most efficient condition for PEUF experiment. Used membranes were successfully regenerated after rigorous washing with water. Finally, the comparison of the performance of the proposed PEUF technique with the existing RO and NF technique were found to be very encouraging. Details experimentations in cross flow mode will help to determine the design parameters for the industrial scale application of PEUF process.

References

1. N. Singh, M. Cherya, Process Design, Economic analysis of a ceramic membrane system for microfiltration of corn starch hydrolysate. J. Food Eng., 1998, 38, 57–67.

2. S. Sachdeva, A. Kumar, Synthesis and modeling of composite poly(styrene-coacrylonitrile) membrane for the separation of chromic acid. J. Membr. Sci., 2008, 307, 37–52.

3. Y. Matsumoto, M. Sudoh, Y. Suzuki, Preparation of composite UF membranes of sulfonated polysulfone coated on ceramics. J. Membr. Sci., 1999, 158, 55–62.

4. B.K. Nandi, R. Uppaluri, M.K. Purkait, Effects of dip coating parameters on the morphology and transport properties of cellulose acetate–ceramic composite membranes. J. Membr. Sci., 2009, 330, 246–258.

5. W. Yoshida, Y. Cohen, Ceramic-supported polymer membranes for pervaporation of binary organic/organic mixtures. J. Membr. Sci., 2003, 213, 145–157.

6. F. Xiangli, W. Wei, Y. Chen, W. Jin, N. Xu, Optimization of preparation conditions for polydimethylsiloxane (PDMS)/ceramic composite pervaporation membranes using response surface methodology. J. Membr. Sci., 2008, 311, 23–33.

7. G.A. Vikhoreva, E.A. Shablyukova, N.R. Kil'deeva, Modification of Chitosan Films with Glutaraldehyde to Regulate Their Solubility and Swelling. Fiber Chemistry, 2001, 33, 206–210.

8. K.M. Song, W.H. Hong, Dehydration of ethanol and isopropanol using tubular type cellulose acetate membrane with ceramic support in pervaporation process. J. Membr. Sci., 1997, 123, 27–33.

9. X. Cao, T. Zhang, Q.T. Nguyen, Y. Zhang, Z. Ping, A novel hydrophilic polymer–ceramic composite membrane. 1. Acrylic acid grafting membrane. J. Membr. Sci., 2008, 312, 15–22.

10. H. Yanagishita, D. Kitamoto, K. Haraya, T. Nakane, T. Tsuchiya, N. Koura, Preparation and pervaporation performance of polyimide composite membrane by vapor deposition and polymerization (VDP). J. Membr. Sci., 1997, 136, 121–126.

11. S. Mimoune, R.E. Belazzougui, F. Amrani, Purification of aqueous solutions of metal ions by ultrafiltration. Desalination 2007, 217, 251–259.

12. P. Cafiizares, A. Perez, R. Camarillo, Recovery of heavy metals by means of ultrafiltration with water-soluble polymers: calculation of design parameters. Desalination, 2002, 144, 279–285.

13. A. Kryvoruchko, L. Yurlova, B. Kornilovich, Purification of water containing heavy metals by chelating-enhanced ultrafiltration. Desalination, 2002, 144, 243–248.

14. K.M. Hassan, T. Fukuhara, F.I. Hai, Q.H. Bari, Kh. Md. S. Islam, Development of a bio-physicochemical technique for arsenic removal from groundwater. Desalination, 249, 224–229.

15. I.A. Katsoyiannis, A.I. Zouboulis, Application of biological processes for the removal of arsenic from groundwaters. Water Res., 2004, 38, 17–26.

16. Y. Zheng, A. Wang, Removal of heavy metals using polyvinyl alcohol semi-IPN poly(acrylic acid)/tourmaline composite optimized with response surface methodology. Chem. Engg. J., 2010, 162, 186–193.

17. H. Ozaki, K. Sharmab, W. Saktaywirf, Performance of an ultra-low-pressure reverse osmosis membrane (ULPROM) for separating heavy metal: effects of interference parameters. Desalination, 2002, 144, 287–294.

18. S.K. Maji, A. Pal, T. Pal, Arsenic removal from real-life groundwater by adsorption on laterite soil. J. Hazar. Mat., 2008, 151, 811–820.

19. L.Y. Blue, M.A. V. Aelstyn, M. Matlock, D.A. Atwood, Low-level mercury removal from groundwater using a synthetic chelating ligand. Water res., 2008, 42, 2025–2028.

20. C.P. Nanseu-Njiki, S.R. Tchamango, P.C. Ngom, A. Darchen, E. Ngameni, Mercury(II) removal from water by electrocoagulation using aluminum and iron electrodes. J. hazar. Mat., 2009, 168, 1430–1436.

21. H.A. Tsai, H.C. Chen, K.R. Lee, J.Y. Lai, Study of the separation properties of chitosan/polysulfone composite hollow-fiber membranes. Desalination, 2006, 193, 129–136.

22. W.S. W. Ngah, C.S. Endud, R. Mayamar, Removal of copper (II) ions from aqueous solution onto chitosan and cross-linked chitosan beads. Reactive & Functional Polymers, 2002, 50, 181-190.

23. J.H. Finley, Spectrometric Determination of Polyvinyl Alcohol in Paper Coating. Analy. Chem., 1961, 33, 1925–1937.

24. S. Rivero, M.A. García, A. Pinotti, Crosslinking capacity of tannic acid in plasticized chitosan films. Carbohydrate Polymers, 2010, 82, 270–276.

25. M.K. Purkait, S. DasGupta, S. De, Removal of dye from wastewater using micellar-enhanced ultrafiltration and recovery of surfactant. Sep. Purif. Technol., 2004, 37, 81–92.

26. A. Jönsson, G. Trägårdh, Ultrafiltration applications. Desalination, 1990, 77, 135–179.

27. J. Labanda, M.S. Khaidar, J. Lloren, Feasibility study on the recovery of chromium (III) by polymer enhanced ultrafiltration. Desalination, 2009**,** 249, 577–581.

28. L.B. Chaudharia, Z.V.P. Murthya, Separation of Cd and Ni from multicomponent aqueous solutions by nanofiltration and characterization of membrane using IT model. J. Hazar. Mat., 2010, 180, 309–315.

29. N. B. Frares, S. Taha, G. Dorange, Influence of the operating conditions on the elimination of zinc ions by nanofiltration. Desalination, 2005, 185, 245–253.

30. A. Bougen, M. Rabiller-Baudry, B. Chaufer, F. Michel, Retention of heavy metal ions with nanofiltration inorganic membranes by grafting chelating groups. Sep. Purif. Technol., 2001, 25, 219–227.

31. T. Balanyà, J. Labanda, J. Llorens, J. Sabaté, Separation of metal ions and chelating agents by nanofiltration. J. Membr. Sci., 2009, 345, 31–35.

32. S. Jana, M.K. Purkait , K. Mohanty, Preparation and characterization of low-cost ceramic microfiltration membranes for the removal of chromate from aqueous solutions. App. Clay Sc., 2010, 47, 317–324.

Chapter V

Preparation and characterization of polyvinyl acetate-ceramic composite membrane by modified dip coating method and application for the fractionation of lysozyme and ovalbumin from chicken egg white

5.1. Introduction and Literature Survey

Recently the use of composite membranes is gaining huge interest due to their higher selectivity, permeation rate, chemical stability and thermal stability [1]. Polymer ceramic composite membranes were widely used for the application of ultrafiltration (UF) [2, 3] and pervaporation (PV) [4-7]. These membranes have different merits such as good structural integrity, better fouling resistance, higher flux and better selectivity [8]. Different combinations of polymeric skin layers and ceramic supports were tried for preparing composite membranes. Ceramic supports were prepared from raw materials such as kaolin [3], zirconia [9] and alumina [4] with pore sizes of 200–2000 nm whereas, the corresponding polymers used were cellulose acetate (CA) [8], polyvinyl acetate (PVAc), polyvinyl pyrrolidone (PVP) [4], styrene acrylonitrile [3] and polydimethylsiloxane (PDMS) [7, 9].

Many methods were reported for the preparation of composite membranes such as spray coating [3], self assembly [6], vapor deposition [10], dip coating [9] and spin coating [5]. Among these dip coating method is easiest and inexpensive and thus most suitable for making composite membranes. Numerous articles reported the characterization, behavior and applications of ceramic-polymeric composite membranes prepared by dip-coating method. Hong and Hong prepared PDMS-ceramic composite membrane with an average pore size of 370 nm and used it for the separation of isopropanol/water mixture [7]. Matsumoto et al. [11] had prepared sulfonated polysulfone-ceramic composite membrane for ultrafiltration applications by dip-coating method. Apart from these, Xiangli et al. [9], Sachdeva and Kumar [3] worked with different composite membranes for PV and UF applications with commercial support and polymer precursors. The critical review of literature revealed

that polymer concentration, dipping time and concentration of cross-linking agent (sometimes) control the thickness of the polymer layer over ceramic support as well as effective pore size and structural integrity. Additionally it was found that, for applying thin coating of PVAc or PVP over ceramic support, free radical graft polymerization was applied by Jou et al. [4], but no work was reported with easy and convenient method such as dip coating.

Composite polymer-ceramic UF membranes can remove higher molecular-weight substances, colloidal materials and organic-inorganic polymeric molecules. Recently, UF membranes were applied for single protein purification or binary protein fractionation. General protein purification techniques used in laboratories (such as electrophoresis, chromatography or affinity purification) have some limitations for large scale production and very difficult to scale-up. At the same time, UF processes can provide a better solution for this requirement.

Lysozyme (LS) is a commercial protein found in tears, saliva, human milk, mucus and in egg white. It is used as a food additive in milk products, cell-disrupting agent for extraction of bacterial intracellular products, a component of ophthalmologic preparations, and as a drug for treatment of ulcers and infections. On the other hand, ovalbumin (OV) is used in chelation therapy, and in different research work such as studying the structure/properties of protein, in proteomics or in immunology. Chicken egg white (CEW) is a potential source of both LS and OV as, it contains about 3.4 % LS and 54 % OV. The molecular weight of OV (45,000 Da) is much higher than that of LS (14,300 Da), thus makes the two proteins to be separated easily by size based membrane separation [12].

Many researchers have studied LS separation from CEW using different methodologies. Lu et al. have used commercial polyether sulfone membrane for the fractionation of LS and OV from CEW and obtained 99% lysozyme transmission with the selectivity of 2400 at pH = 11 [13]. Chang and Chang used a stirred fluidized bed adsorption technique using streamline SP adsorbent [14]. Effectiveness of PEG/salt aqueous two-phase system on the LS separation was investigated by Su and Chiang [15]. Bayramoğlu et al. have used ion-exchange method and obtained maximum absorption of 65.7 mg LS/g of poly(methacrylic acid) brush grafted chitosan beads at pH 6.0 [16]. Ghosh et al. [12] and Wan et al. [17] have used commercial membrane of 30 kDa cutoff and obtained 80–90 % and 94 % pure LS in the permeate respectively.

From the literature, it was found that no studies were reported on flux decline profiles due to fouling on the membrane surface and the variation of rejections of ovalbumin (OV) and transmission of lysozyme (LS) with respect to time. In this study, a novel modified dip-coating method (easier to apply than free radical grafting technique) was proposed to apply a thin UF layer of PVAc over a low cost microporous ceramic support. The effect of polymer solution and dipping time on the effective pore size of the membrane was studied. The prepared composite membranes were characterized by thermogravimetric analysis (TGA) and scanning electron microscopy (SEM), gas and hydraulic permeabilities. The effectiveness of the prepared membrane was observed by the fractionation of OV and LS from CEW. For finding the best pH for the operation, rejection of OV and transmission of LS were studied at a fixed transmembrane pressure while varying the solution pH. Further the variation of fractionation of LS and OV and flux with respect to time was determined at a fixed pressure and pH.

5.2. Materials and Methods

5.2.1 Raw Materials

– 150 mesh natural clay powder (collected from IIT Guwahati campus) was used for the preparation of ceramic support. The chemical analysis of clay was done by X-ray fluorescence (Philips, PW 2440 MagiXPRO) and the result was shown published in our earlier work [18]. Clay powder, kaolin (CDH (P.) Ltd.), sodium metasilicate (Loba Chemie Pvt. Ltd.), sodium carbonate (Rankem, India) and boric acid (Loba Chemie Pvt. Ltd.) were used for the preparation of ceramic support. Polyvinyl acetate (PVAc) (Alfa Aesar) was used for applying a thin layer over the ceramic support and N, N-di-methyl acetamide (DMAc) (Spectrochem (P.) Ltd., India) was used as the solvent of PVAc. 3x crystallized lysozyme (Sisco Research Laboratories, India) and purified egg albumin powder (Loba Chemie, (P.) Ltd., India) was used to calibrate the HPLC for analyzation of lysozyme (LS) and ovalbumine (OV) respectively. pH of the CEW solution was maintained by NaOH (Rankem, India) and HCl (Merck, India) (0.1 N each).

5.2.2 Preparation of the Ceramic Support

Disc shaped ceramic membranes (50 mm diameter and 5 mm thickness) were prepared by paste casting and sintered at 1000 °C from the composition of Membrane B of Chapter III. The membranes were used as ceramic support in this work. Detail of the preparation method was discussed and different parameters were evaluated and reported in Chapter III.

5.2.3 Preparation of the Composite UF Membrane

***Dip-coating Method*:** The well known dip-coating method was followed as reported in literature [8]. PVAc beads were dissolved in DMAc and the ceramic support was dipped in DMAc for 4 h before starting of the coating process. During this, all the air present in the porous structure in the support was displaced by DMAc. After taking out from DMAc, all the surfaces of the support except the top surface were covered by aluminum foil for preventing PVAc deposition. Then, the support was placed in a 250 mL beaker and PVAc solution was poured over it in such a way that the top surface was totally covered by the solution. The supports were kept immersed in to the solution for specific dipping time. At the period of dipping, a thin layer of PVAc was created over the top surface of the support. The coated sample was then taken out from the solution and dried at 175 °C (boiling point of DMAc is 165 °C) for 12 h. During this time, with the evaporation of the solvent (DMAc), a thin layer of the polymer (PVAc) was supposed to appear over the ceramic support. But, this process was not successful although tried many times with different PVAc concentrations and dipping times. Probably, the viscosity of the polymer solution was not enough to create a continuous layer. As a consequence, PVAc were deposited within the macropores of the support, which resulted neither decreasing in pore size nor a thin top layer over the support. A novel modified dip-coating method was tried to overcome this problem.

Modified dip-coating method: Making some changes in the technique of conventional dip coating method, modified dip coating process was organized. Figure 5.1 represents the schematic of the total process. This process requires one polymer and two solvents. The solvents were chosen in such a way that, both the solvents ("Solvent 1" and "Solvent 2") are miscible with each other while only "Solvent 2" dissolves the "polymer". The boiling point of "Solvent 2" should be higher than that of "Solvent 1". In step 1, the ceramic support was dipped into the Solvent 1 for 4 h to displace the air from the pores. The time of dipping was found by trial and error and can vary depending upon the morphology of the support

and the nature of solvent. After that, a required concentration of polymer solution in Solvent 2 was prepared. Then the ceramic support was taken out from Solvent 1 and wrapped with aluminum foil in same way as done in conventional dip coating. In Step 2, the wrapped support was dipped into the polymer solution for specific time. During this time, a thin layer of polymer solution was developed over the ceramic support. The polymer couldn't enter into the pores of the support due to the non-solubility of the polymer in Solvent 1. In Step 3, the support was taken out from the polymer solution and kept in atmosphere on a horizontal surface for 5 min to stabilize the film over the top surface. In Step 4, the support with the top layer was kept in a 250 mL beaker and Solvent 1 was poured into the beaker slowly to cover the top surface. The support was dipped for 5 min. During this step, solvent 2 diffuses out from the film and a thin polymer layer was formed over the ceramic support. Finally, in Step 5, the support with polymer layer was dried at a temperature slightly higher than the solvent 2. In this interim, both the solvents were vaporized and the final composite membrane was formed. Due to the lower boiling point of solvent 1, it evaporated faster and minute penetration of polymer into the pores occurred which made the farm binding of the polymer layer with the ceramic support stronger.

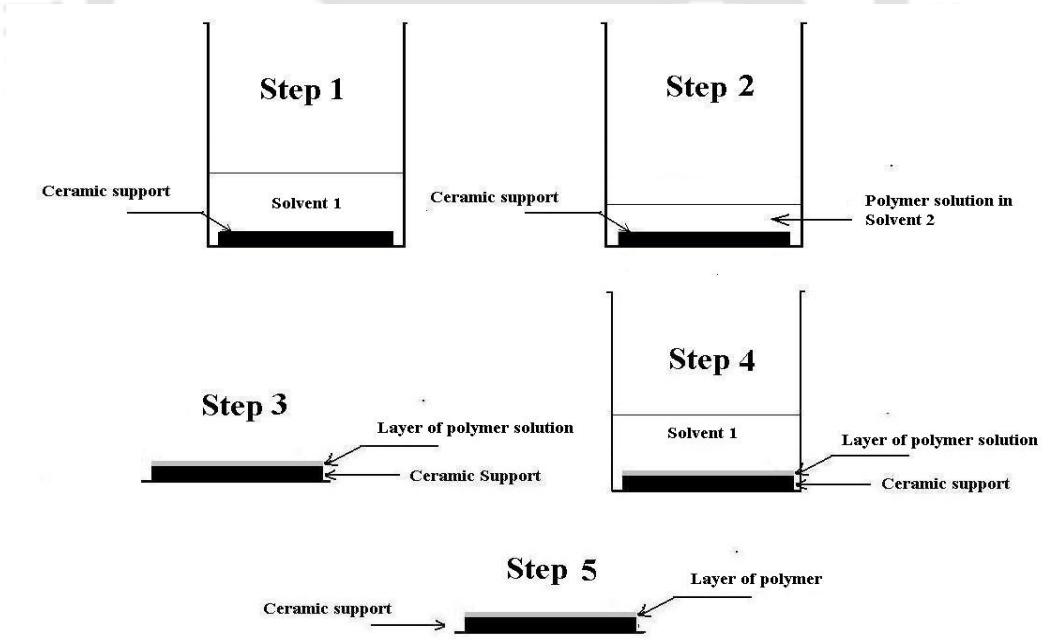

Figure 5.1. Schematic of the modified dip-coating procedure.

In this work, water, DMAc and PVAc were used as Solvent 1, Solvent 2 and polymer respectively. PVAc is soluble in DMAc but not in water; on the other hand DMAc is soluble in water.

The boiling point of DMAc (165 °C) is higher than water (100 °C). The effect of polymer concentration and dipping time over the pore size and morphology of the membrane were studied. Twelve different membranes were prepared using four different polymer concentration (10 %, 20%, 30% and 40%) and three dipping time (30s, 60s and 120s). Nomenclatures of the membranes were shown in Table 5.1.

Table 5.1. Nomenclature of the prepared composite membranes.

Time (s)	PVAc concentration (weight %)			
	10 %	20 %	30 %	40 %
30	M-10-30	M-20-30	M-30-30	M-40-30
60	M-10-60	M-20-60	M-30-60	M-40-60
120	M-10-120	M-20-120	M-30-120	M-40-120

5.2.4 Characterizations of the Support and Membranes

Thermogravimetric analysis (TGA) (Mettler-851e) of PVAc was done under inert atmosphere (nitrogen) and under air from 25 °C to 250 °C at a heating rate of 5 °C/min to study its behavior for thermal application.

The characterization of both support and composite membranes were performed by scanning electron microscopic analysis (Make: Oxford; Model: LEO 1430VP) and permeation experiments (air and water). The broad intension of the SEM experiment was the morphological study aimed to evaluate the effect of dip coating parameters (solution concentration and dipping time) on ceramic matrix blocking and top layer growths as well as checking the sequential change of membrane morphology during dip coating process with respect to the coating parameters. SEM also detects the presence of surface/cross sectional defects such as pinholes and cracks (if any). Air flux characterization aimed to quantify membrane morphological parameters such as average pore size and Viscous/Knudsen flux that contribute to the overall transport. All the composite membranes were subjected to gas permeation test. The theory, process, image and the description of the is shown in Chapter IV.

Chemical stability of the support and the composite membranes were investigated by measuring the weight loss, pore size, air and hydraulic permeability before and after acid and base treatment. The membranes were subjected to a solution of NaOH (0.075 M; pH~13.5) and HCl (0.075 M; pH~1.0) separately for 1 week under atmospheric condition. All the membranes were dried thereafter and the

weight loss was measured. The characterization of all the membranes were performed as discussed in the preceding section.

5.2.5 Ultrafiltration of Chicken Egg White Solution

Three dilute CEW solutions were prepared with different concentrations. The details of the prepared solutions are given in Table 5.2. 1 g, 2 g and 3 g CEW was mixed with 99 mL, 98 mL and 97 mL water with 200 mM NaCl (each) and named as Solution A, Solution B and Solution C. NaCl was used to enhance the solubility of CEW in water. The effect of salt concentration was already studied and it was reported that, over 200 mM salt, the product purity decreases [17]. The lysozyme and ovalbumin concentrations in each solution were determined by HPLC (Series 200, Perkin Elmer). The standard curves were drawn from the pure lysozyme and purified egg albumin powder. The used HPLC column was Perkin Elmer Bio-C18 (5µm; 250×4.6 mm) and the mobile phase was a mixture of 80% acetonitrile and 20% water with 0.1 % trifluroacetic acid. The proteins were detected at 215 nm with a UV-vis detector combined with the instrument [19].

Table 5.2. Solution nomenclature, and compositions.

Solution	Raw material compositions			Protein compositions	
	CEW (gm)	Water (mL)	NaCl (g)	Ovalbumin (mg/mL)	Lysozyme (mg/mL)
Solution A	1	99	1.17	5.421	0.352
Solution B	2	98	1.17	10.842	0.704
Solution C	3	97	1.17	16.263	1.056

All the prepared solutions were subjected to a dead end filtration cell of volume 250 mL. The effective membrane area was ≈ 16×10^{-4} m^2. The schematic of the experimental set up was reported in Chapter III. For all the experiments, 206.8 kPa transmembrane pressure and the lowest pore size UF membrane (M-40-120) with pore size around 9 nm was used. Permeate protein concentrations were measured by HPLC. For observing the effect of pH, Solution B was passed through the UF membrane at pH of 3.0, 5.0, 7.0, 9.0 and 11.0. Rejections of OV and transmission of LS were calculated after 30 min of operation for each experiment. The values of pH were chosen in such a way that it covers the isoelectric point of the both the proteins, lysozyme (pI = 11.0) and ovalbumine (pI = 5.1). Further, the variation in rejection of OV and transmission of LS with respect to time (up to 3 h) was observed for all

the three solutions at pH = 11.0 (determined from previous set of experiment). Finally, flux decline profiles were also observed for Solution A, B and C at pH = 11.0 and up to 3 h. The pHs of the solutions were adjusted by 0.1 N HCl and NaOH solutions.

5.3 Results and discussion

5.3.1 Thermogravimetric Analysis of the Coating Material

The TGA analysis of the coating material (polyvinyl acetate) under air and inert atmosphere was presented in Figure 5.2. It was evident from the figure that there was almost no difference in weight loss pattern of PVAc (up to 450 °C) under both the conditions which proves the non-reactivity of this material with air even at higher temperature. Up to 275 °C, the material shows weight loss of 3.23 % and 4.43 % under air and inert atmosphere respectively, and after that, a sharp fall was observed. Thus, the material was found to be thermally stable up to 275 °C.

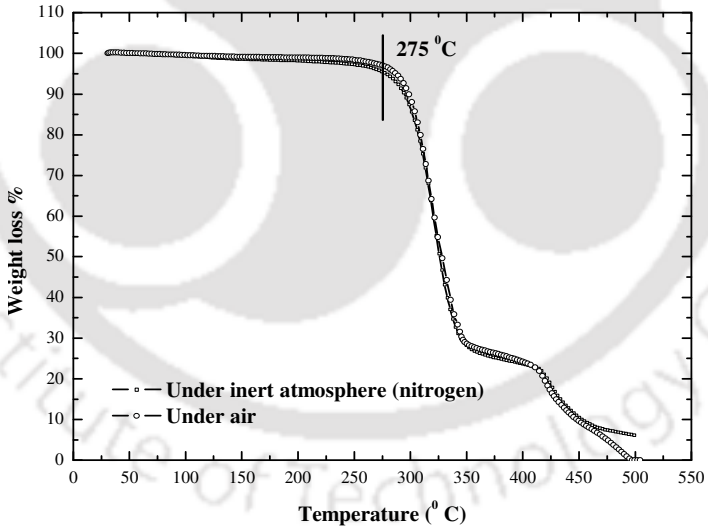

Figure 5.2. TGA of polyvinyl acetate under inert atmosphere (Ar) and air.

5.3.2 Membrane Morphology

The SEM micrographs of the top surface of the ceramic support and composite membranes are presented in Figure 5.3. From the figure it was clear that the surface of the support was covered with the coating material during the process. The extent of coating increased with the concentration of PVAc as well as the duration of coating. From the images of 10% PVAc coated membranes, it was clear that the large pores of the ceramic support were partially covered by the coating material, whereas the extent of coating increased with time. For 20% PVAc coated membranes, a thin layer appeared over the top surface. Again, for 30 % and 40 % PVAc coated membranes, not only the total surface was covered by the coating material but also additional clusters of coating materials were noticed in some locations. It was thus concluded that the effective pore size of the composite membranes were reduced with increase in PVAc concentration as well as dipping time. It was also confirmed from the SEM images that there were no cracks or discontinuous coating over the membrane surfaces.

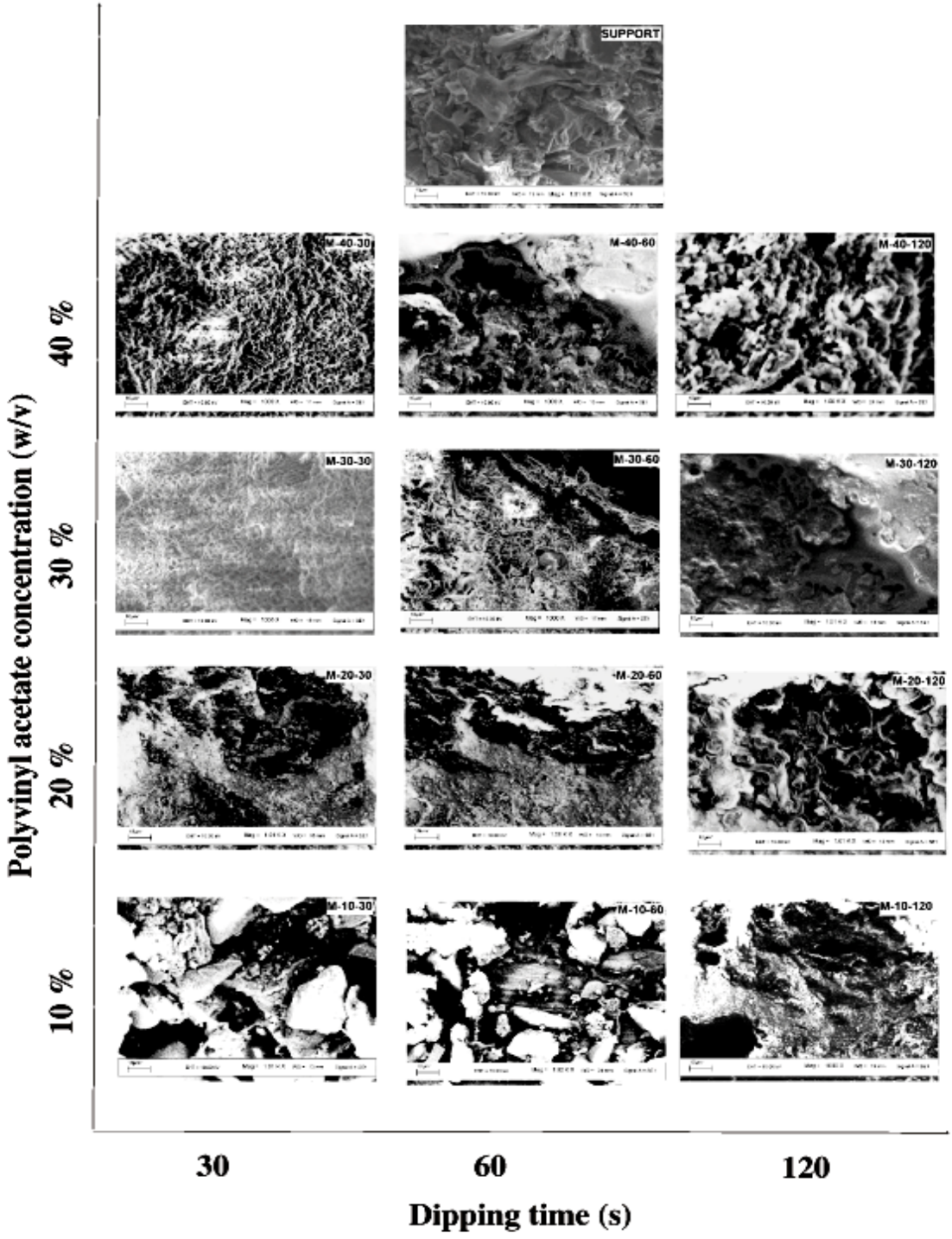

Figure 5.3. SEM micrographs of the top surface of the support and different composite membranes.

5.3.3 Determination of Air Permeability and Pore Sizes

Figure 5.4 shows the variation of effective permeability factor (K) with average pressure (*p*) for the support and as well as composite membranes. Table 5.3 summarizes the parameters evaluated from graphical analysis of the transmembrane flux data. As shown in the table, the permeability of the support was found to be 6.90×10^{-1} $m^3m^{-2}kPa^{-1}s^{-1}$ and that for different composite membranes were varied from 3.75×10^{-2} $m^3m^{-2}kPa^{-1}s^{-1}$ to 2.90×10^{-3} $m^3m^{-2}kPa^{-1}s^{-1}$. The average pore size of the support was found to be 1093 nm and that for composite membranes were varied from 150 to 9 nm. Another observation was that with the increase in the PVAc concentration and dipping time, the contribution of viscous flux decreased and Knudsen flux increased. Viscous flux decreased from 39 % (M-10-30) to 2 % (M-40-120) and Knudsen flux increased from 61 % (M-10-30) to 98 % (M-40-120). This was due to the decrease in the pore sizes with the increase in the PVAc concentration and dipping time, which was also confirmed from the SEM analysis. Nandi et al. also ported similar trend for the membranes prepared by dip coating of cellulose acetate over ceramic support [8].

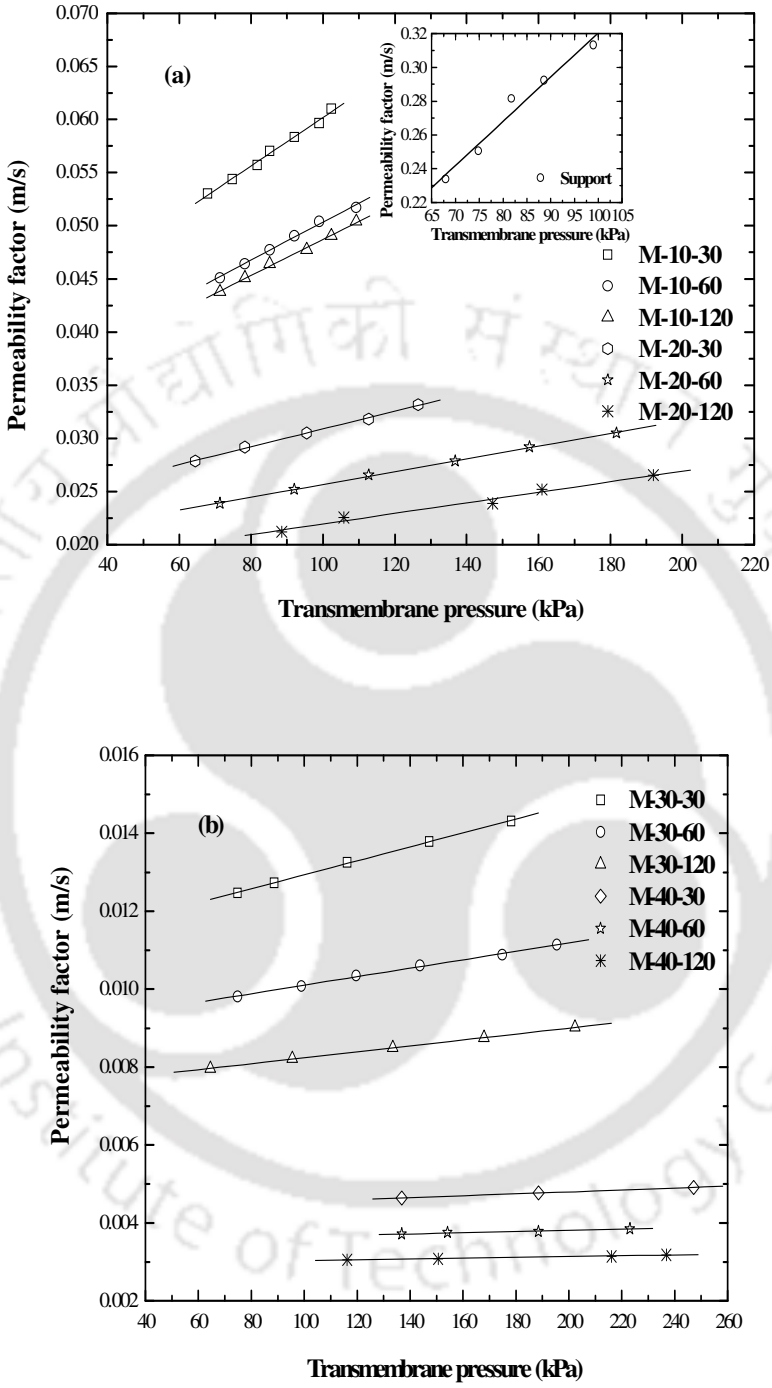

Figure 5.4. Variation of effective permeability factor (*K*) with average pressure (*P*) for (a) Support, M-10-30, M-10-60, M-10-120, M-20-30, M-20-60 and M-20-120 and (b) M-30-30, M-30-60, M-30-120, M-40-30, M-40-60 and M-40-120.

Table 5.3. Various parameters evaluated from graphical analysis of gas permeation results.

Membrane Name	Slope ($\times 10^{7}$) ($m.s^{-1}Pa^{-1}$)	Intercept ($\times 10^{2}$) ($m.s^{-1}$)	Air permeability* ($m^3m^{-2}kPa^{-1}s^{-1}$)	Pore size (nm)	Viscous Flux (%)	Knudsen Flux (%)
Support	26.15	5.89	6.90×10^{-01}	1093	60 – 81	19 – 40
M-10-30	2.27	3.74	3.75×10^{-02}	150	19 – 39	61 – 81
M-10-60	1.78	3.25	3.25×10^{-02}	136	18 – 38	62 – 82
M-10-120	1.69	3.17	3.17×10^{-02}	132	17 – 37	63 – 83
M-20-30	0.83	2.25	2.25×10^{-02}	92	16 – 36	64 – 84
M-20-60	0.60	1.97	1.97×10^{-02}	76	11 – 34	66 – 89
M-20-120	0.49	1.69	1.69×10^{-02}	72	10 – 32	68 – 90
M-30-30	0.18	1.11	1.11×10^{-02}	40	09 – 29	71 – 91
M-30-60	0.15	0.90	9.00×10^{-03}	30	09 – 26	74 – 91
M-30-120	0.074	0.75	7.50×10^{-03}	24	07 – 22	78 – 93
M-40-30	0.024	0.43	4.30×10^{-03}	14	06 – 18	82 – 94
M-40-60	0.014	0.35	3.50×10^{-03}	10	04 – 10	90 – 96
M-40-120	0.011	0.29	2.90×10^{-03}	9	02 – 11	89 – 98

*At 241.3 kPa transmembrane pressure.

5.3.4 Hydraulic Permeability

From the hydraulic permeabilities data presented in Figure 5.5, it was observed that the permeability decreased with increase in PVAc concentrations and dipping times. For 10 % PVAc concentration, the permeability decreased from 1.20×10^{-8} $m^3m^{-2}Pa^{-1}s^{-1}$ to 1.19×10^{-8} $m^3m^{-2}Pa^{-1}s^{-1}$ with an increase in the dipping time of 30 s to 120 s. On the other hand, for 60 s dipping time, the permeability decreased from 1.20×10^{-8} $m^3m^{-2}Pa^{-1}s^{-1}$ to 1.47×10^{-10} $m^3m^{-2}Pa^{-1}s^{-1}$ with the increase in the PVAc concentration of 10 % to 40 %. This was due to the fact that, with increase in both dipping time and polymer concentration, the average pore size of the membrane decreased and top layer thickness increased. The values of hydraulic permeabilities were observed to be lesser than the value of air permeabilities for the same membrane. This was due to the higher density and viscosity of water with respect to air.

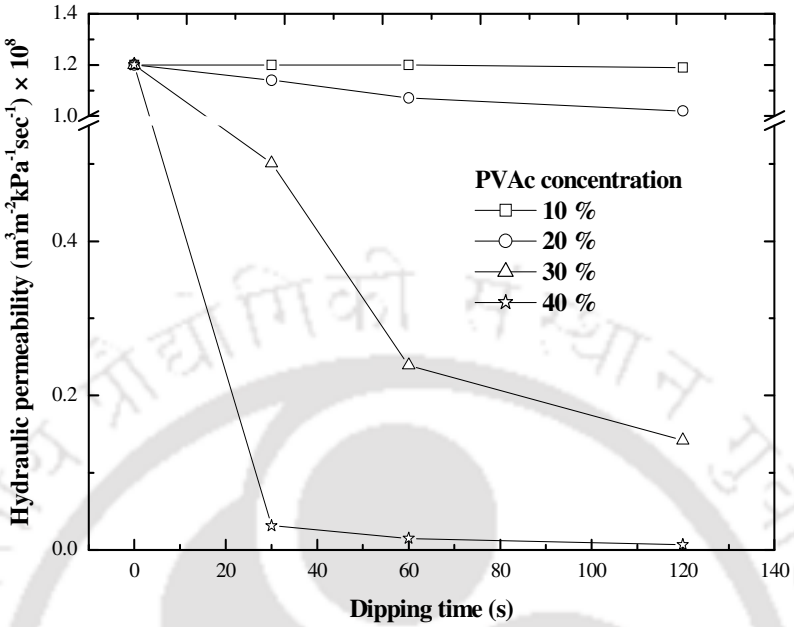

Figure 5.5. Hydraulic permeabilities of the prepared membranes.

5.3.5 Chemical Resistivity

Table 5.4 summarizes the variations in different membrane parameters for the ceramic support and the composite membranes after acid and base treatments. It was seen that the pore size, air and hydraulic permeabilities were slightly increased after both acid and base treatment. The mass loss of the support was found as 5.37 % in acidic solution and 6.89% in basic solution. For composite membranes, the mass loss was varied from 5.46 % (M-10-30) to 5.37 % (M-40-120) in acidic solution and 6.96 % (M-10-30) to 6.89 % (M-40-120) in basic solution. Thus, the mass losses of composite membranes were mainly due to the loss of the ceramic support. Theoretically, the change of water permeabilities (in %) were proportional to the square of changes of pore size, because, both values increased with pore area, assuming the pores are cylindrical and the thickness of the membrane did not change during chemical treatment. Comparing the air permeability of the membranes before treatment (from Table 5.3), it was found that the air permeabilities of M-10-30 and M-40-120 were changed from 3.75×10^{-2} $m^3m^{-2}kPa^{-1}s^{-1}$ and 2.90×10^{-3} $m^3m^{-2}kPa^{-1}s^{-1}$ to 3.93×10^{-02} $m^3m^{-2}kPa^{-1}sec^{-1}$ and 2.97×10^{-03} $m^3m^{-2}kPa^{-1}sec^{-1}$ for acid treatment and 3.84×10^{-02} $m^3m^{-2}kPa^{-1}sec^{-1}$ and 2.95×10^{-03} $m^3m^{-2}kPa^{-1}sec^{-1}$ for base treatment,

respectively. The water permeability of the M-20-60 was changed from 1.14×10^{-8} $m^3m^{-2}kPa^{-1}sec^{-1}$ to 1.29×10^{-08} $m^3m^{-2}kPa^{-1}sec^{-1}$ and 1.23×10^{-08} $m^3m^{-2}kPa^{-1}sec^{-1}$ for acid and base treatment respectively.

Table 5.4. Variation of different membrane parameters after chemical treatment.

After acid treatment				
Membrane	Weight loss (%)	Pore size (nm)	Air permeability* ($m^3m^{-2}kPa^{-1}sec^{-1}$)	Water permeability ($m^3m^{-2}kPa^{-1}sec^{-1}$)
Support	5.37	2310	7.30×10^{-01}	1.27×10^{-05}
M-10-30	5.46	153	3.93×10^{-02}	1.37×10^{-08}
M-10-60	5.45	139	3.45×10^{-02}	1.35×10^{-08}
M-10-120	5.44	135	3.35×10^{-02}	1.34×10^{-08}
M-20-30	5.43	94	2.37×10^{-02}	1.32×10^{-08}
M-20-60	5.41	77	2.06×10^{-02}	1.29×10^{-08}
M-20-120	5.40	73	1.88×10^{-02}	1.18×10^{-08}
M-30-30	5.38	41	1.11×10^{-02}	5.20×10^{-09}
M-30-60	5.38	31	1.29×10^{-02}	2.55×10^{-09}
M-30-120	5.37	24	7.61×10^{-03}	1.50×10^{-09}
M-40-30	5.37	14	4.38×10^{-03}	3.23×10^{-10}
M-40-60	5.37	10	2.53×10^{-03}	1.51×10^{-10}
M-40-120	5.37	9	2.97×10^{-03}	6.53×10^{-11}
After base treatment				
Membrane	Weight loss (%)	Pore size (nm)	Air permeability* ($m^3m^{-2}kPa^{-1}sec^{-1}$)	Water permeability ($m^3m^{-2}kPa^{-1}sec^{-1}$)
Support	6.89	2300	7.25×10^{-01}	1.26×10^{-05}
M-10-30	6.96	152	3.84×10^{-02}	1.35×10^{-08}
M-10-60	6.95	138	3.35×10^{-02}	1.33×10^{-08}
M-10-120	6.95	134	3.25×10^{-02}	1.31×10^{-08}
M-20-30	6.93	93	2.31×10^{-02}	1.27×10^{-08}
M-20-60	6.92	77	2.04×10^{-02}	1.23×10^{-08}
M-20-120	6.91	73	1.83×10^{-02}	1.12×10^{-08}
M-30-30	6.90	40	1.21×10^{-02}	5.14×10^{-09}
M-30-60	6.89	30	9.12×10^{-03}	2.44×10^{-09}
M-30-120	6.89	24	7.57×10^{-03}	1.49×10^{-09}
M-40-30	6.89	14	4.35×10^{-03}	3.22×10^{-10}
M-40-60	6.89	10	3.52×10^{-03}	1.48×10^{-10}
M-40-120	6.89	9	2.95×10^{-03}	6.51×10^{-11}

* At 241.3 kPa transmembrane pressure.

5.3.6 Fractionation of Lysozyme and Ovalbumin from Chicken Egg White

Effect of pH on rejection of OV and transmission of LS: As described in section 2.4, the effect of pH was observed by passing Solution B through the membrane at different pH. The rejections of ovalbumin (OV) and transmissions of lysozyme (LS) were shown in Fig. 6.It was observed that the rejection of OV was highest as pH = 11.0 (62.1 %) and lowest at pH = 5.0 (57.5 %). The transmission of lysozyme was increased with the pH and shown highest at pH = 11.0 (96.7 %). At pH = 3.0, 5.0 and 11.0, the rejection of OV were 60.3 %, 57.5 % and 62.1 % respectively. The LS transmissions were found to be 72.1 % and 96.7 % at pH = 3.0 and 11.0 respectively. This observation complied well with the mechanism of binary protein fractionation [22]. The mechanism says that at pH = pI (isoelectric point) of the specific protein, net charge of the protein becomes zero. Thus at that particular pH, the ceramic support (charged part of the composite membrane) doesn't provide any resistance for the transmission of the protein. The pI of LS and OV are 11.0 and 5.1 respectively. As a result, LS transmission maximizes at 11.0 and the rejection of OV increases with the increase of pH. Thus, with the aim to fractionate both the proteins, the optimum pH was taken as 11.0 (the pI of LS).

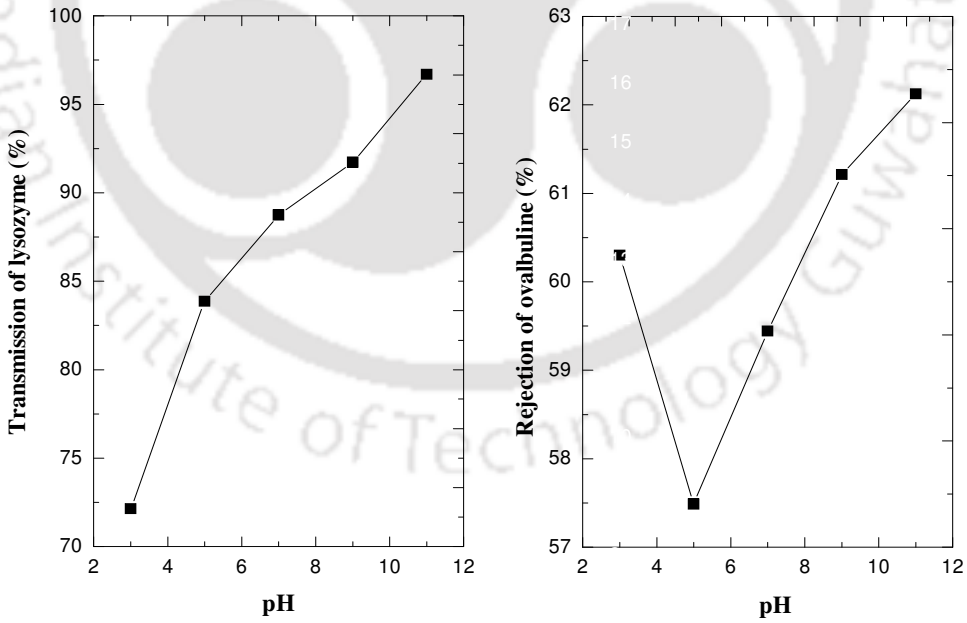

Figure 5.6. Variation of rejection of lysozyme and transmission of ovalbumin (Solution 2) with respect to pH at 206.8 kPa at 30 min of operation.

***Variation of Fractionation of Lysozyme and Ovalbumin with Time*:** Figs. 7 and 8 represent the variation in rejection of OV and transmission of LS with respect to time for solution A, B and C. From Figure 5.7 two trends were observed. Initially for all the solutions, rejection was increasing with the progress of the experiment. Solution B has shown 57.6 % and 90.0 % rejection in 5 and 180 min of the experiment. This was due to the deposition of OV molecules over the surface of the membrane with the continuation of the experiment, thus decreasing the pore sizes which further increased the rejection. Further, Solution A, B and C had shown successive increase in the rejections at a fixed time of the experiment. After 60 min of the experiment, Solution A, B and C have shown 72.7 %, 79.9 % and 80.5 % of rejection. This phenomenon can be explained by the fact that the solid content of the solutions were in an increased order. This accordingly increased the settlement of solid particles over the membrane surface followed by increase in the rejection.

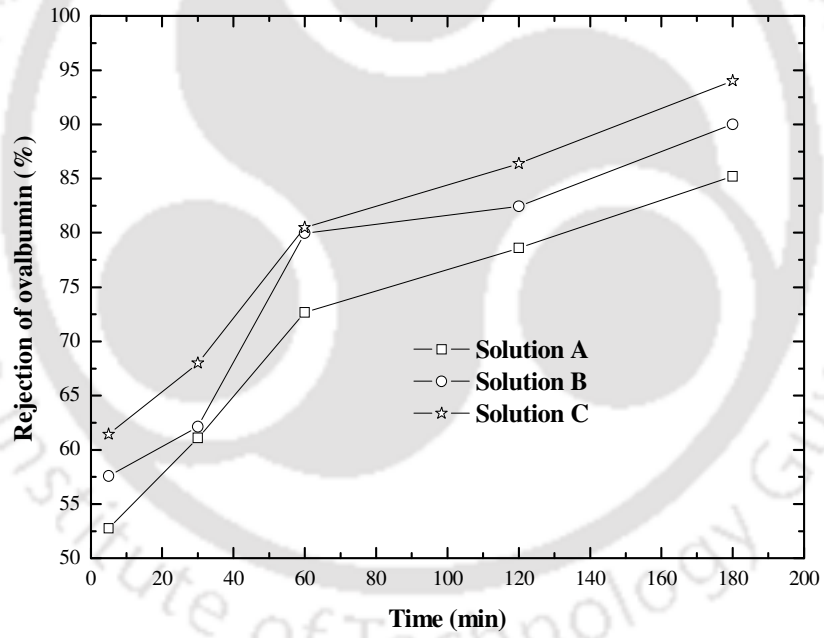

Figure 5.7. Variation of rejections of ovalbumin with respect to time for solution A, solution B and solution C at 206.8 kPa and pH = 11.0.

In Figure 5.8, transmission of LS was observed to decrease with the progress of the experiment for all the solutions. For Solution B, the transmission of LS decreased form 97.5 % to 91.7 % within 5 to 180 min of ultrafiltration. The reason was same as explained for OV earlier. With the progression of time, deposition of solid particles over membrane surface decreased the pore sizes and further

declination in transmission occurred. Another observation was that the transmission shown a consecutive decrease with Solution A, B and C at a constant time of operation. The transmissions of the solution at 30 min of operation were 97.4 %, 96.3 % and 95.5 % respectively. This was again due to the increase in the solid content of the successive solutions. The rate of solid deposition over the membrane surface increased thus transmission decreased.

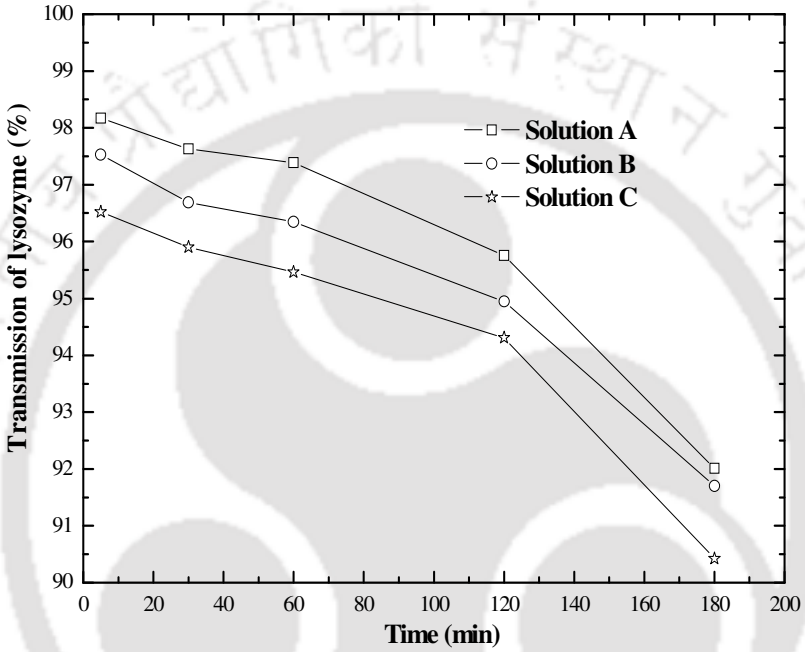

Figure 5.8. Variation of transmission of lysozyme with respect to time for solution A, solution B and solution C at 206.8 kPa and pH = 11.0.

***Flux declination during UF experiment*:** Before the experiment, the stable flux of the membrane (M-40-120) was found to be 4.83×10^{-07} $m^3m^{-2}s^{-1}$ for 206.8 kPa transmembrane pressure. The flux decline profile was observed for Solution A, B and C up to 3 h. at 206.8 kPa (Figure 5.9). During the experiment, the flux was observed to decrease slowly. From the flux decline profiles, two trends were observed. Initially, the flux was decreased very sharply and then the declination was gradual. The first phase flux declination was due to the concentration polarization and the second stage gradual decrease was due to gel formation over the membrane surface [21]. Another observation was that, the flux decline rate increased for higher concentration of chicken egg white. The flux decreased to 8.15×10^{-8} $m^3m^{-2}s^{-1}$, 3.12×10^{-8} $m^3m^{-2}s^{-1}$, and 2.01×10^{-8} $m^3m^{-2}s^{-1}$ in 1702 s, 1879 s and 1917 s for Solution A, B and C

respectively. This was due to the increase in CEW concentration. At higher CEW concentration, more protein molecules were deposited over the membrane surface resulting higher flux declination.

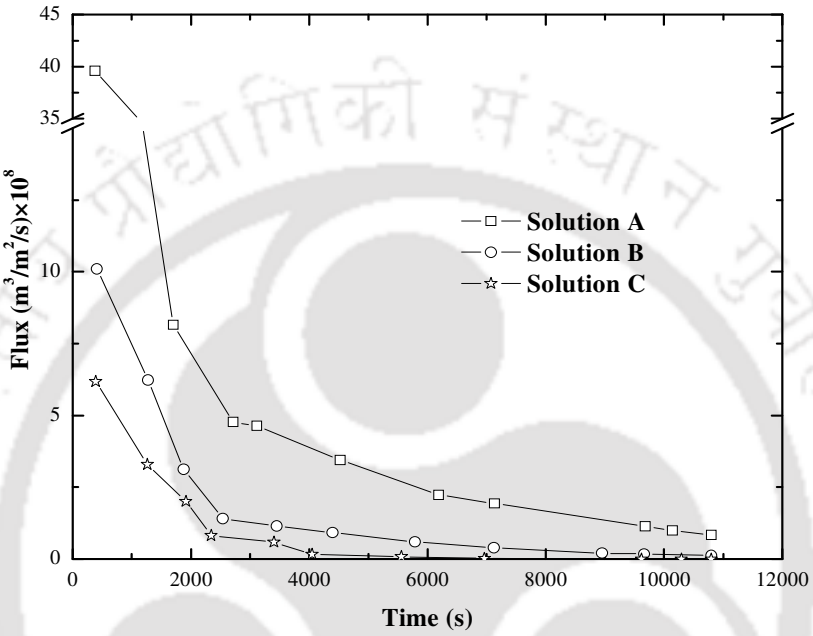

Figure 5.9. Flux decline profiles for solution A, solution B and solution C at 206.8 kPa and pH = 11.0.

5.4. Conclusion

A novel modified dip coating method was applied for the coating of polyvinyl acetate over a low cost ceramic support which was prepared by paste casting followed by sintering. The method of coating was found to be suitable for low viscous polymers. Twelve composite membranes were prepared by varying the polymer concentration (10 %, 20 % 30% and 40 %) and dipping time (30 s, 60 s and 90 s). The pore sizes of composite membranes were found to be within 150 nm to 9 nm. The coating material (PVAc) was found to be thermally stable up to 275 °C. All the membranes were characterized with SEM, gas permeability and water permeability. The pore sizes were found to decrease with the increase in the polymer concentration and dipping time. The lowest pore size membrane (9 nm) was applied for the fractionation of lysozyme (LS) and ovalbumin (OV) for chicken egg white using a dead end

membrane permeation cell. The rejection of OV and transmission of LS was observed at different pH and 11.0 was determined as the optimum pH for fractionation of both the proteins. Three different dilute CEW solutions in water were used for the study and up to 94 % rejection of OV and 98 % transmission of LS was obtained. The results were encouraging and confirmed that such composite membrane can be used for bioseparation of proteins in related industries.

References

1. M. Mulder, Basic principles of Membrane Technology. First Indian Reprint, Springer, India 2007.

2. R.S. Faibish, Y. Cohen, Fouling resistant ceramic supported polymer membranes for ultrafiltration of oil-in-water microemulsions. J. Membr. Sci., 2001, 185, 129–143.

3. S. Sachdeva, A. Kumar, Synthesis and modeling of composite poly(styrene-coacrylonitrile) membrane for the separation of chromic acid. J. Membr. Sci., 2008, 307, 37–52.

4. W. Yoshida, Y. Cohen, Ceramic-supported polymer membranes for pervaporation of binary organic/organic mixtures. J. Membr. Sci., 2003, 213, 145–157.

5. K.M. Song, W.H. Hong, Dehydration of ethanol and isopropanol using tubular type cellulose acetate membrane with ceramic support in pervaporation process. J. Membr. Sci., 1997, 123, 27–33.

6. Y. Chen, F. Xiangli, W. Jin, N. Xu, Organic–inorganic composite pervaporation membranes prepared by self-assembly of polyelectrolytemultilayers on macroporous ceramic supports. J. Membr. Sci., 2007, 302, 78–86.

7. Y. Ki Hong, W.H. Hong, Influence of ceramic support on pervaporation characteristics of IPA/water mixtures using PDMS/ceramic composite membrane. J. Membr. Sci., 1999, 159, 29–39.

8. B.K. Nandi, R. Uppaluri, M.K. Purkait, Effects of dip coating parameters on the morphology and transport properties of cellulose acetate–ceramic composite membranes. J. Membr. Sci., 2009, 330, 246–258.

9. F. Xiangli, W. Wei, Y. Chen, W. Jin, N. Xu, Optimization of preparation conditions for polydimethylsiloxane (PDMS)/ceramic composite pervaporation membranes using response surface methodology. J. Membr. Sci., 2008, 311, 23–33.

10. H. Yanagishita, D. Kitamoto, K. Haraya, T. Nakane, T. Tsuchiya, N. Koura, Preparation and pervaporation performance of polyimide composite membrane by vapor deposition and polymerization (VDP). J. Membr. Sci., 1997, 136, 121–126.

11. Y. Matsumoto, M. Sudoh, Y. Suzuki, Preparation of composite UF membranes of sulfonated polysulfone coated on ceramics. J. Membr. Sci., 1999, 158, 55–62.

12. R. Ghosh, S.S. Silva, Z. Cui, Lysozyme separation by hollow-fibre ultrafiltration. Biochem. Engg. J., 2000, 6, 19–24.

13. J. Lu, Y. Wan, Z. Cui, Fractionation of Lysozyme and Chicken Egg Albumin Using Ultrafiltration with 30-kDa Commercial Membranes. Indus. Engg. Chem. Res., 2005, 44, 7610–7616.

14. Y.K. Chang, I.P. Chang, Method development for direct recovery of lysozyme from highly crude chicken egg white by stirred fluidized bed technique. Biochem. Engg. J., 2006, 30, 63–75.

15. C.K. Su, B.H. Chiang, Partitioning and purification of lysozyme from chicken egg white using aqueous two-phase system. Pross. Biochem., 2006, 41, 257–263.

16. G. Bayramoğlu, G. Ekici, N. Beşirli, M.Y. Arica, Preparation of ion-exchange beads based on poly(methacrylic acid) brush grafted chitosan beads: Isolation of lysozyme from egg white in batch system. 2007, 310, 68–77.

17. Y. Wan, J. Lu, Z. Cui, Separation of lysozyme from chicken egg white using ultrafiltration. Sep. Purif. Technol., 2006, 48, 133–142.

18. S. Jana, M.K. Purkait, K. Mohanty, Preparation and characterization of low-cost ceramic microfiltration membranes for the removal of chromate from aqueous solutions. App. Clay Sci., 2010, 47, 317–324.

19. V.G. Mal'tsev, D.G. Nasledov, S.A. Trushin, T.B. Tennikova, L.V. Vinogradova, I.N. Volokitina, V.N. Zgonnik and Boris G. Belenkii, High-performance liquid chromatography of proteins on short capillary columns. J. High Resol. Chrom., 1990, 13, 185–189.

20. B.D. Halligan, A Tool for Calculating the p*I* and Molecular Mass of Phosphorylated and Modified Proteins on Two-Dimensional Gels. Method. Mol. Biol., 2009, 527, 283–298.

21. A. Jönsson, G. Trägårdh, Ultrafiltration applications. Desalination, 1990, 77, 135–179.

Chapter VI

Preparation of LTA zeolite–cellulose acetate mixed matrix membrane and studies on the rejection of bovine serum albumin

6.1 Introduction and Literature Survey

Membrane based technologies alone or in combination with other methods is advantageous in terms of capital cost and energy efficiency than older established separation processes such as absorption, adsorption and distillation. Recently, membrane technology is applied in various industries such as petrochemical, food, biochemical, pharmaceutical, semiconductor as well as for solving wide range of environmental problems [1].

Among different materials, polymer membranes are most successful commercial membrane and reported to be successfully applied for the separation of several gas and liquid streams. Polymer membranes have several advantages such as easy processing, low cost, good selectivity and permeability while the disadvantages are: low solvent and temperature resistance, lower applicable range of pH and lower life span [2]. On the other hand, zeolite membranes have advantages in terms of high selectivity; long term stability in high temperature and pressure, ease of cleaning and catalytic activation. But zeolite membranes suffer from the problems such as high capital cost, brittleness, low membrane surface per module volume and difficulty in achieving high selectivity in large scale microporous membranes [3].

Future membrane market demands a novel membrane material which will combine the advantages of both polymer and zeolite membranes. Based on this need, a new type of membrane, the mixed-matrix membrane has been developed recently. The mixed-matrix material was generally prepared by uniform dispersion of inorganic materials (mostly zeolites) into a continuous phase of polymer. Mixed-matrix membranes have the advantages of both polymer membrane (low coast and ease of processability) and zeolite membrane (high selectivity and permeability). Addition of small amount of zeolite in the polymer material improves the separation quality to a great extent due to the very specific particle size distribution of zeolites thus creating the uniform pore size distribution, however, polymer

matrix helps in the binding of the zeolite particles within themselves or with the support (for asymmetric membrane) [1].

Kulprathipanja et al. first introduced the term "mixed-matrix membrane" and performed the pioneering study on zeolite/polymer mixed-matrix membrane [4]. Afterwards, both rubbery [5, 6] and glassy polymers [7-9] were used as dispersion phase, whereas verities of inorganic materials such as aluminosilicates [7], silicoaluminophosphate [8] and non zeolite particles [9] were used as dispersed phase.

It was reported that, glassy polymers used to show better performance in terms of continuous matrix formation due to more rigid polymer chains. Additionally those polymer have much higher glass transition temperature thus much acceptable for mixed-matrix membranes. Some of the typical glassy polymers include cellulose acetate, polysulfone, polyimides, polyetherimide, polyvinyl alcohol etc. Mahajan et al. reported mixed-matrix membrane prepared from polyetherimide and polyvinyl acetate with zeolite 4A and used it for the separation of N_2/O_2. [10, 11]. Another study also reported separation of N_2/O_2 with the mixed-matrix membrane prepared from 5A zeolite and polyethersulfone [12].

On the other hand, choosing a zeolite for mixed-matrix membrane material depend on many factors such as: crystal morphology, crystal or particle size, Si/Al ratio, chemical composition etc. In general, small and uniform crystal size zeolite particles are more efficient for the preparation of defect free mixed-matrix membrane [1]. Furthermore, Miller et al. discovered that, lower Si/Al ratio zeolite are more efficient for dispersion within polymer matrix [9].

For maximizing the flux, which represents membrane productivity, the thickness of the membrane should be minimized. For that purpose, similar to commercial polymer membranes, asymmetric geometry containing a skin layer over a porous support is advantageous for mixed-matrix membranes also. Most of the asymmetric mixed-matrix membranes were prepared by phase inversion method [13-15]. In this process, one phase mixed-matrix dope is converted to two phases. First phase is of high ratio zeolite/polymer which creates the membrane and the second phase is of high polymer/zeolite ratio which generates the void/pores. Interfacial polymerization method was also tried by Jia et al. using silicalite-1 zeolite and two component polychmethylsiloxane. Thus, from the above discussion, it was found that no work was reported for the preparation of mixed-matrix membrane by easy and convenient method like dip coating. Further, most of the studies were done in nanofiltration range and applied for gas separation.

In this work, ultrafiltration range mixed-matrix membranes were prepared from cellulose acetate as the polymer material and LTA zeolite as the inorganic material by dip coating method. Zeolite particles were prepared in the laboratory and characterized by XRD and liquid particle size analyzer (LPSA). For studying the effects of dipping time, polymer and zeolite concentration on the pore size, different membranes were prepared varying the said parameters. Membranes were characterized by field emission scanning electron microscopy (FESEM), air permeability and hydraulic permeability. Finally the effectiveness of the membranes were tested by the rejection of bovine serum albumin in batch mode.

6.2 Materials and Methods

6.2.1 Raw Materials

– 150 mesh natural clay powder (collected from IIT Guwahati campus) was used for the preparation of ceramic support. The chemical analysis of clay was done by X-ray fluorescence (Philips, PW 2440 MagiXPRO) and the result was published in our earlier work [16]. Clay powder, kaolin (CDH (P.) Ltd.), sodium metasilicate (Loba Chemie Pvt. Ltd.), sodium carbonate (Rankem, India) and boric acid (Loba Chemie Pvt. Ltd.) were used for the preparation of ceramic support. Sodium aluminate (National Chemicals, India), sodium metasilicate nonahydrate along with sodium hydroxide (Rankem, india) were used for the preparation of LTA zeolite. Cellulose acetate (Loba Chemie, India) was used as the polymeric material for the mixed-matrix membrane whereas acetone (Merck, India) for the solvent of cellulose acetate. Bovine serum albumin (BSA) was purchased from Merck, India to test the feasibility of the prepared membranes for ultrafiltration applications. pH of the BSA solutions were maintained by NaOH (Rankem, India) and HCl (Merck, India).

.2.2 Preparation of the Zeolite

LTA zeolite was prepared following the method discussed in the literature keeping the Na:Al:Si ratios constant [17] 0.967 g NaOH was dissolved in 80 mL water. Then the solution was divided in to two equal volumes. 20.258 g sodium metasilicate was added to one-half solution and 3.45 g sodium aluminate to other solution kept in two capped bottles separately and mixed gently until clear solutions appeared. Then these two solutions were mixed quickly. A thick gel appeared. The composition of the gel can be represented by the molar ratio $3Na_2O:Al_2O_3:2SiO_2:43H_2O$. The gel was heated in a 170 mL

volume teflon lined autoclave at 120 °C for 8 h. Further, the prepared zeolite is washed with distilled water repetitively to neutralize the pH. Finally the zeolite is dried at 100 °C for 12 h.

6.2.3 Characterization of the Prepared Zeolite

The prepared powder was investigated by XRD (Bruke D8, advanced X-ray diffraction measurement system) and the reflections of the result were compared with standard literature to confirm the formation of the zeolite [18]. Further the particle size distribution of the zeolite was analyzed by Liquid Particle Size Analyzer (LPSA) (Malvern, Masterizer-2000; Model: APA-5005) to observe the average particle size and span of the size distribution.

6.2.4 Preparation of the Membrane

Preparation of the ceramic support: Disc shaped ceramic supports (50 mm diameter and 5 mm thickness) were prepared by paste casting followed by sintering at 1000 °C using the composition given in Table 6.1. Detail of the preparation method was discussed and different parameters were evaluated and reported by us in an earlier work [19]. The support was tagged as "Membrane B" in the aforementioned chapter III.

Table 6.1. Composition of the support

Components	Dry basis	Wet basis
Clay	70	56
Kaolin	18	14.4
Sodium carbonate	6	4.8
Sodium metasilicate	3	2.4
Boric acid	3	2.4
Water	--	20

Preparation of the asymmetric mixed-matrix membrane: The well known dip coating method was applied as the fabrication method [20]. Nine membranes were prepared by varying the dipping time, polymer (cellulose acetate) and zeolite (LTA) concentrations. To observe the effect of each parameter, while varying one parameter, other two were kept constant. The nomenclatures of all the nine membranes with respective zeolite %, polymer % and dipping time are shown in Table 6.2.

Table 6.2. Membrane nomenclature

Membrane	LTA %	CA %	Dipping time (s)	Reason
M-2.5-2-60	2.5	2	60	To study the variation of CA%
M-2.5-3-60	2.5	3	60	
M-2.5-4-60	2.5	4	60	
M-2.5-3-30	2.5	3	30	To study the variation of LTA%
M-5.0-3-30	5.0	3	30	
M-7.5-3-30	7.5	3	30	
M-5.0-4-30	5.0	4	30	To study the variation of dipping time
M-5.0-4-60	5.0	4	60	
M-5.0-4-90	5.0	4	90	

For preparing the membranes, required amount of polymer and zeolite particles were added to acetone. Cellulose acetate was properly dissolved in acetone whereas; fine zeolite particles kept suspended due to high viscosity of the polymer solution. Before starting the dip coating process, the ceramic supports were dipped within acetone for 4 h to displace air bubbles from the void spaces. The time of dipping was found by trial and error and can vary depending upon the morphology of the support and the nature of solvent. After taking out from acetone, all the surfaces of the support except the top surface were covered by aluminum foil for preventing polymer/zeolite deposition. Then, the support was placed in a 250 mL beaker and the polymer/zeolite suspension was poured over it in such a way that the top surface was totally covered by the suspension. The supports were kept immersed in the solution for specific dipping time. During the period of dipping, a thin layer of mixed-matrix material was created over the top surface of the support. The coated sample was then taken out from the solution and dried at 100 °C for the removal of acetone. During this time, polymer and zeolite create a thin layer over the ceramic support and pores were generated due to the evaporation of acetone.

Characterization of the membranes: Thermogravimetric analysis (TGA) (Mettler-851e) of cellulose acetate and LTA zeolite were done under inert atmosphere (nitrogen) and under air from 25 °C to 500 °C at a heating rate of 5 °C/min to study its behavior for thermal application. The characterization of the asymmetric mixed-matrix membranes were performed by field emission scanning electron microscopic analysis (Make: Oxford; Model: LEO 1430VP) and permeation experiments (air and water). The broad intension of the FESEM experiment was the morphological study aimed to evaluate the effect of dip coating parameters (dipping time, polymer and zeolite concentrations) on ceramic matrix blocking as

well as to check the sequential change of membrane morphology during dip coating process with respect to the coating parameters. FESEM also detects the presence of surface/cross sectional defects such as pinholes and cracks (if any).

The air and hydraulic permeability experiments were conducted in a dead end permeation cell. Details of the experimental set up were given in Chapter III. Air flux characterization aimed to quantify membrane morphological parameters such as average pore size and Viscous/Knudsen flux that contribute to the overall transport. All the composite membranes were subjected to gas permeation test. Based on the gas permeation data, average pore radius (r_g) was estimated according to the following expression [20]

$$K = 2.133\frac{r_g \cdot \nu \cdot \varepsilon}{l \cdot q^2} + 1.6\frac{r_g^{\,2} \cdot \varepsilon}{l \cdot \eta \cdot q^2} p \qquad (1)$$

where p is the average pressure on the membrane, v (m/s) is the molecular mean velocity of the gas, l (m) is the pore length, q is the tortuosity, η (Pa s) is the viscosity of gas, K (m/s) is the effective permeability factor evaluated as

$$K = \frac{Q \cdot P_2}{S \cdot \Delta P} \qquad (2)$$

where, S (m^2) is the permeable area of the membrane, Q (m^3/s) is the volumetric flow rate, P_2 is the membrane pressure at permeate side (Pa) and ΔP is the transmembrane pressure drop (Pa). In Eq. (1), the first term corresponds to Knudsen permeance and the second term corresponds to the viscous permeance. Eq. (1) can be represented as a straight line in a plot drawn between K and p where the slope and intercept represents the viscous and Knudsen permeabilities of the membranes respectively. Henceforth the values of the slope and intercept obtained from the plot were used to evaluate the percentage contribution of pores (and pore sizes) that contributed towards viscous and Knudsen flow transport mechanisms. In other words, gaseous flux characterization of the ceramic support yielded qualitative information with respect to the pore size distribution applicable for the contribution of Knudsen or viscous flow regimes towards the overall composite membrane flux. The average pore radius (r_g) of the membrane was evaluated using the intercept (A) and slope (B) of the straight line expressed as:

$$r_g = 1.333\frac{B}{A}v\eta \quad (3)$$

The hydraulic permeability experiments were conducted for all the membranes using deionized water and determined by the following equation:

$$J = L_h \cdot \Delta P \quad (4)$$

where, J is the liquid flux ($m^3m^{-2}s^{-1}$), L_h is the hydraulic permeability ($m^3m^{-2}s^{-1}kPa^{-1}$) and ΔP is the transmembrane pressure (kPa).

6.2.6 BSA Rejection Studies

The rejection of BSA was performed to check the feasibility of the prepared mixed-matrix membranes. For the first set of experiments, 1000 mg L^{-1} BSA solution was passed through all the prepared membranes and rejections were observed. In the second set of experiments flux decline profiles were observed for three different concentrations of BSA (viz. 500 mg L^{-1}, 1000 mg L^{-1} and 2000 mg L^{-1}) with lowest pore size membrane (M-5.0-4-90). For all the experiments, the transmembrane pressure was 206.8 kPa and the pH was kept constant at 7.2. Because, with the change in pH, the adsorptive fouling of the membranes may increase and intermolecular attraction between BSA molecules and membrane can predominate which may affect the membrane performance. The feed and permeate BSA concentration was determined by UV-vis spectrophotometer (Thermo Scientific; Chemito, spectroscan UV-2300) at 278 nm. % rejection R of BSA was determined by the following equation:

$$R(\%) = \frac{C_f - C_p}{C_f} \times 100 \quad (5)$$

where, C_f = feed concentration (mg L^{-1}) and C_p = permeate concentration (mg L^{-1}).

6.3. Results and Discussion

6.3.1 Characterization of Zeolite

X-ray Diffraction analysis: The reflections of the powder were shown in Figure 6.1. The peak positions and patterns were compared with other literature to verify the formation of LTA zeolite [18]. The matched peaks are represented by "black dots" in the figure which confirm the powder as LTA zeolite.

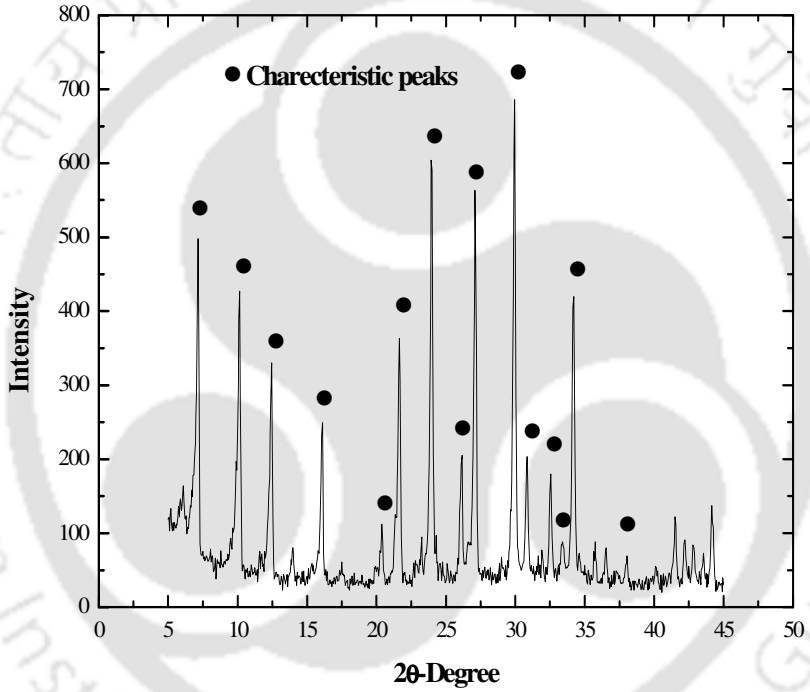

Figure 6.1. XRD analysis of the prepared zeolite (LTA)

Particle size distribution analysis: As described in the section 2.3, the particle size distribution was done to determine the average particle size and the span of distribution (Figure 6.2). The average zeolite particle size was found as 0.8 μm whereas; the maximum and minimum particle size was 3.8 μm and 0.3 μm respectively.

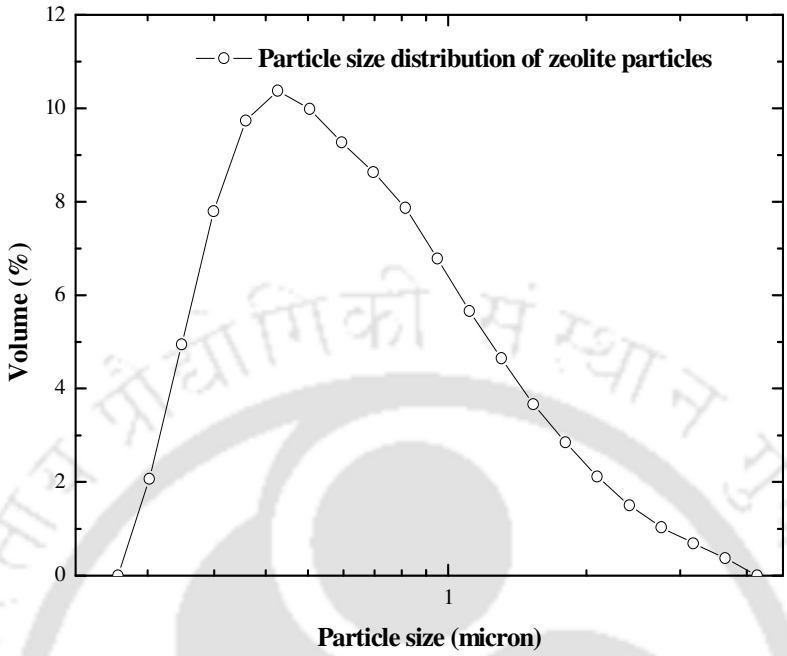

Figure 6.2. Particle size distributions of zeolite particles

6.3.2 Characterization of the Membrane

Thermogravimetric analysis of LTA zeolite and cellulose acetate: The TGA analysis of the mixed-matrix materials (zeolite and polymer) were done separately to observe the thermal stability of the membrane (Figure 6.3). It was observed that initially, up to 175 °C, LTA zeolite has shown 14.4% mass loss. This can be attributed to the loss of loosely bonded water molecules which also proves the hygroscopic nature of the material. Thereafter, up to 500 °C, the material did not shown much mass loss (4.3%). Thus, the zeolite was not degrading thermally up to 500 °C.

On the other hand, the cellulose acetate has shown a mass loss of 6.0% up to 80 °C, which can be due to the loss of moisture. Thereafter up to 300 °C, only 3.8% mass loss and finally drastic falling was observed. Therefore, cellulose acetate was found to be thermally stable up to 300 °C. Consequently, the thermal stability of mixed-matrix membrane was found up to 300 °C.

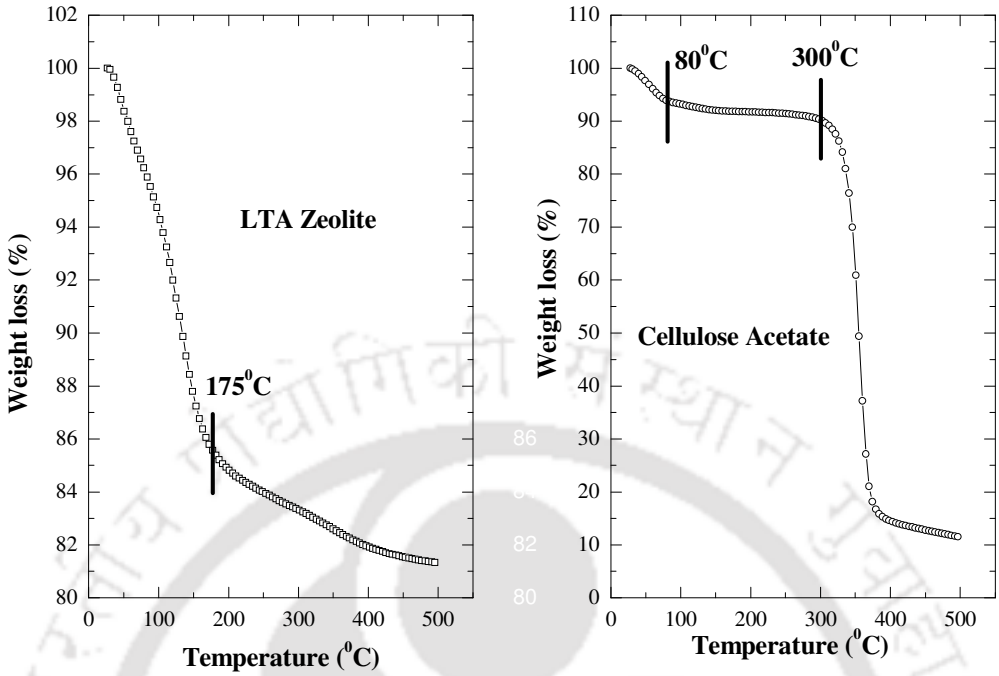

Figure 6.3. Thermogravimetric Analysis of LTA zeolite and cellulose acetate

Membrane morphology: The micrographs of all the top surfaces of the prepared mixed-matrix membranes were obtained by Field Emission Surface Electron Microscopy (FESEM). The images are presented in Figure 6.4. In Figure 6.4 (a), variation of cellulose acetate concentration (2%, 3% and 4%) were shown with a fixed zeolite concentration (2.5%) and dipping time (60 s). Further, the variation of LTA % (2.5%, 5.0% and 7.5%) with fixed cellulose acetate concentration (3%) and dipping time (30 s) was shown in Figure 6.4 (b). The increased ratios of zeolite and polymer were clearly visible from the figures. On the other hand, the effect of dipping time (30 s, 60 s and 90 s) was observed with a fixed polymer (4%) and zeolite (5.0%) concentrations (Figure 6.4 (c)).

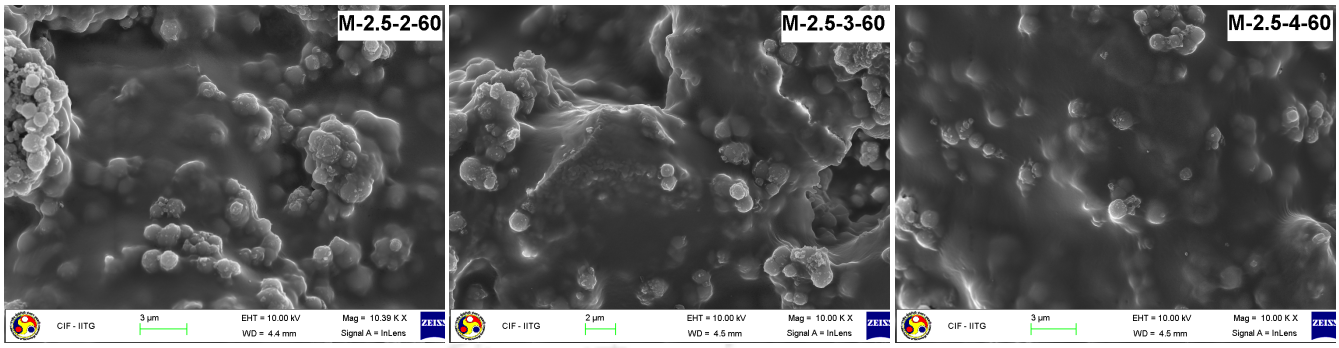

Figure 6.4 (a). Field emission scanning electron microscopy of top surfaces of M-2.5-2-60, M-2.5-3-60 and -2.5-4-60 (variation of CA)

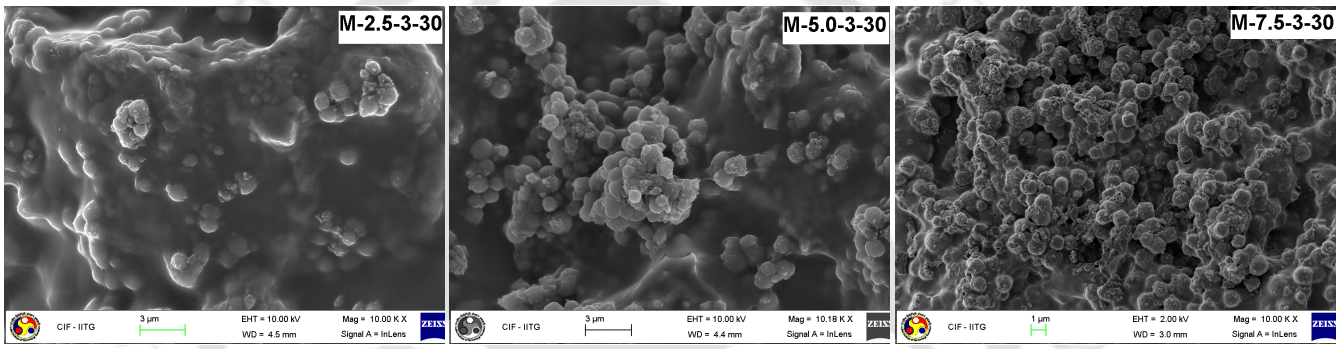

Figure 6.4 (b). Field emission scanning electron microscopy of top surfaces of M-2.5-3-30, M-5.0-3-30 and M-7.5-3-30 (variation of LTA)

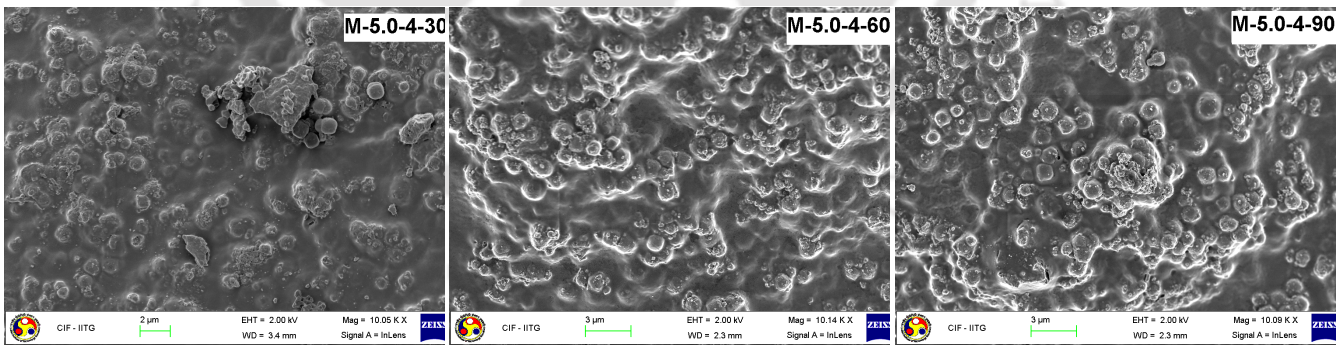

Figure 6.4 (c). Field emission scanning electron microscopy of top surfaces of M-5.0-4-30, M-5.0-4-60 and M-5.0-4-90 (variation of dipping time)

The extent of coating increased with the concentration of polymer, zeolite as well as with the duration of coating. Again, with the increased dipping time, not only the total surface was covered by the coating material but also additional clusters of coating materials were noticed in some locations. It was thus concluded that the effective pore size of the asymmetric membranes were reduced with increase in polymer/zeolite concentration along with the increase in dipping time. It was also confirmed from the FESEM images that there were no cracks or discontinuous coating over the membrane surfaces.

Determination of air permeability and pore sizes: Figure 6.5 shows the variation of effective permeability factor (K) with average pressure (p) for the support and as well as the asymmetric mixed-matrix membranes. Table 6.3 summarizes the parameters evaluated from graphical analysis of the transmembrane flux data.

Table 6.3. Various parameters evaluated from graphical analysis of gas permeation result

Membrane Name	Slope ($\times 10^7$) ($m.s^{-1}Pa^{-1}$)	Intercept ($\times 10^2$) ($m.s^{-1}$)	Permeability* ($m^3m^{-2}kPa^{-1}s^{-1}$)	Pore size (nm)	Viscous Flux (%)	Knudsen Flux (%)
Support	26.15	5.89	6.90×10^{-01}	1093	60 – 81	19 – 40
M-2.5-2-60	0.63	1.92	1.97×10^{-02}	80	13 – 47	53 – 87
M-2.5-3-60	0.43	1.64	1.69×10^{-02}	65	12 – 41	59 – 88
M-2.5-4-60	0.29	1.36	1.36×10^{-02}	52	12 – 27	73 – 88
M-2.5-3-30	0.83	2.25	2.25×10^{-02}	92	16 – 36	64 – 84
M-5.0-3-30	0.14	0.94	1.28×10^{-02}	36	09 – 30	70 – 91
M-7.5-3-30	0.024	0.43	4.30×10^{-03}	14	06 – 18	82 – 94
M-5.0-4-30	0.15	0.90	9.00×10^{-03}	30	09 – 26	74 – 91
M-5.0-4-60	0.046	0.59	6.31×10^{-3}	19	10 – 32	68 – 90
M-5.0-4-90	0.014	0.35	3.50×10^{-03}	10	04 – 10	90 – 96

*At 241.3 kPa transmembrane pressure.

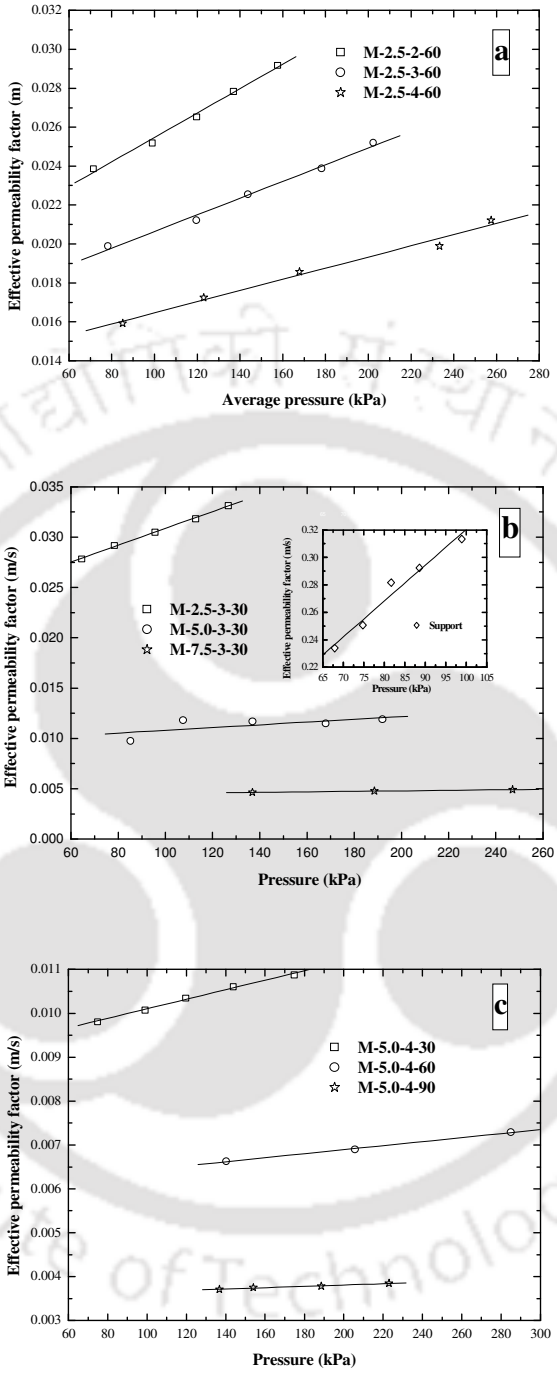

Figure 6.5. Variation of effective permeability factor (*K*) with average pressure (*P*) for a) M-2.5-2-60, M-2.5-3-60 and -2.5-4-60 (variation of CA) b) M-2.5-3-30, M-5.0-3-30, M-7.5-3-30 and support (variation of LTA) and c) M-5.0-4-30, M-5.0-4-60 and M-5.0-4-90 (variation of dipping time)

As shown in the table, the permeability of the support was found to be 6.90×10^{-1} $m^3m^{-2}kPa^{-1}s^{-1}$ and that for different mixed-matrix membranes were varied from 1.97×10^{-2} $m^3m^{-2}kPa^{-1}s^{-1}$ to 3.50×10^{-3} $m^3m^{-2}kPa^{-1}s^{-1}$. The average pore size of the support was found to be 1093 nm and that for mixed-matrix membranes were varied from 80 to 10 nm. Another observation was that with the increase in dipping time, zeolite and polymer concentration, pore sizes decreased, the contribution of viscous flux decreased and Knudsen flux increased. For instance, with the increase in the polymer concentration from 2% to 4% with a fixed LTA zeolite concentration (2.5%) and dipping time (60 s), the pore size decreased from 80 nm to 52 nm. Again, viscous flux decreased from 47% (M-2.5-2-60) to 4% (M-5.0-4-90) and Knudsen flux increased from 53% (M-2.5-2-60) to 96% (M-5.0-4-90). This was due to the decrease in the pore sizes with increase in the polymer/zeolite concentrations and dipping time, which was also confirmed from the FESEM analysis. Nandi et al. also ported similar trend for the membranes prepared by dip coating of cellulose acetate over ceramic support [20].

Hydraulic permeability: From the hydraulic permeabilities data presented in Figure 6.6, it was observed that the permeability decreased with increase in polymer/zeolite concentrations and dipping times. For 2.5% zeolite concentration and 60 s dipping time, the permeability decreased from 3.5×10^{-10} $m^3m^{-2}Pa^{-1}s^{-1}$ to 2.3×10^{-10} $m^3m^{-2}Pa^{-1}s^{-1}$ with an increase in the polymer concentration from 2% to 4%. Comparatively, for 4% cellulose acetate concentration and 5.0% zeolite concentration, the permeability decreased from 9.6×10^{-11} $m^3m^{-2}Pa^{-1}s^{-1}$ to 4.2×10^{-12} $m^3m^{-2}Pa^{-1}s^{-1}$ with increase in the dipping time from 30 s to 90 s. This was due to the fact that, with increase in dipping time, zeolite and polymer concentration, the average pore size of the membrane decreased and top layer thickness increased. The values of hydraulic permeabilities were observed to be lesser than the value of air permeabilities for the same membrane. This was due to the higher density and viscosity of water with respect to air.

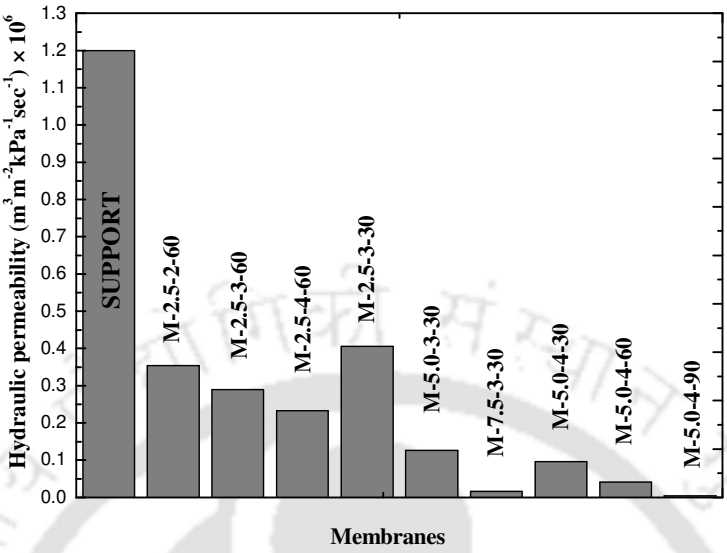

Figure 6.6. Comparing of hydraulic permeabilities of the prepared membranes

6.3.3 Bovine Serum Albumin Rejection

Effect of various membranes on % rejection of BSA: The experimental conditions were explained in the section 2.6. 1000 mg L^{-1} solution (pH = 7.2) was passed through all the prepared membranes and rejection percentage was calculated by Eq 5. The rejections % are reported in Figure 6.7. It was observed that, with the decrease in pore size, rejection was increased. For the membranes with pore sizes of 80 nm (M-2.5-2-60), 36 nm (M-5.0-3-30) and 10 nm (M-5.0-4-90), the rejections were 2.11%, 34.73% and 89.7% respectively. This phenomenon can be explained by the fact that, with the decrease in the pore sizes, more number of BSA molecules could not pass through the pores, thus rejection increased.

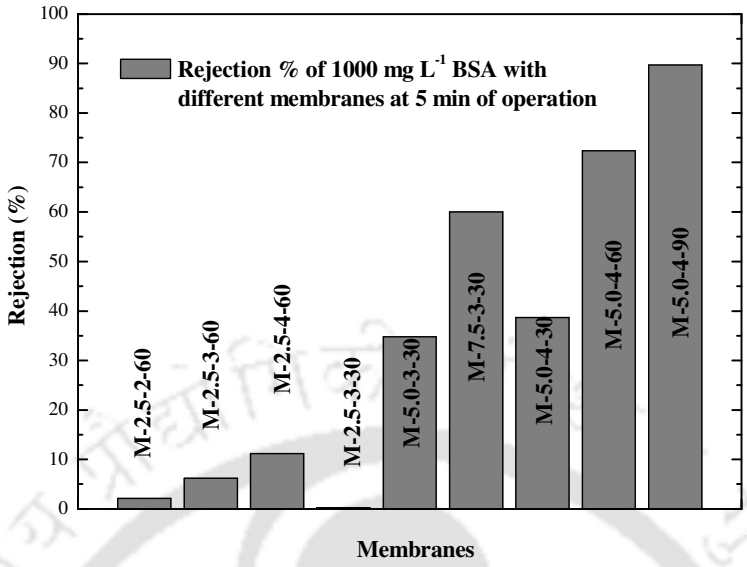

Figure 6.7. Rejection % of 1000 mg L^{-1} BSA with different membranes at 5 min of operation at 206.8 kPa

Variation of rejection with time: Figure 6.8 represents the variation in rejection of BSA with respect to time for 500 mg L^{-1}, 1000 mg L^{-1} and 2000 mg L^{-1} solutions. From Figure 6.8 two trends were observed.

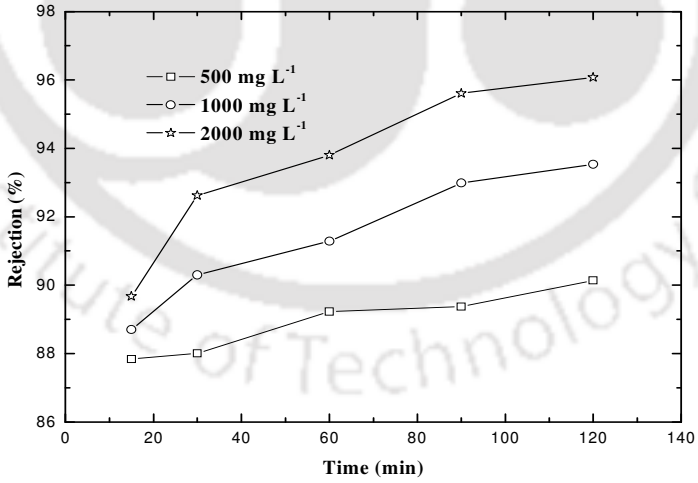

Figure 6.8. Variation of rejection (%) with time with membrane M-5.0-4-90 at 206.8 kPa

Initially for all the solutions, rejection was increasing with the progress of the experiment. 1000 mg L^{-1} solution has shown 88.7% and 93.5% rejection in 15 and 120 min of the experiment. This was due to the deposition of BSA molecules over the surface of the membrane with the continuation of the

experiment, thus decreasing the pore sizes which further increased the rejection. Further, 500 mg L^{-1}, 1000 mg L^{-1} and 2000 mg L^{-1} solutions have shown successive increase in the rejections at a fixed time of the experiment. After 60 min of the experiment, 500 mg L^{-1}, 1000 mg L^{-1} and 2000 mg L^{-1} solutions have shown 89.2%, 91.3% and 93.8% of rejection. This phenomenon can be explained by the fact that the solid content of the solutions were in an increasing order. This accordingly increased the deposition of solid particles over the membrane surface followed by increase in the rejection.

Flux decline during the experiment: Before the experiment, the stable flux of the membrane (M-5.0-4-90) was found to be 4.59×10^{-09} $m^3m^{-2}s^{-1}$ for 206.8 kPa transmembrane pressure. The flux decline profile was observed for 500 mg L^{-1}, 1000 mg L^{-1} and 2000 mg L^{-1} up to 2 h at 206.8 kPa (Figure 6.9).

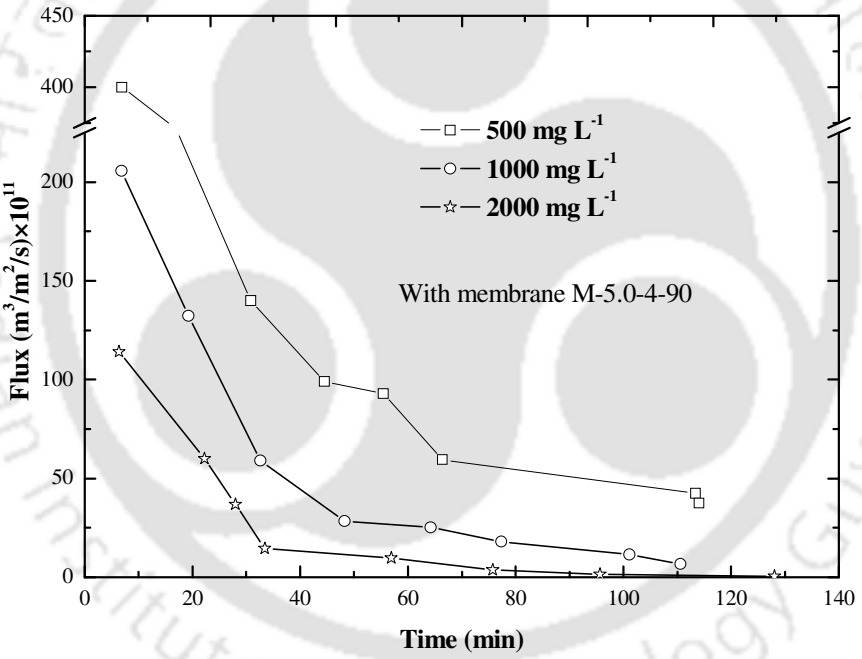

Figure 6.9. Flux decline profiles with membrane M-5.0-4-90 at 206.8 kPa.

During the experiment, the flux was observed to decrease slowly. From the flux decline profiles, two trends were observed. Initially, the flux was decreased very sharply and then the declination was gradual. The first phase flux declination was due to the concentration polarization and the second stage gradual decrease was due to gel formation over the membrane surface [21]. Another observation was that, the flux decline rate increased for higher concentration of BSA. The flux decreased to 9.91×10^{-10} $m^3m^{-2}s^{-1}$, 2.84×10^{-10} $m^3m^{-2}s^{-1}$, and 1.45×10^{-10} $m^3m^{-2}s^{-1}$ in 44.5 min, 48 min and 33.5 min for 500 mg

L^{-1}, 1000 mg L^{-1} and 2000 mg L^{-1} BSA solutions respectively. This was due to the increase in BSA concentration. At higher BSA concentration, more molecules were deposited over the membrane surface resulting higher flux declination.

6.4 Conclusion

Asymmetric mixed-matrix membranes were prepared using cellulose acetate as the polymer, LTA zeolite as the inorganic material and sintered clay as porous support for ultrafiltration applications. LTA zeolite was prepared in laboratory and characterized by XRD and LPSA. The mixed-matrix material was found thermally stable up to 300 °C. Easy and convenient dip coating method was used for the fabrication of the membranes. Nine membranes were prepared by varying the dipping time, zeolite and polymer concentrations and the effect of the parameters over the pore size and morphology were studied in detail. Membranes were characterized by FESEM, gas and hydraulic permeability. The pore sizes were found between 80 nm to 10 nm. Finally the applicability of the membranes was tested by the rejection of bovine serum albumin (BSA). Over 96% rejections were observed whereas; the rejection was increased with the decrease in the pore sizes and with the progress of the experiment. The initial flux declination during the experiment was sharp and afterwards a steady declination was observed. Thus, mixed-matrix membrane can be prepared using the combination of LTA zeolite and cellulose acetate by dip coating method which can be successfully applied for ultrafiltration application.

References

1. S. Kulprathipanja, Zeolites in Industrial Separation and Catalysis. Wiley-VCH Verlag GmbH & Co., Weinheim, 2010.

2. M. Mulder, Basic Principles of Membrane Technology, Springer. 2007.

3. J. Caro, M. Noack, P. Kölsch, R. Schäfer, Zeolite membranes – state of their development and perspective. Micropor. Mesopor. Mat., 2000, 38, 3–24.

4. S. Kulprathipanja, E.W. Funk, S.S. Kulkarni, Y.A. Chang, Separation of a monosaccharide with mixed matrix membranes. US Patent 4735193, 1988.

5. H.J.C. Hennepe, D. Bargeman, M.H.V. Mulder, C.A. Smolders, Zeolite-filed silicon rubber membranes: part 1. Membrane pervaporation and pervaporation results. J. Membr. Sci., 1987, 35, 39-55.

6. P. Jha, J.D. Way, Carbon dioxide selective mixed matrix membranes formulation and characterization using rubbery substituted polyphosphazene. J. Membr. Sci., 2008, 324, 151-161.

7. S. Hussain, W.J. Koros, Mixed Matrix hollow fiber membranes made with modified HSSZ-13 zeolite in polyetheremide polymer metrix for gas separation. J. Membr. Sci., 2007, 288, 195-207.

8. G. Ciobanu, G. Carja, O. Cioban, Structure of mixed matrix membranes made with SAPO-5 zeolite in polyurethane matrix. Micropor. Mesopor. Mat., 2008, 115, 61-66.

9. S.J. Miller, A. Kuperman, D.Q. Vu, Mixed matrix membranes with low silica-to-alumina ratio molecular sieves and methods for making and using these membranes. US Patent 7138006 B2, 2006.

10. R. Maharajan, W.J. Koros, Factors controlling successful formation of mixed matrix gas separation materials, Ind. Engg. Chem. Res., 2000, 39, 2692-2696.

11. R. Maharajan, W.J. Koros, Mixed matrix membrane materials with glassy polymers. Poly. Engg. Sci., 2002, 42, 1432-1441.

12. T.W. Pechar, S. Kima, B. Vaughan, E. Maranda, M. Tsapatsis, H.K. Jeong, C.J. Cornelius, Fabrication and characterization of polyimide-zeolite L mixed matrix membranes for gas separation. J. Membr. Sci., 2006, 277, 195-202.

13. S. Hussain, W.J. Koros, Mixed matrix hollow fiber membranes made with modified HSSZ-13 zeolite in polyetherimide polymer matrix for gas separation. J. Membr. Sci., 2007, 288, 195-207.

14. A.F. Ismail, T.D. Kusworo, A. Mustafa, Enhanced gas permeation performance of polyethersulfone mixed matrix hollow fiber membrane using novel Dynasylam Ameo silane agent. J. Membr. Sci., 2008, 319, 306-312.

15. L.Y. Jiang, T.S. Chung, C. Cao, Z. Huang, An investigation to revitalize the separation performance of hollow fiber with a thin mixed matrix composite skin for gas separation. J. Membr. Sci., 2005, 252, 113-125.

16. S. Jana, M.K. Purkait, K. Mohanty, Preparation and characterization of low-cost ceramic microfiltration membranes for the removal of chromate from aqueous solutions. App. Clay Sci., 2010, 47, 317-324.

17. A. Malekpour, M.R. Millani, M. Kheirkhah, Synthesis and characterization of a NaA zeolite membrane and its applications for desalination of radioactive solutions, Desalination, 2008, 225, 199-208.

18. A. Tavolaro, P. Tavolaro, LTA zeolite composite membrane preparation, characterization and application in a zeolitic membrane reactor, Catal. Comm., 2007, 8, 789-794.

19. S. Jana, M.K. Purkait, K. Mohanty, Preparation and Characterizations of Ceramic Microfiltration Membrane: Effect of Inorganic Precursors on Membrane Morphology, Sep. Sci. Technol., 2011, 46, 33-45.

20. B.K. Nandi, R. Uppaluri, M.K. Purkait, Effects of dip coating parameters on the morphology and transport properties of cellulose acetate–ceramic composite membranes. J. Membr. Sci., 2009, 330, 246-258.

21. A.S. Jönsson, G. Trägårdh, Ultrafiltration applications, Desalination, 1990, 77, 135-179.

Chapter VII

Conclusion and Future Scope of work

This chapter discusses the major conclusion drawn from the present investigation and the future works which can be done as an advancement of the current study.

7.1 Conclusion

This work deals with the preparation, characterizations and applications of low-cost ceramic microfiltration and composite ultrafiltration membranes. During the first phase of the work two low-cost microfiltration membranes were prepared from locally available clay of IIT Guwahati. Membrane A was prepared from clay only and Membrane B was prepared from clay with addition of small amount of other chemicals. Sodium carbonate, sodium metasilicate and boric acid were added to increase the mechanical strength of the Membrane B. The pore sizes of the prepared membranes sintered at 1000 °C were 3.75 μm (Membrane A) and 4.5 μm (Membrane B). All the membranes were characterized by Scanning Electron Microscopy (SEM), X-Ray Diffraction (XRD), water permeability and chemical stability test. It was found that with increase in the sintering temperatures, the pore size increased and porosity decreased. The overall performance of Membrane B was better than Membrane A. Membrane B was thus used for the removal of chromate ions from aqueous solution by Micellar Enhanced Microfiltration (MEMF) using cetylpyridinium chloride (CPC) as the surfactant. Different CPC/ $K_2Cr_2O_7$ ratios were tried and it was found that for the ratios > 10, 100 % rejections were achieved.

In the next stage of the study, more finer particles of kaolin were used with clay in different proportion for making lower pore sized membranes. Five number of microfiltration membranes were prepared with different compositions of clay, kaolin and other binding materials. The effect of sintering temperature on membrane pore size and porosity were studied and similar trends as previous work were found. Further, the effect of precursor particle size on membrane pore size and pore density was studied. Prepared membranes pore sizes were found to be 4.58 μm, 2.28 μm, 0.71 μm, 0.49 μm, and 0.31 μm at 1000 °C sintering temperature for the

average precursor particle size of 34.66 μm, 30.37 μm, 26.07 μm, 21.79 μm and 17.51 μm respectively. The relationships of average particle diameter [$D_{1,0}$], surface weighted mean diameter [$D_{3,2}$], volume weighted mean diameter [$D_{4,3}$] and specific area [A_{sp}] with average pore size and the relationships of average particle diameter [$D_{1,0}$] and quartile ratio [$_{25}X_{75}$] with pore density were found to be represented by second order polynomials. Thus, it was concluded that pore diameter and density can be predicted directly from the particle size distribution of membrane precursors even before preparing the membranes.

Further, the lowest pore size microfiltration membrane (pore size 0.31 μm) was used for the removal of crystal violet dye by a hybrid process of advanced oxidation (AOP) followed by microfiltration. For the complete removal of dye, the ratios of the reactant and dye were found as: $[H_2O_2]/[Dye] \geq 10$ and $[H_2O_2]/[FeSO_4] \leq 10$. The effects of the dye, ferrous sulfate heptahydrate and hydrogen peroxide concentration on the degradation of dye were studied in detail and it was found that the rate of degradation of the dye decreased with the increase in the dye concentration and increased with the increase in the concentration of $FeSO_4 \cdot 7H_2O$ and H_2O_2. For the quick and complete removal of AOP post product, microfiltration was applied. The EDX and FTIR analyzation of the crystal violet and the membrane retentate clearly showed the oxidization of the aromatic group and chlorine from the dye molecular structure. The conductivity, pH, TDS and density of the feed and permeate were compared. It was observed that the dissolved solids were totally removed, density and pH shown minute changes and conductivity value wasn't changed at all. Thus, the proposed hybrid process showed a better option for the removal of such dye molecules from aqueous solution.

With an aim to prepare ultrafiltration range membranes, the lowest pore size MF membranes thus prepared were impregnated with chitosan crosslinked with glutaraldehyde by dip coating method. Ceramic disc shaped membrane with a pore size of 1093 nm was used as the support and three different concentrations of chitosan (1.0 %, 1.5 % and 2.0 %) at different dipping times (240 s, 480 s and 720 s) were used for the preparation of ultrafiltration membrane. The average pore sizes of the chitosan impregnated membranes were calculated using gas permeability data and found to be within 760 nm to 13 nm. The average pore size decreased with increase in both the chitosan concentration and dipping time. The 13 nm pore size membrane was applied for the removal of mercury and arsenic from synthetic groundwater by polymer

enhanced ultrafiltration (PEUF) using polyvinyl alcohol (PVA) as the chelating agent. Concentration of heavy metal in the permeate was observed to be increased with its concentration in feed and decreased with increase in the polymer concentration. Another observation was that the permeate heavy metal concentration was increased with the progress of the experiment which was due to the convective transport of the chelate complexes through the membrane. The performance of the proposed PEUF technique was compared with the existing RO and NF technique and was found to be very encouraging.

Another attempt was done for the preparation of ultrafiltration range composite membrane by a novel dip coating method. The method was especially applicable for low viscous polymer solutions. In a nutshell, a thin film of polymer solution was applied over ceramic support by dip coating method and further dipped in another solvent for removing the solvent of the polymer. Polyvinyl acetate (PVAc) was used as the polymer in this work. Four polymer concentrations (10 %, 20 % 30% and 40 %) and three dipping times (30 s, 60 s and 90 s) were studied for the preparation of membranes with pore sizes within 150 nm to 9 nm. All the membranes were characterized with SEM, gas permeability and water permeability. The lowest pore size membrane (9 nm) was applied for the fractionation of lysozyme (LS) and ovalbumin (OV) for chicken egg white using a dead end membrane permeation cell. pH 11.0 was found as optimum for the transmission of LS and rejection of OV. Up to 94 % rejection of OV and 98 % transmission of LS was obtained. The results were encouraging and confirmed that such composite membrane can be used for bioseparation of proteins in related industries.

Finally another study was done on the preparation and characterization of mixed matrix membrane using cellulose acetate and LTA zeolite by the usual dip coating method. LTA zeolite was prepared in laboratory by hydrothermal synthesis. Nine membranes were prepared by varying the dipping time, zeolite and polymer concentrations and the effect of the parameters over the pore size and morphology were studied in detail. Membranes were characterized by Field Emission Scanning Electron Microscopy (FESEM), gas and hydraulic permeability. Pore sizes were found to be within 80 nm to 10 nm and applicability of the membranes were tested by the rejection of bovine serum albumin (BSA). Over 96 % rejection of BSA was observed, thus, the method of dip coating for preparation of mixed matrix membrane showed good promise for preparation of UF range membrane.

In a bottom-line, the whole study showed fabrications and characterizations of low cost ceramic microfiltration and asymmetric composite ultrafiltration membranes with some applications such as removal of chromate ion, dye and heavy metals by hybrid processes like MEMF, AOP followed by MF, PEUF. Novel modified dip coating method was proposed which was especially applicable for the coating of low viscous polymers. Prepared membrane by this method was applied for the fractionation of lysozyme and ovalbumin from chicken egg white. Another study was done on the preparation and characterization of asymmetric ultrafiltration mixed matrix membranes using LTA zeolite and cellulose acetate as inorganic material and polymer respectively. The applicability of the membranes in ultrafiltration range were tested by the rejection of bovine serum albumin.

7.2 Scope of Future Work

Research findings in this work provided good number of insights with respect to fabrication, characterization and applications of clay supported composite membranes. Some recommendation for future works are described in this section

Preparation and applications of microfiltration membrane

1. Poisonous permanganate (MnO_4^-) ion removal studies by Micellar Enhanced Microfiltration (MEMF) may be investigated.
2. The MEMF studies with other cationic surfactants such as: cetyl trimethylammonium bromide (CTAB), hexadecyl trimethyl ammonium bromide (HTAB) or with cetyl trimethylammonium chloride (CTAC) may be undertaken.
3. Investigation for the relationship of optimum level of binding material with the average particle size of the membrane precursors.
4. Advanced Oxidation Process (AOP) followed by microfiltration (MF) studies on other dyes such as: brilliant green, eosin yellow etc. may be taken up.

Preparation and applications of ultrafiltration membrane

1. Removal studies on other heavy metal (such as: Pb, Zn, Sn etc.) by Polymer Enhanced Ultrafiltration (PEUF).
2. Use of other polymers (such as: chitosan, ethylenediaminetetraacetic acid etc) which were known for making chelate compounds for the PEUF providing the specific membrane pore size is sufficient to restrict the passage of the polymer.
3. The novel dip coating method can be applied for other polymers such as: polysulfone or polyvinyl propylene.
4. A correlation of membrane thickness (Can be found by SEM) with dipping time and solution concentration for a particular system can be found.

Research Output

International Peer Reviewed Journals

S. Jana, M.K. Purkait, K. Mohanty, Preparation and characterization of low-cost ceramic microfiltration membranes for the removal of chromate from aqueous solutions, **Applied Clay Science**, 47, 2010, 317-324.

S. Jana, M.K. Purkait, K. Mohanty, Removal of Crystal Violet by Advanced Oxidation and Microfiltration, **Applied Clay Science**, 50, 2010, 337-341

S. Jana, M.K. Purkait, K. Mohanty, Preparation and Characterizations of Ceramic Microfiltration Membrane: Effect of Inorganic Precursors on Membrane Morphology, **Separation Science and Technology**, 46, 2011, 33-45.

S. Jana, Anirban Saikia, M. K. Purkait, K. Mohanty, Chitosan based ceramic ultrafiltration membrane: Preparation, characterization and application to remove Hg(II) and As(III) using polymer enhanced ultrafiltration, **Chemical Engineering Journal**, 170, 2011, 209-219.

S. Jana, M.K. Purkait, K. Mohanty, Clay supported polyvinyl acetate coated composite membrane by modified dip coating method: Application for the purification of lysozyme from chicken egg white. **Journal of Membrane Science**, 382, 2011, 243-251.

S. Jana, M.K. Purkait, K. Mohanty, Polymer enhanced ultrafiltration of mercury using chitosan impregnated ceramic membrane, **Desalination and Water Treatment**, 37, 2012, 1-10.

Manuscripts under review

S. Jana, M.K. Purkait, K. Mohanty, Preparation, Characterization and Application of Mixed-matrix Ultrafiltration Membrane from LTA Zeolite and Cellulose Acetate.

Book Chapter

S. Jana, M.K. Purkait, K. Mohanty, *Preparation and Applications of Zeolite Membranes: A Review* in **Membrane Technology & Applications** (Eds: K. Mohanty and M.K. Purkait), CRC Press, USA. (Article in Press).

Conference Proceedings

S. Jana, M.K. Purkait, K. Mohanty, Preparation and Characterization of Clay Based Microfiltration Membrane: Role of Precursor Particle Size on Surface Morphology, CHEMCON 2010, 27-29 December 2010, Annamali Nagar, India.

S. Jana, M.K. Purkait, K. Mohanty, Removal of Arsenic (As) and Mercury (Hg) from Drinking Water by Complexation-Ultrafiltration with Polyvinyl Alcohol, GIST 2010, 26-27 December, 2010, Pune, India.

Appendix:

Error Analysis

Error in a scientific measurement usually does not mean a mistake or blunder. Instead, the terms "error" and "uncertainty" both refer to unavoidable imprecision in measurements. When an experiment is repeated for more than once, then there is an obvious observation of the fluctuation in the results. So, in the laboratory more often data were combined to obtain the final quantity. Whereas, 'error analysis' determines the accuracy of calculations and reliability of the reported experimental data.

Especially, two types of errors were considered during this study viz.

Systematic error: Systematic errors are biases in measurement which lead to the situation where the mean of many separate measurements differs significantly from the actual value of the measured attribute. All measurements are prone to systematic errors, often of several different types. Sources of systematic error may be imperfect calibration of measurement instruments (zero error), changes in the environment which interfere with the measurement process and sometimes imperfect methods of observation can be either zero error or percentage error.

Random error: Random errors are errors in measurement that lead to measurable values being inconsistent when repeated measures of a constant attribute or quantity are taken. The word random indicates that they are inherently unpredictable, and have null expected value, namely, they are scattered about the true value, and tend to have null arithmetic mean when a measurement is repeated several times with the same instrument. All measurements are prone to random error. The concept of random error is closely related to the concept of precision. The higher the precision of a measurement instrument, the smaller the variability (standard deviation) of the fluctuations in its readings.

Error during the measurement of concentration

Throughout the study, different concentrations were measured with the help of UV-vis spectrophotometer and High Performance Liquid Chromatography (HPLC). For that, calibration curves were drawn from the known concentrations of the specific species. Both the instrument provide measurement with four digit precession after the decimal and during repetition, only fourth digit variation was observed. The coefficient of determination (R^2) for the calibration curves were varied between 0.9891 (calibration of ovalbumin in HPLC) to 0.9994 (calibration of crystal violet in UV-vis

spectrophotometer). Thus during the measurement of concentrations, maximum error occurred was 1.09 %.

Error during the measurement of the permeate flux

Gas and air permeability experiments were done to determine the pore sizes of the prepared membranes. Except this, during the application of the membranes, different liquid streams were passed through the membranes and permeabilities were determined. All the experiments were repeated for 3-5 times and statistical method was obtained for calculating the error in the permeate flux. Determination of standard deviation is the best method for estimation of the uncertainty. The method is as follows:

If, p_1, p_2, p_3 …. p_n are the n number of measurements of a particular quantity p, then the mean value (viz. $\overline{p}$) is defined as

$$\overline{p} = \frac{p_1 + p_2 + p_3 + ... + p_n}{p} = \frac{1}{p}\sum_{i=1}^{n} p_i$$

The root mean square (RMS) deviation was expressed as Δp and calculated by the equation:

$$\Delta p = \sqrt{\frac{(p_1 - \overline{p})^2 + (p_2 - \overline{p})^2 + ... + (p_n - \overline{p})^2}{n-1}}$$

Using this method, the Δp values during the measurement of pore sizes for the microfiltration membranes were varied between 0.0024 to 0.0107, for the chitosan impregnated membrane 0.0946 to 0.0582, for the polyvinyl acetate composite membrane 0.0708 to 0.0074 and for mixed matrix membrane was 0.1439 to 0.0726. And, during the other studies, maximum error in permeate flux was occurred during the removal of mercury (Δp = 0.0824).